INVESTIGATING THE MOLECULAR MECHANISM OF ENDOTHELIAL EROSION OF ATHEROSCLEROTIC PLAQUES

SATTA SANDRO

A thesis submitted in partial fulfilment
of the requirements of
Manchester Metropolitan University
for the degree of Doctor of Philosophy

Department of Life Sciences
Manchester Metropolitan University

2019

LIST OF FIGURES

LIST OF ABBREVIATIONS

4eBP-1	4e-binding protein-1
ACC	Acetyl-CoA Carboxylase
ACS	Acute Coronary Syndrome
ACS-IFC	Acute Coronary Syndrome with an Intact Fibrous Cap
AF	Attachment Factor
AMPK	AMP-activated Protein Kinase
Apaf-1	Apoptosis Protease Factor 1
APC	Anaphase-Promoting Complex
ARE	Antioxidant Response Element
ATF3	Activating Transcription Factor 3
ATF4	Activating Transcription Factor-4
Atg	Autophagy-related genes
BAG3	Bcl2-associated athanogene 3
BCA	Bicinchoninic acid-Assay
BDGI	Bone Marrow Stromal cell-derived Growth Inhibitor
BECN1	Beclin 1
BrdU	Bromodeoxyuridine
BSA	Bovine Serum Albumin
C1	Complex -1
CAMKK2/CaMKKβ	Calcium/calmodulin-dependent Protein Kinase 2 beta
CBP	cAMP-response-element-binding protein
CDKs	Cyclin Dependant Kinases
CFD	Computational Fluid Dynamic
CHD6	Chromo-ATPase/helicase DNA-binding protein 6
Chq	Chloroquine
CIP/KIP	CDK interacting protein/Kinase inhibitory protein
CKI	Cyclin Dependant Kinase Inhibitors
CMA	Chaperone-Mediated Autophagy
CsCL	Caesium Chloride
CSE	Cigarette Smoke Extract
CUL3	Cullin 3
Cyc	Cyclins
DAB	Diaminobenzidine
DAMP	Damage-Associated Molecular Pattern
DBS	Double Strand Break
DGR	Double Glycine Repeat

EB3	End-binding Protein 3
EC	Endothelial Cell
ECL	Enhanced Chemiluminescence
ECM	Extracellular Matrix
eNOS	endothelial Nitric Oxide Synthase
ER	Endoplasmic Reticulum
ESS	Elevated Shear Stress
ESSTC	ESS in combination with CSE+TNFα
FCS	Fetal Bovine Serum
FDA	Food and Drug Administration
FFA	Free Fatty Acid
FoV	Field of View
Fra-1	Fos Related Antigen-1
FRB	FKBP12/Rapamycin-Binding
GABARAP	Gamma-aminobutyric acid receptor-associated protein
GAPDH	Glyceraldehyde 3-phosphate dehydrogenase
GCL	Glutamate Cysteine Ligase
GCLC	Glutamate—Cysteine Ligase Catalytic subunit
GCLM	Glutamate-Cysteine Ligase Modifier Subunit
GF-AFC	Glycylphenylalanyl-aminofluoroumarin
GPx	Glutathione Peroxidases
GR	Glucocorticoid Receptor
GSH	Glutathione
GSK-3	Glycogen Synthase Kinase 3
HCAECs	Human Coronary Artery Endothelial Cells
HIF1α	hypoxia-inducible factor 1α
Hip	HSP70-interacting protein
HMOX	Heme Oxygenase
Hop	HSP-organising protein
HRP	Horseradish peroxidase
HS	Heat Stress
HSC70	Heat Shock Cognate 70
HSF1	Heat shock factor 1
HSP70	Heat Shock Protein 70
HSP90	Heat Shock Protein 90
HSPA1B	Heat Shock Protein 70k 1B
HSPs	Heat Shock Proteins
HYAL2	Hyaluronidase 2

HUVECs	Human Umbilical Vein Endothelial Cells
ICC	Immunocytochemistry
IFN γ	interferon-γ
IKKβ	Inhibitor of nuclear factor Kappa-B Kinase Subunit beta
IL-1β	Interleukin 1 beta
IL-2	Interleukin-2
IMS	Industrial Methylated Spirit
iNRF2	NRF2 Inhibitor
IP3	Intracellular inositol 1,4,5-trisphosphate
IPA	Ingenuity Pathway Analysis
IRF	Interferon regulatory factor 1
IVR	Intervening Region
Kbp	Kilo-base pairs
Keap1	Kelch-like erythroid cell-derived protein with CNC homology-associated protein 1
KLF	Kruppel-like Factor
LAMP1	Lysosomal-Associated Membrane Protein 1
LC3	Microtubule-associated Protein – Light Chain 3
LDL	Low Density Lipid
LSS	Lamina Shear Stress
MAF	Musculoaponeurotic Fibrosarcoma
MAPK	Mitogen-Activated Protein Kinase
MAPLC3	Microtubule-associated proteins
MCP-1	Monocyte Chemoattractant Protein-1
MI	Myocardial Infarction
MMF	Monomethyl Fumarate
MMP	Matrix Metalloproteinase
MOI	Multiplicity of Infection
MPO	Myeloperoxidase
MRI	Magnetic Resonance Imaging
MTE	Multi Tissue Expression
MTN	Multi Tissue Northern blot
mTOR	mammalian Targets of Rapamycin
NADPH	Nicotinamide Adenine Dinucleotide Phosphate
NBD	Nucleotide Binding Domain
NE	Neutrophil Elastase
NES	Nuclear Exporting Signal
NETs	Neutrophil Extracellular Traps
NFE2L2	Nuclear Factor, Erythroid 2 Like 2

NFκB	Nuclear Factor Kappa-light-chain-enhancer of activated B cells
NO	Nitric Oxide
NOX2	NADPH Oxidase 2
NQO1	NAD(P)H Quinone Dehydrogenase 1
NRF2	Nuclear Response Erythroid 2-like 2
O_2°	Oxygen Radicals
OCT	Optical Coherence Tomography
OKL38	Ovary, Kidney and Liver Protein 38
OSGIN1	Oxidative Stress Induced Growth Inhibitor 1
OSGIN2	Oxidative Stress Induced Growth Inhibitor 2
OSI	Oscillatory Shear Index
OSS	Oscillatory Shear Stress
Pa	Pascal
PAD4	Peptidyl Arginine Deiminase 4
PAI	Plasminogen Activator Inhibitor
PAMP	Pathogen-Associated Molecular Pattern
PARP	poly-ADP-ribose polymerase
PAS	Phagophore Assembly Site
PBS	Phosphate Buffered Saline
PCR	Polymerase Chain Reaction
PE	Phosphatidylethanolamine
PECAM	Platelet Endothelial Cell Adhesion Molecule
PFA	Paraformaldehyde
Pfu	Plaque forming units
PGAM	Phosphoglycerate Mutases
PI	Propidium Iodide
PI3K	Phosphatidylinositol 3-Kinase
Pifithirin α	2-(2-Imino-4,5,6,7-tetrahydrobenzothiazol-3-yl)-1-p-tolylethanone hydrobromide
PKA	Protein Kinase A
PMA	Phorbol 12-myristate 13-acetate
PMN	Polymorphonucleates
PPP1R15A	Protein Phosphatase 1 Regulatory Subunit 15A
ProTα	Prothymosin-alpha
PRTN3	Proteinase 3
PTEN	Phosphatase and Tensin Homolog
PVDF	Polyvinylidene Difluoride
Re	Reynolds Number
RFU	Relative Fluorescent Units

RNS	Reactive Nitrogen Species
ROCK	Rho-associated Protein Kinase
ROS	Reactive Oxygen Species
RT	Reverse Transcriptase
RXRα	Retinoids X Receptor α
S40	Serine-40
S6K1	S6 kinase 1
SA-β-gal	Senescence-associated Beta-galactosidase
SASP	Senescence-Associated Secretory Phenotype
SBD	Substrate Binding Domain
SDS	Sodium Dodecyl Sulfate
SEM	Scanning Electron Microscopy
SEM	Standard Error of the Mean
SH3GLB1/Bif-1	SH3 Domain Containing GRB2 Like, Endophilin B1/Bax interacting factor 1
siRNA	Small Interfering RNA
SLC3A2	Solute Carrier Family 3 Member 2
SMC	Smooth Muscle Cell
SRXN1	Sulfiredoxin 1
SSB	Single Strand Break
STAT1	Signal Transducer and Activator of Transcription 1
STAT2	Signal Transducer and Activator of Transcription 2
TAWSS	Time Averaged Wall Shear Stress
TBS	Tris Buffered Saline
TCFAs	Thin Capped Fibro-Atheromas
TF	Transcription Factor
TLR2	Toll Like Receptor factor 2
TNFα	Tumour Necrosis Factor alpha
TRIM24	Tripartite Motif Containing 24
TXNRD1	Thioredoxin Reductase 1
Ublc	Ubiquitin-like conjugation
UPR	Unfolded Protein Response
UTR	Untranslated Region (UTR)
VCAM	Vascular Cell Adhesion Molecule
VEGFR	Vascular Endothelial Growth Factor Receptors
Ver	Ver155008
ZO-1	Zonula Occludins-1
β-TrCP	β-transducin repeat-containing protein

LIST OF TABLES

LIST OF TABLES APPENDIX

ABSTRACT

Nearly a third of heart attacks are caused by endothelial erosion, where the endothelial layer overlying atherosclerotic plaques detaches, initiating blood clot formation. Understanding the processes involved that mediate plaque erosion is the central aim of this research, in particular, the signalling pathways involved in endothelial cell (EC) dysfunction. Endothelial dysfunction caused by the combined action of inflammatory mediators and oxidants derived from cigarette smoke are known to promote coronary atherosclerosis and increase the likelihood of myocardial infarctions and strokes. Endothelial dysfunction is modified by the hemodynamic environment that the endothelial cell is exposed to, with disturbed flow found at bifurcations and curved sections of artery amplifying the effects. This plays a major role in the initiation and progression of atherosclerosis, with disease developing and progressing most rapidly in regions of oscillatory, low and disturbed wall shear stress. This reduces the bioavailability of nitric oxide as well as increasing oxidant stress, the magnitude of response to inflammatory cytokines, rates of apoptosis and permeability. On the contrary, normal physiological shear stress (12–16 dynes/cm2 in the coronary circulation) induces an athero-protective phenotype in endothelial cells predominantly mediated by activation of transcription factors KLF2, KLF4 and NRF2, all of which combine to activate a program of gene expression and epigenetic changes that reduces endothelial dysfunction. Endothelial erosion tends to occur overlying stenotic atherosclerotic plaques, exposed to very elevated levels of shear stress. Overexpression of NRF2 and NRF2 regulated genes OSGIN 1 and 2 promote EC detachment. In addition, expression of OSGIN1 and OSGIN2 increased under these conditions and also in the aortas of mice exposed to cigarette smoke. Sustained high level expression of OSGIN1+2 resulted in cell cycle arrest, induction of senescence, loss of focal adhesions and actin stress fibres, and dysregulation of autophagy. Furthermore, EC detachment observed by overexpression of either NRF2 or OSGIN1+2 did not depend on apoptosis and could be partially rescued by inhibition of HSP70 using Ver155008, or AMP kinase activation using metformin. These findings demonstrate that under elevated flow, smoking-induced hyperactivation of NRF2 can trigger endothelial cell detachment, highlighting a novel mechanism that could contribute to ACS involving endothelial erosion overlying stenotic plaques.

ACKNOWLEDGEMENTS

There are many people to whom I owe gratitude, and would like to thank, for helping me to reach this point.

I would like to first say a very big thank you to my supervisors Stephen White and Yvonne Alexander for their endless support, guidance and direction, and for allowing me the freedom to work independently and take the investigation down the paths I found the most fascinating.

Completing this work would have been all the more difficult were it not for the support provided by the other members in the Cardiovascular group at Manchester Metropolitan University, which has been a source of friendship as well as good advice and collaboration. My thanks go to Raya, Fadel and Moa for the laughs and for making my PhD time lighter and more enjoyable, which would have been much harder without their support.

I would like to thank Manchester Metropolitan University not only for providing the funding which allowed me to undertake this research, but also for giving me the opportunity to attend conferences and meet so many interesting people.

I greatly appreciate the support received through the collaborative work with Mario Sechi, especially for trying to convince me that working in science is more satisfying than escaping to Mexico.

I would like to thank my family and friends for their ongoing support and for allowing me escape when I needed it. Without their encouragement, I am not sure I would have made it anywhere near this far. A special thanks goes to Kristina for supporting me along the way and understanding me when I needed the most.

Lastly, my thought goes to my dad, never forgotten, who I hope is going to be proud of me for what I have achieved until now.

NOVELTY STATEMENT

The findings arising from this thesis define the permissive hemodynamic environment in which endothelial erosion occurs. To our knowledge, this is the first study that highlights a completely novel mechanism that regulates endothelial adhesion, which potentially contributes to a third of acute coronary syndrome and proposes a therapeutic route.

LIST OF PUBLICATIONS ARISING FROM THIS THESIS

1. **Submitted: Sandro Satta**, Michael McElroy, Alex Langford-Smith, Glenn Ferris, Jack E Teasdale, Yongcheol Kim, Giampaolo Niccoli, Ajime Tom Tanjeko, Jef Serre, Georgina G Hazell, Graciela Sala Newby, Ping Wang, Jason L Johnson, Martin J Humphries, Ghislaine Gayan-Ramirez, Peter Libby, Filippo Crea, Hans Degens, Frank Gijsen, Thomas Johnson, Amir Keshmiri, Yvonne Alexander, Andrew C Newby, Stephen J White **Title:** 'A pivotal role for Nrf2 in endothelial detachment– implications for endothelial erosion of stenotic plaques'.

2. **Sandro Satta**, Michael McElroy, Alex Langford-Smith, Glenn Ferris, Jack E Teasdale, Yongcheol Kim, Giampaolo Niccoli, Ajime Tom Tanjeko, Jef Serre, Georgina G Hazell, Graciela Sala Newby, Ping Wang, Jason L Johnson, Martin J Humphries, Ghislaine Gayan-Ramirez, Peter Libby, Filippo Crea, Hans Degens, Frank Gijsen, Thomas Johnson, Amir Keshmiri, Yvonne Alexander, Andrew C Newby, Stephen J White **Title:** A pivotal role for Nrf2 in endothelial detachment– implications for endothelial erosion of stenotic plaques. 2019 14th SYMPOSIUM BVBCD2019, LONDON (Conference abstract)

3. **Sandro Satta,** Michael Mcelroy, Georgina Hazell, Jack Teasdale, Graciela Sala-Newby, Jason Johnson, Frank Gijsen, Tom Johnson, Yvonne Alexander, Amir Kesmiri, Andrew Newby and Stephen White. **Title:** Nrf2-mediated upregulation of OSGIN1 and OSGIN2 triggers cell detachment through dysregulated autophagy – a potential mechanism for endothelial erosion overlying stenotic plaque. 2018 ANNUAL MEETING OF THE BRITISH ATHEROSCLEROSIS SOCIETY, CAMBRIDGE (Conference abstract)

4. **Sandro Satta,** Georgina Hazell, Jack Teasdale, Graciela Sala-Newby, Tom Johnson, Andrew Newby, Yvonne Alexander & Stephen White. **Title:** OSGIN1 and OSGIN2 regulate adhesion of HCAEC and potentially contribute to endothelial erosion of plaques. 2018 1st SUMMER SCHOOL EVBO POSTER, DRESDEN (Conference abstract)

5. **Sandro Satta,** Georgina Hazell, Jack Teasdale, Graciela Sala-Newby, Tom Johnson, Andrew Newby, Yvonne Alexander & Stephen White. **Title:** OSGIN1 and OSGIN2 regulate adhesion of HCAEC and potentially contribute to endothelial erosion of plaques. 2018 INTERNATIONAL VASCULAR BIOLOGY MEETING, HELSINKI (Conference abstract)

6. **Sandro Satta**, Ayman M. Mahmoud, Fiona L. Wilkinson, M. Yvonne Alexander, and Stephen J. White (2017), Oxidative Medicine and Cellular Longevity Volume 2017, Article ID

9237263, **Title:** 'The Role of Nrf2 in Cardiovascular Function and Disease'

7. **Sandro Satta,** Georgina Hazell, Jack Teasdale, Alasdair Peachey, Graciela Sala-Newby, Jason Johnson, Yvonne Alexander, Andrew Newby, Stephen White. **Title:** Cigarette smoke extract and TNFα provoke cell detachment at elevated shear stress. 2017 BSCR/BAS SPRING MEETING, MANCHESTER (poster) (Conference abstract)

8. **Sandro Satta,** Jack Teasdale, Georgina Hazell, Andrew Newby and Stephen White. **Title:** Does chronic hyperactivation of Nrf2 trigger heart attacks? 2016 NORTHERN VASCULAR BIOLOGY, HULL (poster) (Conference abstract)

LIST OF SCIENTIFIC MEETINGS ATTENDED

1. 2019 14th SYMPOSIUM BVBCD2019 LONDON (ORAL PRESENTATION)
2. 2018 ANNUAL MEETING OF THE BRITISH ATHEROSCLEROSIS SOCIETY, CAMBRIDGE (Poster)
3. 2018 1st SUMMER SCHOOL EVBO. DRESDEN (Poster).
4. 2018 INTERNATIONAL VASCULAR BIOLOGY MEETING, HELSINKI (Poster).
5. 2017 BSCR/BAS SPRING MEETING, MANCHESTER (Poster).
6. 2016 NORTHERN VASCULAR BIOLOGY, HULL (Poster).

PRIZES: NOMINATIONS AND AWARDS

1. 1st prize winner: oral presentation 2019 14th SYMPOSIUM BVBCD2019, LONDON
2. Awarded a travel Bursary from British heart foundation to attend 14th SYMPOSIUM BVBCD2019, LONDON.
3. 1st prize winner: 2018 ANNUAL MEETING OF THE BRITISH ATHEROSCLEROSIS SOCIETY, CAMBRIDGE.
4. 1st prize winner: 2018 1st SUMMER SCHOOL EVBO. DRESDEN.

CHAPTER 1: INTRODUCTION

CHAPTER 1: INTRODUCTION

1.1 Atherosclerosis: An historical perspective

Between 1504-08 Leonardo da Vinci met a hundred-year-old man in a hospital in Florence who suddenly passed away in his bed without any sign or movement. Leonardo did an autopsy to ascertain the cause of what he describes as a "peaceful death". He referred to atherosclerosis as a failure of blood flow caused by a vessel thickening, which is not able to feed the heart. In 1852 Johnson reported a thickening of arterioles of the kidney [1] and less than 200 hundred years later the word atherosclerosis was coined by Marchand in 1904 [2]. However, many others before him had already spoken about this pathology. Jean Frederic Lobstein in the "*Traité d'anantomie pathologique"* in 1829-33 firstly used the term "arteriosclerosis" to describe calcified arterial lesions [3] and in 1903, Mönckenberg used the word "medial calcific sclerosis" [4]. Although atherosclerosis is thought of as a modern disease correlated with contemporary lifestyle, in 2013 Thompson *et al* studied 137 mummies from four parts of the world [5]. Ancient populations such as Egyptians, Peruvians, Puebloans and Unagans were imaged and traces of atherosclerosis was found in all of them. Furthermore, atherosclerosis affects not only human kind but even animals, either in captivity or in the wild and they can develop spontaneous atherosclerosis lesions [6]. In the past 20 years, many studies were carried out on this pathology and new knowledge has been acquired to better understand atherosclerosis [7], but the whole mechanism is still unclear. What we know is that atherosclerosis can lead to acute coronary syndromes (ACS) which is the acute manifestation of ischemic heart disease or heart attack and is the main cause of morbidity and mortality in the world [8].

1.2 Acute coronary syndromes

Atherosclerotic plaques are responsible for narrowing or blockage of the coronary arteries due to their development on the artery walls. The majority of plaques remain asymptomatic, in some cases they become obstructive (stable angina) and in other cases elicit acute thrombosis which may lead to an ACS. Approximately 66% of ACS occur overlying plaques with a physically disrupted fibrous cap (plaque rupture), while 31% occur overlying plaques with an intact fibrous cap, where the endothelial cells have detached, exposing the underlying matrix (endothelial erosion) [9]. Plaque rupture has received much attention during the years, and research has made considerable inroads into

understanding the pathophysiological mechanism of this process. Post mortem observations and recent advances in intravascular imaging, particularly optical coherence tomography (OCT)-based methods, have allowed ruptures to be distinguished from erosion in patients with ACS [10-13].

OCT-defined – acute coronary syndrome with an intact fibrous cap (ACS-IFC) - erosion is a diagnosis by exclusion of rupture or the presence of calcified nodules and is not without controversy [14]. However, OCT-defined ACS-IFC has a similar frequency to that defined by histological studies of erosion, supporting its relevance [15, 16]. Moreover, the largest study to date that has utilised OCT-diagnosis of plaque rupture or erosion in 822 STEMI patients [16], identified a propensity for plaque erosion in smokers and women <50yrs, compared to plaque rupture patients, this is consistent with post mortem observations [10, 14, 17]. Yet other traditional risk factors for acute coronary syndromes (for example, diabetes, hyperlipidaemia and hypertension) are segregated with plaque rupture, highlighting that the mechanisms of regional intimal endothelial detachment in patients differ from those of plaque rupture and require better definition.

A third cause of ACS which represents luminal thrombus in 2-5% of cases is a calcified nodule [18]. Calcified nodules seem to be observed in older patients and these have a higher rate in diabetes, whereas plaque rupture or erosion is observed more commonly in younger patients [11]. Jia *et al* reported the majority of calcified nodules (62%) were in the left anterior descending artery and 30% of them in the mid-right coronary artery. It was also described that compared to plaque rupture and erosion, calcified nodules were found in smaller vessels. Heavy calcification in these arteries commonly showed large plates of calcified matrix surrounded by areas of fibrosis, inflammation and neovascularization [19]. The precise mechanism of vascular calcification remains incompletely understood and further investigation is necessary.

1.3 Plaque-associated thrombus formation

The majority of ACS are related with plaque-associated thrombus formation, which can trigger malignant arrhythmogenesis, infarction and cardiomyopathy [20]. Despite the systemic exposure of the endothelium to high cholesterol, diabetes and other risk factors for the development of atherosclerosis, atherosclerotic plaques do not appear randomly within arteries, but develop at branch points (bifurcations) or curved sections of arteries

[21] where the endothelial layer is exposed to disturbed flow patterns. This suggests that the response of endothelial cells to disturbed (athero-prone) flow, alters cell behaviour in a way that renders the arterial wall sensitive to plaques. This is contrasted with sections of artery that experience normal laminar stress, these appear to resist atherosclerotic plaque development. Progression of atherosclerosis can lead to significant plaque burden accumulating in the artery wall over time and in order to understand this mechanism it is necessary to understand the dynamics that lead to plaque development

1.4 Endothelial Shear Stress

Endothelial shear stress is defined as "the tangential stress derived from the friction of the flowing blood on the endothelial surface of the arterial wall" [22]. It is calculated in Newton [N]/m2, Pascal [Pa] or dyne [dyn]/cm2. Endothelial shear stress is the product of the blood viscosity (μ) multiplied by the spatial gradient of blood velocity at the wall (Figure 1.1)

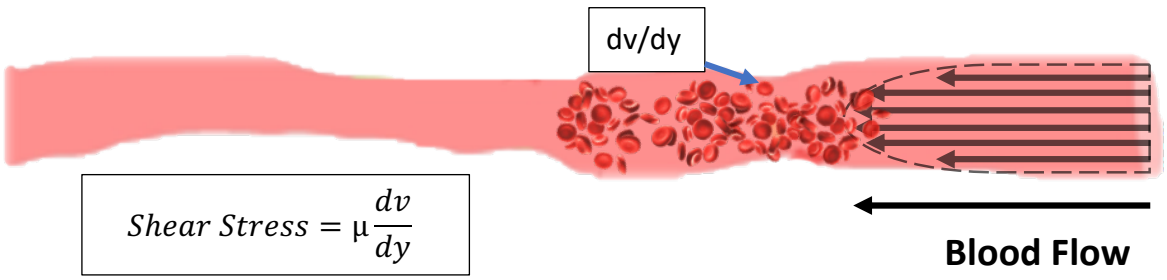

Figure 1.1). Schematic representation of endothelial shear stress. Shear stress is proportional to the product of the blood viscosity (μ) multiplied by the spatial gradient of blood velocity at the wall (dv/dy).

Inside the arterial wall, the nature of the flow is dependent on its velocity but also on the presence of geometric irregularity. Flow can be laminar or disturbed in accordance with the vessel geometry [23]. Laminar flow can be divided into undisturbed or disturbed, for the presence of areas where it reverses, but the velocity appears to be constant [24]. On the contrary, turbulent flow is characterized by changes in velocity at any point, even if the overall flow velocity is comparable to a steady flow. In order to determine the nature of flow, Reynolds number (Re) is used. For low Re values the flow is considered laminar, while for high values, above 2.000, is considered turbulent [25]. Inside the arterial wall another variable must be considered as well as the complex geometric configuration, this is the pulsatile nature of the arterial blood flow. In straight arterial area lamina shear stress (LSS), it is pulsatile, unidirectional and its magnitude varies between 10-20 dyn/cm2. In the area where the flow is disturbed, mostly in the arterial bifurcation segments, pulsatile flow

generates low flow and oscillatory shear stress (OSS). OSS peculiarity is its significant change in flow direction and its magnitude during systole and diastole which results in a very low velocity with a magnitude less than 10 dyn/cm2 [26, 27].

1.4.1 Vessel morphology and hemodynamics: atherosclerotic plaque formation and its progression

Laminar flow or LSS (10-20 dyn/cm2) developes in the straight area of the artery which has been demonstrated to be athero-protective and promotes endothelial cell (EC) survival and inhibits coagulation [28, 29]. In contrast, OSS or disturbed flow is observed in arterial bifurcations or curved sections of artery, with reduced time-averaged shear stress with endothelial exposure to multi-directional flow [30]. ECs in these regions develop a pro-inflammatory phenotype which is characterised by poor alignment and high turnover, higher levels of oxidative stress, greater response to inflammatory cytokines and a reduction in bioavailable nitric oxide (NO). Furthermore, evidence supports that disturbed flow increases endothelial permeability, and triggers an increase in secretion of inflammatory mediators and adhesion molecule expression which contribute to the development of atherosclerosis [31, 32]. Progression of atherosclerosis can lead to significant plaque burden accumulating in the artery wall over time.

Remodelling of the artery during plaque development affects the impact of disease on blood flow to the distal tissue. Expansive remodelling describes the expansion of the artery to accommodate the growing plaque, preventing the lumen diameter from being compromised. Conversely, restrictive remodelling results in a reduction of the lumen as the plaque grows. It may be possible for plaques to go through different phases of expansive and constrictive remodelling (Figure 1.2). The drivers for expansive or restrictive remodelling are not fully defined, but may include the haemodynamic environment, endothelial dysfunction, the degree of inflammation and lipid deposition, all modulating the cells of the artery wall (Figure 1.3).

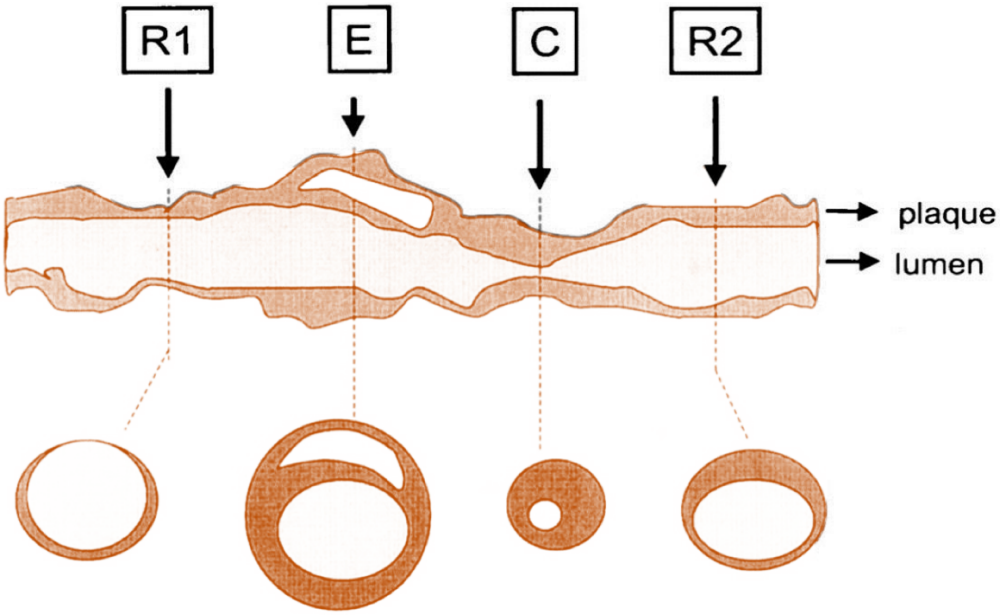

Figure 1.2). Schematic presentation of the different remodelling modes. The mode and extent of arterial remodelling is mostly based on a comparison with 1 or 2 reference sites. In post-mortem studies, often the vessel area in the section with the least amount of plaque (R1) is used as a reference. In intravascular ultrasound studies, the average vessel area of a proximal (R1) and distal site (R) with an angiographic normal lumen being used as a reference. Expansive remodelling (E) is then present when: (vessel area R1+R2)/2> vessel area culprit lesion. However, constrictive remodelling [C] is evident when: (vessel area R1+R2)/2< vessel area culprit lesion. Expansive remodelling is often associated with the presence of atheroma and inflammatory cells [20].

The behaviour of ECs, because of their mechanosensory nature, is finely regulated by shear stress. They respond to flow in a unique way, and the haemodynamic environment which they are exposed to affects EC shape, provokes cytoskeleton arrangement, regulates their metabolism, proliferation and their response to inflammatory stimuli [33]. Noteworthy, the monolayer of ECs on a protrusion plaque are exposed to different type of shear stress, in fact upstream in the proximal area the main shear is elevated (50-300 dyn/cm^2), whilst downstream in the distal area is disturbed or turbulent, as shown in Figure 1.3. It has been reported that the apoptotic response is regulated by a disturbed flow or OSS, rather than LSS or elevated shear stress (ESS). ECs located upstream of the plaque in the proximal area did not show any apoptotic mechanism activation pathway [34-37].

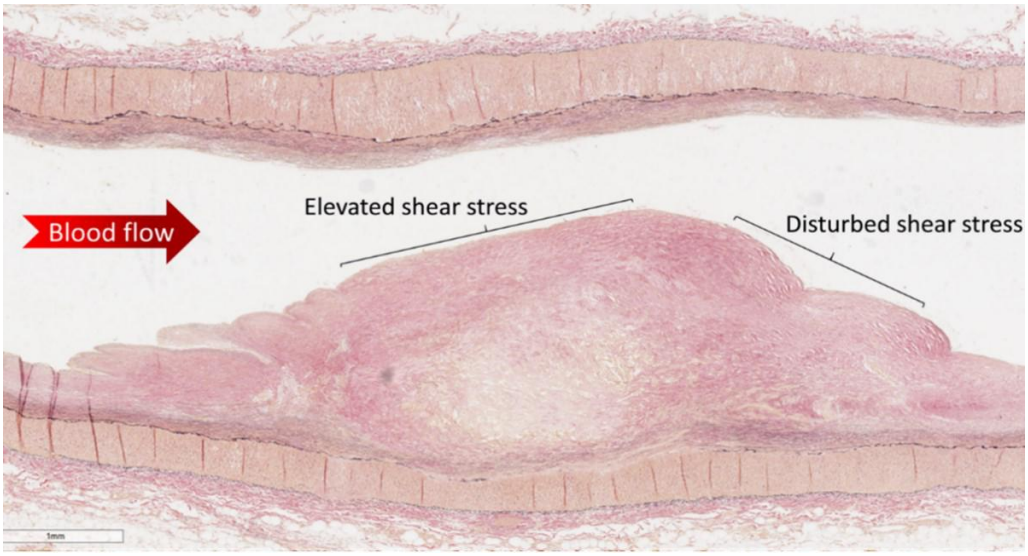

Figure 1.3). Plaques that protrude into the lumen of the artery expose the endothelial cells to very elevated shear stress. Shear stress related to the third power of the radius of the vessel, so an artery where the lumen is decreased by 50%, exposed endothelial cells to an 8-fold increase in shear stress. Advanced stenotic plaques can severely restrict the vessel lumen exposing the endothelium overlying the plaque to very elevated flow rates and consequentially shear stress (which relates to the third power of the radius). This can exceed 100 dynes/cm2 [21].

1.4.2 Ruptured plaque Vs Eroded Plaque

Plaques that rupture or erode are found to contain morphological and molecular differences (Figure 1.4), which suggests a distinct pathological process.

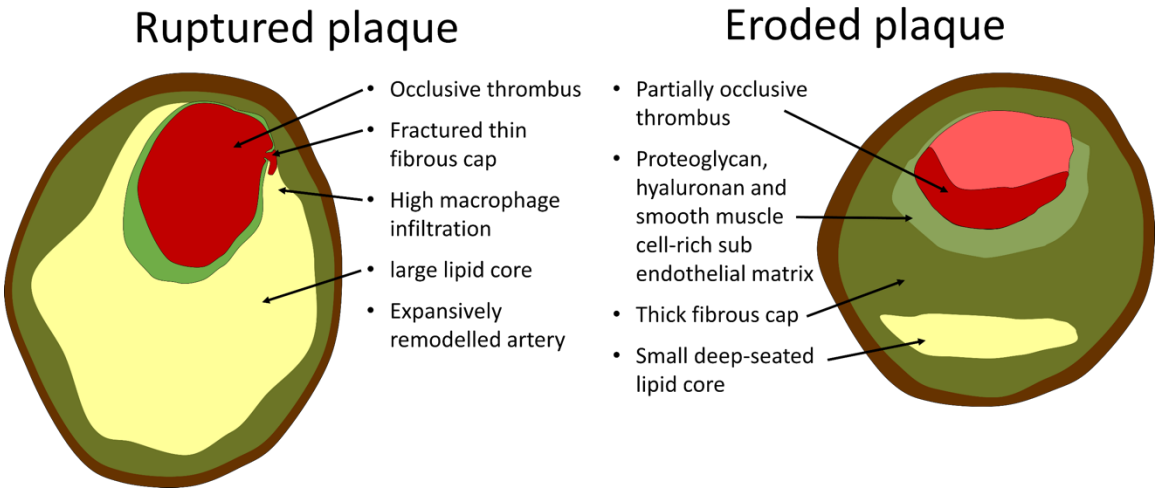

Figure 1.4). Representation of eroded and ruptured atherosclerotic plaques. Eroded plaques generally show thick fibrous caps with absent or deep-seated necrotic cores and the thrombi are less frequently occlusive. They contain an altered matrix below the erosion, with more versican and hyaluronic acid and greater numbers of smooth muscle cells (SMC). On the other hand, ruptured plaques have thin, fractured fibrous caps with a high proportion of underlying macrophages and a large lipid core [38].

Most plaque ruptures, also known as vulnerable plaque, occur in the up-stream section of the plaque. Typical plaque rupture has a large atheromatous core, filled by macrophage foam cells and debris accumulated due to their death. The fibroatheroma is exposed to the highest levels of shear stress and strain, this may contribute to cap rupture. In addition, an increase of proteolytic digestion of collagen by macrophages, and increased intra-plaque pressure from rupture of the vasa-vasorum [39] are suggested to play a significant role in plaque rupture. In coronary arteries, ruptured caps are less than 65 μm, and this morphological characteristic gave rise to the nomenclature of thin capped fibro-atheromas (TCFAs), where the lipid-rich necrotic core of the plaque is prone to rupture [40]. In the event of rupture of the vulnerable plaque, the thrombogenic material within the plaque gets exposed to the blood, promoting its coagulation. This process triggers the thrombus formation, provoking an ACS event.

Ruptured and eroded plaques are different in terms of cellular and extracellular matrix (ECM) composition. The ruptured plaque often shows internal elastic lamina expansion and are characterised by a high number of inflammatory cellular components such as macrophages and T-lymphocyte–derived mediator interferon-γ (IFN γ) [41]. Macrophages, once stimulated by inflammatory mediators, overexpress matrix metalloproteinase (MMP) and other proteases. T-lymphocytes inhibit vascular SMC production of interstitial collagen. Both cellular types provoke a significant reduction in the proteoglycan and versican ECM composition [10, 42, 43], but greater presence of calcification has been reported [44]. Noteworthy is the typical presence of systemic inflammation which promotes fibrin and plasminogen activator inhibitor (PAI-1) production. PAI-1 is considered the main inhibitor for fibrinolysis which further increases the thrombogenicity in the solid state of the plaque [44]. In this scenario, clinical studies have shown that low amounts of lipid would ameliorate the composition of the ruptured plaque [45, 46]. This finding was supported by animal and human studies through the use of intracoronary imaging and magnetic resonance imaging (MRI) where a decrease in lipids reduces the size of the lipid core, switching to more fibrous tissue atherosclerotic plaque [47, 48]. In a world where a better therapy is prevention, preventive therapies such as hypertension monitoring, low density lipid (LDL) lowering, and smoking cessation were not enough to avoid ACS events. Therefore, it is possible a less responsive pathway which is not controlled by the risk factors mentioned above is responsible, shifting attention from the rich-lipid-

core atherosclerotic plaque pathway to the fibrous tissue atherosclerotic plaque pathway [49, 50].

1.4.3 Eroded Plaques: clues in the literature

Eroded plaques do not present positive lamina remodelling, and in contrast to ruptured plaques, they are SMC and proteoglycan rich [10]. Furthermore, they are high in versican, glycosaminoglycan, hyaluronan but low in biglycan [42]. Most importantly, eroded plaques are more fibrotic with a thicker cap and little or absent necrotic core [10, 42], with a grade of culprit lesion stenosis slightly smaller for eroded compared to ruptured plaques (ruptured vs eroded: 52 vs 45 % of diameter stenosis) [10, 51-53]. Interesting observations have been reported by *Farb et al,* where the presence of the two different types of plaques are related with age. It was noticed that the age of the patients with erosion of overlying stenotic plaques were lower than the ones suffering with rupture plaques. This observation validates the fact that in coronary arteries the average stenosis size increases with age [10].

How endothelial erosion starts is not well understood, and the loss of ECs after analysis of post-mortem arterial sections don't prove that lack of endothelial monolayer precedes the thrombotic event. Although the temporal cascade of events is not clear, the loss of ECs exacerbates and amplifies the progression of the intact fibrous cap thrombus atheroma. Eroded plaques, differently to ruptured, present a more organised morphology which suggests a longer life-span. This has been assessed up to one week before the clinical symptoms appear [43, 54]. In fact, in the case of cap-rupture the high presence of thrombogenic material such as fibrin and PAI-1, other tissue factors and the presence of abundant neutrophils forming neutrophil extracellular nets promote the immediate occlusion of the arterial vessel [43, 53, 55].

In terms of the mechanism promoting erosion of overlying stenotic plaques, the monolayer of ECs is exposed for much longer compared to plaque rupture to two different shear stresses. It is possible to speculate that there are potentially two or more distinct mechanisms contributing to erosion of plaques; ESS in the proximal/upstream area and OSS in the distal/downstream area.

In this complicated scenario there are multiple hypotheses to be considered. A possible reason for desquamation of the EC monolayer can be due to a loss of the tethers between ECs and SMCs. Potentially it can be the leading cause of EC detachment and subsequent

cell death [56]. The EC membrane adheres through ligand/receptor complex of the integrin family, in particular β-1 integrins, laminin and collage type IV. A 72kDa collagenase type IV also known as gelatinase A or matrix metalloproteinase-2 (MMP2) but not MMPs 1,8, and 13, could participate in endothelial erosion [57, 58]. MMP14 can be induced by pro inflammatory cytokines, which further activates the form of pro-MMP2 and facilitates the EC adherent molecules complex. In the presence of OSS in the distal area of the plaque, the apoptotic mechanism seems to be dominant. According to Tedgui's group, ECs downstream of the stenosis showed markers of programmed cell death [59]. The percentage of apoptosis in the downstream area of stenosis was 6-fold higher than upstream (distal 18.8±3.3 vs 2.7±1.2 proximal, $P<0.001$) suggesting the potential role of OSS as an apoptotic mechanism activator.

1.4.4 Eroded Plaques: the role of OSS and apoptosis

We propose OSS and programmed cell death appears to orchestrate the erosion process, at least in the downstream stenosis. It is of note, that apoptotic marker expression has been detected in ECs specifically at the distal site of atherosclerotic plaques, but not at the proximal region.

The observation that disturbed flow promotes apoptosis [59] has led to the hypothesis that EC apoptosis not only promotes atherogenesis but also endothelial erosion. In support of this mechanism, it had been observed that the upregulation of Toll like receptor factor 2 (TLR2) is a crucial player in atherosclerosis development in mice [60, 61] and also promotes endothelial apoptosis [61]. Furthermore, it has been reported that using a TLR2 agonist exacerbates endothelial dysfunction by increasing E-selectin, Vascular cell adhesion molecule (V-CAM) 1, thus leading to the ultimate stage of apoptosis [62, 63]. In addition,neutrophils, which are considered the first line of defence, can entrap microorganisms through the creation of neutrophil extracellular traps (NETs) [64]. Neutrophil traps lead to the formation of a condensed structure of chromatin, histones and proteins to promote microbial death named as NETosis [65] and is described in more detail in section 1.5. Neutrophils have been found in the atherosclerotic plaque region [66] and might play a role in promotion of basement membrane degradation and weakening EC adherence through the secretion of MMP2 and MMP9. Co-culture of neutrophils and ECs also demonstrate an increase in the rates of endothelial apoptosis [67]. For all these reasons, erosion of plaques has been described as an apoptotic mechanism occurring on

endothelial cells through several signals, which leads to morphological changes at cytoplasmic and nuclear levels.

In the presence of cell death by nuclear fragmentation, proteins or lipid are structurally altered and become dysfunctional, intracellular faults occur, and the innate immune response is activated, which promotes phagocytic clearance of the cell bodies [68]. Therefore, it is plausible that when OSS leads to EC apoptosis, an innate response contributes to the apoptotic process. Elegant work in 2008 by *Mullik et al,* demonstrated an overexpression of innate TLR2 in ECs of atherosclerotic mice in the distal area of stenosis, exposed to OSS [69]. Together with this observation, the same study established that loss of TLR2 function reduces leukocyte accumulation in the atheroma. Furthermore, in the hyperlipidemic LDL receptor–deficient (LDLr -/-) murine model, the complete deletion of TLR2 in mice showed atheroprotective effects. Additional experiments on human coronary artery endothelial cells (HCAECs) showed higher expression of TLR2, but not Toll-like receptor 4 (TLR4), if exposed to OSS or static conditions compared to LSS [70]. The result led to the proposal that TLR2 expression is an early stage atherogenesis enhancer, stimulating superficial erosion through EC dysfunction and leukocyte accumulation [71, 72]. Further experiments by Libby's group strengthened the concept by providing evidence that stimulation of ECs co-cultured with polymorphonucleates (PMN) leads to superficial erosion [73] through the use of TLR2 agonists, which enhance a granulocyte chemoattractant IL-8 expression, as well as E-selectin, ICAM-1 and VCAM-1 [66]. Much stronger induction of these mediators was enhanced by the use of the proinflammatory stimulus, tumour necrosis factor alpha (TNFα). In addition, it has been established that in long-term heavy smokers there is an elevation in circulating markers of inflammation (TNFα included), which could potentially play a part in atherosclerotic plaque development [38, 74], exacerbating EC dysfunction. This observation points out the fact that TLR2 only slightly triggers an innate immune activation response, on the other hand, an immune response is proinflammatory stimulus concentration dependent. Although TLR2 seems less efficient than TNFα, exposure of ECs to lipoteichoic acid (a TLR2 ligand) reduces vascular endothelial cadherin (VE-cadherin/CD144) by 50%, promoting EC monolayer detachment and the expression of leukocyte adhesion molecules. In the event of EC desquamation, neighbouring cells rapidly migrate to recover the gap and ensure intimal integrity, but when ECs are exposed to TLR2 agonists, migration and subsequent

repair is reduced [66]. However, a key question remaining to be answered is what activates TLR2 in order to trigger the cascade of events downstream? As mentioned in the previous section, eroded plaques are rich in proteoglycans. Kolodgie *et al* observed that during the process of eroded plaques, there was accumulation of both proteoglycans and hyaluronan [42, 75]. It was speculated that portions of them act as "endogenous danger signals" and assemble a ligand/receptor TLR2 complex [76, 77], contributing to EC dysfunction and monolayer erosion. In order to prove this hypothesis, ECs were cultured on a hyaluronan matrix. Elevation of E-selectin, VCAM-1 and IL-8 was observed, as well as the activation of caspase-3, which is a crucial enzyme involved in apoptosis [59, 78]. Other molecules such as ox-LDL, fatty acids and peptidoglycans, derived from bacteria or pathogens, can engage with TLR2 contributing to EC detachment [79-81].

The process of endothelial erosion in ECs exposed to OSS on the distal area of stenosis, appears to occur in two distinct stages. The first stage starts with the TLR2+ligand which promotes a low level of innate response initiating the EC detachment process. During the second stage, PMN chemoattractant molecules recruit granulocytes, potentially activating the arterial intimal surface by triggering proteinases and generating reactive oxygen species (ROS), in a process described as neutrophil extracellular trap, known as NETs or NETosis [82].

1.5 NETosis

Neutrophils in the innate immune response process are the most copious cell type, they are broadly armed with antipathogens stored in granules and uncontrolled stimulation can damage the host tissue. Based on the stimuli received, membrane receptors trigger either a survival or suicidal pathway [82-86]. In the first case, nuclear DNA is released into vesicles in the extracellular space without compromising membrane integrity, typically in response to platelets or Gram+ bacteria respectively via TLR4 or TLR2 [87] and it is a ROS-independent mechanism. The second type, NETosis is triggered by phorbol 12-myristate 13-acetate (PMA), IL-8, INF-α and γ [82, 88] via NADP-oxidase activation in a ROS dose-dependent manner [87, 89]. Despite which pathway is activated, the molecular components are analogous and are mostly constituted of proteolytic enzymes such as neutrophil elastase (NE), cathepsins, proteinase 3 (PRTN3), myeloperoxidase (MPO) and gelatinase, along with the presence of histones [90, 91]. Most of the neutrophil DNA is

transcriptionally inactive and gets condensed into heterochromatin by the regulation of peptidyl arginine deiminase 4 (PAD4) and by reducing the histones positive charge and weakening histone-DNA binding [91], which is absolutely crucial to activate NET release in the event of an insult [92, 93].

1.5.1 NETs involvement in the scenario of erosion of overlying stenotic plaques

NETs have been observed during the inflammation processes or infection [94] and atherosclerosis is characterised by a chronic inflammatory process in the vascular wall due to endothelial dysfunction and SMC proliferation [95]. Therefore it is a fair assumption that there is an involvement of NETs in this process. In the circumstance of eroded plaque, proteoglycans and hyaluronan are the main component of the fibrotic core, and additionally OSS triggers an EC apoptotic response. In this scenario, where there are a large number of hyaluronan and cellular fragments, several of these potentially engage with TLR2 and stimulate an innate immune response. Once EC desquamation is initiated, platelets and neutrophils have access to subendothelial structures. Herein, platelets activated by contact with collagen can adhere to it through glycoprotein VI, furthermore they can bridge fibrin binding, trigger granulocytes NETosis [9], and develop platelet-rich thrombus attached to DNA strands derived from neutrophil extracellular traps. The abundant presence of NETs has been observed on human atherosclerotic eroded plaques but with a morphology correlated with plaque rupture [66] in the presence of OSS. This is intriguing because ECs are exposed to the same OSS only in the distal area and not all along the plaque. It is at the distal end where the most abundant presence of NETs has been reported [9], therefore a potential mechanism driven by other players might happen in the proximal area of the eroded plaque exposed to ESS.

1.6 Elevated shear stress and High-Risk Plaque: An Emerging Concept

Recently, ESS has been considered as a possible cause of development for atherosclerotic plaques. As well as OSS, ESS induces specific changes in EC morphology and behaviour. A recent study reported that in 77.8% of cases thrombi is localised in the zone of high endothelial shear stress, suggesting that ESS and plaque geometry are responsible for EC detachment [96]. Atherosclerotic plaques with a stenosis of 40% expose ECs to a 5-fold higher shear stress, and a 75% stenosis showed a 64-fold higher flow, interestingly blood flow seems not to be affected until the stenosis overcomes 75% [97]. As mentioned before,

LSS is around 10-12 dyn/cm^2 but every change in the morphology of the artery wall exposes ECs to abnormal shear stress. In 2006 Moraweitz's group applied an *in vitro* shear stress of 50 dyn/cm^2 which reported production of ROS, NADPH oxidase 2 (NOX2) expression and nicotinamide adenine dinucleotide phosphate (NAPDH) oxidase [98]. The Kruppel-like factor (KLF) family KLF2,4 and 6 were reported to regulate EC phenotype in response to shear [99], in particular KLF4 was established to activate atheroprotective gene expression programs in combination with KLF2 [100] and nuclear response erythroid 2-like 2 (NRF2) [101]. Interestingly in human umbilical vein endothelial cells (HUVECs), both genes KLF2 and KLF4 showed a ~10-fold increment between OSS and ESS [102]. The role of NRF2 was determined by its inhibition through small interfering RNA (siRNA) which showed the pivotal role of NRF2 in cellular defence mechanisms against the toxicity of electrophiles and ROS [101].

Despite increasing evidence, there are very few data linking ESS to clinical events, primarily due to the fact that the interplay between atherosclerosis, risk profiles, endothelial dysfunction, eroded plaque and ESS is driven by an unclear NRF2 mechanism and is highly dynamic and not easy to understand.

1.7 Previous work leading up to this project

Previous work carried out by Dr Stephen White and others showed that EC behaviour is deeply affected by both cyclic strain and shear stress because of their mechanosensitive nature. It has been extensively reviewed that OSS promotes the development of an inflammatory EC phenotype, which is proatherogenic [34, 103, 104]. ECs exposed to LSS on the contrary resist inflammation, promote EC quiescence and it appears to be atheroprotective [105-107]. ECs overlying stenotic plaques, during advanced atherosclerosis, are exposed to ESS exceeding 300 dynes/cm2 [108-110], however the response of ECs on exposure to ESS is not very well studied. Dr Stephen White and collaborators investigated the permissive flow dynamic environment for the development of erosion using OCT scan analysis where a high definition image of the lumen profile underneath the adherent thrombus was imposed on bi-plane angiography data in order to reconstruct the coronary artery geometry (Figure 1.5).

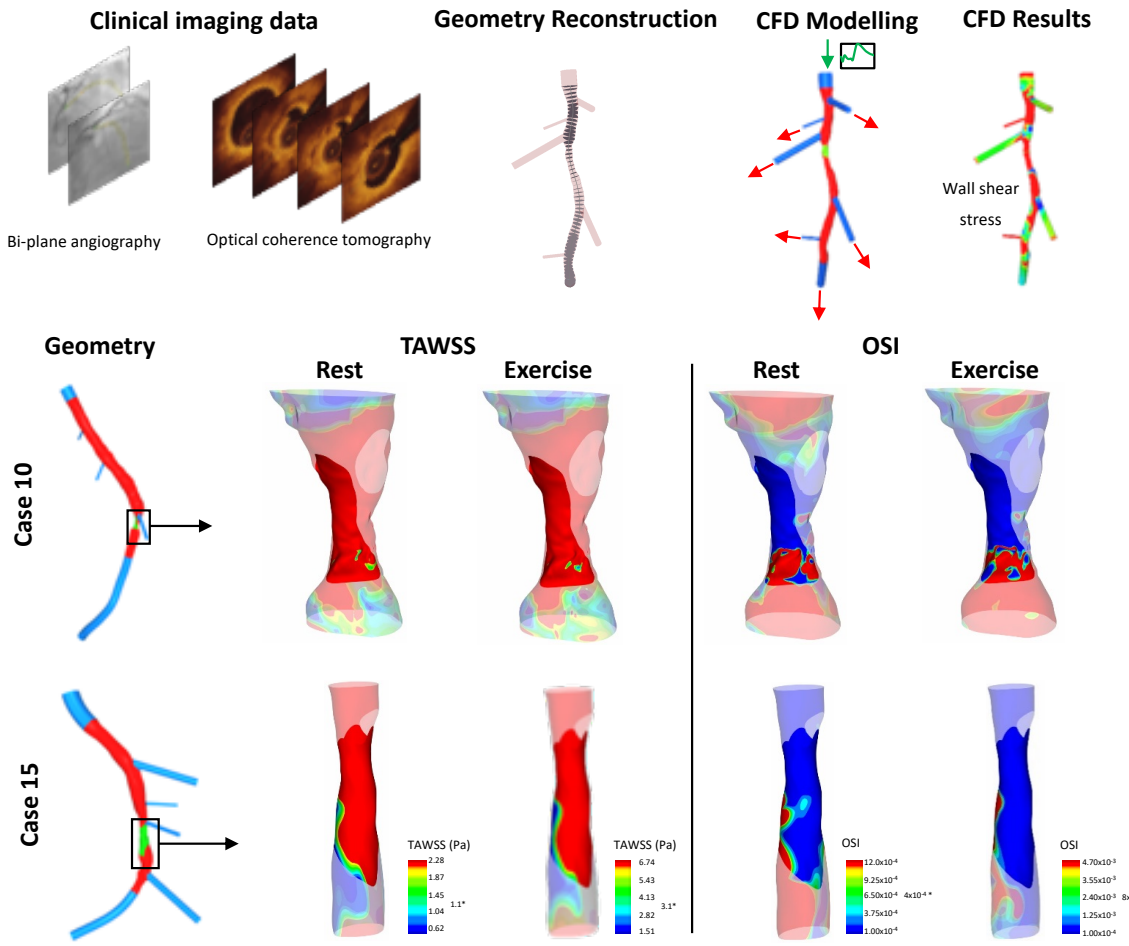

Figure 1.5). Coronary artery geometry reconstruction of the permissive flow environment of erosion. For the high accuracy reconstruction in the red section hybrid OCT/bi-plane angiography was used. For the reconstruction of the blue section bi-plane angiography analysis was used alone. Adherent thrombus is shown in green. OCT was used in order to measure the side-branch diameter. Pulsatile flow conditions were simulated for four cardiac cycles. Depending on the location of the culprit lesion, separate waveforms were used for the right, left/left anterior descending and circumflex arteries. Flow results were post-processed to quantify additional wall shear-based haemodynamic metrics of interest. Thrombus were shown in the opaque portion of the metrics, conversely the lumen area is shown in the semi-transparent portion. The metrics represented were time-averaged wall shear stress (TAWSS) and oscillatory shear index (OSI). In the legend the minimum and maximum values were referred to the lower and upper quartiles of the respective metrics.

During this study 17 cases were analysed, among them 14 culprit plaques revealed a 60% area of stenosis in agreement with histological data shown by Virmani's lab [10, 51, 111, 112]. Both resting and stress conditions were simulated using artery-specific waveforms by computational fluid dynamic (CFD), and it was confirmed that ESS was the predominant flow characteristic on the adherent thrombi sites. TAWSS was increased by ~6.5-fold in the area of plaque stenosis. No increase in oscillatory shear index (OSI) was observed in nine of fourteen of the adherent thrombi's sites.

A modest increase of oscillatory shear index (OSI) was observed only in five cases (Figure 1.6). The last three of the seventeen cases showed little or no stenosis and low changes in TAWSS values, but significant elevation in OSI. These data suggest that erosion of the overlying stenotic plaque is led by two different flow dynamic environments which promotes two distinct mechanisms [113].

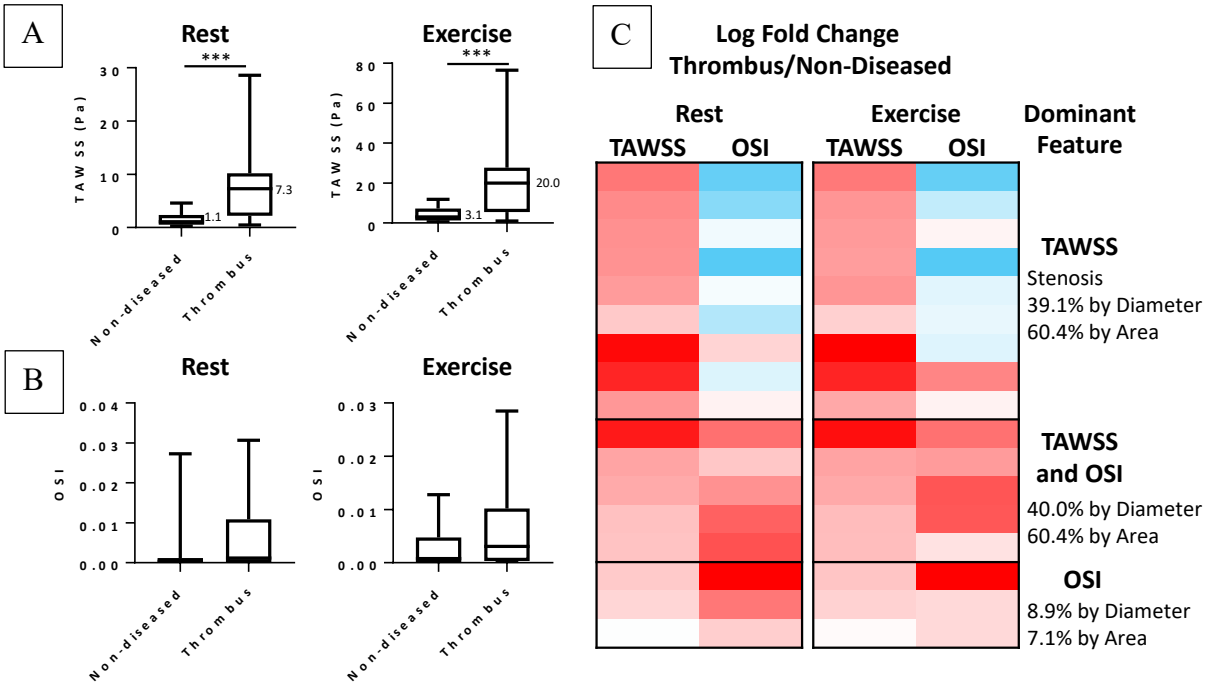

Figure 1.6). 17 cases of erosion of atherosclerotic plaques were examined. A) Simulation of the pulsatile flow dynamic environment at 'rest' and 'exercise' for 4 cardiac cycles were analysed. TAWSS in the area and under adherent thrombus was calculated by CFD. (Wilcoxon signed rank test was used between the two sections: Thrombus Vs non-diseased sections, *** $p<0.001$. B) No statistically significant difference was observed. C) Heatmap displays the log2 fold change between the two areas: non-diseased and thrombus-covered sections. Red colour indicates an increase and blue a decrease.

These data show that endothelial erosion is predominantly occurring in the area exposed to ESS and further work carried out in HCAECs exposed to cigarette smoke extract (CSE) and TNFα showed different EC responses to flow. HCAECs exposed to LSS for 72hrs failed to tackle the TNFα inflammatory effect, but conversely CSE activated the anti-oxidant response pathway, reducing inflammation in ECs [114].

Interestingly, the anti-inflammatory effect was observed under the combination of ESS, CSE and TNFα through the enhancement of expression of NRF2-regulated genes. In particular, the anti-inflammatory effects of CSE could therefore be mediated by an NRF2-

dependent process by the activation of activating transcription factor 3 (ATF3), which has been shown to be regulated by NRF2 [115] and this correlation was further confirmed by NRF2 adenoviral overexpression [116]. However, the ATF3 anti-inflammatory effect does not directly suppress nuclear factor kappa-light-chain-enhancer of activated B cells (NFκB) activity but promotes a negative-feedback loop which suppresses inflammation. In addition, ESS in combination with CSE and TNFα, significantly enhanced the transcription level of Heme Oxygenase (HMOX) 1, Glutamate-Cysteine Ligase Modifier Subunit (GCLM), NAD(P)H Quinone Dehydrogenase 1 (NQO1), Sulfiredoxin 1 (SRXN1) and Oxidative Stress Induced Growth INhibitor 1 (OSGIN1) [116].

NRF2 chronic activation, driven by ESS+TNFα+CSE, promoted cell detachment (Figure 1.7A) in the flow model apparatus (Figure 1.7B) and adenoviral overexpression of NRF2 led to antiproliferative effect on HCAECs (Figure 1.7C), suggesting that hyperactivation of the NRF2 antioxidant system is detrimental for EC homeostasis [113].

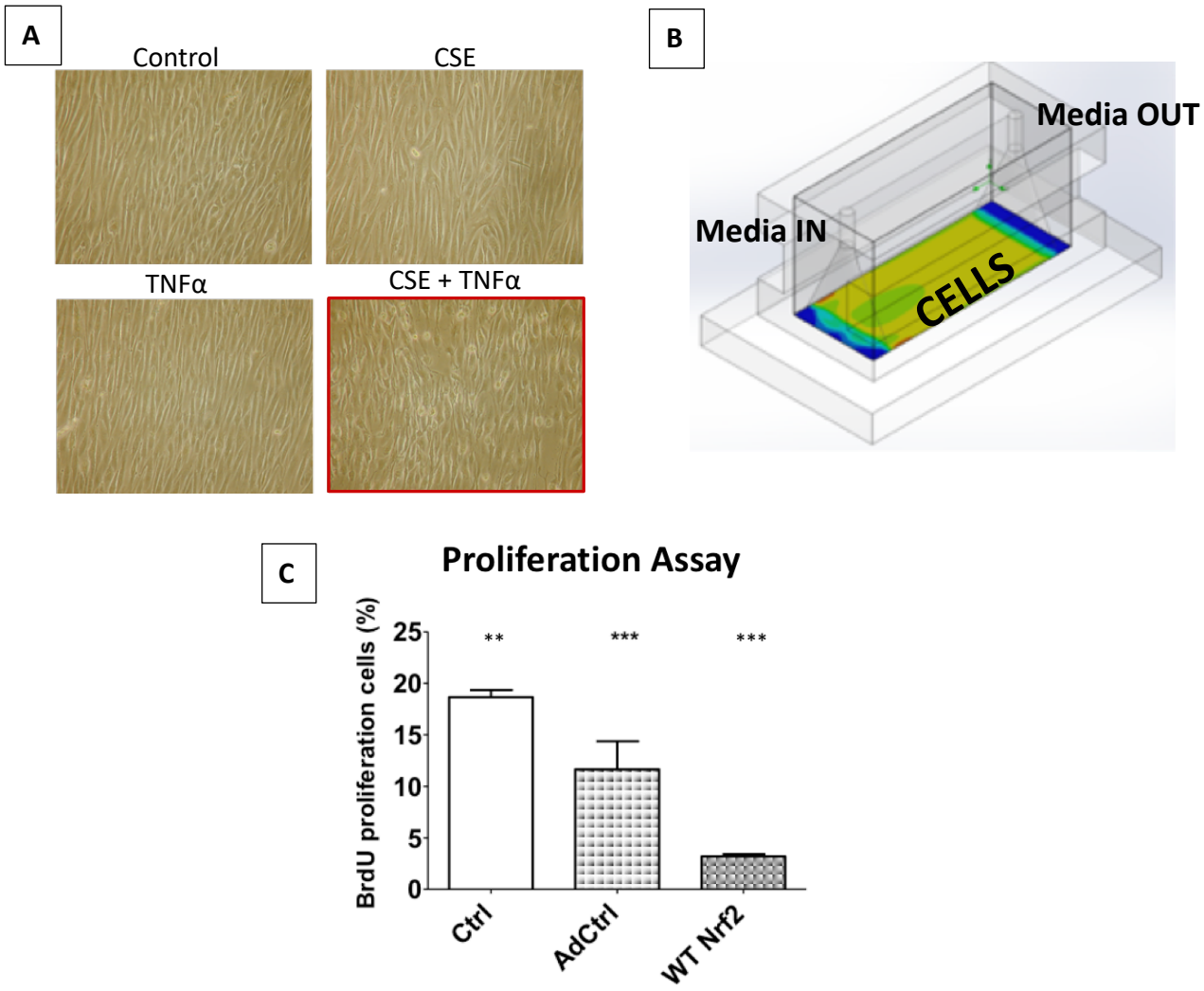

Figure 1.7). A) Schematic representation of the flow system chamber. HCAECs seeded on a glass slide and exposed to flow. The slide was placed in the chamber and flow passed through the inlet to the outlet. **B)** $2.5x10^5$ cells were seeded onto a gelatine covered (0.1%) glass slide and left to settle for 24 hrs. Subsequently ECs were exposed to ESS for 72 hrs. CSE, TNFα and combination of both were added into the media. Combination of ESS + CSE + TNFα showed around 30% of cell detachment. **C)** Wild-type NRF2 was overexpressed using adenoviral vector. BrdU proliferation assay was carried out on HCAECs and percentage of BrdU positive cell was calculated from 6 different donors (mean ± SD One-way ANOVA Bonferroni *P<0.05 and **P<0.01, compared with AdCtrl).

All these data together highlighted that hyperactivation of the NRF2 signaling pathway might be responsible for endothelial detachment in atherosclerotic plaques when ECs are exposed to ESS in combination with the presence of ROS insults (e.g. smoking). Although previous work showed that EC detachment under ESS is promoted by NRF2

hyperactivation, further study on NRF2 and NRF2-regulated genes is vital in order to shed light on the molecular mechanism leading to erosion of stenotic plaques and to identify the principal responsible for EC detachment and will be the focus of this PhD programme of work.

1.8 NRF2

There are multiple defensive strategies to prevent free radical toxicity, which are dynamically regulated to protect from oxidative insults and preserve cell function [117]. Excessive production of ROS and dysregulation of the antioxidant defence system in the endothelium provokes cellular damage and dysfunction. NRF2 has been identified as a major regulator of the oxidant/antioxidant balance. The NRF2/ARE signalling was first discovered in 1966 by Moi *et. al.* during studies based on B-globin [118]. Its role was identified the following year where it was discovered to be deeply involved in the mechanism related to the expression of oxidant and antioxidant enzymes [119]. NRF2-regulated gene expression is primarily controlled by Kelch-like erythroid cell-derived protein with CNC homology-associated protein 1 (Keap1), which leads to constant NRF2 degradation. In the event of oxidative insults, NRF2 disengages from Keap1 and translocates into the nucleus and is capable of binding to a DNA sequence known as antioxidant response element (ARE) [120]. NRF2/ARE signalling is highly conserved and regulated in all species and controls a wide panel of genes, among these are glutamate cysteine ligase (GCL), which contributes in the glutathione "synthesis", and NQO-1, HMOX1 which reduces the level of ROS involved in cell damage [121].

1.8.1 NRF2 and Keap1 structures

NRF2 belongs to the Cap'n'collar family of transcription factors (TF), and contains a region leucine zipper (CNC– bZIP) structure characterised by a sequence of 605 amino acids, divided into Neh1 to Neh7 domains [122]. CNC-bZip is localised into Neh1 and contains a motif responsible for heterodimerization with MAF proteins and DNA binding [123]. KEAP1 recruits Neh2 through binding to ETGE and DLG motifs, which cyclically associates and dissociates from the Kelch-domain in an opened and closed form. Normally KEAP1 retains NRF2 in the cytoplasm, ubiquitylated and degraded by the proteasome [118, 124]. The carboxy-terminal Neh3 domain of NRF2 is required for transcriptional activation through binding with chromo-ATPase/helicase DNA-binding protein 6 (CHD6) [125]. Neh4 and

Neh5 are N-terminal domains with distinct transactivation properties and, in tandem, promote NRF2 interaction with nuclear co-factor RAC3/AIB1/SRC-3 and cAMP-response-element-binding protein (CBP) [122, 126], which augments NRF2/ARE activation by acetylation of NRF2 [127]. Additionally, a redox-sensitive nuclear exporting signal (NES)-like motif has been identified in the NRF2-Neh5 transactivation domain which further regulates NRF2 cellular localisation [128]. NRF2 regulation is further negatively controlled by two motifs (DSGIS and DSAPGS) in the serine-rich Neh6 domain. Phosphorylation of the serine residues by glycogen synthase kinase 3 (GSK-3) allows the interaction with the β-transducin repeat-containing protein (β-TrCP), engaging with the receptor for Skp1–Cul1–Rbx1/Roc1 ubiquitin ligase complex and promoting NRF2 degradation through KEAP1-independent mechanism [129]. The final Neh7 domain is responsible for NRF2/ARE signalling inhibition via interaction with retinoids X receptor α (RXRα) [130]. Keap1 is a 69 kDa protein, it is part of BTB-Kelch family that assembles with the cullin 3 (CUL3) which contains E3 ubiquitin ligase (E3) protein to form a Cullin–RING E3 ligase or NRF2 inhibitor (iNRF2) complex for the degradation of NRF2 [131, 132]. It is a highly redox-sensitive member, containing 27 cysteine residues and is characterised by five domains. The N-terminal region, a BTB dimerization domain (Broad-Complex, Tramtrack, and Bric a' brac), which includes Cys151 residue [133], a cysteine-rich intervening region (IVR) domain with two cysteine domain residues Cys273 and Cys288 which are stress sensors [134]. A Kelch double glycine repeat (DGR) motif containing 6 Kelch repeats and a C-terminal region, which acts as an NRF2 repressor, specifically binds to the Neh2 domain on NRF2 [135].The Cys273, 288, and 297 are highly sensitive to oxidation and are localised in the IVR domain [136, 137].

1.8.2 Regulation of NRF2 activity

In normal homeostatic conditions, NRF2 always engages with Keap1 in the cytoplasm and constantly degrades, therefore is barely detectable. Oxidative insults can free NRF2 which translocates into the nucleus and heterodimerises with MAF proteins [138], c-Jun/Fos with the Fos related antigen-1 (Fra-1) and activating transcription factor-4 (ATF4), triggering NRF2/ARE complexes.

The core sequence TGANNNNGC is crucial for the NRF2/ARE complex [139], and evidence suggests that some of the flanking nucleotides are essential as well as the NNN sequence, which appear to be critical for ARE function, although this is still not completely

understood [140]. Proteins such as p21, involved in inhibition of cell cycle, and p62 are considered the main autophagy markers and the WTX tumour suppressor can interfere with the NRF2/KEAP1 complex promoting its disruption. In particular, p62 sequesters Keap1 inside the autophagosome, whilst p21 binds NRF2 on its DLG motif which stops Keap1 from binding NRF2 and therefore impairs its ubiquitination [141, 142].

Aside from its regulatory role in the NRF2–ARE pathway, KEAP1 has been found to interact and negatively regulate inhibitor of nuclear factor kappa-B kinase subunit beta (IKKβ). IKKβ is targeted for degradation through autophagy in the absence of HSP90 (heat shock protein 90), which is a chaperone protein assisting in protein folding. Keap1 is thought to prevent HSP90 binding to IKKβ, which triggers its autophagic degradation. Additionally, KEAP1 decreases the phosphorylation of IKKβ possibly by concealing the residues to which phosphate groups are otherwise attached. Overall, the outcome of the KEAP1–IKKβ interaction is the negative regulation of NF-κB through stabilization of IKBα [143].

Keap1 is thought to deplete NRF2 from the cytoplasm, however the F-box protein β-TrCP, a component of the Skp1–Cullin1–β-TrCP E3 ligase complex, controls nuclear NRF2 levels [144, 145]. The mechanism of degradation via β-TrCP differs considerably from the KEAP1 mode of action, as it only recognizes and binds to phosphorylated substrates. The kinase that phosphorylates and marks NRF2 for β-TrCP binding is GSK3β. Interestingly, p65 is also a substrate for GSK3β phosphorylation, which is thought to modulate p65 DNA binding affinity, but can have both positive and negative effects on NFκB depending on the cellular context [129, 146].

Several factors may promote Keap1 dissociation from CUL-E3 ligase complex, including oxidized phospholipids [147], NO, zinc, alkelans [148], cigarette smoke (CSE), as well as fresh aqueous CSE [116, 149, 150], nonetheless not all forms of ROS seem to weaken the Keap1/NRF2 complex depending on cell type and context-specific factors. Of particular interest in atherosclerosis, TNFα promotes the activation of NRF2 in both ECs [116] and monocytes [151], and LSS promotes NRF2 nuclear translocation through a KLF2-dependent mechanism [152], as well as via lipid peroxide and COX2-derived 15-deoxy-12,14-prostaglandin J2 (15d-PGJ2) intermediates, amplified by phosphoinositol 3-kinase/Akt signalling, and unexpectedly through endothelial nitric oxide synthase (eNOS) independent activity [101, 153-155]. Finally, naturally occurring compounds have been reported to disrupt NRF2/KEAP1 complex, such as isoliquiritigenin [145] sulforaphane [156], sulfuretin

[157] and 2-trifluoromethyl-2-methoxychalone [143] which suggests a potential diet involvement in terms of modulation of ARE-dependent gene expression in atherosclerosis and other inflammatory diseases.

1.8.3 NRF2 Additional regulatory systems

NRF2 sequestration and degradation by Keap1 is not the exclusive form of regulation, other forms of NRF2 gene regulation exist. NRF2 ubiquitination and further degradation by the proteasome are induced by the β-TrCP–Skp1–Cul1–Rbx1 E3 ubiquitin ligase complex [129, 146] through phosphorylation of the Neh2 domain and profoundly differs from the KEAP1 mode of action. GSK3β is the kinase that phosphorylates and allows NRF2/β-TrCP binding. Intriguingly, NFκB is itself a substrate for GSK3β phosphorylation [158, 159] and is currently proposed to have a dual role in the regulation of NRF2 activity [160]. It has been reported in pharmacological and genetic studies that there is an active cross-talk between NRF2 and NFκB, where nuclear translocation of NRF2 inhibits the interaction between p65, a protein involved in NFκB heterodimer formation, and p300 [161]. NRF2 regulated gene HMOX1 seems to have the main role on NRF2-mediated NFκB inhibition. High level of HMOX1 in ECs leads to suppression of NFκB-mediated transcription of VCAM-1 and adhesion molecules such as E-Selectin [162]. NFκB transcriptional activation is controlled by p38 [163] and NRF2 nuclear translocation is strongly decreased following p38 mitogen-activated protein kinase (MAPK) inhibition [164], supporting mutual regulation between NRF2 and NFκB signalling pathways. Although, the majority of KEAP1 binds to NRF2 in the cytoplasm, a KEAP1 binding site with [165] prothymosin-alpha (ProTα) has been observed [166] as a potential role for Keap1 to engage with NRF2 and trigger its degradation. Inside the nucleus NRF2 has to compete with B-zip proteins BACH1 which form dimers with MAF proteins through their BTB domain, preventing the NRF2/ARE complex [167-169]. In the event of BACH1 phosphorylation on its residue Y486, the BACH1/ARE complex is disengaged, provoking BACH1 nuclear export and triggering NRF2-dependent gene expression [170]. Although the actual phosphorylation sites in NRF2 or KEAP1 are mainly unknown, it is certain that the PKC phosphorylation occurs on the Serine-40 (S40) residue of NRF2 to facilitate its NRF2/KEAP1 dissociation and NRF2 nuclear translocation (Figure 1.8) [171].

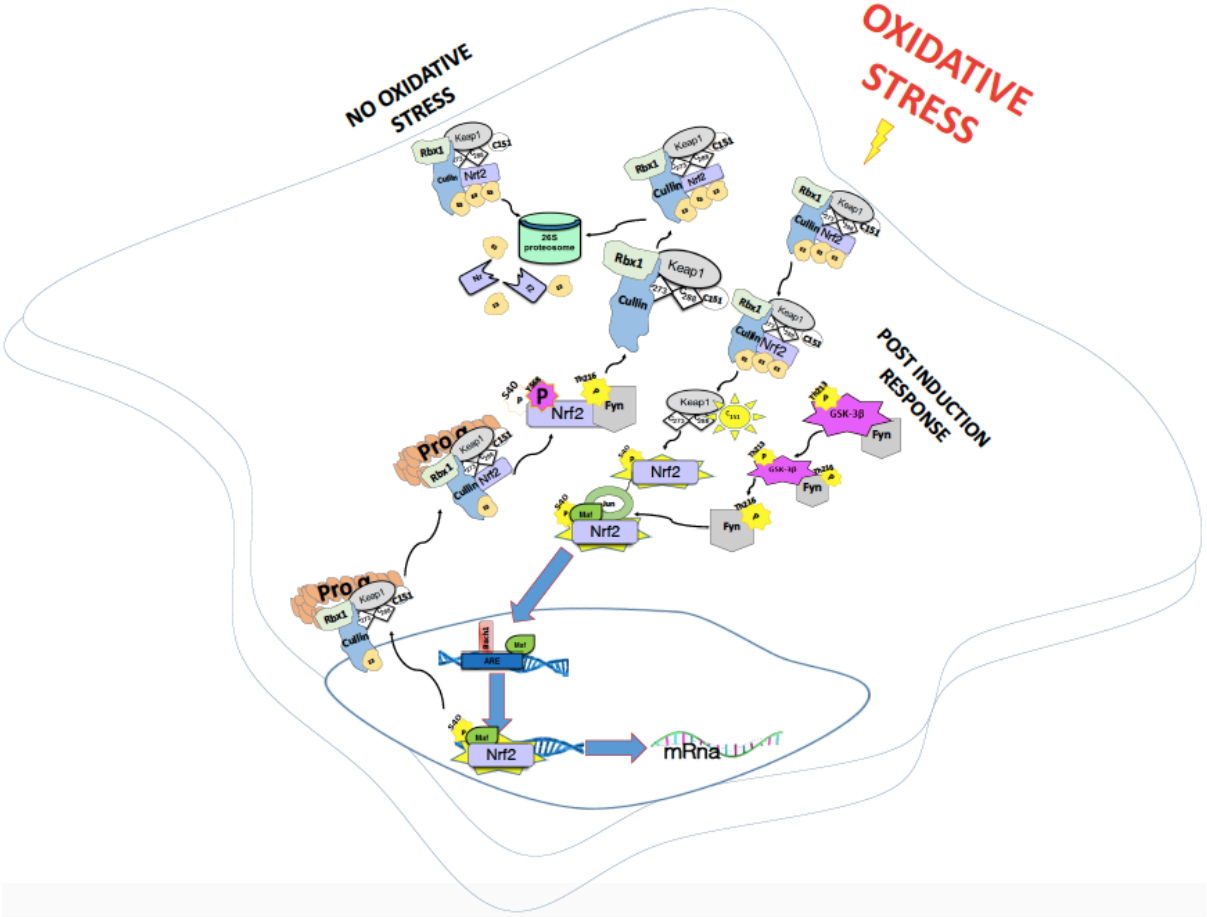

Figure 1.8). Schematic representation of the intricate NRF2 regulation mechanism in homeostatic conditions and in response of oxidative stress. In homeostatic conditions NRF2/Keap1 inhibitor complex constantly degrades NRF2 by presenting it to the 26 proteasome. In the presence of oxidative stress, phosphorylation of the cysteine 151 on Keap1 weakens the bind NRF2/Keap1 allowing NRF2 nuclear translocation. Phosphorylation of the sub-unit S40 enhance NRF2/ARE complex in a competitive way against BACH1 (NRF2 antagonist). NRF2/ARE is now ready to proceed to activate NRF2 regulated genes.

1.8.4 The role of NRF2 in endothelial dysfunction

ROS insults and PI3K-Akt signalling triggered by LSS, induce the activation of NRF2 [155]. In human aortic endothelial cells (HAECs), activation of NRF2 regulates overexpression of GSH, Glutathione peroxidases (GPx) and HMOX1, [172] and adenoviral NRF2 overexpression with its anti-inflammatory properties, down-regulates the expression of interleukin 1 beta (IL-1β), monocyte chemoattractant protein-1 (MCP-1), TNFα and VCAM1 [173]. In addition, up-regulation of NRF2/ARE/HO-1 signalling protects human ECs against TNFα activation [174].

In the event of disturbed flow by stenosis and/or ESS, Nitric Oxide bioavailability diminished, whilst oxygen radicals (O_2°) increased, the NRF2 protective role is compromised and the EC monolayer becomes prone to atherogenesis [175]. A study carried out in Alexander's group demonstrated that free fatty acid (FFA)-induced damage to HUVECs produced excessive ROS production at the expense of reduced gene and protein expression of HO-1, NRF2 and NQO-1 in ECs [176]. The NRF2 protective mechanism might be due to the NRF2/KEAP1 complex which binds mitochondrial outer membrane by phosphoglycerate mutases (PGAM)-5 and directly senses mitochondrial ROS production [177]. NRF2 endothelium protection against ROS may also be regulated by the catalytic subunit of glutamate—cysteine ligase catalytic subunit (GCLC) which reduces glutathione (GSH) biosynthesis [178]. In HUVECs and HCAECs, in the presence of ROS, it has been reported there is an increase of NRF2 nuclear translocation and transcriptional activity [179], highlighting a role for NRF2 in protecting against endothelial dysfunction.

Interestingly, it has been demonstrated that NRF2 has the ability to control its abundance inside cells, inducing NRF2 inhibitor complex gene expression for self-degradation [180] which might suggest that either hypo- or hyper-activation of NRF2 may be detrimental to the cell. According with this hypothesis, several studies in mice have shown that the NRF2 chronic activation [181], by knockout of Keap1, provokes postnatal lethality, whereas NRF2 knockouts are viable even though they are hyper-susceptible to oxidative stressors. Furthermore, NRF2 double knock out (NRF2-/-) mice overall showed protective effects against atherosclerosis lesion formation [182].

These findings suggest that there is a delicate balance of NRF2 expression that needs to be maintained in order to preserve normal EC physiology, which is challenging the belief that the role of NRF2 is always protective.

As mentioned in section 1.5 smoking is an undiscussed risk profile contributing to the development of eroded plaques, and high levels of TNFα have been reported in heavy smokers, in addition to the proximal/upstream area of the stenotic plaques causing exposure of cells to ESS.

In vitro studies on HUVECs and HCAECs have been carried out by White's group to better understand the processes involved in endothelial erosion, which overcome the lack of a spontaneous experimental animal model. Initial studies on HUVECs examined the EC response comparing OSS, LSS and ESS. In particular, the response of ESS exposure by ECs

appears to be similar to amplify the atheroprotective effect of LSS. Upregulation of metallothioneins, HSP70 family and KLF2/KLF4 axis was reported, with the reduction of ERK1/2 and IL-6 signalling. A comparison of transcriptional analysis between ESS and LSS showed NRF2 placed in the top seven enriched sites in the upregulated gene list [102]. Following this result, further studies have demonstrated that hyperactivation of NRF2 through pharmacological activators by using sulforaphane or isoliquiritigenin were added to the culture system with CSE and TNFα. Further activation of NRF2 triggered almost complete cell detachment, indicating chronic hyperactivation of NRF2 may contribute, rather than protect, from cell loss. However, NRF2 regulates many genes, among which some are protective, therefore, inhibition of NRF2 is not a viable option. Confluent monolayers of HCAECs were exposed to OSS, LSS or ESS and treated with CSE and/or TNFα. Cell detachment was observed at ESS with the addition of both CSE and TNFα (~30% cell loss). Interestingly, treatment with apoptosis inhibitor (Z-VAD-FMK) or matrix metalloproteinase inhibitor (GM6001) did not prevent cell loss [113], proposing an alternative mechanism to what was previously described. HCAECs exposed to CSE showed upregulation of HMOX1 (strictly controlled by NRF2 changing level), GCLM, OSGIN1 and PAR4, and a 2-hour exposure to CSE showed predominantly NRF2 nuclear localisation and therefore its activation [150]. Transcriptional analysis on HCAEC exposure to ESS, CSE and TNFα showed a maximal increase of two genes Oxidative Stress Growth INhibitor (OSGIN) 1 and 2 during EC detachment [113]. Furthermore, NRF2 stratified signature analysis in human and rat identified 15 genes, 2/3 of the genes were activated by NRF2. Among these musculoaponeurotic fibrosarcoma (MAF)-F, solute carrier family 3 member 2 (SLC3A2), OSGIN1, OSGIN2, Heat shock protein 70k 1B (HSPA1B), Protein phosphatase 1 regulatory subunit 15A (PPP1R15A), GCLC, SRXN1 and HMOX1 appeared in 75% of all the categories analysed [183].

1.9 Oxidative Stress Growth INhibitor 1 (OSGIN1)

OSGIN1, also referred to as ovary, kidney and liver protein 38 (OKL38) or bone marrow stromal cell-derived growth inhibitor (BDGI), was initially identified in 2001 by Huynh *et al*. as a pregnancy-induced growth inhibitor with a major role in breast epithelial cell growth regulation and differentiation during pregnancy and tumorigenesis. The original name OKL38 was based on the predominant protein expression in in ovary, kidney and liver and

a predicted size of 38kDa [184]. Other isoforms were later identified with a molecular mass protein size of 52kDa and 61kDa [185]. In humans the OSGIN1 gene is situated on chromosome 16, with around 18 kilo-base pairs (Kbp) and is comprised of 8 exons and 7 introns. OSGIN1 is composed of a single 1434-bp ORF, it encodes for 477-amino acid residue protein and an isoelectric point of 6.63. The 5'-untranslated region (UTR) is composed of 146 bp, and the 3'-UTR of 186 bp [185]. OSGIN1 expression was evaluated through Multi Tissue Northern blot (MTN) and Multi Tissue Expression (MTE) array which revealed that in physiological conditions it is ubiquitously expressed across all tissues with predominance for kidney and liver [186, 187].

Two highly conserved domains were found within OSGIN1, the first is a Bthiol_YpdA domain and the second is a NAD (P)-binding Rossmann-like domain, these domains overlap on the C-terminal region of OSGIN1 [188]. Intriguingly the Bthiol_YpdA domain has been found within a protein family of oxidoreductases present only in bacteria whereas the NAD(P)-binding Rossmann-like domain seems to be a common domain for protein families such as NADP oxidoreductase coenzyme F420-dependent and NAD-dependent glycerol-3-phosphate dehydrogenase-like. The existence of these two domains within OSGIN1 supports the theory of OSGIN1 activity in response of oxidative stress [171, 189]. Alternative splicing at the 5' UTR of OSGIN1 was discovered and interestingly this splicing pattern resulted in it becoming alike to the human thioredoxin reductase 1 (TXNRD1) gene [190, 191], it may therefore be the case that both genes are regulated in similar manner [187, 192]. Seven potential OSGIN1 transcripts have now been identified, six of them showed evidence for protein encoding and the seventh, which was the first originally identified OSGIN1 as 38kDa, has been reported to be incomplete once analysed in the Ensembl browser. For this reason, the majority of the studies on OSGIN1 focus only on the two isoforms stated above for the 52 and 61 kDa ORFs, even though the existence of other isoforms might result in differential biological functions downstream. Furthermore, the complexity of OSGIN1 is not only related to its sequence and the various splicing forms but appears to be highly conserved among species, suggesting a fundamental role through evolution. The human OSGIN1 protein sequence shares significant homology with rats and mice for overall protein sequence, 81% and 89% respectively. Interestingly, homology analysis established a similarity of around 40-65% to several unknown/undefined proteins between species such as Aspergillus Nidulans, Caenorhabditis briggsae, Caenorhabditis

elegans, Danio rerio, Homo sapiens, Mus Musculus and Rattus norvegicus. In 2005, it was demonstrated to have an antiproliferative effect on human breast cancer cells by inducing cellular apoptosis and cell cycle arrest [185]. These findings support OSGIN1 as a tumour suppressor gene, however the mechanisms underlying this effect were not determined. Loss or decreased levels of OSGIN1 expression has been associated with the carcinogenesis of the liver and kidney and could be correlated to adverse outcomes and reduced survival rates in patients [186, 193]. The contribution of OSGIN1 to cardiovascular disease has received very little attention, however its expression was shown to be induced by high superoxide levels and was suggested to protect cells against oxidative stress [194, 195]. In response to oxidative stress or DNA damage, OSGIN1 was shown to interact with p53 and translocate to the mitochondria in order to induce a cytochrome c release during apoptosis [195, 196]. Similar results were described recently by Brennan *et al* in astrocytes incubated with monomethyl fumarate (MMF), proposing an OSGIN1-p53 cross-activation through NRF2 nuclear translocation. In the case of MMF incubation, NRF2, NQO1, OSGIN1 and p53 activation was reported. Interesting data showed that NRF2 siRNA decreases the level of NQO1 and OSGIN1, siRNA-NQO1 doesn't affect OSGIN1 without MMF but after MMF (30μM) siNQO1 increases OSGIN1 levels. Noteworthy, siRNA-p53 did not have any effect on OSGIN1 transcriptional levels (Figure 2d Brennan *et al* [197], which opens up discussions about the real involvement of OSGIN1 in the apoptotic process, especially considering that MMF *per se* has been reported to have an apoptotic pathway activation effect [198].

Considering that the mechanism of OSGIN1 in inflammatory disease such as atherosclerosis is still elusive, its level under homeostatic conditions was explored using a BioGPS gene annotation portal (www.biogps.org), which enables a comparison of OSGIN1 expression level in both cells and tissue (Figure1.9).

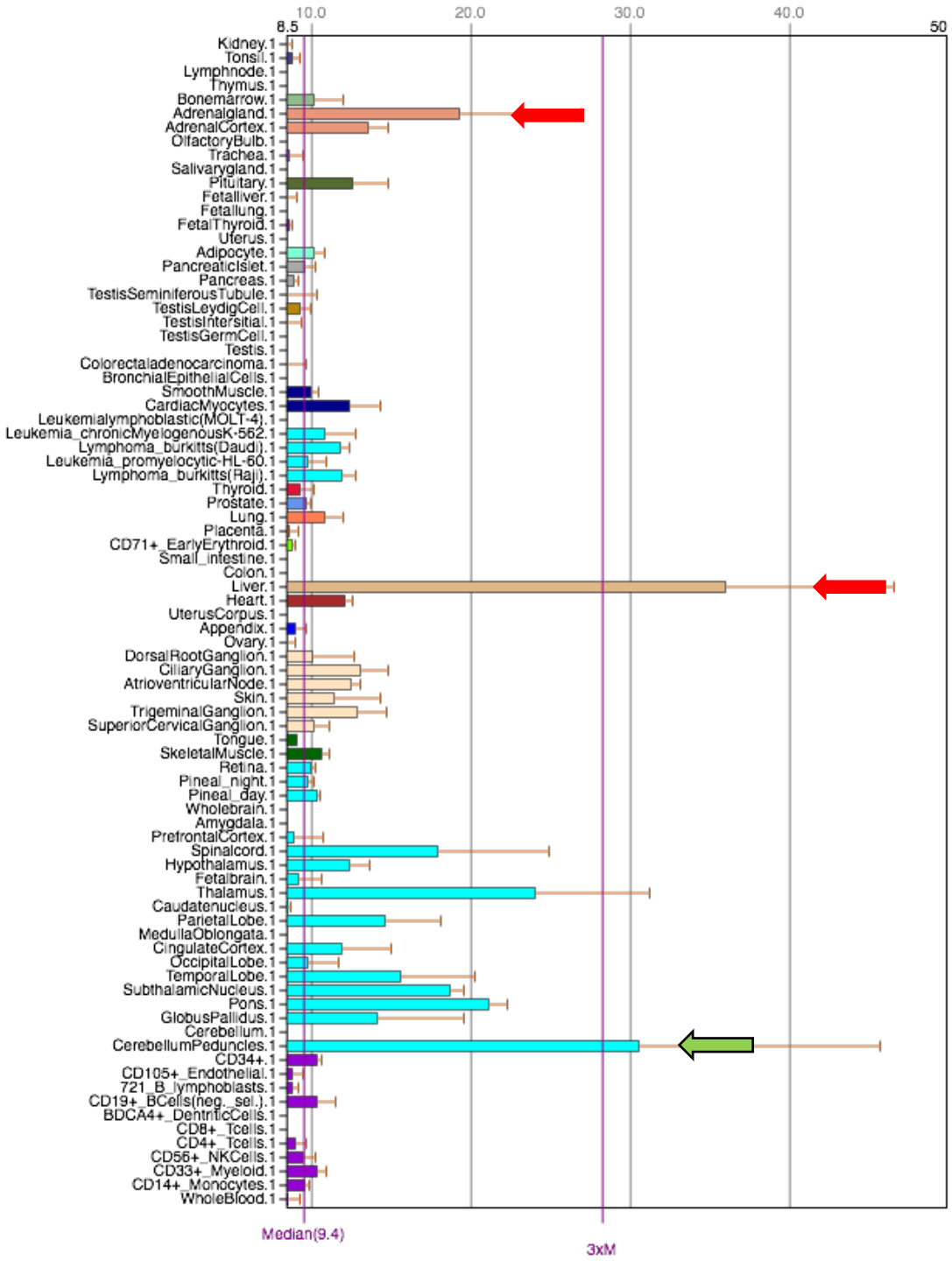

Figure 1.9). OSGIN1 expression across different tissues and primary cells. Red arrows indicate pronounced expression of OSGIN1 in adrenal gland and liver.

In physiological conditions the highest value for OSGIN1 appears in the adrenal gland and liver and only little expression in endothelial cells (Green arrow Figure 1.9), therefore its overexpression in ECs has to be led by external inputs. In 2017, Wang and colleagues

identified OSGIN1 as a novel smoke-inducible gene in the airway epithelium. OSGIN1 transcriptional levels were enhanced in smokers, both small and large airway epithelium, and Lentiviral OSGIN1 overexpression reported the involvement of OSGIN1 in the autophagy mechanism activation. Transcriptional and translational expression of the main autophagy-related genes MAP1LC3B, SQSTM1/p62 and GABARAPL1 were enhanced using CSE or Lenti-OSGIN1, supporting the hypothesis that OSGIN1 is an autophagy-relevant gene. However, protein accumulation of SQSTM1/p62 was reported during this work which might suggest a dysfunctional autophagy mechanism [199] which could lead to cellular senescence. [200-204].

1.9.1 Oxidative Stress Growth INhibitor 2 (OSGIN2)

OSGIN2 is still a poorly characterized homolog of OSGIN1, in physiologic conditions it is mostly expressed in the superior cervical ganglion, kidney and in muscular tissue, and similarly to OSGIN1 there is little expression reported in ECs (www.biogps.org) (Figure1.10). OSGIN2 is located in chromosome 8 in humans with more than 4 Kbp, it contains 6 exons and 5 introns. OSGIN2 has a mass protein size of 62kDa and encodes for 549-amino acid residue proteins with an isoelectric point of 7.39. A total of four other isoforms have been identified, all of them encoding for proteins. Two have a molecular weight of 56kDa, distinct from the last one which is 23kDa and contains only 5 exons and 4 introns. Similar to OSGIN1, OSGIN2 also contains a NAD(P)-binding Rossmann-like domain and furthermore, protein alignment analysis reports that the homology between OSGIN1 and 2 is up to 50%, as shown in figure 1.11, which might suggest a similar role or that it is part of same pathway. As well as OSGIN1, OSGIN2 is also highly conserved among species which implies a crucial role during evolution. No studies exist on the role and function of OSGIN2 in cells, or what are the causes and consequences of its activation and hence is the focus of this PhD. There is only one article in the literature from 1999 [205] where the gene was sequenced.

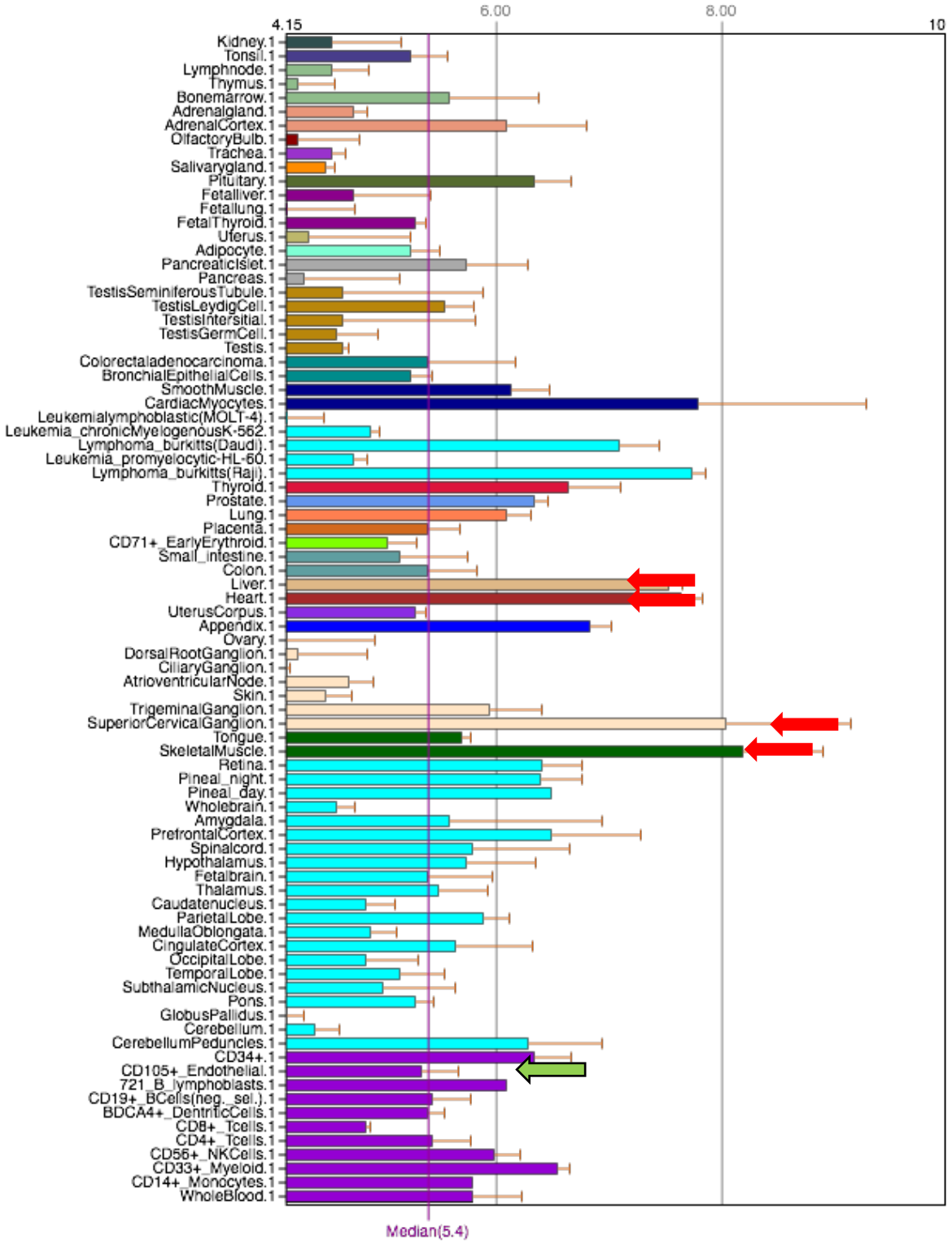

Figure 1.10). OSGIN2 expression across different tissues and cell lines. Red arrows indicate pronounced expression of OSGIN1 in brain and muscular tissue-related (red arrows). OSGIN2 expression in ECs is indicated by a green arrow.

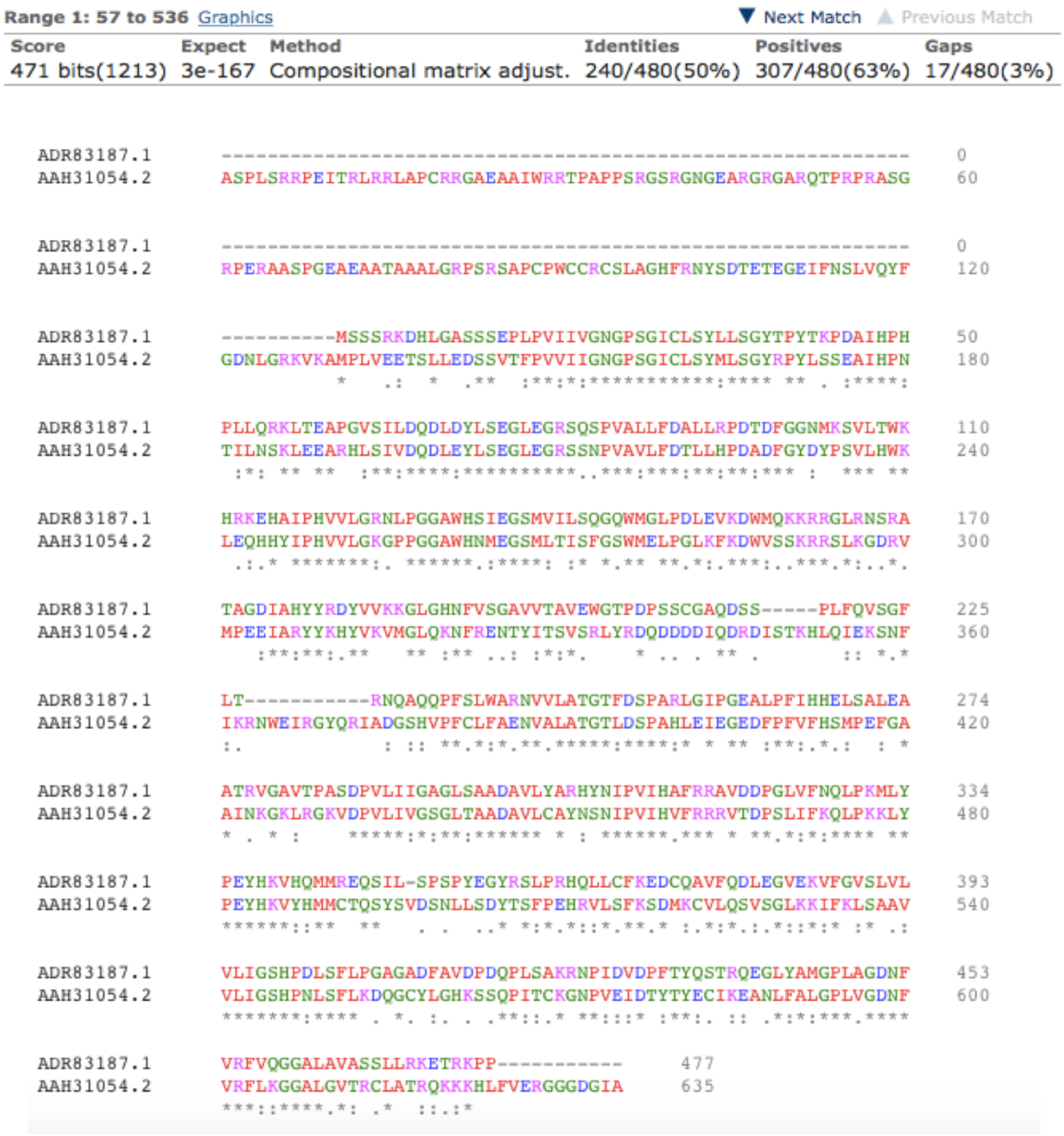

Figure 1.11). CLUSTALO protein sequence alignment of *Homo sapiens* OSGIN1 and OSGIN2.

1.10 Autophagy and its mechanism

The etymology of the word "autophagy" derives from Greek and literally means "eating of self". It was coined in 1966 by the Belgian Christian de Duve who observed it in rat liver, mitochondria and other intra-cellular organelles degraded within lysosomes after perfusion with glucagon, a pancreatic hormone [206]. Today our knowledge is much broader in terms of the molecular understanding and physiological significance of autophagy because of the effort of many laboratories [207-209], however precise mechanisms underpinning the process are still not completely elucidated. Although the

importance of autophagy in the mammalian system is now well established, most of the progress in understanding this mechanism has been made in yeast (Saccharomyces cerevisiae) [209-211], where 32 different autophagy-related genes (Atg) have been screened, many of which are conserved in worms, plants and mammals, highlighting the importance of this mechanism through species [207].

There are four defined types of autophagy: macro-autophagy or canonical autophagy, micro-autophagy, chaperone-mediated autophagy (CMA) and mitophagy. Another "type" has been introduced by Levine and colleagues who coined the term autosis for the cell death process led by autophagy which exhibits distinct features such as focal perinuclear swelling [212], but the use of this new term is still strongly debated [213]. The first three types promote proteolytic degradation of cytosolic components within the lysosome, mitophagy instead, is considered as a removal process of damaged mitochondria through autophagy which is critical for maintaining proper cellular functions. While each is morphologically distinct, all these different pathways culminate to degrade damaged or non-functional components such as nucleotides, amino-acids, proteins and intracellular organelles within the lysosome and reused [214, 215]. Every step is highly regulated and has different functions which consists of sequestration, delivery to lysosome, proteins or components of degradation and subsequent utilization of products degraded (Figure 1.12).

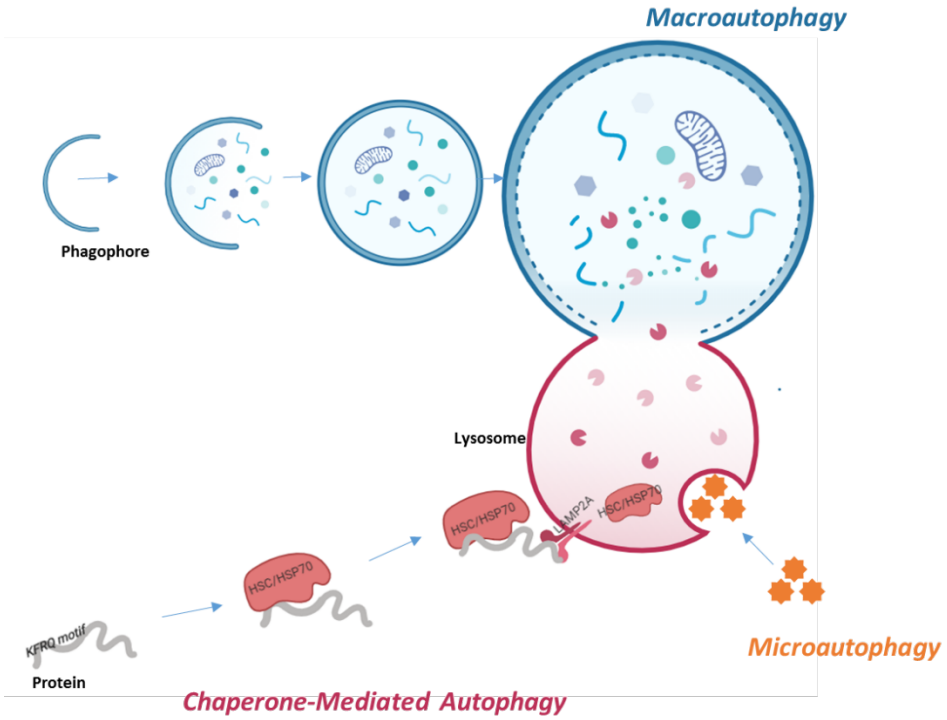

Figure 1.12). Schematic representation of the three different types of autophagy. During macroautophagy multi-step are necessary for the formation of the autophagolysosome. Phagophore membrane develops around the cargo. Endosome with protease and hydrolase enzymes engages with the phagophore releasing its content inside the autophagosome degrading the cargo. In the process of microautophagy the cargo is not surrounded by phagophore membrane, but it is engulfed inside the lysosomal vesicles. In CMA a protein shows a KFERQ motif which is recognised by HSC/HSP70. HSC/HSP70 bind the protein and present it to LAMP2A receptor on the lysosomal vesicles. Next, the complex of HSC/HSP70 and the protein is transported inside the lysosomal vesicle for degradation or recycling.

The capability of cells to renew their intracellular components and to degrade undesired molecules reduces with age [429]. Failure during the autophagy process is considered to have a significant contribution to reduce tissue function of old organisms. In fact, reduced recycling of cellular damaged organelles, cell components and proteins underlies the inability of old cells to respond to oxidative stress, and to adapt to stress conditions.

1.10.1 Macroautophagy

In contrast to microautophagy and CMA, which are the other two cytoplasmic autophagy mechanisms, macroautophagy involves *de novo* synthesis of double-membrane vesicles for the auto-phagosome formation which is used to surround and sequester the cargo following translocation into the lysosome [216]. Autophagy is highly conserved from yeast to mammals, and it is in yeast that the formation of autophagosomes begins at a single perivacuolar site called the phagophore assembly site (PAS) [217]. However, in mammalian

cells the generation of the phagophore is initiated, according with several studies, in the cytoplasm [218] within endoplasmic reticulum (ER)-associated structures called omegasomes [219, 220]. Once the phagophore is created it begins to expand, the source of membrane material for its expansion is still unknown and strongly debated [221], but Golgi complex [222], ER [219, 220], plasma membrane [223, 224] and mitochondria [225] are among the options. The factors that cause the phagophore membrane to bend and to create spherical shapes are not yet known but it seems that the membrane wraps around the cargo changing its shape accordingly [226] until its completion in a double-membrane autophagosome. At this point the external membranes fuse with the lysosomal membrane creating the autolysosome [227], the cargo gets exposed to the acidic lumen, hydrolases and proteases which leads to its degradation. At this stage, all the content is brought back into the cytoplasm via lysosome permease enzymes and the cell can finally recycle it and use it as energy or in biosynthetic processes [216].

1.10.2 Macroautophagy machinery

Induction of autophagosome formation is regulated by several Atg genes that were discovered in yeast [221], this process in mammalian cells is driven by Atg1, 13 homologs, from Unc-51-like kinase family ULK1 or 2 and RB1-inducible coiled-coil 1 (RB1CC1/FIP200) homolog of yeast Atg17 [228-231]. The complex ULK1/2-Atg13-RB1CC1, also known as autophagy induction complex, is regulated by mammalian targets of rapamycin (mTOR) complex-1 (C1), which is normally associated with ULK1/2-Atg13-RB1CC1 complex inactivating it. However, in particular conditions such as starvation, or in cells incubated with rapamycin, mTORC1 dissociates from the induction complex by dephosphorylation of ULK1/2-ATG13-RB1CC1 sites, triggering macroautophagy [230, 231].

Once macroautophagy is activated the complex responsible for the nucleation of the phagophore is the ATG14-containing class III phosphatidylinositol 3-kinase (PI3K) complex [232] and its subunits C3 and R4 together with Beclin 1 (BECN1). The completion of the autophagosome process is not yet clear and more studies are needed. What is known is that two are the potential regulator involved in generating autophagosome membrane curvature. The first is AMBRA1 and the second one is the SH3 Domain Containing GRB2 like, Endophilin B1/Bax interacting factor 1 (SH3GLB1/Bif-1) which generate the autophagosome membrane curvature through their interaction with BECN1 [222, 233, 234]. The expansion of the phagophore is modulated by two conjugative systems, the first

in the mammalian ortholog complex Atg5, Atg7, Atg12 and Atg16L1 which has been shown to work exactly in the same way as yeast [235-237], it associates with the phagophore and dissociates once the autophagosome is completed [235, 238]. This complex is inhibited by the Golgi protein RAB33A engaging with ATG16L1 and by the acetyltransferase KAT2B/p300 binding Atg5, Atg7, and Atg12 [232, 239]. The second system regulating the phagophore expansion is regulated by the Gamma-aminobutyric acid receptor-associated protein/ Microtubule-associated proteins (GABARAP/MAPLC3), where the Atg4 cysteine processes GABARAP by exposing its glycine residue at the C terminus protease, followed by interaction with E1-like enzyme Atg7 which activates the processed GABARAP/MAPLC3 and in turn modulates and activates the E2-like enzyme Atg3 [240]. Here, GABARAP glycine residue conjugates to phosphatidylethanolamine (PE), forming the complex GABARAPL/MAPLC3-PE [240-242]. Very little is known about the disjunction process, but it appears to be a critical step in macroautophagy, which can promote dysfunctional macroautophagy in the case of faults in the cleavage process [243, 244]. In the complex GABARAPL/MAPLC3, MAPLC3 has been well characterised and it seems to work in two different forms, one is not processed, and it has been named as MAPLC3A or LC3A. The second form PE-conjugated is MAPLC3B or LC3B, this process is enhanced by starvation, ROS and other type of insults [245, 246], and its synthesis during macroautophagy is fundamental in determining autophagosome size [247].

1.10.3 Regulation of Macroautophagy

Extracellular and intracellular stresses are responsible for triggering macroautophagy [221]. Two main pathways are involved in macroautophagy activation, both regulated by starvation. The first is cAMP-dependent protein kinase A (PKA) and the second is the mTOR pathway [248]. PKA negatively regulates autophagy under nutrient-rich conditions [249], partially by phosphorylation of LC3 by PKA [250]. Studies have shown a cross-talk between PKA and mTOR pathways, it has been demonstrated that PKA can positively regulate mTOR through phosphorylation of mTORC1 or by inactivation of the AMP-activated protein kinase (AMPK) [251, 252]. AMPK is considered the major energy-sensing kinase within cells, it responds to intracellular levels of AMP/ATP and regulates several cellular processes, among which is macroautophagy [253, 254]. AMPK is activated by AMP binding and deactivated by ATP [255], when it binds to AMP it can directly inhibit mTOR [256] or negatively regulate it via phosphorylation of the tuberous sclerosis proteins 1 and 2

(TSC1/2) complex which inhibits the mTORC1 in mTOR [257, 258]. Furthermore, it has been reported in cases of external stimuli such as ER and ROS stresses, increases in the concentration of Ca^{2+} [259] activating calcium/calmodulin-dependent protein kinase 2 beta (CAMKK2/CaMKKβ) and leads to ULK1 phosphorylation by AMPK activation and finally induction of macroautophagy [260-264]. Another way for ER and ROS stress to induce macroautophagy is by accumulation of unfolded protein response (UPR) signalling, however this mechanism in not completely understood and there are debates about whether it is a pro-survival mechanism or whether it promotes autophagic cell death (autosis) [212, 221, 265].

1.10.4 Chaperone-Mediated Autophagy (CMA)

CMA is a different type of autophagy which has only been described in mammalian cells. Conversely to macroautophagy and microautophagy which can both sequester components in a non-specific way in the cytoplasm, CMA is highly specific. The typical substrate for CMA is a pentapeptide targeting motif biochemically associated to the KFERQ sequence which appears to be contained in almost 30% of the cytosolic protein [266]. CMA acts as a protein quality control which has the potential to degrade a wide range of substrate proteins, lipid-binding proteins, protein subunits and a transporter in vesicular trafficking [267]. The KFERQ sequence of the substrate protein is shielded by its three-dimensional structure which avoids contact with the CMA heat shock protein 70 (HSP70) family, the heat shock cognate 70 (HSC70) and the sequence itself. In the case of unfolding or incorrect folding of the protein, the HSP70 and HSC70 are free to interact with the target and promote its degradation by lysosome [268, 269]. The HSP70/HSC70 complex can deliver the misfolded proteins across the lysosomal membrane presenting the cargo to lysosomal-associated membrane protein1 (LAMP1) and 2A (LAMP2A) [270-272]. Herein, the cargo after translocation in the lysosomal lumen gets degraded, the HSP70/HSC70/LAMPs dissociates, and a new cycle begins [273]. Not much is known about CMA regulation, this process seems sensitive to oxidative stress, damaging toxins and starvation, but its molecular mechanism in still not clear [267, 274-276]. It appears that the HSP70/HSC70 complex and LAMP can be related with macroautophagy, where CMA acts as a support in the clearance of some ubiquitinated organelles and protein complexes, selectively tagged by the presence of SQSTM1/p62 and NBR1, thus promoting their degradation via lysosomes [277-279]. Furthermore, CMA, has been reported to be strictly

regulated and modulated by Bcl2-associated athanogene 3 (BAG3) and HSP70. HSP70 interacts with proteins on the basis of their hydrophobicity or other amino acid motifs and regulated their refolding/unfolding and/or degradation. The role of HSP70 is still far from being understood, however has been shown that it might be involved in inhibiting cell death blocking procaspase 9 activity through direct bind with the apoptosis protease factor 1 (Apaf-1) [431], and furthermore, it has been reported that HSP70 blocks and inhibits caspase3 [432] showing anti-apoptotic effects. Antiapoptotic effect through inhibition of caspase 3 was reported to be also related to BAG3 [433] and, recently, it was reported that HSP70/BAG3 complex acts as main player for proteotoxicity-induced signalling, which controls protein aggregation [434]. Among many roles, HSP70/BAG3 complex seems to be involved in impairing migration and adhesion molecules and once again it seems to promote cell survival suggesting an enhancement against apoptosis [435-437]. Of high interest the HSP70/BAG3 complex binds to SQSTM1/p62 which links to the autophagosomes protein LC3B itself, and during this process, higher levels of cathepsin activity was reported [438] which might be involved in modulation of the ECM. That suggests that autophagy pathways mediated by HSP70/BAG3 is crucial for protein quality control and regulation also known as proteostasis, especially in response to ROS or during ageing.1.10.6 The role of Autophagy in atherosclerosis

Autophagy has a fundamental role in atherosclerosis, which suggests that autophagic flux regulation might be considered as a treatment for atherosclerosis. It has been established in vitro and in vivo that different types and degrees of autophagy affect ECs, SMCs and macrophages, which are well known to be crucial in stenotic plaque development [292].Scanning electron microscopy (SEM) has shown that in the atherosclerotic plaques the presence of autophagic characteristic such as increments in vacuoles and accumulation and aggregation of inclusion bodies was observed [293]. Furthermore, pro-atherosclerosis factors like ER stress, hypoxia, inflammation, ROS and shear stress have been shown to trigger autophagy [294-296].

It has been established that autophagy plays a crucial role against apoptosis and ROS, supporting the haemodynamic function in the cell and tissue physiological conditions [22]. On the other hand, dysfunctional autophagy can lead to cell structure disruption [297] and too much autophagy can promote cell death or autosis [298]. Furthermore, as stated(section 1.13.1), different types of shear stress can either protect or promote

atherosclerosis and modification of the flow can regulate autophagy, inducing the conversion of LC3A to LC3B and reducing the autophagic flux marked by SQSTM1/p62 accumulation [299]. In the case of excessive ROS insult, impairment of autophagy has been reported and has been shown to be responsible in triggering cellular senescence [300, 301]. Cellular senescence can be promoted by overexpression of Cdk inhibitors such a p16, which is commonly accepted as the main senescence marker. p19 and p21 both provoke cell cycle arrest in S-phase [302] and were recognised in 2012 by Capparelli et al. to be responsible for triggering autophagy [303]. In addition, chronic inhibition of mTOR mechanism triggers premature senescence [304], all this evidence provides a relationship between autophagy and cellular senescence. However, further studies are necessary to understand whether senescence is inducing autophagy or vice-versa, but what it is now clear is that autophagy and senescence are correlated [305].

1.10.7 Autophagy and Vascular Aging

Impairment of autophagic flux has been proposed as a possible cause of vascular ageing which might contribute to a wide range of vascular pathology, such as atherosclerosis and calcification. Ageing is the main risk factor leading cardiovascular disease and [306] it has been demonstrated that induction of autophagy in mice can improve life span. Although the link between ageing and autophagy is still not clear, it has been speculated that autophagy might contribute to vascular functionality against arterial stiffening, and impaired endothelial relaxation [307, 308]. Several factors have been shown to influence vasculature ageing, with enhanced levels of ROS providing a unifying theme. In this context, autophagy has been showed to modulate the global redox state [309]. Dysfunctional autophagy has been linked with cardiovascular disease, which is exacerbated by oxidative stress [310]. This dualism between ageing and impairment of autophagy was highlighted in a study on mice carried out by La Rocca et al [311], where the level of SQSTM1/p62 in ECs was higher in old mice vs young suggestive of a dysfunction on the process of autophagy and reduction of autophagic flux responsible for SQSTM1/p62 accumulation. While the mechanism was not definitively identified, pharmacological treatment to increase autophagic flux have shown efficacy in two murine studies, where stimulating autophagy reverses aspects of arterial ageing, such stiffening and EC dysfunction, [312, 313]. The convergence between autophagy and cardiovascular disease, in particular related with ageing and therefore with senescence of cells might be the key

to interpretation in order to prevent or minimize the cellular damage caused by their disfunction.

1.11 The link between to cellular senescence and autophagy

In contrast to quiescence, which is considered temporary, senescence is an irreversible cell loss of proliferative potential and can occur in G1, G1/S or G2 cell cycle check points [314]. Cdk inhibitors such as p16 and p21, the main markers of senescence, and their ectopic expression leads to a senescence-associated secretory phenotype (SASP) [315]. Young *et al.* proposed a correlation between a transitory senescence and autophagy which can promote cell cycle arrest [316]. Similar observations were reported by Cho and Hwang in 2012, where cells exposed to serum starvation were positive for senescence-associated β-galactosidase (SA-β-gal), this is a commonly accepted marker of high lysosomal activity. Furthermore, they reported lysosomes biogenesis, mTOR inhibition and induction of autophagy [317]. Interestingly, SA-β-gal and p16, which increase with ageing, are positive in senescent cells [318], as well as unbalanced autophagy activation, and the expression of these markers can be enhanced by mTOR dependent or independent mechanisms, which leads to a senescence phenotype caused by p21-induced cell cycle arrest [319, 320]. In this complicated scenario, mTOR can restrain autophagy but in case of events promoting mTOR inhibition, autophagy can be triggered and induced in a feedback loop manner. In order to assess the relationship between autophagy, cell cycle arrest and senescence an interesting study was carried out *in vitro* by Capparelli *et al.* inhibiting pharmacologically Cdk4/6. As expected, cell cycle arrest was induced with p16 and p21 upregulation, as well as an increased SA-β-gal, lysosomal activity and activation of autophagy markers. Interestingly, the same outcome was observed with ROS exposition rather than chemical inhibitors which leads to speculation that the involvement of senescence-autophagy down stream of NRF2 activation are part of the same metabolic program. A previous study has shown that interferons (IFN)-α–β–γ are pivotal to promote cell cycle arrest over cell division [321-323], and in ECs to be further responsible for p16 activation and triggering senescence [324].

Finally, overexpression of p16 and p21 resulted in higher autophagic marker expression such as LAMP1 and LC3B, cell morphology appears flatter or hypertrophic, all of which is consistent with a senescent phenotype [303]. During the active senescence process, cells

enlarge in size without proliferative potential which shows high metabolic activity by mTOR dependent and independent-mechanisms and leads to cytoskeletal rearrangement and disruption by the increased activity of lysosomes [297].

1.12 Cellular senescence and cellular proliferation

Cellular senescence is described as a permanent proliferative arrest of cell cycle [344]. Normal cells can only go through a finite number of divisions due to a process termed cellular or replicative senescence which involves telomere erosion [345]. Interestingly, senescent cells have been observed to be resistant to apoptosis through secretion of soluble factors, which are collectively known as the SASP [346-349]. Accumulation of senescent cells have been reported in humans and primates with advancing age [350, 351], due to a critical telomere shortening, triggering a DNA damage repair mechanism, similar to DNA breaks and inducing permanent cell cycle arrest.

Free radical, ROS and reactive nitrogen species (RNS)-mediated cellular stress can induce senescence, leading to the impairment of both the function and regenerative potential of a tissue and promoting inflammation in aged organisms [352-354]. The senescence mechanism can be induced by molecular damage such as DNA double strand break (DBS) which, for example, is led by oncogenic RAS expression and radiation and recognised by damage sensors like ATM/R kinases [355, 356]. Senescence can also occur during different stages of the cell cycle based on the insult that the cell receives. It has been observed that in the case of RAS expression, p53 promotes the upregulation of $p21^{Cip/Waf}$, leading to Rb phosphorylation and prohibiting S-phase entry [357].

Conversely, in response to heat stress (HS), $p21^{Cip}$ overexpression leads to cell cycle arrest only in the early S-phase and stops cells from progressing to the G2-M phase. This scenario seems to be related to a single strand break (SSB) in the DNA [358]. Cellular senescence can be also induced by reactive oxygen species (ROS) through activation of the RAS-RAF–MEK–ERK cascade, activating p38 MAPK which leads to the upregulation of p53 and p21 [359]. Sustained cellular stress or replicative senescence then triggers permanent cell cycle arrest, maintaining cellular senescence and permanently inhibition of the cell-cycle through upregulation of CDK4/6 inhibitor $p16^{InkA}$ [360] and p21 [361, 362]. A deficiency in one of the cell cycle checkpoints may induce genetic instability [363, 364]. Upon induction of senescence and subsequent block in proliferation, the cell undergoes morphological and phenotypic changes described as the senescence-associated phenotype.

1.12.1 Cellular senescence and ROS

The most common features of cellular senescent phenotype include cell size enlargement, multinucleated cells [361, 365, 366], lysosomal accumulation with increased β-galactosidase activity [367], as well as alterations in chromatin rearrangement, metabolic reprogramming or autophagy modulation (cellular morphology of OSGIN1+2 overexpressing cells can be viewed in section 3.4.5). Although the main role of cellular senescence is to protect the tissue from cellular damage accumulation and malignant transformation, once this process is corrupted it becomes deleterious, several findings have been described by Childs *et al* [368]. Accumulation of senescent cells within a tissue occupies space, reducing tissue functionality and is a key process in the reduction of tissue performance in aging. Considering that excessive exposure to ROS can trigger cellular senescence and NRF2 is the main regulator in response to oxidative stress insult, it is crucial to elucidate the role of NRF2 in cellular senescence and whether NRF2-controlled genes are involved in this cellular signalling pathway, which may shed light on how they modulate this process. Furthermore, the constant activation of NRF2 in smokers is a known risk factor for plaque erosion formation and, as previously stated, NRF2 stimulation leads to the transcription of OSGIN1 and OSGIN2 in ECs. For this reason, research and development of new antioxidant molecules might contribute to prevent or at least partially reduce the activation of this mechanism.

1.13. Cellular proliferation and cell cycle

Howard and Pele first described the cellular cycle and its phases in 1951. This mechanism is highly conserved and controlled by many mechanisms that allow or restrain the progression through the phases [334]. The cyclins (cyc) are the main family of proteins responsible for controlling the progression of the cycle, which are controlled by the cyclin dependent kinases (CDKs) and their inhibitors (CKI). These families are crucial for progression through all the checkpoints within the cell cycle. 21 cyc have been described, however, only four are required for cell cycle regulation, they are CDK1, CDK2, CDK4 and CDK6 [335, 336]. CDK2, 4 and 6 are pivotal for progression through G_1 phase, CDK2 is also required for progression through S-phase, while CDK1 for progression through G2-M phases. CKIs, such as CDK interacting protein/Kinase inhibitory protein (CIP/KIP) (which include p21, p27 and p57) and INK (p15, p16, p18 and p19) control all these phases, binding CDK complexes and provoking cell cycle arrest [337] [338]. P21 was the first CKI member

identified, which binds to E/CDK2 inhibiting G_1->S-phase transition, and A/CDK1-2 resulting in the inhibition of the S>G_2-M transition phase [339]. Furthermore, recent studies have shown that p21 can be activated by p53-dependent and p53-independent mechanisms [340]. p21 also plays an important role in regulating apoptosis through DNA-repair activity or protein-protein interaction, where p21 has the ability to bind proteins which promote apoptosis, inhibiting their activity [341]. In 2005 a study of Bone Marrow Stromal Cell-derived by Wang *et al* did not investigate whether OSGIN1 was promoting apoptosis but did described the role of OSGIN1 on cell cycle inhibition for the first time.

1.13.1 Cellular proliferation and Apoptosis

Cell cycle arrest has most commonly been associated with the apoptotic signalling pathway and is involved in many processes, such as tissue development and homeostasis, which needs to be meticulously regulated by balancing both cell proliferation and apoptosis. It has been reported that the molecules required during the apoptosis process are those related to the G1 phase, the S-phase and controlled by p53 [342]. Moreover, in 1998 [343] Browne *et al* observed that caspase 3 was able to cleave poly-ADP-ribose polymerase (PARP) to induce cell cycle arrest and apoptosis and identified the caspase inhibitor Z-VAD-FMK inhibits apoptosis. Since this evidence has been reported, it seems clear that there is a precarious balance in the intricate network and crosstalk between autophagy-senescence pathways and cell cycle and will be part of the investigation of this PhD programme of work

CHAPTER 2: MATERIALS AND METHODS

CHAPTER 2: MATERIALS AND METHODS

2.1 Cell culture

Primary HCAECs (passage 2) were purchased from PromoCell and cultured in endothelial cell media (Endothelial cell GM MV2, PromoCell, Germany) supplemented with 5% fetal bovine serum (FCS) (PromoCell, Germany), 100 U/ml penicillin, 100 µg/ml streptomycin in a humidified incubator supplemented with 5% CO2, passaged at a 1:3 ratio every 3 to 5 days. Cell passages 4-6 were used in this study. Cells from different donors were used for each experimental replicate, typically n=3 or n=6 for the analyses presented here.

2.1.1 Passaging HCAECs

Confluency of HCAECs was regularly evaluated and cells were passaged once confluence was reached. From a T25, MV2 media was aspirated and cells were washed with 5ml of sterile 1X Phosphate Buffered Saline (PBS) twice. 1X trypsin-EDTA (3ml) (Life Technologies) was added to cells ensuring full coverage (Tables 2.1-2.2).

Table 2.1: Comparison of cell culture flasks

Flask	Size (cm2)	Cell number (seeded)	Media vol (ml)	PBS 1X vol (ml)	Trypsin 1x vol (ml)
T-25	25	$2.5x10^5$	5	5	3
T-75	75	$5.0x10^5$	15	10	5
T-175	175	$1.5x10^6$	25	15	8

Table 2.2: 0,1% gelatine coated glass slide

Glass slide	Cell number	Media vol (ml)	PBS 1X vol (ml)
76x26 cm2	$2.5x10^5$	3	5

HCAECs were incubated at 37°C, 5% CO_2 for 5mins. Once cells were visibly dislodged, trypsin was neutralised adding (6ml) MV2 media. Cell suspension was collected and centrifuged at 300 g. The supernatant was discarded, and cell pellet was resuspended in 1ml of fresh MV2 media and aliquoted into a new T-75 flask at a cell density of $1x10^6$ cells/cm2.

2.2 Cell Counting

Cell monolayers were trypsinised using 1X trypsin/EDTA solution. Once they were dislodged, trypsin was neutralized adding double volume of media compared to trypsin. Content was centrifugated at 300g and the pellet re-suspended in a suitable volume of medium (appropriate for number of cells, typically 10ml). 10 µL cell suspension was mixed 50/50 with 10µl of 0,4% trypan blue solution before counting using a BioRad TC20™ automated cell counter.

2.3 Slide surface coating

Glass slides, measuring 76x26 cm^2 were sterilized using Industrial Methylated Spirit (IMS) 70% and left to dry for 1 h inside a class 2 cabinet under air flow. Rubber gaskets were placed on top of the glass slide and coated with 0.1% gelatine (attachment factor (AF) Gibco, Life Technologies) for a minimum of 24 hrs at 4°C.

2.4 Cloning of OSGIN1 and 2 and preparation of adenoviral vector

OSGIN1 and OSGIN2 were cloned into pCpG-free MCS plasmid (Invivogen). The coding regions were amplified by Polymerase Chain Reaction (PCR) using KOD proofreading DNA-polymerase, introducing a 5' BglII site and 3' NheI site by Dr S White. Once inserted into the respective sites in pC-G-free MCS, the whole expression cassette was shuttled into pDC511 (Microbix Biosystems, Canada) for adenoviral vector production by Dr Sala-Newby (University of Bristol). Viral stocks were amplified and purified using a caesium chloride (CsCl) gradient and titrated by plaque assay. Viruses were used at a total of 400 pfu/cell for all experiments.

2.5 Cytotoxicity, viability and apoptosis analysis

Apotox-Glo triplex assay (Promega, Madison, USA) was performed in the HCAECs to provide a luminescent assay quantifying cell viability, cytotoxicity and an apoptosis assay, according to manufacturer's instructions. The principle behind this assay is the capability for the glycylphenylalanyl-aminofluoroumarin (GF-AFC) substrate to enter into live cells where it is cleaved by the live-cell protease to release AFC. The bis-AAF-R110 substrate cannot enter live cells but instead can be cleaved by the dead-cell protease to release R110. This allows measurement of fluorescence at the following two wavelength sets:

- 400Ex/505Em (Viability)
- 485Ex/520Em (Cytotoxicity)

The second part of the assay uses the Caspase-Glo Assay Technology by providing a luminogenic caspase-3/7 substrate, which contains the tetrapeptide sequence DEVD, in a reagent optimized for caspase activity, luciferase activity and cell lysis.

Briefly, apoptosis is determined by measuring the luminescence of the luminogenic substrate containing the DEVD sequence. Following caspase cleavage, a substrate for luciferase (amino luciferin) is released, resulting in the luciferase reaction and the production of light. The reagent relies on the properties of a proprietary thermostable luciferase.

HCAECs were seeded into a 96 well plate at a density of $5x10^4$ cells per well and transduced with AdOSGIN1 (200 multiplicity of infection (MOI) +200MOI AdCtrl) and AdOSGIN2 (200MOI +200MOI AdCtrl) or control virus AdCtrl (E1/E3 deleted 400 MOI). Transduction was carried out for 16hrs and media was subsequently replaced. Cells analysis was performed 40 hrs after AdOSGIN1 and AdOSGIN2 infection. Results were normalized to DMSO treated control cells. Experiments were performed five times with eight replicates per condition.

2.6 Caspase-3 activity assay

Caspase-3 activity was measured using a caspase-3 activity assay kit (Promokine kit). This assay is based on a fluorometric immunosorbent enzyme assay performed in a multititer plate, according to the manufacturer's instructions. Briefly, a 96 well multititer plate was coated with human caspase-3 monoclonal antibodies and blocked to prevent nonspecific binding. Then, cellular lysates were incubated in the coated wells for 1.5 h at 37°C. After a washing step, the caspase-3-specific substrate Ac-Asp-Glu-Val-Asp-7-amino-4-(trifluoromethyl) coumarin (DEVD-AFC) was added and cleaved by the active enzymes to generate free fluorescent AFC. Fluorescence was measured at λ max = 505 nm after 3 h of incubation with the substrate and normalized by the protein content of each sample. Each treatment was carried out in 5 wells.

2.7 Orbital shaker system as a model of shear stress

HCAECs were seeded at $2x10^5$ cells per well in a 6 well cell culture plate with 3ml of MV2 media. Cells were cultured to achieve a confluent monolayer of cells. The plates were then cultured on the centre of the orbital shaker (model PSU-10i; Grant-Bio) at 210 rpm, within an incubator at 37°C with 5% CO_2. CFD assessment under these conditions has been

previously published [325] demonstrating that HCAECs in the centre of the well experience complex multidirectional flow with a shear stress of 5 dyn/cm^2, while in the periphery the flow is pulsatile and unidirectional with shear stress of 13 dyn/cm^2 (Figure 2.1).

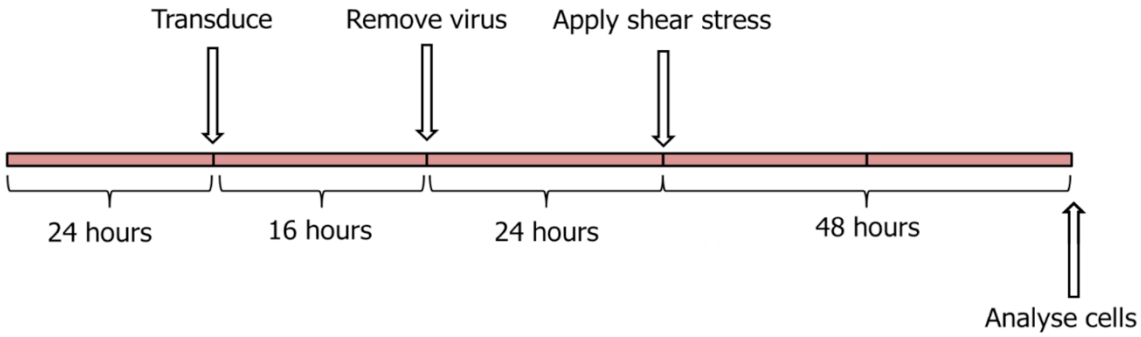

Figure 2.1). Timeline of experiments on the orbital shaker system as a model of shear stress. 2.5x10^5 HCAECs per well were seeded in a 6 well plate. Cells were given 24 hrs to adapt before adenoviral transduction for 16 hrs. MV2 media was replaced and cells were left in static conditions for 24 hrs. On day 5 the cells were exposed to flow for 48 hrs.

2.7.1 Sample collection from the orbital shaker

At the end of the experiment, the orbital shaker was stopped, and plates were removed. The media including any detached cells were quickly collected in 2 ml Eppendorf tubes, centrifuged at 300g for 5 minutes to pellet cells, which were then resuspended in 1ml. 90μl of resuspended cells were mixed with 10μl 0.2% trypan blue for counting and analysis of cellular integrity, using a BioRad TC20™ automated cell counter. Adherent cells were washed with cold 1X PBS and imaged using a Leica M165 FC stereomicroscope at 4x magnification, 6 micrographs per well, with 2 Fields of view (FoV) taken of the central region exposed to multidirectional flow and 4 photographs in the peripheral areas of the well exposed to unidirectional flow. Subsequently, HCAECs were lysed using 300μl of lysis buffer (RIPA buffer; Sigma) with 1:1000 protease and phosphatase cocktail inhibitor (Sigma). HCAECs were scraped into 300μl of lysis buffer and collected in a 1.5 ml Eppendorf tubes for further analysis.

2.7.2 Cell lysis for protein analysis

For western blot analysis, 24 well plates were removed from the incubator and immediately placed on ice. Culture media was removed, and cells were washed twice with 1ml of cold 1X PBS. HCAECs were lysed with cold RIPA buffer (Sigma) containing 1X HaltTM protease inhibitor cocktail (Thermo Scientific) and 1X phosphatase inhibitor cocktail (Cell Signalling). The resulting cell suspension from each well was collected and placed into a

cold 1.5 ml Eppendorf tubes. The samples were sonicated three times for 20 seconds each and centrifugated at 14000 rpm for 10 minutes at 4°C. The supernatant was placed into a new tube and stored at -80°C for further use.

2.7.3 Protein quantification and normalisation

Before western blot analysis the protein samples were quantified and normalised at 20ng in order to ensure equal loading at 20µl. Bicinchoninic acid-assay (BCA), according to the manufacturer's instructions, using Pierce BCA Protein Assay (Thermo Scientific, Rockford, USA) was used. Standards were made by serial diluting albumin (2000 µg/ml) in RIPA buffer containing protease and phosphatase inhibitors.

Table 2.3: BCA Standards

Standards	**Albumin concentration (µg/ml)**
A	2000 µg/ml
B	1600 µg/ml
C	1200 µg/ml
D	800 µg/ml
E	400 µg/ml
F	200 µg/ml
G	0 µg/ml

The colorimetric reaction was carried out in a 96 well plate with 10µl of standards or samples (in triplicate) and 190 µl of working solution (50:1 ratio of reagent A/ reagent B) for a total volume of 200µl per well. The plate was incubated at 37°C for 30 minutes to allow the reaction to progress. The absorbance was then determined at 562nm with correction by the blank average to improve the precision of the reading. Sample concentration was calculated from the standard curve generated from the known standards. Standardisation of samples was achieved through dilution to match the concentration of the least concentrated sample. After normalisation, 20µg for each sample was prepared by adding 5 µl of 2X laemmli loading dye [4% sodium dodecyl sulfate (SDS), 20% glycerol 0.004% bromophenol blue.0.125M Tris-Cl, pH 6.8] which was supplemented with 10% 2-mercaptoethanol, added immediately before use. Proteins were denatured in

preparation for resolving on acrylamide gels by incubating at 100°C for 5 minutes followed by 2 minutes on ice.

20ng of protein were loaded in 10% polyacrylamide gel. Gels were stained by using instant blue for 16 hrs and quantified the densitometry of western blot bands (Figure 2.2).

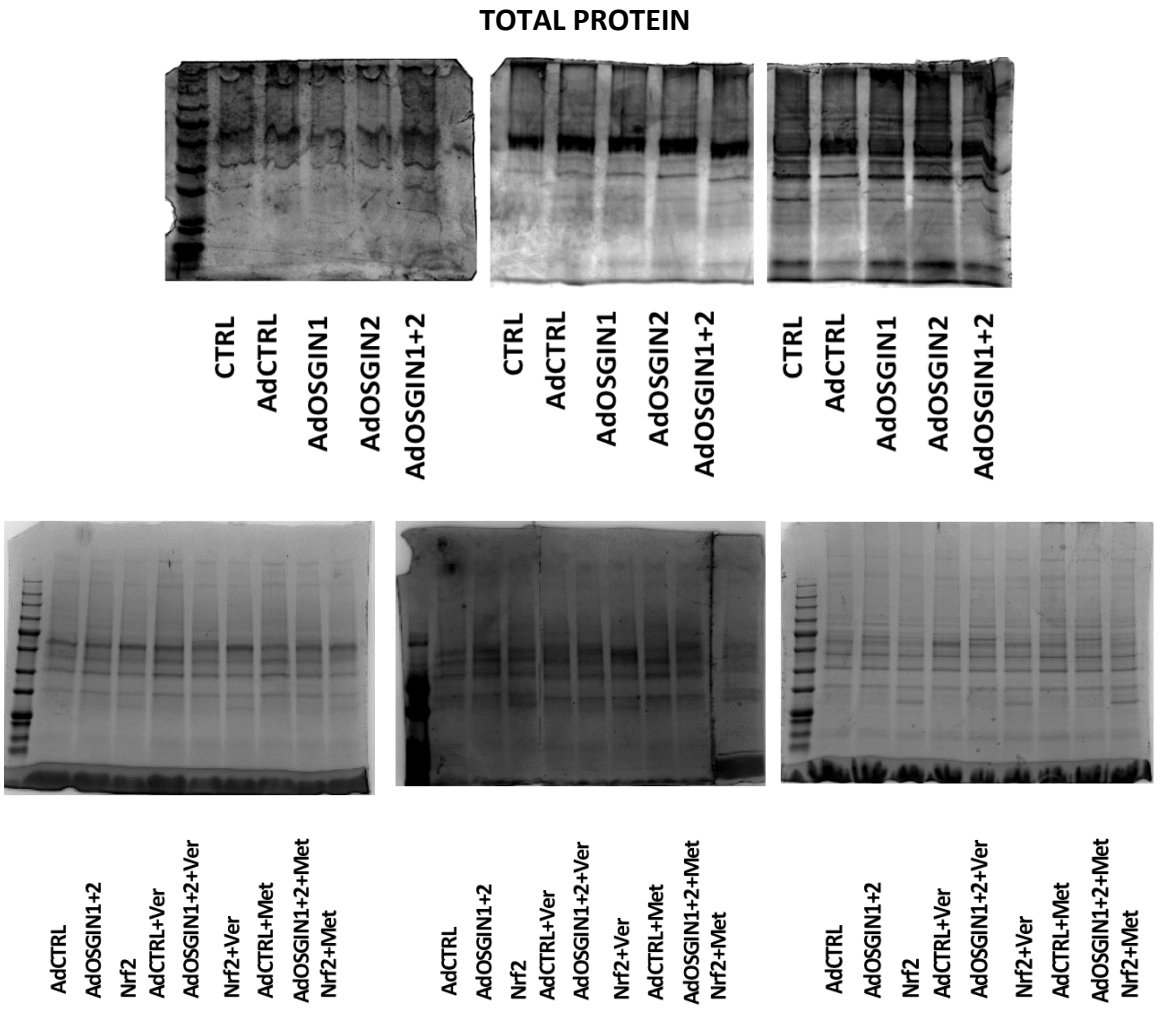

Figure 2.2). HCAECs were lysed and densitometry of western blot bands was calculated.

2.7.4 SDS-PAGE and transfer of protein to membrane

Samples were loaded into TGX FastCast premixed 10% acrylamide gels (1mm, BioRad) along with the protein ladder (SpectraTM Multicolor Broad Range Protein Ladder; Thermo Scientific). The gel sandwich was placed into a gel tank (BioRad) and filled with 1X running buffer [3.03 g of Tris base, 14.4 g of glycine, and 1.0 g of SDS dissolved in 1L of ddH_2O]. Electrophoresis was performed at 120 V until the samples progressed through the stacking gel into the resolving gel, after which it was increased to 160 V for 1 hr to allow proteins to migrate and separate according to their molecular weight. After disassembling the

apparatus, the cassette was opened and the gels were incubated with a towbin buffer 1X [3.03 g Tris base, 14.4 g glycine and Methanol (100 ml for semidry transfer system and 200 ml for wet transfer system) in a total volume of 1L of ddH_2O] for 15 minutes before the transfer reaction. Transfer onto pre-prepared membranes Amersham Protran supported nitrocellulose (0.45 µm pore size) or polyvinylidene difluoride (PVDF) membrane (Immobilon supported (0.45 µm pore size) was achieved using either a semidry transfer system (protein size less than 90 kDa, BioRad Trans-Blot SD Cell Semi-Dry Transfer), or wet transfer apparatus (protein size more than 90 kDa, Invitrogen™ Novex™ XCell SureLock). Transfer apparatus was set up according to manufacturer's instructions and electrophoresis was carried out at 18 V for 1 hr for the semidry system and 35 V for 1 hr for the wet transfer apparatus. After completion, the membranes were rinsed in Tris buffered saline (TBS) Tween-20 (Sigma) (TBS-T) 1X and used for immunoblotting.

2.7.5 Immunoblotting

Membranes were blocked in Bovine Serum Albumin (BSA) (Sigma) or Milk (Marvel Dried Skimmed Milk) (see Table 1 Appendix for full information) in TBS Tween-20 (Sigma) (TBS-T) for 1 hr and then incubated with the appropriate primary antibody (Table 1 Appendix) at 4°C overnight. Membranes were washed 3 times for 5 minutes before incubation with appropriate horseradish peroxidase (HRP) conjugated-secondary antibody for 1 hr at room temperature with gentle agitation. Membranes were washed again for 3 times for 5 minutes and incubated with 2ml of enhanced chemiluminescence (ECL) solution (Immobilon ECL substrate A and substrate B 1:1) for 2 minutes. Images were captured using the BioRad blot scanner. All experiments were conducted in triplicate.

2.8 RNA extraction

For RNA analysis, a confluent layer of ECs in a 24 well plate were placed on ice, culture media was removed and HCAECs were washed twice with cold 1X PBS. Cells were lysed using 300µl RTL Buffer (NORGEN) with (1% v/v MercaptoEthanol). Wells were scraped using a scraper and the buffer/cell suspension was collected in cold 1.5 ml Eppendorf tubes, RNA/DNAse nuclease free. Eppendorf tubes were stored in a -80°C freezer ready for RNA extraction.

Subsequently, Total RNA was extracted using the RNeasy Mini Kit (NORGEN) according to the manufacturer's protocol. Briefly, Norgen Kit lysis buffer was used for cell lysis. gDNA was removed through DNA binding column by centrifugation. 200 µl of 96 – 100% ethanol was added and centrifugated in an RNA binding column. After several washes and centrifugation steps the RNA was eluted and the concentration measured by nanodrop (One Microvolume UV-Vis Spectrophotometer - Thermo Scientific).

2.8.1 Measuring RNA concentration

RNA sample concentrations were measured using a NanoDrop (One Microvolume UV-Vis Spectrophotometer - Thermo Scientific). A blank was measured using elution buffer (NORGEN). The relative purity of samples was assessed by examining the 260/230 and 260/280 ratio, with optimal results reading between 1.95 and 2.05 for the 260/280 ratio and 2.0-2.2 for the 260/230 ratio.

2.8.2 Reverse transcriptase-polymerase chain reaction (RT-PCR)

250 ng of RNA was reverse transcribed into cDNA with a random primer by Quantinova reverse transcriptase (RT) (Quantinova) following manufacturer's instruction in a final volume of 20µl. RNA was normalised at 250 ng in order to ensure equal loading. Samples were incubated at 25°C for 5 minutes, 42°C for 30 minutes and 85°C for 5 minutes. 1 µl of cDNA product (relative to RNA amount) was amplified by standard PCR with Taq DNA polymerase (Sensifast, SybrGreen, LOW-ROX Kit, Bioline) and primers (final concentration 60 µM). 20 µl of final product were diluted with 30 µl of nuclease free water for a final volume of 50 µl.

2.8.3 Real-time PCR

Primers were designed using NCBI PrimerBlast and directed to a region of the gene that was incorporated in all splice forms with primers that spanned an intron to prevent

genomic DNA amplification. For each gene, SYBR Green incorporation was used in place of a labelled probe (primer sequences Table 3 Appendix). Glyceraldehyde 3-phosphate dehydrogenase (GAPDH) mRNA quantification was used as a house keeping gene control for each sample. 10 µl PCR reactions containing 4 µl Sybr® Green PCR Master Mix, cDNA template 1 µl, optimised primers 2 µl (final concentration of 1 µM) and 3 µl of H_2O were performed in duplicate for all samples. PCR thermal cycle parameters were: initial 95°C enzyme activation step of 5 minutes, with 40 cycles of 95°C, 15 seconds, 65°C to 70°C anneal step for 30 seconds and 72°C extension step for 30 seconds using Applied Biosystem detector (Applied Biosystem) (Dissociation curve and Amplification plots example Figure 2.3).

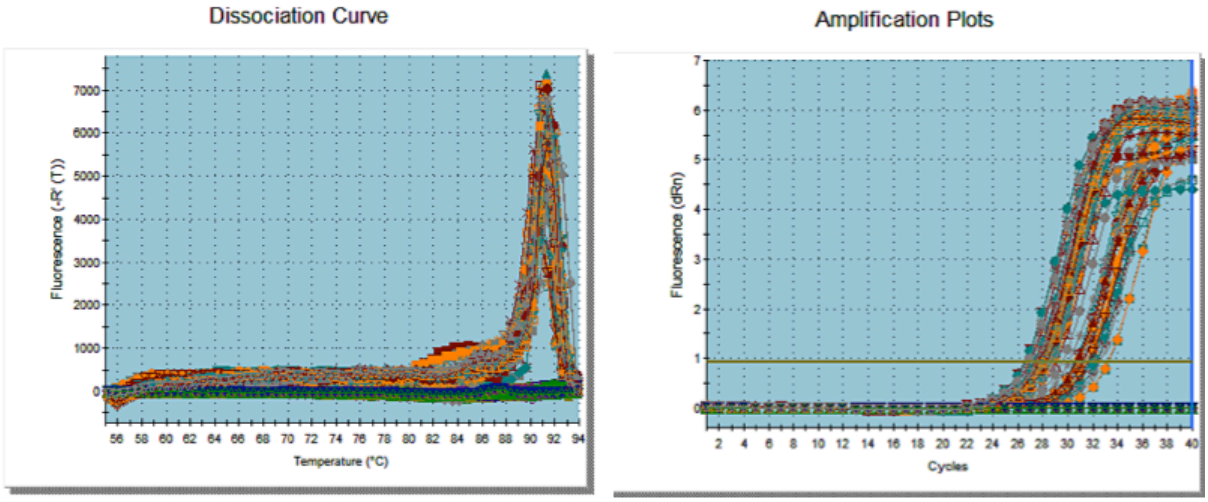

Figure 2.3) Example of dissociation curve and amplification plots during Sybr green qPCR reaction. All primers showed only one pick in relation to the dissociation curve which confirmed their specificity for the gene selected. Amplification plot value was used to calculate relative mRNA abundance and was defined as the ratio of target gene expression level to GAPDH mRNA expression. Primer sequences can be found in Table 3 (Appendix).

2.8.4 RNAseq data analysis

Illumina workflow with the TruSeq® Stranded mRNA Sample Preparation Kit was used in order to prepare Strand-specific RNA-seq libraries. On the Illumina platform of HiSeq4000 65bp paired-end reads were generated from each sample. FastQC was used to analyse the fastq files generated [326], any contaminated barcodes and low-quality reads were trimmed using Trimmomactic. STAR-2.5.3a was used for all library alignments to the hg38 assembly of the human genome and only the unique alignments were reported for each

read. The mapped reads were also counted with STAR at gene level against gencode.v25.annotation.gtf. All the statistical analysis of data were analysed using R programming [327]. Normalisation of the counts data was made and R package RUVSeq was used in order to remove the donor effect. R package of DESeq2 was used to evaluate differentially expressed genes between groups of experimental data sets. The cluster analysis was carried out on the DE genes identified with DESeq2 using a padj cut off of 0.05 with gplots [328] Through the use of Ingenuity Pathway Analysis (IPA), it was possible to generate the predicted upstream regulators and altered canonical pathways (QIAGEN Inc. https://www.qiagenbioinformatics.com/products/ingenuity-pathway-analysis).

2.9 Proliferation analysis using Bromo-deoxyuridine (BrdU) incorporation assay

To quantify proliferation, BrdU incorporation was assessed for a period of 4 hrs at the end of each experiment. $5x10^4$ HCAECs were seeded in 24 well plates. The next day ECs were transduced with adenoviral vector for AdOSIN1, 2 and both together. After 16 hrs, the media was replaced and on the morning of day 5, BrdU (10 µM, Sigma) was added to the media. BrdU was incubated with the ECs for 4 h. Cells were washed (ice-cold PBS) and fixed in 70% ethanol. The incorporated BrdU was detected by immunocytochemistry (ICC) using a mouse anti-BrdU primary antibody (1/500, Sigma B8434), biotinylated goat anti-mouse secondary (1/250, Sigma) and Extravidin-HRP (1/250, Sigma E2886), and visualised with diaminobenzidine (DAB) staining. Counterstaining was done by using hematoxylin (Mayer's Hematoxylin Sigma) for 2 minutes. 10 images at 10X magnification were taken from each well by using M165 FC stereomicroscope for assessment of BrdU staining. Results were calculated counting the percentage of BrdU positive cells (stained in brown see chapter 3 section 3.4.3) compared to the total number of cells per each FoV.

2.9.1 Cell size calculation

Cellular size was analysed using FIJI Image J particle analyser. Five FoV were evaluated per conditions. Firstly, set scale was established in order to obtain measurements in the metric system. Next, the images were modified to 16-bit and endothelial cell size was calculated using analyse particles plug-in (shown below).

FIJI Image J custom particle analyser plug-in code was modified in order to exclude overlap which improved the accuracy of cell size measurement. Cell area was measured and optimised based on 4 different measurements, as shown in figure 2.4. Custom code

particle analyser was designed to measure the external cell size edge (1), the internal oval shape of the cell (2), the long internal axis delimited inside the cell (3) and the internal circumference area. During the calculation only the areas which were measured at least twice, are selected (overlapping measurements are removed from the calculation) in order to obtain accurate measurement area (5).

Custom Code:

```
call("ij.plugin.filter.ParticleAnalyzer.setFontSize", size);
call("ij.plugin.filter.ParticleAnalyzer.setLineWidth", width);
Where pxls = µm
void createEllipse(ImagePlus imp) {
      IJ.showStatus("Fitting ellipse");
      Roi roi = imp.getRoi();
      if (roi==null)
         {noRoi("Fit Ellipse");
Finds the index of the upper right point that is guaranteed to be on convex hull
   int findFirstPoint(int[] xCoordinates, int[] yCoordinates, int n, ImagePlus imp) {
      int smallestY = imp.getHeight();
      int x, y;
      for (int i=0; i<n; i++) {
         y = yCoordinates[i];
         if (y<smallestY)
         smallestY = y;
      }
      int smallestX = imp.getWidth();
      int p1 = 0;
      for (int i=0; i<n; i++) {
         x = xCoordinates[i];
         y = yCoordinates[i];
         if (y==smallestY && x<smallestX) {
            smallestX = x;
            p1 = i
....
if (roi==null && imp.getOverlay()==null) {
         IJ.error("Create Mask", "Selection, overlay or threshold required");
         return;
/** Converts a line selection into an area selection. */
   public static Roi lineToArea(Roi roi) {
      Roi roi2 = null;
      if (roi.getType()==Roi.LINE) {
         double width = roi.getStrokeWidth();
         if (width<=1.0)
            roi.setStrokeWidth(1.0000001);
         FloatPolygon p = roi.getFloatPolygon();
         roi.setStrokeWidth(width);
         roi2 = new PolygonRoi(p, Roi.POLYGON);
         roi2.setDrawOffset(roi.getDrawOffset());
      } else {
         roi = (Roi)roi.clone();
         int lwidth = (int)roi.getStrokeWidth();
         if (lwidth<1)
            lwidth = 1;
         Rectangle bounds = roi.getBounds();
         int width = bounds.width + lwidth*2;
         int height = bounds.height + lwidth*2;
         ImageProcessor ip2 = new ByteProcessor(width, height);
         roi.setLocation(lwidth, lwidth);
         ip2.setColor(255);
         roi.drawPixels(ip2);
         ip2.setThreshold(255, 255, ImageProcessor.NO_LUT_UPDATE);
         ThresholdToSelection tts = new ThresholdToSelection();
         roi2 = tts.convert(ip2);
         if (roi2==null)
            return roi;
         if (bounds.x==0&&bounds.y==0)
            roi2.setLocation(0, 0);
         else
            roi2.setLocation(bounds.x-lwidth/2, bounds.y-lwidth/2);
      }
```

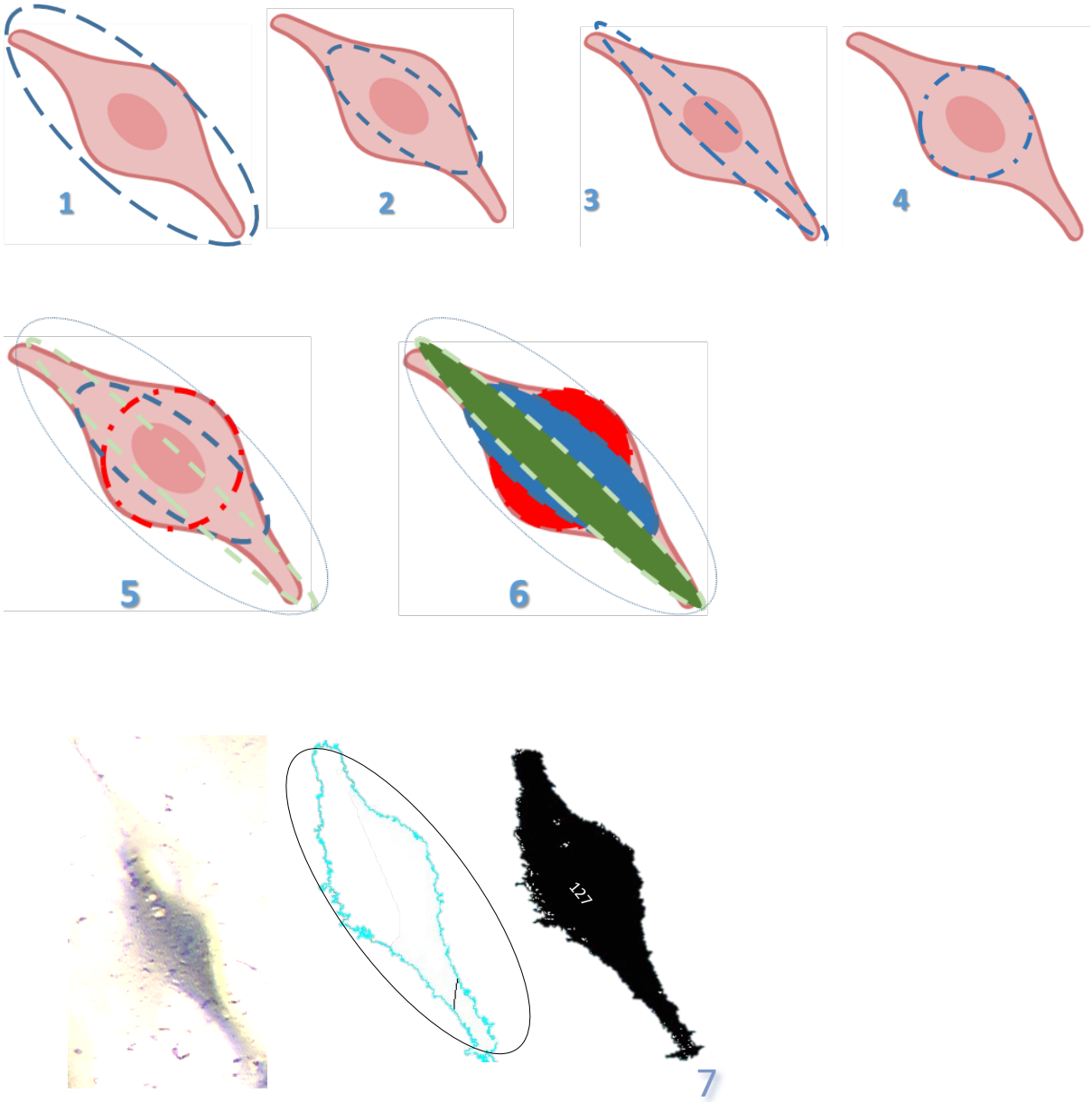

Figure 2.4). Schematic representation of the FIJI Image J analyser particle plug-in. (1) measures the external edge of the cell to delimitate the area of measurement. (2) measures the internal cell oval shape area. (3) measures the cell area along the long axis. (4) measures the internal cell circumference. (5 and 6) show the total cell area calculation, without measuring the overlapping segments. (7) represents a real cell on the left, cell edge measurements are shown in the centre and final area calculation is shown on the right image.

2.9.2 Immunocytochemistry

AdOSGIN1 and AdOSGIN2 transfected HCAECs were fixed in cold 4% paraformaldehyde for 10 minutes. Cells were permeabilised with 0.1% triton, blocked in 20% goat serum and probed with rabbit anti-OSGIN1 (1:100, Biorbyt) and rabbit anti-OSGIN2 (1:75, Biorbyt), and rabbit anti-VE-cadherin (Cell Signalling) followed by goat anti rabbit Alexa Fluor 488 (1/200, Invitrogen). Further staining was carried out with mouse anti-Vinculin (1/400,

Sigma), mouse anti-βcatenin (1/200, BD Transduction Laboratories), mouse-mab137 (1/100, Sigma), followed by goat anti mouse Alexa Fluor 594 (1/200, Invitrogen). In combination with the previous staining, rhodamine-labelled Phalloidin (1/250, Sigma), or anti-Tubulin (Already conjugated (Green) (1/1000, Abcam)) were added. Autophagic marker expression related to classical autophagy and CMA were evaluated. Anti-HSP70 (1:400, Abcam), anti-p62 (1:200, Abcam) and anti-LAMP1 (1:100, Abcam) were used to verify protein accumulation (antibody titration Table 2.4).

Table 2.4. Primary Antibodies used in ICC analysis

Antibody	**Type**	**Dilution**	**Company**
OSGIN1	Rabbit	1:100	(Biorbyt orb100666)
OSGIN2	Rabbit	1:75	(Biorbyt orb185683)
VE-cadherin	Rabbit	1:400	(Cell Signalling D87F2)
β-Catenin	Mouse	1:100	(BD Transduction Laboratories 610153)
Vinculin	Mouse	1:400	(Sigma V4505)
Mab113	Mouse	1:100	(Abcam ab92824)
Tubulin	Already conjugated (Green)	1:1000	(Abcam ab64503)
Phalloidin	Already conjugated (Red)	1:250	(Sigma P1951)
HSP70	Rabbit	1:400	(Abcam ab45133)
LAMP1	Rabbit	1:100	(Abcam ab24170)
SQSTM1/p62	Mouse	1:200	(Abcam ab56416)

Secondary Antibody description

Alexa fluor488	Anti-mouse or rabbit	1:200	Invitrogen
Alexa fluor647	Anti-mouse or rabbit	1:200	Invitrogen

2.9.3 Immunofluorescence on Mouse Aortas

N = 10 mice were exposed to cigarette smoke [329] for 3 months, and a second group (n= 9 Ctrl) of mice not exposed to cigarette smoke were used as controls. The mice were harvested, and aortas were isolated and embedded in optical OCT media for sectioning. 8μM frozen sections were fixed in ice cold acetone before immunofluorescence was performed using the antibodies described in 2.9.2.

2.9.4 Senescent-associated β-galactosidase staining

4% Paraformaldehyde (PFA) fixed HCAECs were rinsed with ice-cold PBS pH 6.0 and submerged in SA-β-Gal staining solution [1 mg/ml 5-bromo-4-chloro-3-indolyl β-d-galactopyranoside (X-gal), 5 mM $K_4Fe(CN)_6$, 5 mM $K_3Fe(CN)_6$, 150 mM $NaCl_2$ and 2 mM $MgCl_2$ titrated with 1M NaH_2PO_4 to pH 6.0] and incubated for 16 hrs at 37°C. After staining, HCAECs were rinsed with ice-cold PBS pH 6.0 micrographs were taken with a Leica M165 FC stereomicroscope. Blue stained cells were considered positive for senescence and quantified (see chapter 3 section 3.4.6). The percentage of positive cells were calculated compared to the total number of cells in the well.

2.10 Flow cytometric analysis

For cell cycle analysis, cells (1×10^5) were washed twice with ice-cold PBS and dislodged with 1.5 ml 1X trypsin/EDTA. Subsequently, trypsin was neutralised adding 5 ml of MV2 media. Cells were centrifugated (300 g) for 5 min at 4°C and the pellet was resuspended in 500 µl 1X PBS. 500 µl of cell suspension was fixed adding 3 ml of ice cold 75% ethanol drop by drop and stored for 16 hrs at -20° C. The following day the cell suspension was centrifuged at 500 g for 10’ at 4° C, the EtOH was aspirated and pellet was washed with 2 ml 1X PBS. Cell suspension was incubated with 25 µl of Propidium Iodide (PI) (1mg/ml) and 10 µl (20mg/ml) of RNase in 1X PBS for 30 min at 37°C in the dark. Samples were stored at 4°C before analysis. Cell analysis was performed using a FACScan flow cytometer (FACS Calibur, BD Transduction Laboratories). Data obtained from the cell cycle distributions were analysed using Modfit software.

2.11 Computational docking

In-silico analysis was performed on a HP Pavilion workstation (Intel(R) core i7-2600 @ 3.4 GHz, 8 GB) installed with Windows 7 operating system. The structure of the inhibitor VER-155008 was constructed, modelled, and energy minimized in neutral form by standard molecular mechanics procedures. The crystal structures of human HSP70 NBD in complex with Ver155008, and HSC70/BAG1 in complex with another small molecule inhibitor, were retrieved from the RCSB Protein Data Bank (PDB ID: 4IO8; resolution: 2.58 Å, and PDB ID: 3LDQ; resolution: 1.9 Å, for HSP70 and HSC70, respectively). The selection of proteins was achieved utilizing a well-established cross docking protocol [330, 331]. The target proteins were prepared using AutoDock 4.25. Briefly, water molecules and other ions were

removed while hydrogen atoms were added using the ADT module implemented in AutoDock. The charges were adjusted using Gasteiger charges module for proteins implemented in AutoDock. Docking was performed with AutoDock version 4.2 using the empirical free energy function and the Lamarckian protocol. The results were analysed for the presence of hydrogen bonding, hydrophobic and π-π interactions between hits and the active site of the protein.

2.12 Statistical analysis

Data are presented as means ± standard error of the mean (SEM) of ≥3 independent experiments. Each individual experiment used HCAECs from a different donor. One-way ANOVA test was used to determine the difference between three or more groups. Two-way ANOVA was used to evaluated 3 or more groups with more than one variable. P-values <0.05 were considered statistically significant. Graph pad prism software was used to perform statistical analysis (GraphPad Software, La Jolla, CA).

CHAPTER 3:
THE EFFECT OF OSGIN1 AND OSGIN2 ON ENDOTHELIAL CELL PROLIFERATION

CHAPTER 3: THE EFFECT OF OSGIN1 AND OSGIN2 ON ENDOTHELIAL CELL PROLIFERATION

Previous work by Dr White's lab and others established that elevated shear stress imposes a significant effect on endothelial behaviour and renders endothelial cells very sensitive to mediators of endothelial dysfunction [102]. Endothelial erosion tends to occur overlying stenotic atherosclerotic plaques, exposed to very elevated levels of shear stress [16]. Smoking is a particular risk factor for endothelial erosion [16, 53] and is known to induce endothelial dysfunction [332, 333]. The White group have extended this work, investigating the haemodynamic environment permissive for plaque erosion, through reconstruction of arterial geometries from OCT-defined erosion cases with computation fluid dynamic assessment of flow.

In an attempt to better understand the mechanism behind endothelial plaque erosion and due to a lack of a spontaneous experimental animal model, White's group manufactured an *in vitro* model of erosion. As mentioned above, smoking is one the few risk profiles known to increase endothelial erosion development, and in the lungs the level of inflammation (TNFα) is much higher in smokers vs non-smokers. Therefore, confluent monolayers of HCAECs were exposed to OSS, LSS or ESS and treated with CSE and/or TNFα. Cell detachment is observed at ESS with the addition of both TNFα and CSE. Treatment with an apoptosis inhibitor (Z-VAD-FMK) or an MMP inhibitor (GM6001) does not prevent cell loss [113]. Transcriptomic analysis indicated strong activation of NRF2, which were confirmed by further analysis [116]. In homeostatic conditions NRF2 is considered cytoprotective [74, 116, 122]. To determine the role of NRF2 in cell detachment, pharmacological activators of NRF2 (sulforaphane or isoliquiritigenin) were added to the culture system with CSE and TNFα. Further activation of NRF2 triggered almost complete cell detachment, indicating chronic hyperactivation of NRF2 may contribute, rather than protect from cell loss and that chronic activation of NRF2, may contribute to pathology, promoting endothelial detachment.

To evaluate this theory, the current project aims to investigate the effects of OSGIN1 and OSGIN2, which are significantly elevated under conditions of cell detachment in the '*in vitro* model of erosion' and are regulated by NRF2 [102]. Defining the role these genes play

in cell biology and any contribution they have in cell detachment of ECs may open up novel therapeutic strategies.

This project's initial aims were to evaluate the mechanism underpinning cigarette smoke extract induced two NRF2 regulated genes, OSGIN1 and OSGIN2, and determine whether their chronic upregulation mediates the detrimental effects of NRF2 activation. We hypothesise that OSGIN1 and 2 could potentially play a role in endothelial erosion. The first objective investigated the role of OSGIN1 and OSGIN2 using HCAECs transduced with AdOSGIN1 or AdOSGIN2 or both together.

In 2012 Hu *et al* described the role of OSGIN1 on U2OS cells as a target gene of p53, a gene involved in apoptosis and cell cycle. It has been suggested that p53 has a proapoptotic role by regulating the cytochrome *c* release in mitochondria [196]. Hu *et al* observed that p53 promoted the trans- and co-localization of OSGIN1 from the nucleus to the mitochondria. This led to the formation of mega-mitochondria and an increase in the levels of ROS during the apoptotic process. Therefore, we investigated the cellular location of OSGIN 1 and 2 was investigated to gain insight into potential mechanisms that might influence endothelial cell detachment *in vitro* and thus reflect endothelial erosion which occurs *in vivo*. Furthermore, previous work in White's lab showed that endothelial detachment in the *in vitro* erosion model was not prevented by the use of apoptosis inhibitors, supported by the findings observed during this PhD programme of work [113], suggesting that the process behind endothelial detachment and erosion of plaques may not be related with an apoptotic process. In order to investigate whether AdOSGIN1 and AdOSGIN2 may or may not promote apoptosis, or regulate apoptosis associated genes, multiple experiments were carried out during this PhD project and the results are reported in section 3.2

3.1 Aim and objectives:

Aim: Establish whether OSGIN1 & 2 regulate senescence, apoptosis and necrosis in a dependent or independent manner and determine how these processes may influence endothelial proliferation and detachment.

This will be addressed in the following objectives:

- Smoking is a recognised risk profile leading to endothelial erosion. OSGIN1 and 2 mRNA level is significantly higher in HCAECs exposed to ESS, TNFα and CSE compared to the control in an *in vitro* model of erosion previously developed in Dr White's lab. It has been observed that OSGIN1 and 2 mRNA are upregulated under conditions of EC detachment. Unfortunately, no model of erosion in animals has been officially established. For this reason, protein expression of OSGIN1 and 2 are assessed in sections of aorta of mice exposed to cigarette smoke for 3mo, in order to link together and also validate the *in vitro* OSGIN1 and 2 data with an *in vivo* model.
- Hu *et al* described the role of OSGIN1 as a target gene of p53. It was reported trans- and co-localization of OSGIN1 from the nucleus to the mitochondria. Formation of mega-mitochondria was observed alongside the activation of a process of apoptosis. Herein, ICC staining of OSGIN1 and 2 intend to verify their localisation. Furthermore, a mitochondrial marker is used to evaluate the presence of mega-mitochondria.
- Wang *et al* [185] observed that OSGIN1 inhibited cell proliferation via induction of cell cycle arrest. Cell cycle arrest might be part of the erosion process of endothelial cells. In order to elucidate the role of OSGIN1 and 2 in HCAECs, a BrdU incorporation assay and PI flow cytometry analysis is carried out. Furthermore, in order to strengthen this data, mRNA level of p21 were assessed.
- Constant cell cycle arrest might be related to the activation of senescence pathway. SA-β galactosidase staining is carried out in order to show the association between OSGIN1 and OSGIN2 and cellular senescence. mRNA level of $p16^{InkA}$, which is the main marker indicating cellular senescence process, is evaluated by qPCr.
- Endothelial erosion has been described as an apoptotic process related at least in the distal side of the plaque, which is exposed to OSS. The molecular process on the proximal area and maximal lumen area of stenosis of the eroded plaque which are exposed to ESS have not yet been studied. ECs are mechanosensors and different flow exposure suggests a diverse molecular mechanism. In order to determine whether OSGIN1 and OSGIN2 are involved with cellular apoptosis, caspase assays and western blot analysis were carried out.
- Loss in cell viability and cytotoxicity might also lead to erosion of ECs. In order to determine whether OSGIN1 and OSGIN2 are involved in the reduction of cell vitality and whether their

overexpression is pushing for necrosis, cell viability and level of cytotoxicity in HCAECs is evaluated.

3.2 RESULTS

Dr White's previous work demonstrated a concomitant upregulation of two Nrf2-regualted genes OSGIN1 and OSGIN2 which demonstrates a complex shear-dependent pattern of regulation, with the highest level of expression at elevated flow with the addition of CSE and TNFα [113, 116]. HCAECS (PromoCell) were grown in EC media MV2 (C-22121, PromoCell). Confluent monolayers of HCAECs were exposed to flow for 24 hrs before receiving 3 sequential treatments of 5 ng/ml of TNFα, 10% v/v CSE and combination of both, 16 hrs apart in order to study the stable effects of these treatments on cells.

CSE was created by drawing mainstream (through the cigarette filter) cigarette smoke from a Marlborough Gold cigarette (most popular brand) through 10mls of HCAEC media. The volume of smoke drawn through the media equates to 7 to 8 puffs of an average smoker and therefore approximates to smoking half a cigarette. The CSE was filtered and diluted 10-fold to generate 100mls of CSE in media. One cigarette would therefore equate to 200ml of CSE in media and considering an average person would have approximately 5 litres of blood volume, 10% of the CSE would directly correlate to 25 cigarettes. CSE was applied every 16 hrs for the 3 treatments, based on the activity profile of NRF2 monitored through regulation of HMOX1 transcriptional activity [150].

HCAECs were exposed OSS, LSS and ESS in combination of 5 ng/ml of TNFα, 10% v/v CSE or both together. HCAECs exposed to ESS+CSE+TNFα showed ~30% of detachment compared to the control (ESS). Further analysis showed the highest upregulation of mRNA level of OSGIN1 and OSGIN2 on HCAECs exposed to ESS+CSE+TNFα (Figure 3.1).

Furthermore, the expression of OSGIN1 and OSGIN2 was evaluated in tissue generated from previously performed murine experiments, where mice were exposed to cigarette smoke for 3 months. Immunohistochemical analysis of aortas demonstrated significantly higher protein expression of OSGIN1 and OSGIN2 particularly in the endothelial lumen and tunica intima, compared to control mice (Figure 3.2)

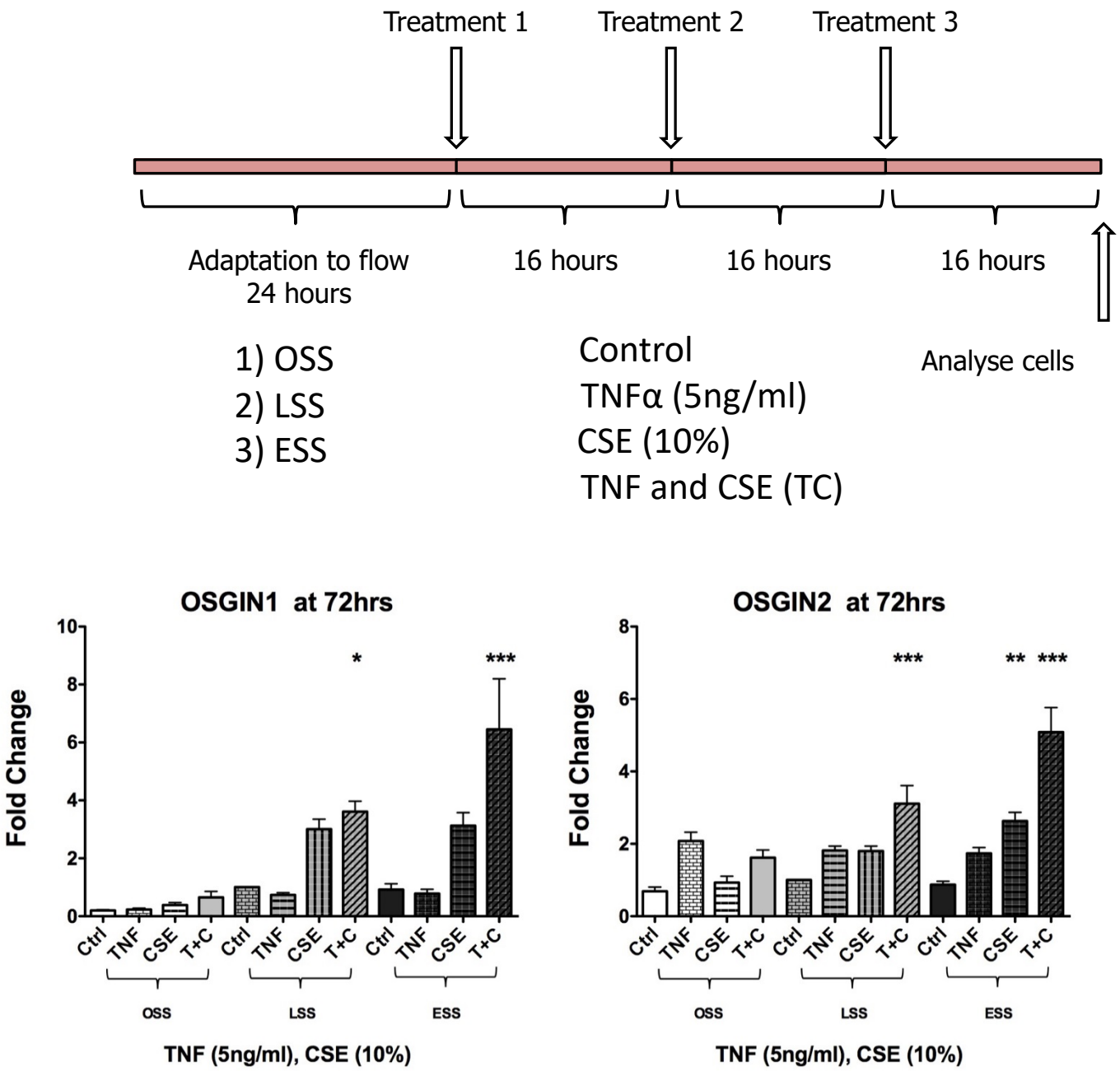

Figure 3.1). OSGIN1 and OSGIN2 mRNA expression in HCAEC cultured for 72hr under OSS, normal laminar (15 dynes/cm2 - LSS) or elevated laminar shear stress (75 dynes/cm2 - ESS). HCAECs were seeded on a 01% gelatine coated glass slide. Cells were exposed to shear stress for 24 hrs to adapt as shown in the timeline above, before 3 treatments of 5 ng/ml of TNFα, 10% v/v CSE, or the combination of both. Treatments were applied to the cells, 16 hrs apart under OSS, LSS or ESS conditions for 72 hrs. Addition of CSE and TNFα (5ng/ml) under ESS resulted in the highest expression of both genes. *P<0.05, **P<0.01, ***p<0.001 OSGIN1 or OSGIN2 vs control.

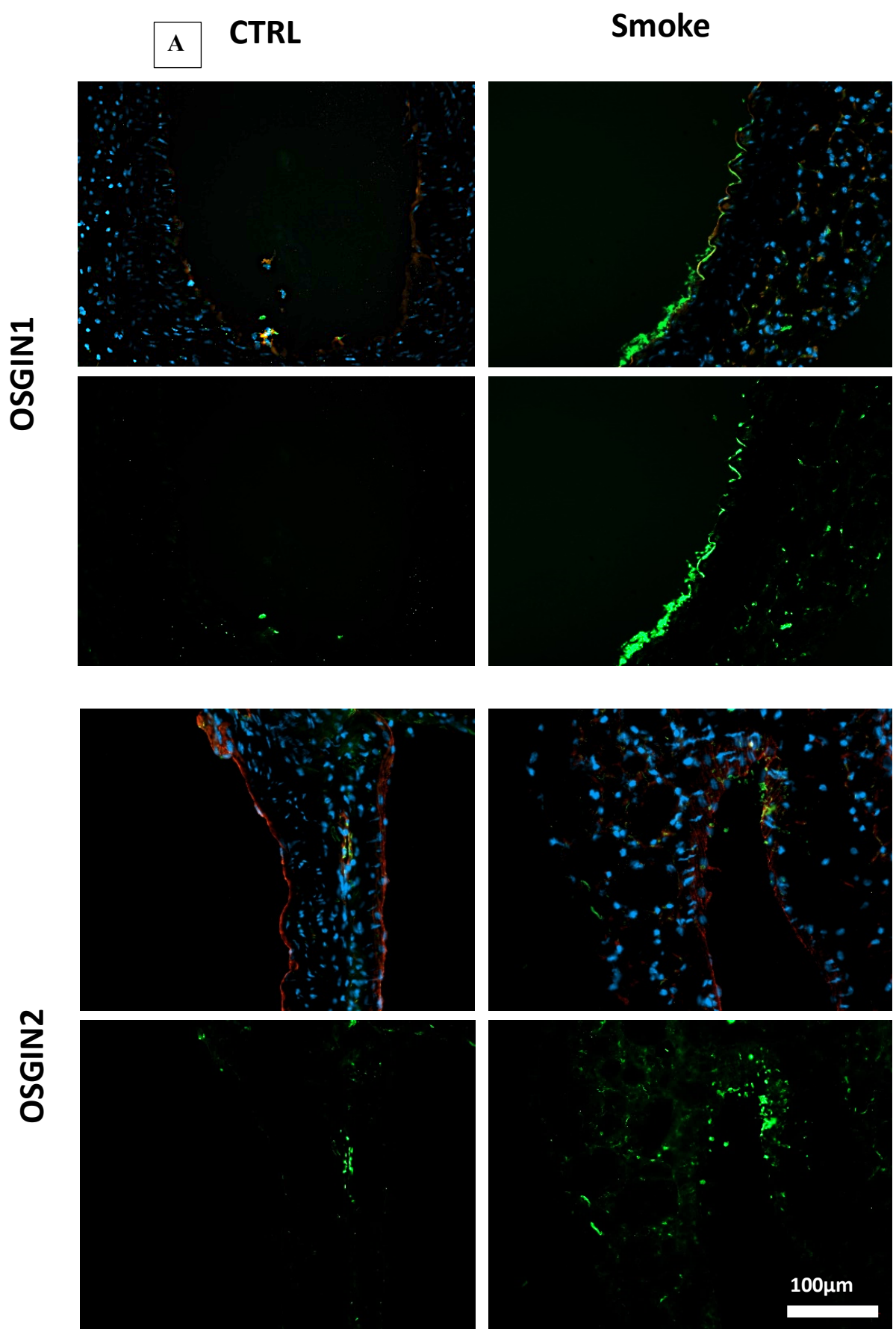
A
CTRL
Smoke
OSGIN1
OSGIN2
100µm

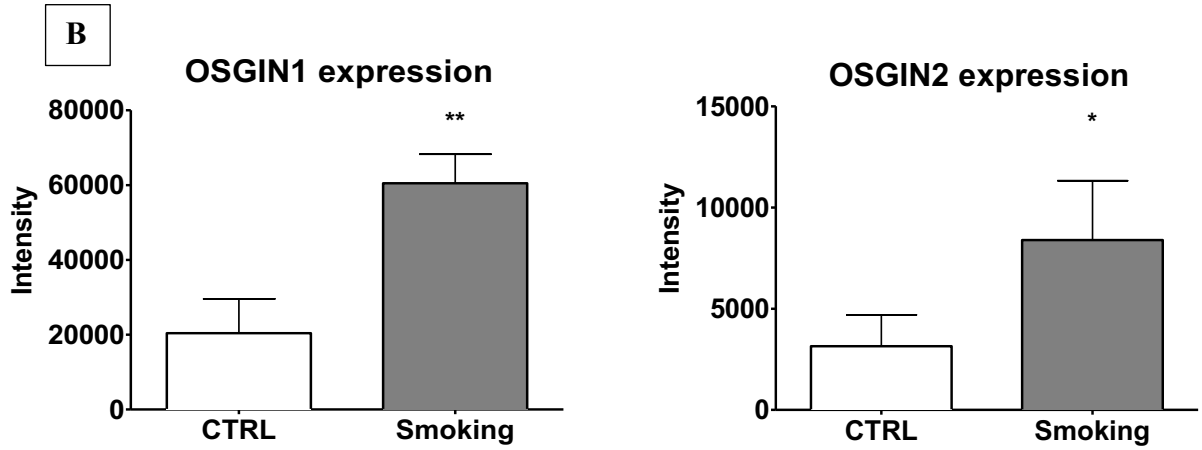

Figure 3.2). **A:** Immunofluorescent analysis of OSGIN1 and OSGIN2 expression in the aortas from mice exposed to cigarette smoke for 3 months vs control. Top two images for each antibody with DAPI counterstain and endothelial marker (rhodamine-labelled GSL1, 1/100 Vector Labs for OSGIN1 and goat anti-CD31, 10μg/ml Bio-Techne AF3628). Bottom two images for each antibody are just the green channel allowing assessment of OSGIN1 or OSGIN2 staining. OSGIN1 was predominantly localised to the endothelium, while OSGIN2 was found throughout the aorta. Images closest to the median values are presented. **B:** Immunohistochemical staining was carried out on 8μM sections of aortas from mice exposed to cigarette smoke for 3 months vs control. Expression of OSGIN1 and 2 were significantly increased in mice exposed to smoke. **P<0.01, n=8 OSGIN1, v 7 control; *P<0.05 n=7 OSGIN2 v 7 control; T-test).

3.4.1 Adenoviral overexpression of OSGIN1 and OSGIN2: mRNA and protein expression validation

To investigate the effects of OSGIN1 and OSGIN 2, adenoviral vectors overexpressing each of the genes were created under the control of human EF1α promoter with mCMV enhancer. Validation of these vectors to elevate OSGIN1 and 2 expression was performed by transducing HCAECs with each vector *in vitro.* Adenoviral OSGIN1 and OSGIN2 overexpression of mRNA by qPCR (Figure 3.3) and protein (Figure 3.4) by western blot, clearly demonstrated that both vectors elevated OSGNI1/2 expression. These experiments were performed in static culture, where the level of OSGIN1 and 2 is normally very low. For consistency with other experiments and to allow the combined overexpression of both vectors total plaque forming units (pfu)/cell of 400 was used. The control was an E1/E3 deleted 'empty' AdCtrl, used at 400 pfu/cell. For individual vector analysis, 200pfu/cell of vector and 200 pfu/cell control was used, for OSGIN1+2 overexpression 200 pfu/cell of each vector was used.

Table 3.1): Adenoviral vector plaque forming units

Adenoviral Vectors	Plaque forming units (pfu)/cell		
AdCtrl	400 pfu/cell AdCtrl		
AdOSGIN1	200 pfu/cell AdOSGIN1	+	200 pfu/cell AdCtrl
AdOSGIN2	200 pfu/cell AdOSGIN2	+	200 pfu/cell AdCtrl
AdOSGIN1+2	200 pfu/cell AdOSGIN1	+	200 pfu/cell AdOSGIN2

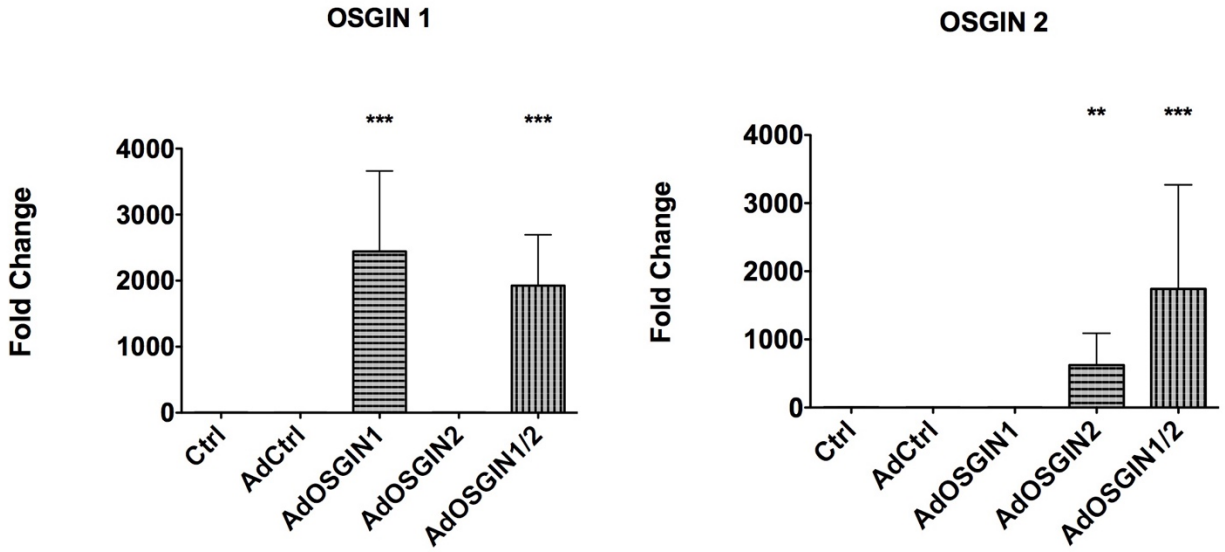

Figure 3.3). **A) B)** Adenoviral transduction of OSGIN1 and OSGIN2 on HCAECs. Real-time PCR for validation of AdOSGIN1 and AdOSGIN2 overexpression level was carried out. Cells were seeded on day 1 into 6 well plates, transduced with adenoviral vector the 2nd day (total pfu/cell of 400). 200 pfu/cell active vector (AdOSGIN1, AdOSGIN2) and 200pfu/cell of control virus were used for single gene transduction; for both OSGIN1 and 2 overexpression this consisted of 200pfu/cell of both vectors; AdCtrl (E1/E3 'empty' Ad vector), was used as the control (400pfu/cell). Virus was removed on 3rd day. ***p<0.001 of AdOSGIN1, AdOSGIN2 and AdOSGIN1+2 in comparison to AdCtrl.

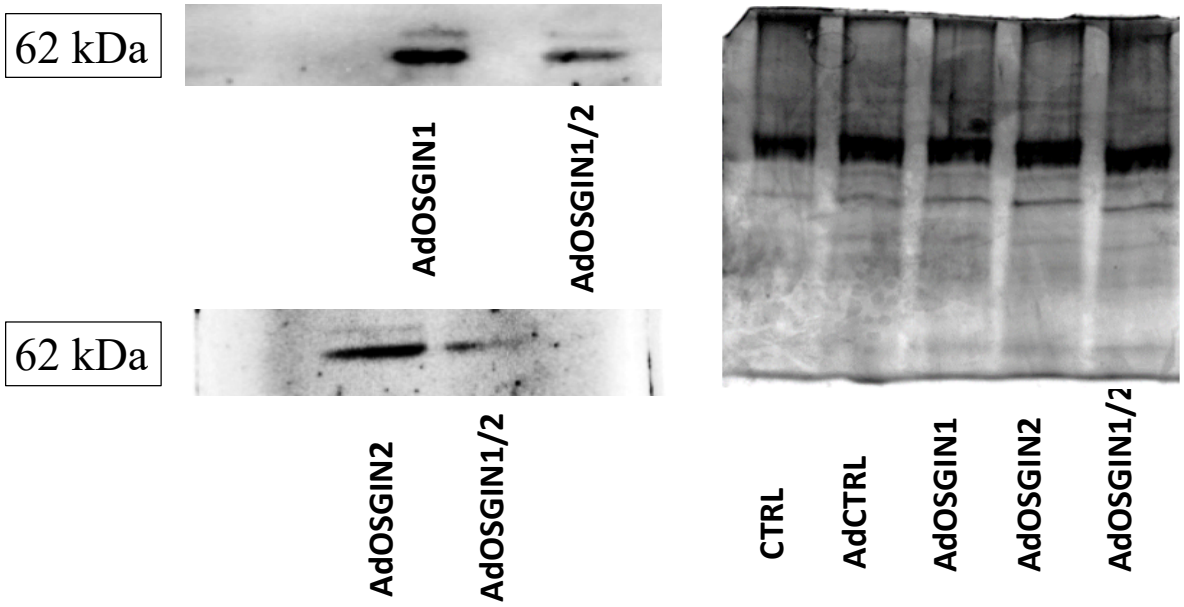

Figure 3.4). Western blot analysis shows overexpression of OSGIN1 and 2 protein levels following Adenoviral overexpression. Adenoviral transduction of OSGIN1 and OSGIN2 on HCAECs. Cells were seeded on day 1 into 24 well plates, transduced with adenoviral vector the 2nd day (total pfu/cell of 400). 200 pfu/cell active vector (AdOSGIN1, AdOSGIN2) and 200pfu/cell of control virus were used for single gene transduction; for both OSGIN1 and 2 overexpression this consisted of 200pfu/cell of both vectors; AdCtrl (E1/E3 'empty' Ad vector), was used as the control (400pfu/cell). Virus was removed on 3rd day. The 4th day the media was removed, cells were washed with 1X PBS. Cell lysis was carried out with following total protein quantification by using BCA Assay Kit (Thermo fisher). 20μg of total protein was loaded in each lane of the polyacrylamide gel.

3.4.2 Cellular localisation of OSGIN1 and OSGIN2

To assess the cellular localisation of both genes and examine the possibility of mitochondrial localisation, ICC analysis of AdOSGIN1 and 2 transduced HCAEC was performed (Figure 3.5).

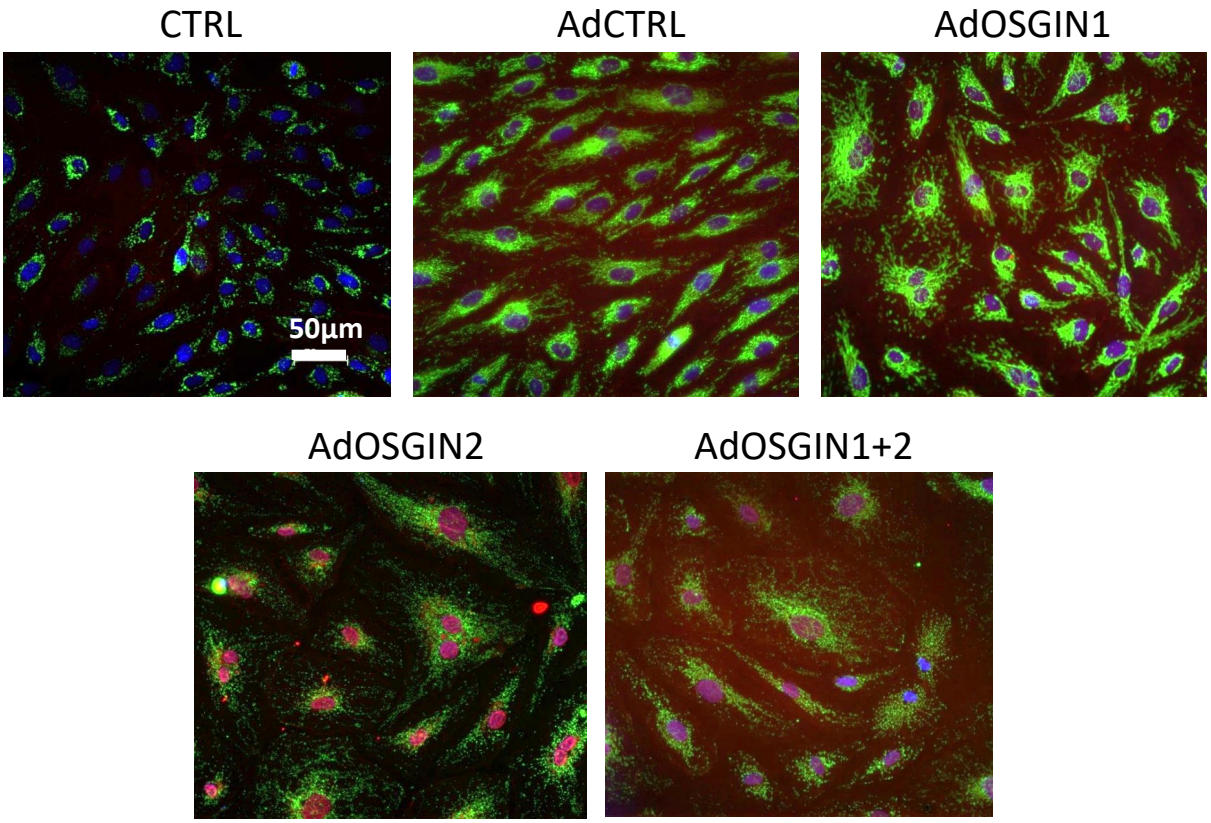

Figure 3.5). Ab byorbyt immunocytochemical staining for OSGIN1 and OSGIN2 (in red) shows nuclear localisation for OSGIN1 & OSGIN2. Mitochondrial staining (in green) confirmed no translocation of OSGIN1 and OSGIN2. Adenoviral transduction of OSGIN1 and OSGIN2 on HCAECs. Cells were seeded on day 1 into 8 well chamber plate previously coated with 0.1% gelatine. Transduction with adenoviral vector was carried out the 2nd day (total pfu/cell of 400). 200 pfu/cell active vector (AdOSGIN1, AdOSGIN2) and 200pfu/cell of control virus were used for single gene transduction; for both OSGIN1 and 2 overexpression this consisted of 200pfu/cell of both vectors; AdCtrl (E1/E3 'empty' Ad vector), was used as the control (400pfu/cell). Virus was removed on 3rd day. The 4th day the media was removed, cells were washed with 1X PBS and fixed in PFA 4% for 20'before immunostaining.

Both OSGIN1 and 2 proteins demonstrated nuclear localisation and did not show any mitochondrial localisation in HCAECs, in accordance with Whang *et al* [199] and in contrast to Hu *et al* [196] where it was shown mitochondrial translocation.

3.4.3 OSGIN1 and OSGIN2 affect cellular proliferation and promotes multinucleated ECs.

In order to investigate whether the overexpression of OSGIN1, OSGIN2 and both together affected cellular proliferation, the BrdU incorporation assay was carried out in HCAECs. This experiment was carried out in five conditions summarised in figure 3.6.

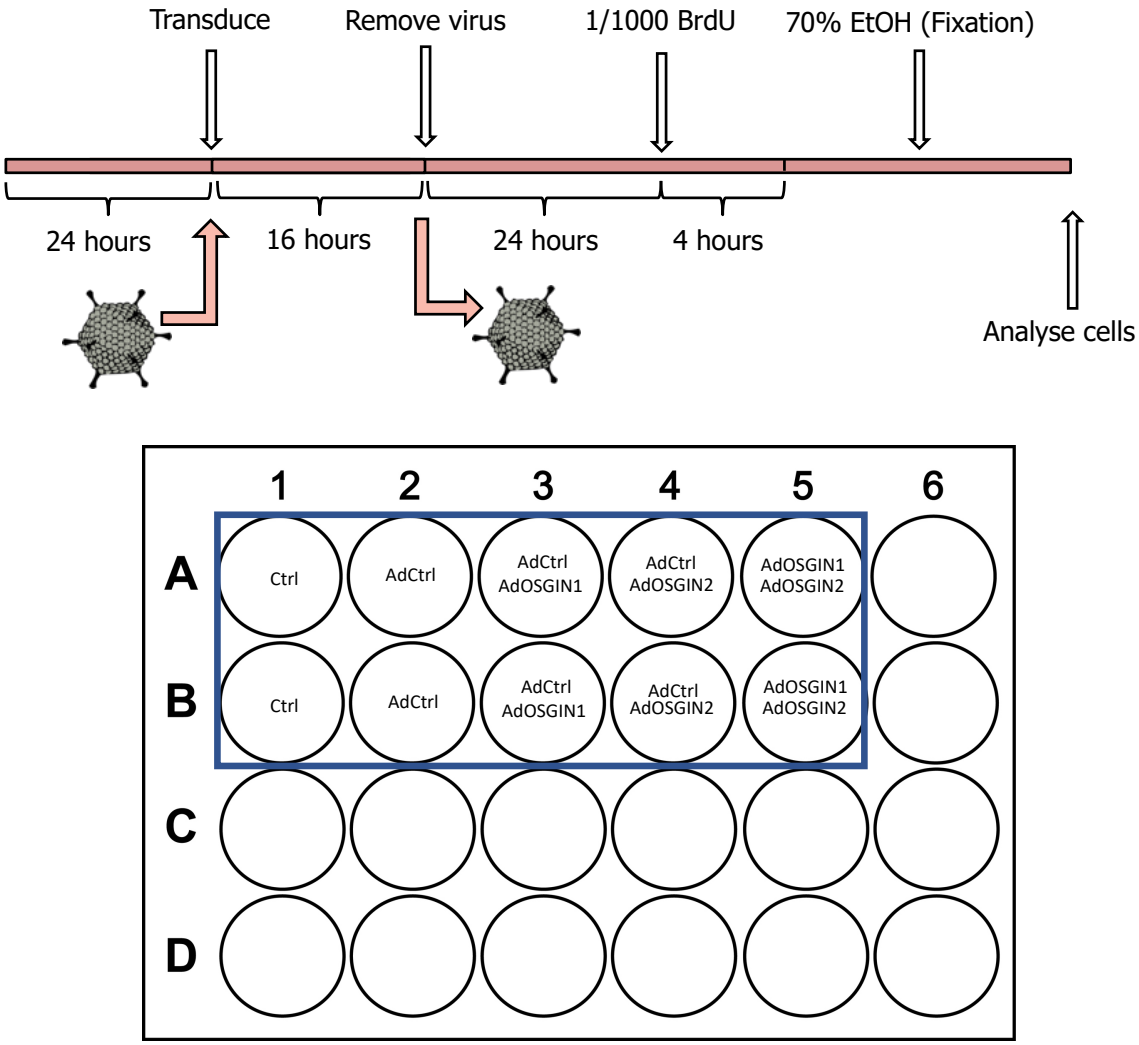

Figure 3.6). Schematic representation of BrdU incorporation assay experiments. The experiments were carried out in duplicate, $5x10^4$ HCAECs were seeded in a 24 well plate. This was repeated 3 times with different batches of HCAEC. After 24 hrs, ECs were transduced with adenoviral vector AdCtrl, OSGIN1, OSGIN2 and AdOSGIN1+2. 16 hrs later the media was replaced. After 24 hrs ECs were incubated with 1:1000 BrdU (10 µM, Sigma). Cells were washed (ice-cold PBS) and fixed in 70% ethanol. The incorporated BrdU was detected by *ICC* using a mouse anti-BrdU primary antibody (1/500, Sigma B8434), biotinylated goat anti-mouse secondary (1/250, Sigma) and Extravidin-HRP (1/250, Sigma E2886), and visualised with DAB staining. Counterstaining was made by hematoxylin (Mayer's Hematoxylin Sigma) for 2 minutes. 10 images at 10X magnification were taken from each well by using M165 FC stereomicroscope for assessment of BrdU staining. Results were calculated counting the percentage of BrdU positive cells (stained in brown see chapter 3 section 3.4.3) compared to the total number of cells per each FoV.

Three different batches of HCAECs were analysed in duplicate in a 24 well plate. HCAECs were split into the 24 well plates on the first day of the experiment, transduced with virus on day 2, which was removed on day 3 with fresh media added. BrdU was added to the media on day four, for the last 4 hrs before fixing and analysis, giving a snapshot of DNA replication for the last 4 hrs of the experiment. Both changes in BrdU incorporation and

morphological differences were observed. AdOSGIN2 showed a higher percentage of BrdU positive cells compared to uninfected control or AdCtrl cells (Figure 3.7A and B). In addition, an increase in cell size with AdOSGIN2 and AdOSGIN1+2 overexpression was observed (quantified in section 3.5) compared to the other conditions.

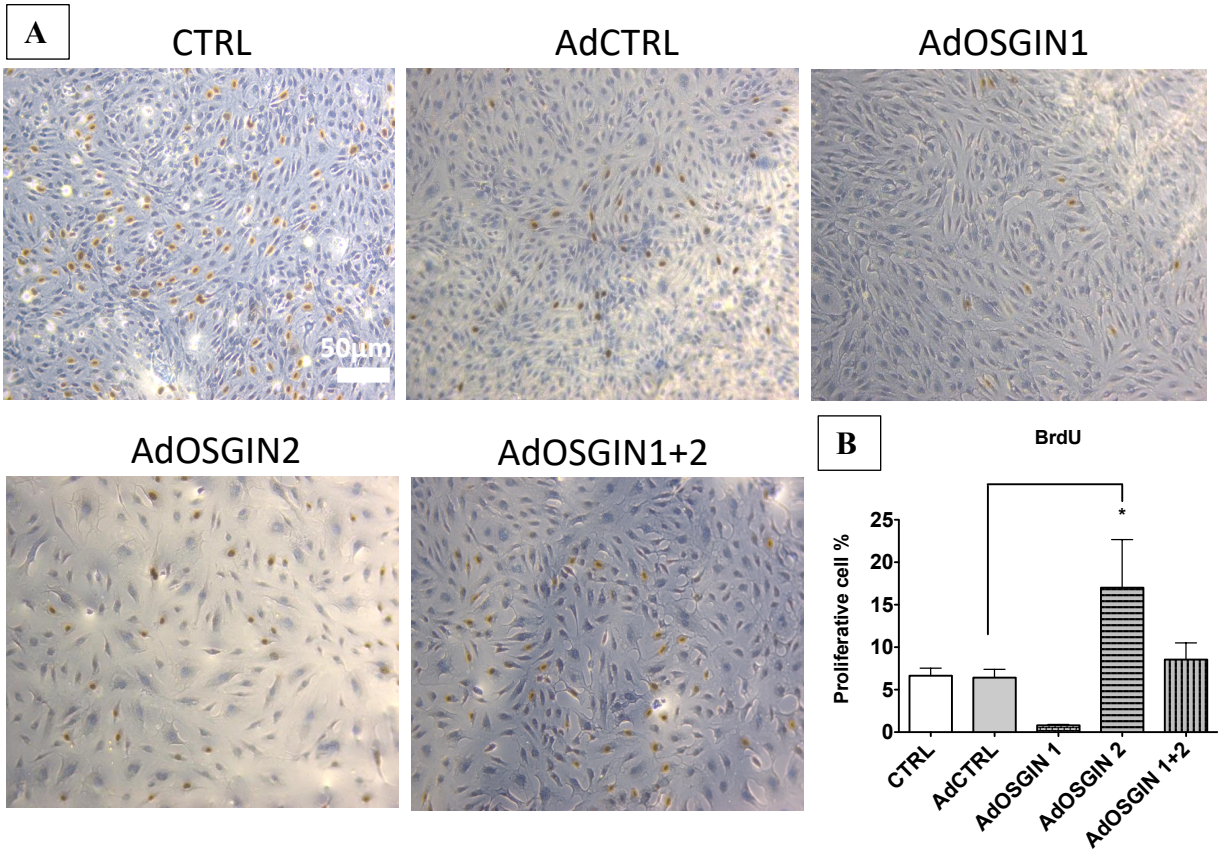

Figure 3.7). A) Proliferation of HCAECs was analysed using the BrdU incorporation assay. HCAECs transfected with AdOSGIN2 show a lower number of cells compared with the other conditions. Furthermore, the cells are bigger in size and have a high rate of replication. HCAECs transfected with ad OSGIN1+2 show a cell size similar to the ad OSGIN2 overexpression conditions, but higher numbers of cells. **B)** The graph shows the effect of OSGIN1, OSGIN2 and OSGIN1+2 ad transfection on cell proliferation. * P<0.05, in comparison with HCAECs on AdOSGIN2 condition VS AdCtrl overexpression.

AdOSGIN1+2 overexpression resulted in numerous multinucleated cells that were not stained by BrdU. The BrdU incorporation occurs during S-phase, so only gives a snapshot of DNA replication after OSGIN1+2 overexpression (Figure 3.8A). BrdU negative cells (highlighted by white arrows) may reflect cells that underwent S-phase prior to BrdU addition, without completing cytokinesis, with the higher numbers in treated conditions suggesting a block of cell cycle between the S-phase and G2-M phase. Calculation of total number of nuclei per cell showed significant increment of multinucleated cells in AdOSGIN2 and AdOSGIN1+2 conditions (Figure 3.8B).

3.4.4 BrdU incorporation assay limitation

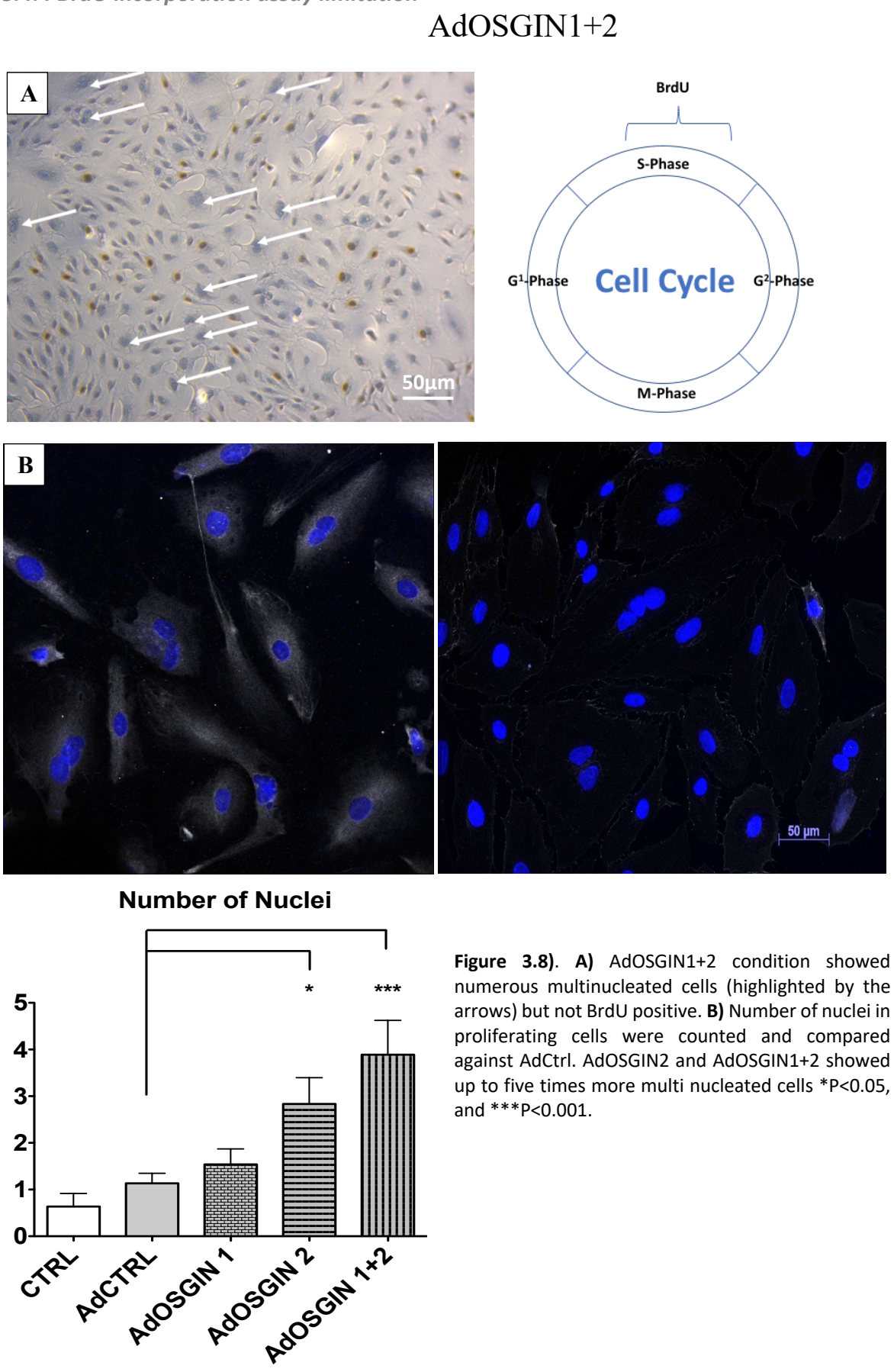

Figure 3.8). **A)** AdOSGIN1+2 condition showed numerous multinucleated cells (highlighted by the arrows) but not BrdU positive. **B)** Number of nuclei in proliferating cells were counted and compared against AdCtrl. AdOSGIN2 and AdOSGIN1+2 showed up to five times more multi nucleated cells *P<0.05, and ***P<0.001.

3.4.5 OSGIN1 and OSGIN2 promote morphological changes in ECs

Multiple analysis was performed in order to dissect the role of OSGIN1 and OSGIN2 and the combination of both in HCAECs. After adenoviral overexpression of the two NRF2-regulated genes, EC morphological changes were observed (Figure 3.9-3.10). Analysis demonstrated that OSGIN2 and 1/2 overexpression significantly increased cell size (Figure 3.10) and height (Figure 3.11) leading to an overall increase in cell volume. Five random FoV per condition were analysed using "FIJI Image J custom particle analyser" (custom code described in section 2.8.1) excluding edges overlap in order to obtained more accurate cell size measurement (Figure 3.10).

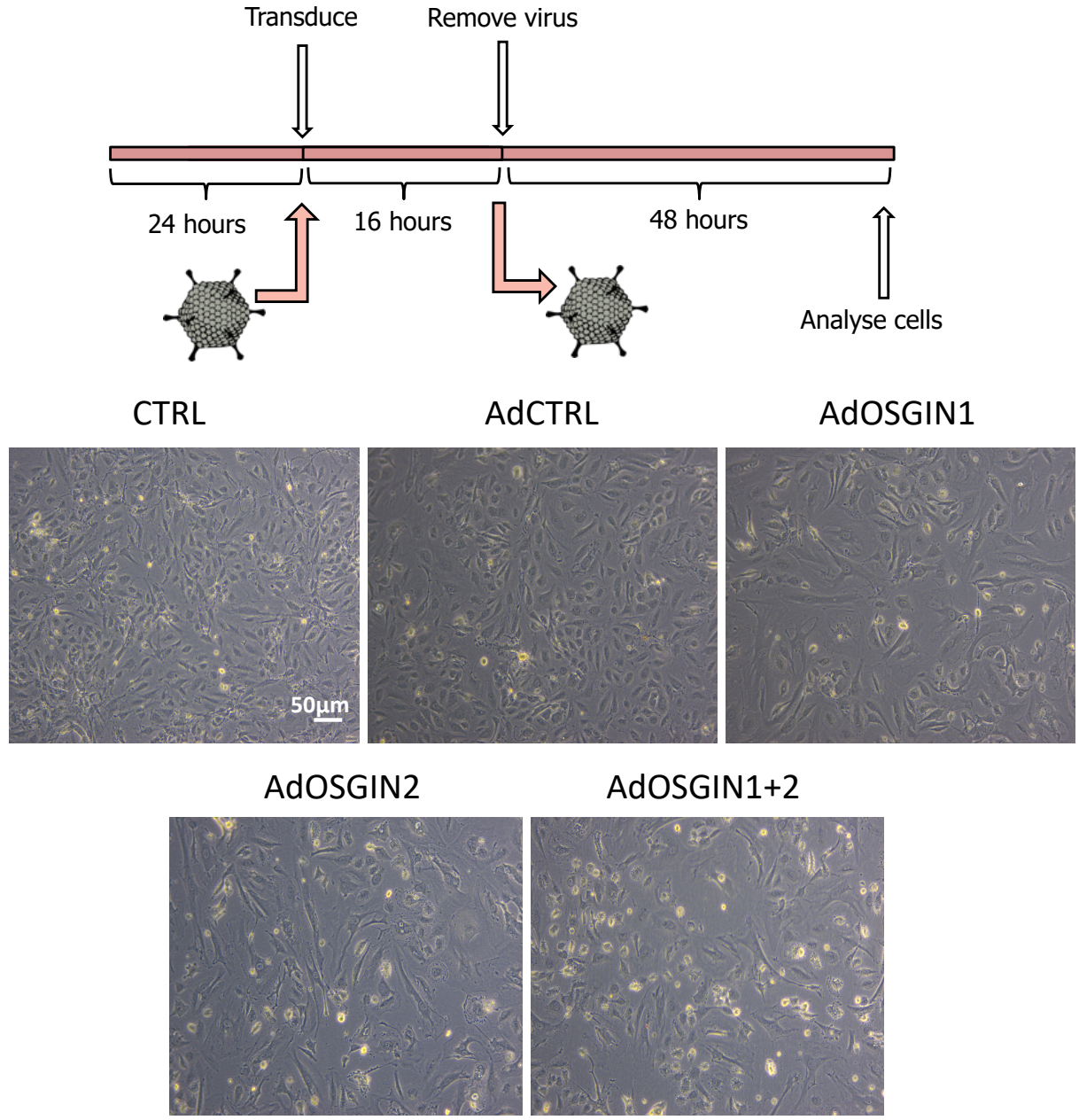

Figure 3.9). HCAEC were seeded into 6 well-plates at 2.0x10^5 cells per well on day 1. Transduction with adenoviral vector was carried out the 2nd day (total pfu/cell of 400 as previously described (section 3.3). 200 pfu/cell active vector (AdOSGIN1, AdOSGIN2) and 200pfu/cell of control virus were used for single gene transduction; for both OSGIN1 and 2 overexpression this consisted of 200pfu/cell of both vectors; AdCtrl (E1/E3 'empty' Ad vector), was used as the control (400pfu/cell). Virus was removed on 3rd day, with cell fixation and image capture 48 hrs later. Five FoV were taken per condition and analysed, representative phase contrast images presented above, with analysis below (Figure 3.10). Three independent experiments were performed, using HCAECs from different donors. HCAECs in static condition after adenoviral overexpression of OSGIN1, OSGIN2 and both together showed increment in size and enlargement followed by retraction and increase height with final detachment (Measurements are shown below).

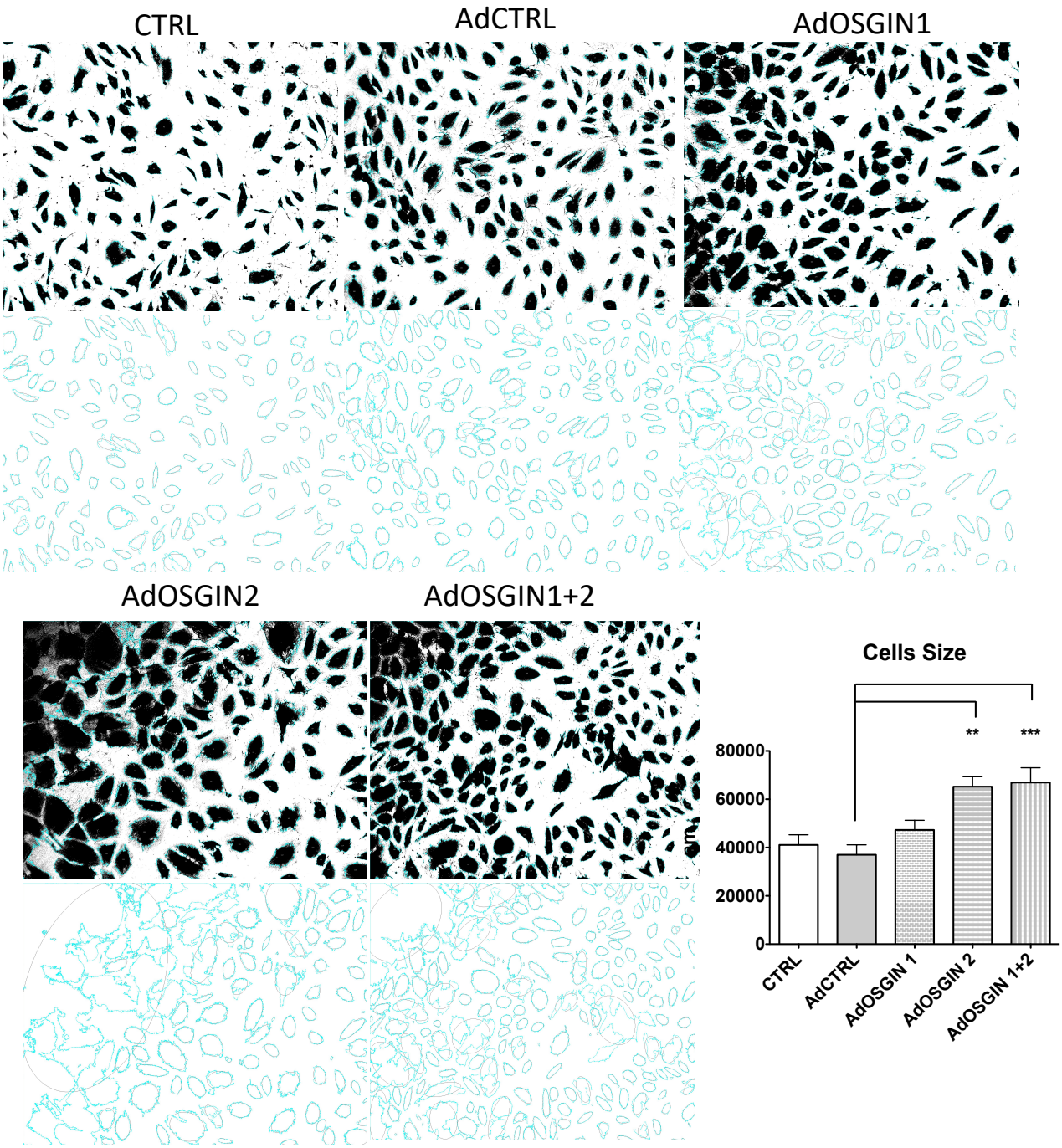

Figure 3.10). HCAEC area analysis was evaluated through FIJI Image J custom particles analyser. Five FoV were analysed, and each cell area was automatically measured. AdOSGIN2 and AdOSGIN12 condition showed an increment in cell size with almost double the size compared to the control and AdCtrl. **p<0.01 AdOSGIN2 and ***p<0.001 AdOSGIN1+2 vs AdCtrl as described above.

Confocal analysis of HCAEC transduced with AdOSGIN1+2 revealed not only that the cells spread out to occupy a greater surface area, they also increased in thickness. Reconstruction of a 3D model from 50 immunostained HCAEC (in triplicate) confocal microscopy Z-Stack plans, demonstrated that the average cell thickness increased by 5-

fold (Figure 3.11). The consequences for such a change in cell shape on exposure to elevated flow might be predicted to amplify the frictional effect of the blood flow on an EC.

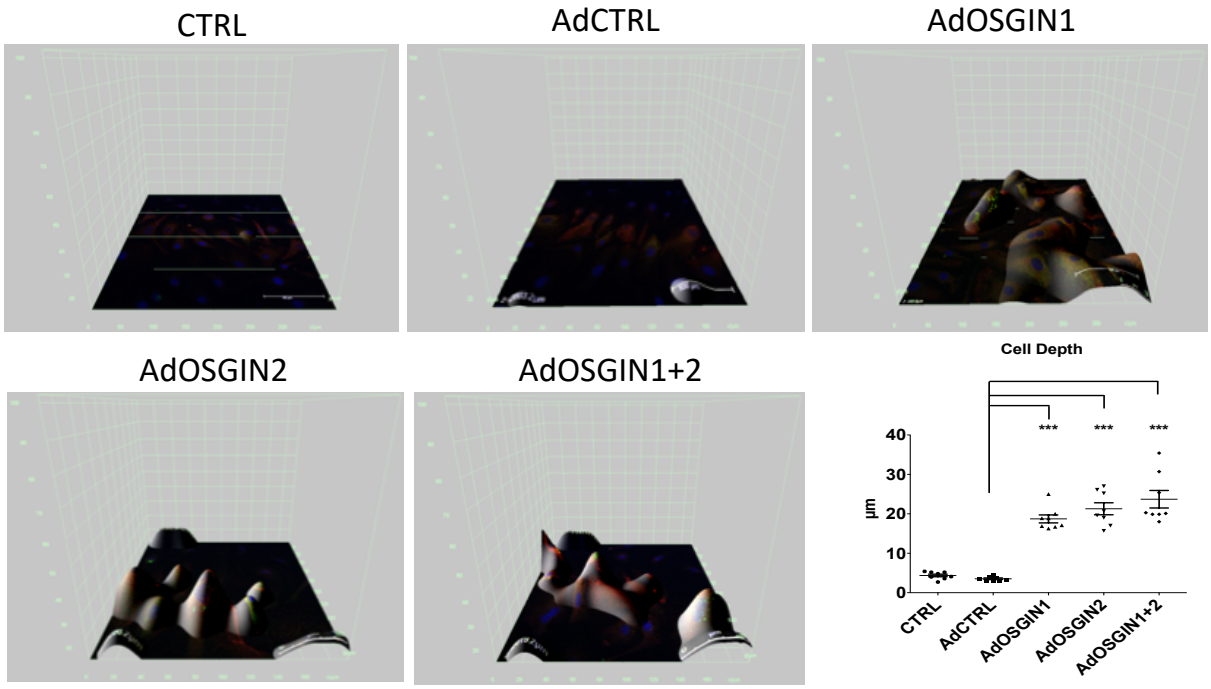

Figure 3.11). HCAECs were seeded at 2.5x10^5 cells per well in a 0.1% gelatine coated 8 well chamber slide and transduced with AdOSGIN1, AdOSGIN2 or both at a total of 400pfu/cell as described above Figure 4.1. 3D cell model was created using Leica software confocal image stack in combination with FIJI Image J: image to stack from 50 layers of confocal images (0,6 μm thicknesses each layer). Maximum Cell depth was recorded for 50 cells in each condition (n=3; ***p<0.001 one-way Anova).

3.4.6 OSGIN1 and OSGIN2 promote cell cycle arrest in HCAECs

In order to strengthen the observations of a block in cell cycle, and investigate any signature of apoptosis, further analysis of the effect of OSGIN1+2 was obtained using flow cytometry analysis, which allows the measurement of DNA content, where PI is used to bind and quantify DNA stoichiometrically. Cell division briefly is composed of five phases: G_0, G_1, G_2 and M, where M-phase is responsible for mitosis and cytokinesis. Abnormal progression through the cell cycle and induction of senescence may manifest itself as an accumulation of cells in one of the phases mentioned above. In order to investigate effects of OSGIN1+2 upregulation on advancement through the cell cycle, cell proliferation was firstly evaluated by the BrdU incorporation assay, followed by flow cytometry analysis. Through this method, it was possible to quantify cell cycle phases G1, S, G2 and M phases. HCAEC replication was synchronised using Nocodazole (0.4μg/ml) for 4 hrs before media

was replaced with fresh media and the cells were left to grow for 48 hrs before analysis (Figure 3.12).

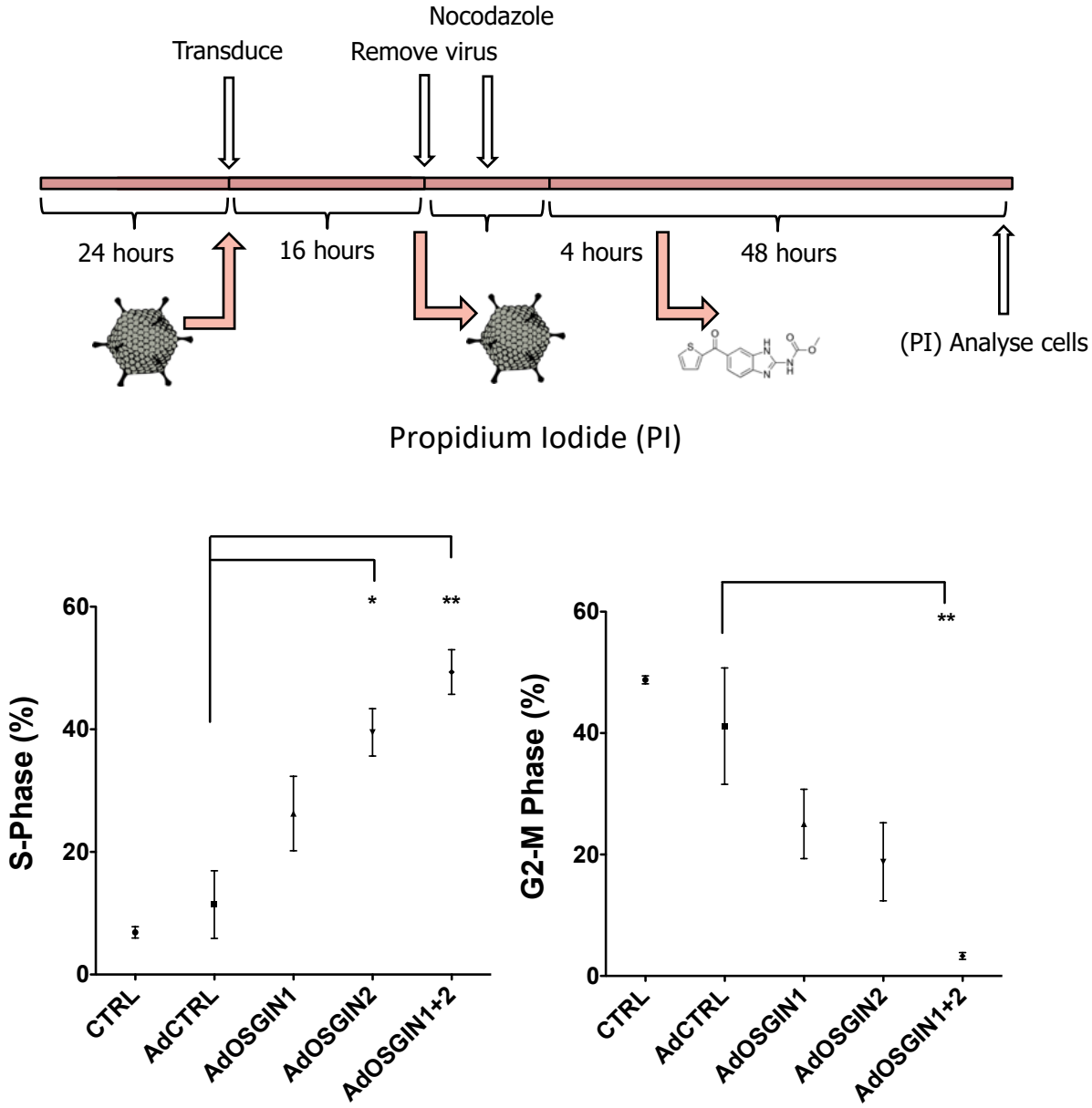

Figure 3.12). 10^5 of HCAECs were seeded in a 6 well plate. Cells were transduced by using adenoviral vector in order to overexpress OSGIN1, OSGIN2 and both together (400MOI). The Virus was removed after 16 hrs and media replaced with Nocodazole-containing media for 4 hrs, following which, the cells were washed x2? PBS and fresh media added. After 48 hrs media was removed, the cells were washed with PBS 1X and collected. After centrifugation, HCAECs were resuspended and PI (1mg/ml) was added. Flow cytometry PI staining showed an increasing level of S phase in OSGIN2 and OSGIN1+2 over-expression conditions, and a decreased number of cells in G2 phase, compared to the AdCtrl-transduced cells (n=3) * $p<0.05$ and ** $p<0.01$.

Flow cytometry analysis in figure 3.12 showed a significant increase of cells in S-phase in HCAEC transduced with AdOSGIN2 and AdOSGIN1+2. Concomitant with this, only a really low percentage of cells (<3%) were able to progress through S-phase and reach the G_2-M phase, confirming OSGIN1+2 overexpression blocks cell cycle progression. Furthermore, there was no sign of apoptotic bodies in the flow cytometry analysis. Further examination of p21 expression which, as stated above, is the main CKI responsible for the checkpoint between S-phase -> G_2-M phase showed significant increase expression level. p21 mRNA analysis by qPCR demonstrated a ~3-fold increase in for AdOSGIN1+2 VS AdCtrl (Figure 3.13).

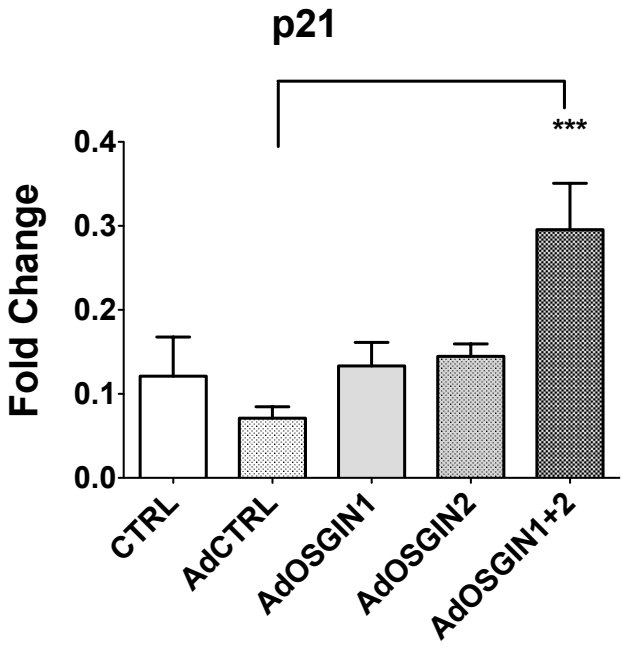

Figure 3.13). Real-time PCR on p21 showed greater mRNA abundance in AdOSGIN1+2 (N=6). Cells were seeded on day 1 into 6 well plates, transduced with adenoviral vector the 2nd day (total pfu/cell of 400). 200 pfu/cell active vector (AdOSGIN1, AdOSGIN2) and 200pfu/cell of control virus were used for single gene transduction; for both OSGIN1 and 2 overexpression this consisted of 200pfu/cell of both vectors; AdCtrl (E1/E3 'empty' Ad vector), was used as the control (400pfu/cell). Virus was removed on 3rd day. The 4th day the media was removed, cells were washed with 1X PBS. Cell lysis was carried out with following RNA purification and quantification. cDNA was obtained by retro transcription PCR reaction before real time PCR quantification. ***P<0.001 of AdOSGIN1+2 in comparison to AdCtrl.

Furthermore, it has been shown that senescent cells stop proliferating and are characterised by an increase of expression of p16 ^{ink4a} mRNA level [369], therefore the gene

expression level of p16 ^{ink4a} was evaluated (Figure 3.14) in order to confirm the aims. p16^{inkA} transcriptional level was statistically higher (3.2-fold) in the AdOSGIN1+2 condition which confirms a lack of proliferation, this is in agreement with data in the literature [360].

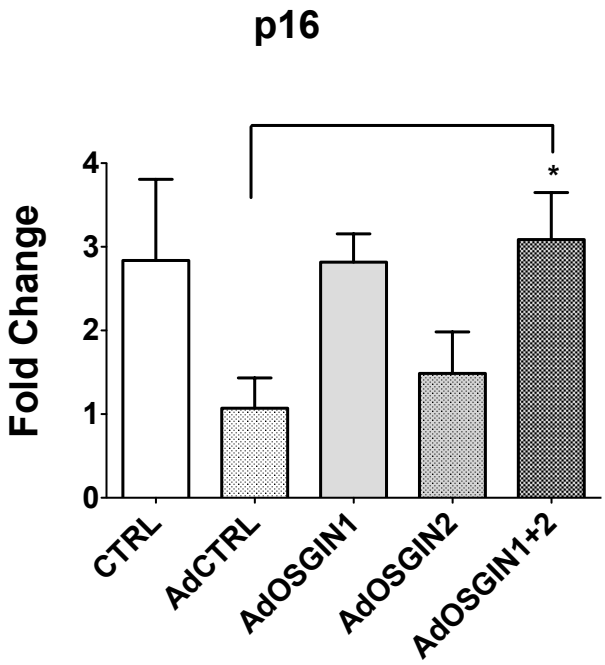

Figure 3.14). Real-time PCR on p16 showed higher expression level in AdOSGIN1+2 (N=6). Cells were seeded on day 1 into 6 well plates, transduced with adenoviral vector the 2nd day (total pfu/cell of 400). 200 pfu/cell active vector (AdOSGIN1, AdOSGIN2) and 200pfu/cell of control virus were used for single gene transduction; for both OSGIN1 and 2 overexpression this consisted of 200pfu/cell of both vectors; AdCtrl (E1/E3 'empty' Ad vector), was used as the control (400pfu/cell). Virus was removed on 3rd day. The 4th day the media was removed, cells were washed with 1X PBS. Cell lysis was carried out with following RNA purification and quantification. cDNA was obtained by retro transcription PCR reaction before real time PCR quantification. *P<0.05 of AdOSGIN1+2 in comparison with AdCtrl.

3.4.7 OSGIN1 and OSGIN2 are associated with cellular senescence and promoting ECs detachment

To further examine if AdOSGIN1 or 2 promoted senescence, transduced cells were stained for SA-β-galactosidase activity, using a classical β galactosidase senescence associated stain (pH 6.0) (Figure 3.15). OSGIN1 and OSGIN2 overexpression clearly showed more than 50% of cells positively stained for senescence-associated β-galactosidase activity, and interestingly the combination of OSGIN1 and 2 showed 85% of senescent cells including numerous 'phase-bright' cells that appear to be in the process of detaching (Phase-bright, red arrows).

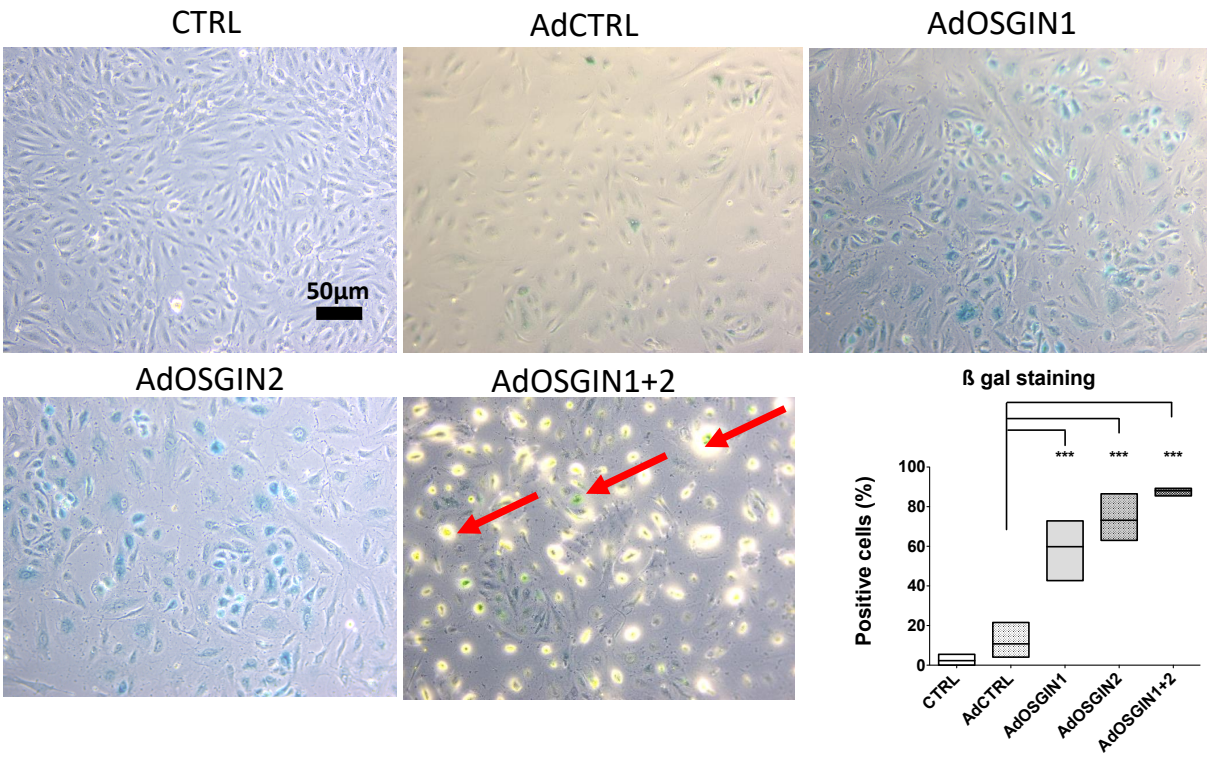

Figure 3.15). SA-β-galactosidase senescence staining of HAECs transfected with adenoviral (OSGIN1, OSGIN2 and OSGIN1+2). Overexpression by ad of AdOSGIN1 and AdOSGIN2 induces senescent phenotypes in HCAECs. AdOSGIN1+2 overexpression shows green/blue senescent cells (red arrows) detached or in progress of detaching. Briefly, cells were cultured in a 24 well plate in duplicate for five days and subsequently fixed with 4% PFA in PBS. Cells were washed with 0.1M phosphate buffer at pH 6.0 supplemented with 2 mM MgCl2. Cells were stained with SA-β-galactosidase for 4 hrs at 37°C. Cells were washed and imaged using a light microscope. SA-β-galactosidase positive cells were quantified using Image J software. One-way ANOVA Bonferroni ***p<0.001 AdOSGIN1, AdOSGIN2 and AdOSGIN1+2 vs AdCtrl (n=3).

The β galactosidase senescence stain is normally used as marker of senescence, however it has been established that it detects an increased accumulation of a classic acid lysosomal β-galactosidase, which becomes detectable at pH 6.0 [370].

3.4.8 OSGIN1 and OSGIN2 do not promote an apoptotic mechanism

To assess the impact of OSGIN1 and 2 overexpression on apoptosis, two different assays and three independent western blots of PARP were carried out. Apotox glow (Promega) and caspase-3 activity assay kit (Promokine kit) were used in order to measure apoptotic mechanism. Apotox glo kit measures the luminogenic substrate, following caspase cleavage containing the DEVD sequence (see section 2.5). With the second kit, a fluorometric immunosorbent enzyme was measured. Promokine caspase assay was performed in a multititer plate coated with human caspase-3 monoclonal antibodies and blocked to prevent nonspecific binding. Cellular lysates were incubated in the coated wells for 1.5 h at 37°C. After washing, a caspase-3-specific activated fluorogenic substrate

assessed caspase 3 activity (see section 2.6). Caspase activity was also evaluated by western blot analysis to investigate PARP cleavage, which is considered the main target for caspase 3. Anti-PARP protein was detected as a single band, however, double bands which are indicative of cleavage, were not observed in any of the three western blots (Figure 3.16C).

Therefore, it was possible to establish that EC detachment exposed to ESS, is not related to apoptosis activity.

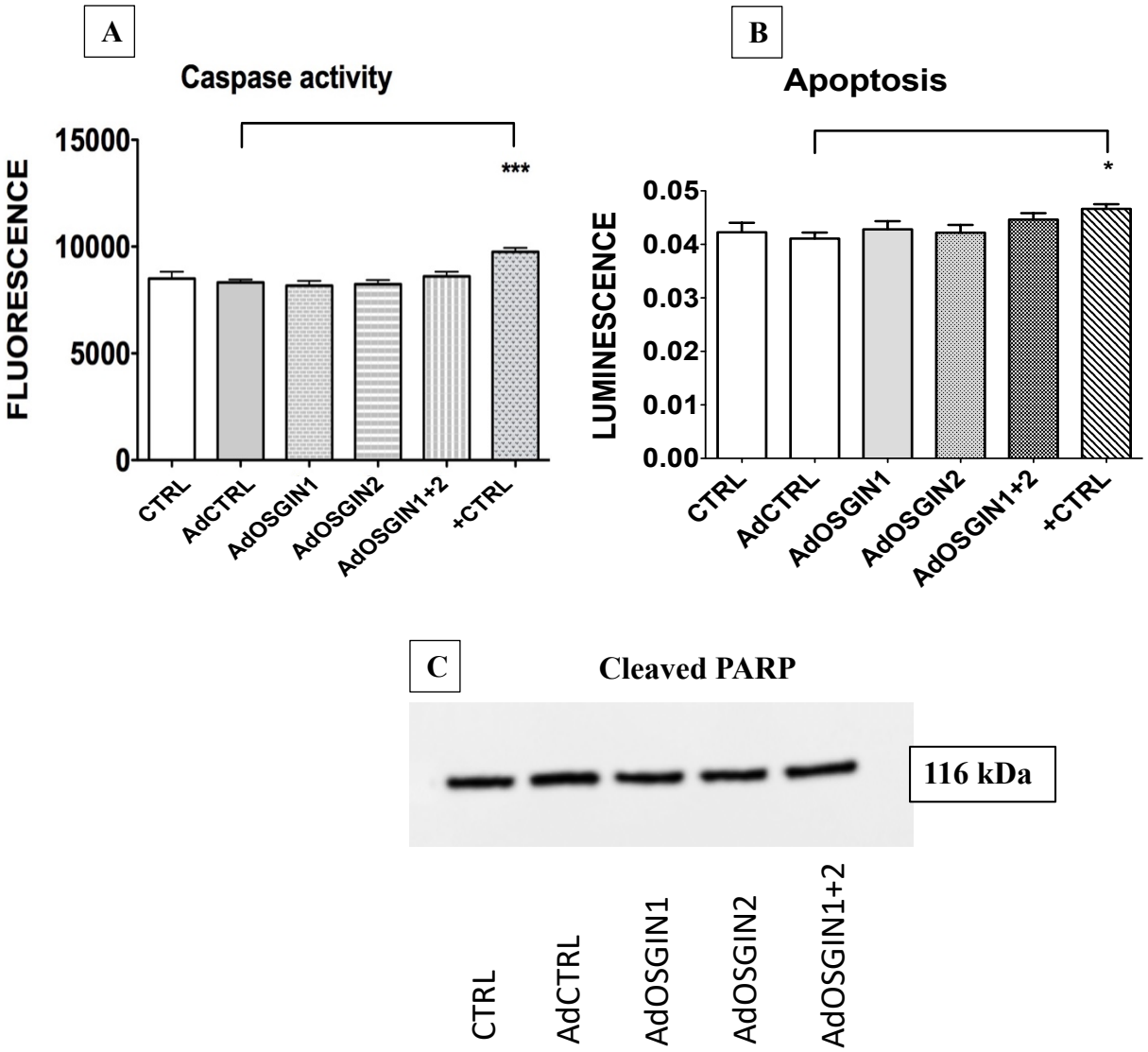

Figure 3.16). **A)** Caspase 3/7 activity of HCAECs transfected with adenovirus overexpressing OSGIN1, OSGIN 2 and both together, compared to AdCtrl transfections and positive control (0.2mM H_2O_2). The caspase 3/7 activity was measured using Caspase-Glo 3/7 assay. *** $p < 0.001$. **B)** Apoptotic activity was evaluated using Apo tox glow assay (Promega) AdOSGINs overexpression did not show any apoptotic activity. *$p < 0.05$. Data are presented as mean ± SEM (n = 3). **C)** Total PARP antibody in western blotting showed no PARP cleavage by caspase-3. No second band was reported in any sample suggesting no apoptosis activity.

3.4.9 Viability and cytotoxicity are not affected by OSGIN1 and OSGIN2

Another form of cell death related to cellular stress by infection or toxin is necrosis. Necrosis, in contrast to apoptosis, is an irreversible mechanism leading to a rupture of the plasmatic membrane [371]. Necrosis activates the inflammatory response and leads to an uncontrolled release of apoptotic protein [372]. Considering necrosis as one of the options related to cell growth inhibition, a necrosis/viability assay was carried out and the results are displayed below (Figure 3.17).

In order to further assess the effect of OSGIN1 and 2 overexpression, the Apo Tox Glo assay (Promega) also quantifies markers of necrosis and cell viability. Necrosis is assessed by measurement of the bis-AAF-R110 substrate which cannot enter live cells but instead can be cleaved by the dead-cell protease to release R110 and viability through the GF-AFC substrate which enter into live cells where it is cleaved by the live-cell protease to release AFC. In most circumstances, viability and cytotoxicity measurement will be inversely proportional to each other. Apotox Glo kit measures vitality/cytotoxicity reading the relative fluorescent units (RFU) for viability 400Ex/505Em, and therefore the cytotoxicity assay RFU (485Ex/520Em) values will be low, or vice versa (see section 2.5 for details).

No reduction in cell vitality or increase in necrosis was observed after 40h hrs following transduction, as shown in Figure 3.17 A-B).

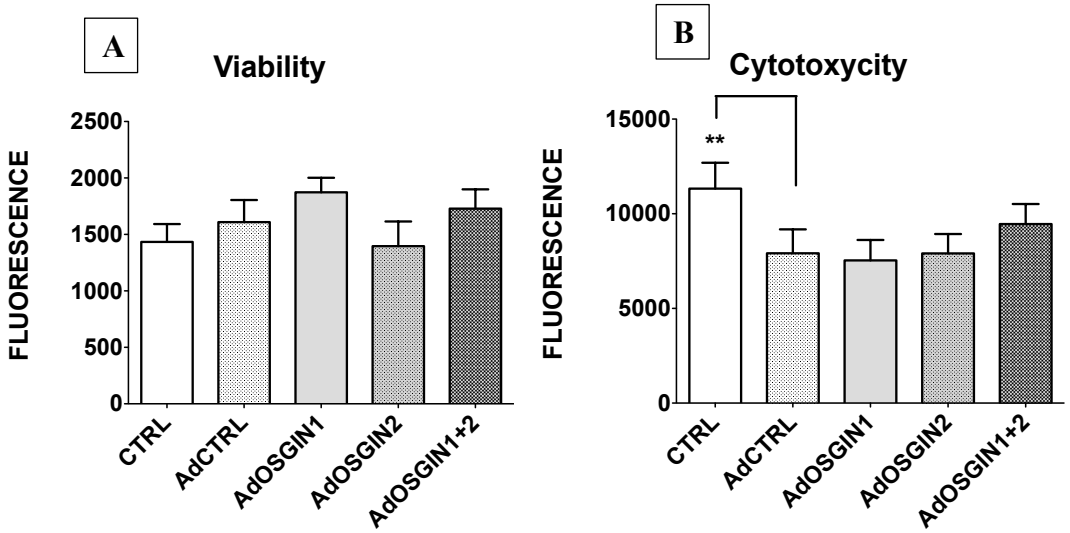

Figure 3.17). **A)** Cell viability assay for HCAECs. The cell viability was measured post transfection at 24 hrs (adenovirus overexpression of OSGIN1, OSGIN2 and both together) and did not cause a significant decrease in cell viability. **B)** Overexpression of OSGIN1, OSGIN2 and both together did not cause a significant increase or decrease in necrosis. Viability and necrosis were measured using the Promega Apotox Glo assay kit. **p < 0.01 Data are presented as mean ± SEM (n = 3).

3.5 Discussion

Previous work carried out by Dr Stephen white explored the flow environment permissive for the development of plaque erosion, identifying that the majority of erosions occur on the proximal face of stenotic plaques that experience elevated flow. Emulating these conditions and combining them with TNFα and CSE created an *in vitro* model of erosion that experienced 30% cell loss under the conditions used. Pharmacological activation of NRF2 using sulforaphane and isoliquiritigenin, triggered almost complete endothelial detachment indicating that hyperactivation of the NRF2 antioxidant system exacerbated detachment, rather than protecting endothelial cells. I extended these observations (chapter 5) confirming that NRF2 activation can induce cell detachment.

This results chapter describes the effects of overexpression of OSGIN1 and OSGIN2, which were observed in the *in vitro* model of erosion. OSGIN1 and 2 protein increment was also confirmed in sections of aorta of mice exposed to cigarette smoke for 3mo, validating the gene expression changes observed in the *in vitro* model. Furthermore, nuclear localisation suggests that the mechanism described by Hu *et al* may not be the direct consequence of OSGIN1 overexpression but may be due to p53 in combination with the apoptosis signalling pathway. This could also be due to the fact that the experiment was done on osteosarcoma cancer cells. Although it is unclear how the OSGINs (Oxidative Stress Growth INhibitor's) acquired their name, they did indeed inhibit cell replication. BrdU analysis identified numerous multinucleated cells that were not positively stained, which showed experimental limitation but at the same time suggested a blockage during cellular cycle. In order to evaluate this hypothesis, HCAECs transduced with adenoviral vectors were analysed by flow cytometry. Continued elevated expression levels of OSGIN1 and 2 resulted in cell cycle arrest during the S-phase which permits nuclear division, but inhibiting cytokinesis promoting the accumulation of multinucleated cells which indicates a failure during mitosis [365]. This was consistently observed in all microscopic analyses and evaluation using PI staining combined with flow cytometry. Further analysis confirmed the association with markers of a senescence pathway which involved an increased level of p21. P21 upregulation suggests it binds with A/CDK1-2 to promote the inhibition of the S>G_2-M transition phase progression, which fits with the observed data. In addition, HCAECs overexpressing OSGIN1, OSGIN2 and OSGIN1+2 also demonstrated an increase of SA-β-gal staining, which catalyses the hydrolysis of β-galactosides into monosaccharides.

Consistent with this, an elevated level of $p16^{Ink4A}$ mRNA, which is known to be the best described biomarker of cellular senescence, was significantly increased in HCAECs overexpressing OSGIN1+2.

It is important to highlight that within this context; cell viability was not affected. Interestingly, none of the experiments showed apoptosis (Figure 3.16 A-B-C). This is in accordance with the inclusion of a caspase inhibitor having no effect on cell detachment in the *in vitro* model of erosion [113] and supporting a recent paper published by Brennan *et al.* [197]. This is in line with the activation of senescence pathway and its nature to be anti-apoptotic, which supports the hypothesis of a separate molecular mechanism for erosion to that reported by Professor Peter Libby's group [9]. His group and others showed that oscillatory shear stress is one of the multiple processes that leads to superficial EC erosion. This particular flow environment strongly correlates with the predisposed sites for atherosclerosis [373-375]. EC activation results in inflammation and apoptosis [376, 377] and might trigger thrombosis [378] and EC erosion.

Previous work in White's lab [113] and independent studies [16, 379], showed that EC detachment mainly occurs in the areas exposed to ESS. This haemodynamic environment results in the regulation of EC function and dysfunction through alternative mechanisms, which elicits a very distinctive gene expression pattern [102, 116]. ESS, in combination with CSE and TNFα, activates OSGIN1 and 2 which are responsible for cell cycle arrest promoting a senescence-like response. They influence endothelial proliferation and promote detachment in an apoptosis and necrosis independent manner. Together, these observations suggest a separate mechanism that would promote detachment of EC located in the proximal area of an eroded plaque (exposed to ESS) compared to the distal area exposed to OSS.

3.6 Key findings:

The key findings of the experiments described in this chapter are:

- In order to validate the OSGIN1 and 2 data obtained using the *in vitro* model of erosion, ICC staining on OSGIN1 and 2 was carried out on sections of aorta of mice exposed to smoke for 3mo. OSGIN1 and 2 ICC staining showed their protein accumulation particularly in the endothelium and in the tunica media.

- OSGIN1 and 2 localisation in HCAECs were evaluated by ICC staining. ICC showed the presence of OSGIN1 and 2 only in the nuclei, and no trans-localisation in the mitochondria was observed at the moment of the evaluation (40 hrs after adenoviral transduction). Furthermore, no mega-mitochondria were observed for OSGIN1, OSGIN2 and OSGIN1+2 conditions compared to the AdCtrl.
- HCAEC proliferation rate was evaluated after adenoviral overexpression of OSGIN1, 2 and both together. BrdU proliferation assay showed significant increase of BrdU positive cells with OSGIN2 overexpression, compared to the AdCtrl. Further analysis using flow cytometry identified a block in cell cycle occurred in the condition of OSGIN2 and OSGIN1+2 overexpression. Cell cycle arrest was observed during the S-phase (up to 60%), with less than 3% of the ECs entered in G2-M phase. Furthermore, an increase in p21 mRNA abundance (CKI for the S>G_2-M transition phase) was observed.
- Markers for activation of the senescence pathway were also evaluated. SA β-galactosidase staining was carried out on HCAECs 40 hrs after adenoviral overexpression of OSGIN1, 2 and both together. A significant increment in the number of SA β-galactosidase positive stained cells was observed in the condition of AdOSGIN1, 2 and AdOSGIN1+2. SA β-galactosidase also suggested a lysosomal accumulation associated with an autophagic mechanism which have been evaluated in the chapter 4. In addition, abundance of $p16^{InkA}$ mRNA was detected by qPCr in AdOSGIN1+2, which indicates a permanent blockage of the cell cycle. Furthermore, EC detachment was observed in AdOSGIN1+2 condition which showed that the combined overexpression of the two genes is not tolerated by ECs in static conditions.
- AdOSGIN1 and AdOSGIN2 overexpression promoted EC detachment without apoptosis signalling pathway activation, which suggests a different molecular mechanism ongoing when ECs are exposed to ESS.
- In HCAECs, cell viability and cytotoxicity were also evaluated in order to assess whether OSGIN1 and OSGIN2. No significant changes were observed in viability and cytotoxicity suggesting that OSGIN1 and 2 are promoting cell detachment in a cell death independent manner.

3.7 Summary:

This study is the first one to report endothelial detachment of endothelial cells in a static *in vitro* model using adenoviral-mediated overexpression of OSGIN1 and OSGIN2. Furthermore, it is the first study to suggest a non-apoptotic mechanism for endothelial erosion, which is promoted by NRF2 activation under elevated flow.

AdOSGIN1+2 combination promotes cellular senescence and blocks cell proliferation in the stage of S->G_2-M, showing a dysfunctional cell cycle.

The series of experiments reported in the next chapters aim to describe in depth the molecular mechanism behind OSGIN1 and 2 mediated endothelial detachment and shed light, for the first time, on a novel mechanism that might promote endothelial erosion, along with potential therapeutic interventions to prevent this pathology.

Table 3.2 Summary of the effect of OSGINs on HCAECs

	CTRL	**AdCTRL**	**AdOSGIN1**	**AdOSGIN2**	**AdOSGIN1+2**
p21	No change	No change	No change	No change	Increased
p16	No change	No change	No change	No change	Increased
B-gal	No change	No change	Increased	Increased	Increased
S-phase	No change	No change	No change	Increased	Increased
G2-M phase	No change	No change	No change	No change	Increased
Cell depth	No change	No change	Increased	Increased	Increased

CHAPTER 4: OSGIN1 AND OSGIN2 PROMOTES CELL STRUCTURE DESTABILISATION AND DYSFUNCTIONAL AUTOPHAGY

CHAPTER 4: OSGIN1 AND OSGIN2 PROMOTES CELL STRUCTURE DESTABILISATION AND DYSFUNCTIONAL AUTOPHAGY

4.1 Cytoskeletal structure and adhesion molecule complex function in EC permeability

A confluent monolayer of EC line all vessels of the circulatory system, from the major arteries to the smallest capillaries. For this reason, EC structure plays a pivotal role on the correct functioning and performance of the endothelium which continuously adapt in response to environmental stimuli, chemical and mechanical stress [382-385]. Cigarette smoke, a recognised risk profile of plaque erosion, which has been associated with vascular wall injuries by EC damage [386, 387]. *In vivo* studies have also shown that acrolein and crotonaldehyde, two major components in the cigarette smoke, activate NADPH oxidase which leads to higher production of ROS [388, 389]. It has also been reported that cigarette smoke operates concomitantly with IL-1β to alter the normal trafficking of β-catenin in the vascular endothelium, impairing cell-cell contact [388]. They also suppress the tensin homolog (PTEN) and chromosome 10 phosphatase, which increase β-catenin and VE-cadherin phosphotyrosine resulting in VE-cadherin/β-catenin membrane complex disassembly [390]. Furthermore, metals present in cigarette smoke causes the loss of microtubule function and subsequent depolymerisation by catalysing the oxidation of cellular proteins. This process disrupts cytoskeletal structure proteasome-dependent degradation of α-tubulin which results in EC contraction and increment in endothelial leakage and permeability [391].

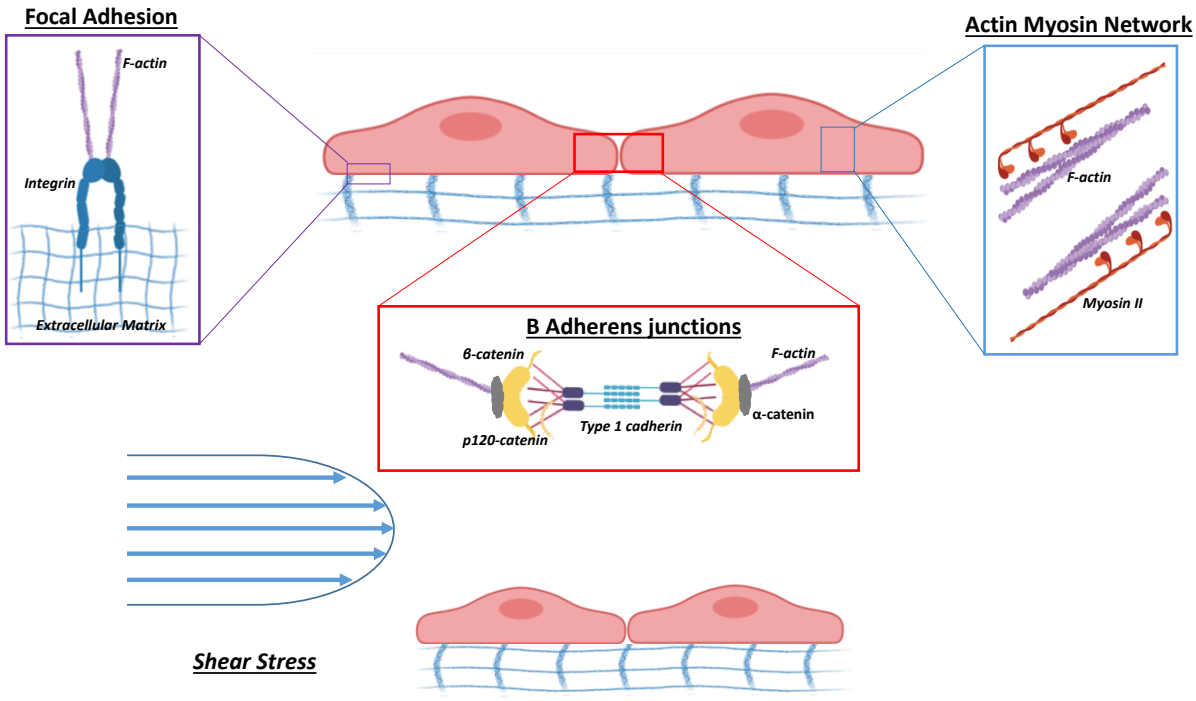

Figure 4.1). Schematic representation of the adhesome, cell-cell junctions and actin-myosin network complex. EC response to flow is modulated by cadherin and integrins. Phosphorylation of adherens junctions and vinculin in focal adhesions, respectively in Y822 and Y100 and Y1065 has been shown to ensure EC adherence strength, which selectively binds to β-catenin and actin [392], [393]. Mechanotransductor EC response to flow by a cross-talk of focal adhesions and adherens junctions transmit mechanical forces of shear stress to a network of contractile actin–myosin. Integrins and cadherins are interconnected to the actin-myosin complex and mechanical stress signal travels from EC neighbouring cells.

Mechanical forces are experienced simultaneously on focal adhesion and adherens junctions by the endothelium, which responds to flow by balancing the strain across both adhesion systems [394]. This behaviour is pivotal for EC function against biomechanical forces. How precisely ECs cope with biomechanical forces remains unclear [394], although several studies have been carried out in order to understand this mechanism. Nagafuchi and Takeichi demonstrated that cadherin/β-catenin complex binds α-catenin, which is responsible for recruiting filaments of actin [395]. In 2014 Buckley *et al* showed that a link between adherens junction and the actin cytoskeleton is necessary for tissue development and homeostasis. Using an optical trap-based assay it was shown that the minimal cadherin-catenin complex binds to actin filaments under force, which could explain how this complex transduces mechanical forces at cell-cell junctions [396]. This concept has been challenged by Gates and Peifer in 2005 proposing the idea that α-catenin is able to interact with other binding partners such as α-actin, zonula occludins-1 (ZO-1) which is a cell-cell tight junction, and vinculin [397]. This complex has not yet been isolated, but

impressive biochemical and genetic data indicates this complex needs to be looked at in a more dynamic perspective. In fact, the model proposed showed that catenins provide a stable tether between actin in the cytoskeleton and cadherin [397]. Adhesion molecule impairment has been reported during the event of atherosclerosis and it has been established that the protein complex mentioned above is crucial for preserving endothelium permeability. Endothelial dysfunction, in fact, is described as a morphological alteration which affects and increases permeability in the endothelium which now allows SMC infiltration, and at the same time there is passive diffusion of particles (e.g. Low density lipoprotein) [384]. The chronology of events that lead to plaque formation is still debated, Tabas *et al* [398] proposed the apo-B lipoprotein infiltration as the first event but others, like Libby *et al,* [399] have suggested that endothelial dysfunction is key for this process, and it may be caused by inflammation and oxidative stress as an initial factor. Although there are discrepancies in the literature, the importance of cadherins, catenins, vinculin and actin proteins for the correct functionality of ECs regarding the protection of the tissue against noxious blood components and inflammatory cells have been commonly accepted [400].

Endothelial cell-cell junctions are pivotal against thrombosis and inflammatory reactions, and their impairment or disruption increase vascular permeability modifying ECs response in terms of interaction with SMC and pericytes, contact cell-inhibition, lumen functionality and intracellular signalling [401]. The main support in terms of cell-cell junction is provided by vascular endothelial cadherin (VE-cadherin), which are connected to the cytoplasm by β-catenin and p120-catenin [402]. It is still unclear whether the VE-cadherin and β-catenin complex interact with actin filaments, but interestingly several binding proteins like vinculin [403], Eplin and actinin [404] have been found to bind with α-catenin [405]. In endothelial cell junctions a bond between VE-cadherin, β-catenin and actin was observed, which allows vinculin to link with α-catenin, bridging the complex VE-cadherin-actin [406, 407] (Figure 4.2). In 2012 Komarova *et al* it has been reported that VE-cadherin can be critical in modulation microtubules and therefore cytoskeletal rearrangement. This process, which is possible through the activation of End-binding protein 3 (EB3), is important for the adherent junction protein complex and also to control vascular permeability [408].

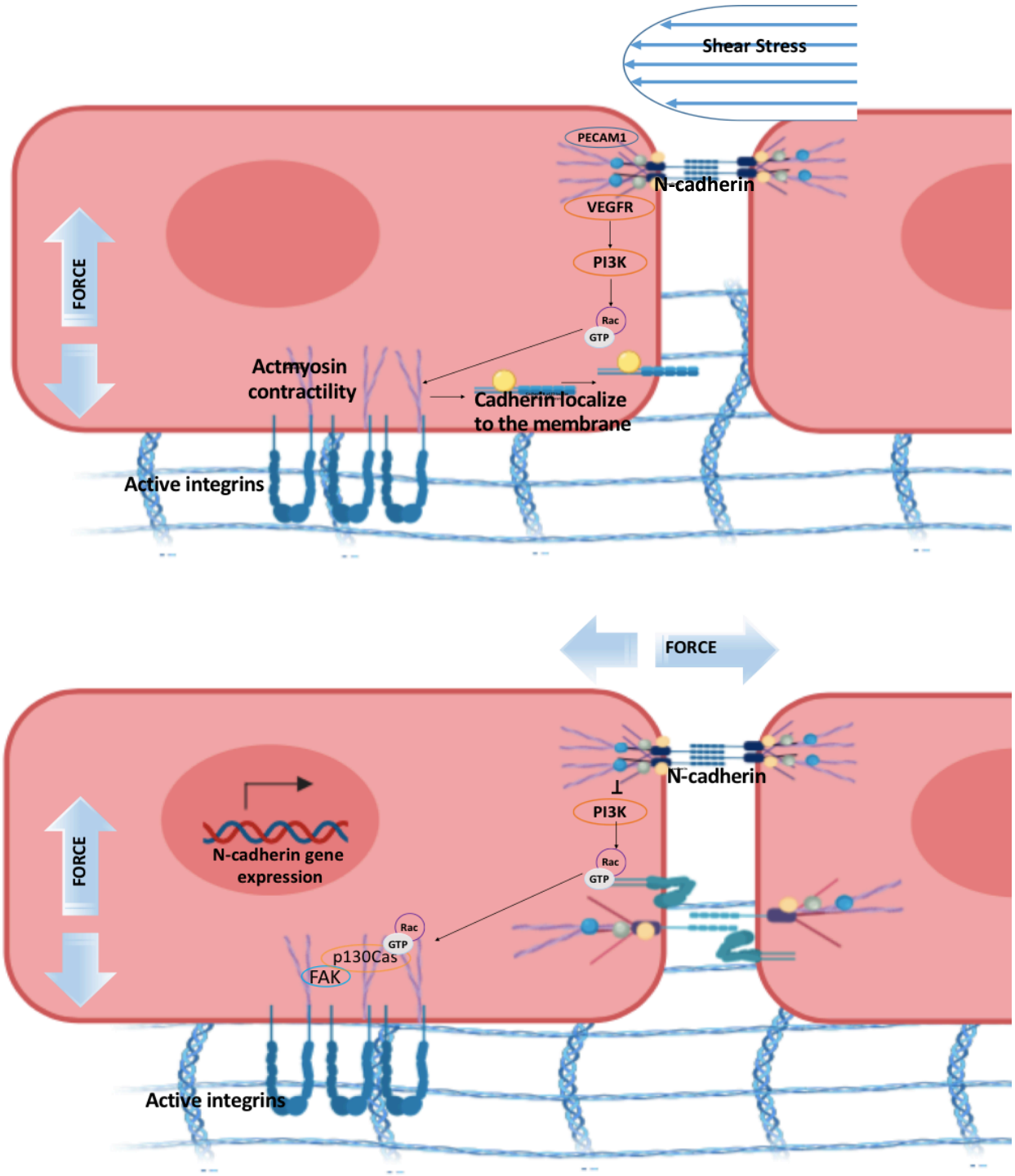

Figure 4.2). Cell response to flow involved different mechanochemical signals. VE-cadherin (together with Platelet Endothelial Cell Adhesion Molecule (PECAM) and Vascular Endothelial Growth Factor Receptors (VEGFR)) mediates integrin regulations by PI3K and Rac complex. Equally, actomyosin contractility regulates VE-cadherin localisation on cell-cell junctions. These two mechanisms mutually regulate the interaction of ECM-focal adhesion and stabilise cell-cell contact.

4.2 The Interconnections between Autophagy and Adhesome

ECs are constantly exposed to mechanical forces such as shear stress and vasculature strain. Integrins and cadherin are the main proteins responsible in controlling cell-cell contact and EC adhesion inside the cell, and remodelling ECM outside of it (Figure 4.2) [394]. Failure to maintain these interactions, such a loss in the connection between integrin and ECM, leads to apoptotic cell death [409, 410]. Furthermore, integrin-focal adhesion responds to extracellular changes with intracellular changes, including autophagy [411, 412]. It has been reported that activation of the autophagy pathway is induced by the loss of integrin-focal adhesion complex, and vice versa autophagy is inhibited by a stable integrin-mediated ECM attachment [413]. Autophagy targets β1 integrin and degrades focal adhesion proteins and induces their turnover [414-416]. Anti-apoptotic signals have also been observed. It has been discovered that ECM detachment induces anti-apoptotic signals, which allows cell survival and the possibility for the cell to re-establish a contact with ECM [413]. One of these anti-apoptotic signals is activation of the autophagy pathway which has been reported to be due to the impairment of integrin-focal adhesion [417-419]. Fascinatingly, it has been shown that focal adhesion and myosin, which are the regulators of cellular contractility, are substrates for the autophagy dependent adhesion mechanism [420]. Myosin can also be activated and modulated by GTPase RhoA through Rho-associated protein kinase (ROCK) [421], and additionally it can be targeted by SQSTM1/p62-dependent autophagy [422]. Noteworthy, SQSTM1/p62-dependent autophagy seems to be involved in cytokinesis. The autophagy activation pathway seems to protect cells against detachment-induced cell death (anoikis) [423], which would support the hypothesis that degradation of GTPase RhoA by autophagy triggers anti-anoikis response by limiting focal adhesion maturation [417]. This would induce a reduction in terms of tension at unanchored integrin sites in cells depleted of their natural roots, and in the presence of ESS would lead to EC erosion of overlying stenotic plaque.

4.3 The Interconnections between CMA and Adhesome

SQSTM1/p62-dependent autophagy is not the only autophagy pathway interacting with the adhesome. It was observed that Filamin A, which acts as a cross-linker for actin cytoskeleton, is also responsible for linking integrins to actin and in the focal adhesion it is

recruited in a tension-dependent manner in response to tensional stress [424]. Interestingly it has been reported that Filamin A unfolds in response to tension, this conformational change triggers CMA [425], in particular CMA-BAG3 complex which contains the E3 ligase, promoting filamin A ubiquitylation. Next, SQSTM1/p62 promotes the degradation of the ubiquitylated filamin A [420]. Ulbricht *et al* suggested that tensional force induces autophagy by increasing autophagosome-LC3 complex formation which might be one of the mechanism responsible for triggering autophagy [425] (Figure 4.3). Localized tension at focal adhesions could also be one mechanism through which autophagy is spatially and temporally regulated.

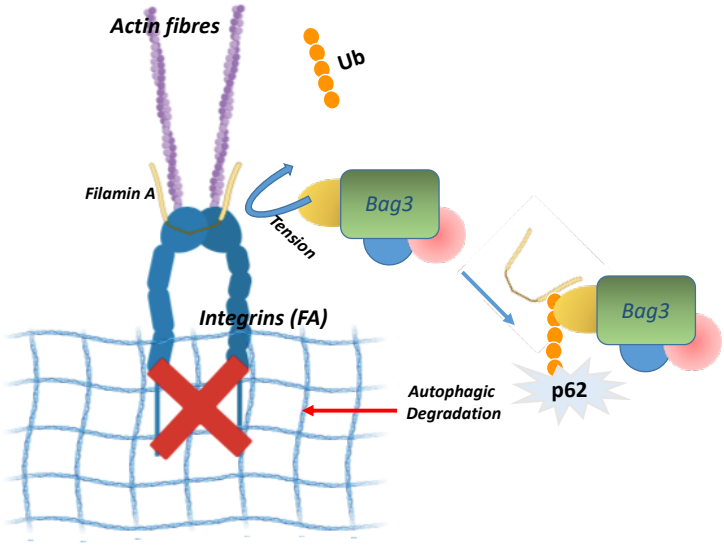

Figure 4.3). Tensional force response promotes flamin A conformational changes. Flamin A supports focal adhesion and appears to be sequestered by BAG3 complex during activation of CMA. Once flamin A is sequestered, SQSTM1/p62 binds with BAG3 complex, recruits E3-ubiqutin ligase and promotes flamin A degradation which results in impairment of focal adhesion-ECM interaction and cell detachment.

4.5 Putative mechanism of action of OSGIN1 and OSGIN2 in ECs

As previously described in section 1.2, atherosclerosis develops mostly in the presence of arterial bifurcations and disturbed shear stress. This environment allows SMC replication and migration into the intima, with associated matrix production, proinflammatory signal enhancement and atherosclerosis development [439]. Concurrently, there is an increase in flow-induced permeability that allows greater flux of lipoproteins into the intima. LDL is trapped in the thickened matrix, becomes oxidised by ROS, promote leukocyte recruitment from the blood to the artery and drive inflammation [103]. There is also

evidence that EC apoptosis contributes to plaque development by enhancing EC permeability [59]. On the contrary, laminar shear stress has been considered protective, through mitigation of the inflammatory process, increased nitric oxide production, reduction in permeability and reduced levels of apoptosis [440]. In 2017 an interesting study by Vion *et al* aimed to assess the correlation between shear stress and defective autophagy. It was reported that in a model of atherosclerosis in mice, a genetic inactivation of endothelial autophagy promotes plaque burden only in straight arterial area exposed to LSS, which usually are resistant to atherosclerotic plaque development [441]. For this reason, during this project was hypothesised that *in vitro* model with AdOSGIN1 and 2 overexpression via the combination of ESS, TNFα and CSE could be related to dysfunctional autophagy. Furthermore, there are several types of autophagy and none of them have been enterally understood. Therefore, it was necessary to evaluate whether AdOSGIN1 and AdOSGIN2 were responsible for autophagy process and possibly which type of autophagy was involved.

4.6 Aim and objectives:

Aim: Establish whether OSGIN1 and 2 are responsible for impairing adhesion molecules, disrupting cell-cell contact and cytoskeletal structure. Furthermore, lysosomal accumulation suggests the involvement of OSGIN1 and OSGIN2 in autophagy process. Establish whether OSGIN1 and OSGIN2 trigger autophagy pathway.

This will be addressed in the following objectives:

- Cytoskeletal structure, cell-matrix and cell-cell contacts signal into the cell regulate many aspects of cell behaviour, therefore it was important to perform Immunocytochemical staining to elucidate whether adenoviral overexpression of OSGIN1 and OSGIN2 regulate these important cell processes.
- The cellular function of OSGIN1 and 2 are poorly defined. In order to shed light on the effects of OSGIN1 and 2 upregulation, RNAseq transcriptomic analysis was performed. Analysis using Inginuity IPA canonical pathway will be evaluated to add functional information to understand their role within the cell.

- Bioinformatic analysis of the genes regulated by OSGIN1 and 2 suggested a role in altering autophagy. We therefore validated these results and assessed the effects of OSGIN1 and 2 upregulation of the processing of autophagic vesicles.
- It has been shown that NRF2 is involved on CMA modulation. Stress induced activation of elevated levels of CMA is an important process in responding to diverse types of cellular stress. CMA might contribute in the mechanism of endothelial detachment due to enhanced expression of NRF2 regulated genes OSGIN1 and OSGIN2. In order to shed light on the link between EC detachment and autophagy, HSP70, HSP72 and BAG3 mRNA levels were evaluated through qPCr analysis. Furthermore, HSP70 is evaluated through western blotting analysis. This is pivotal to understand the impact of CMA on EC detachment.

4.7 Results

4.7.1 OSGIN1 and OSGIN2 compromise cytoskeletal structure, disrupt adhesion molecules and impair cell-cell contact

An in-depth analysis of cell structure was performed using immunocytochemistry. Immunocytochemical staining on a confluent layer after AdOSGIN1 and AdOSGIN2 overexpression showed significant detrimental effects on cell-cell contact (Figure 4.4), cell structure (Figure 4.5) and focal adhesion molecules (Figure 4.6). Firstly, we analysed the intensity and localisation of β catenin (Figure 4.4). β-catenin is a marker of intercellular junctional stability, its association with the membrane is maintained through association with junctional cadherins. The representative images in figure 4.4 demonstrate that OSGIN1 or 2 overexpression not only reduced association with cell-cell junctions but also reduced overall levels.

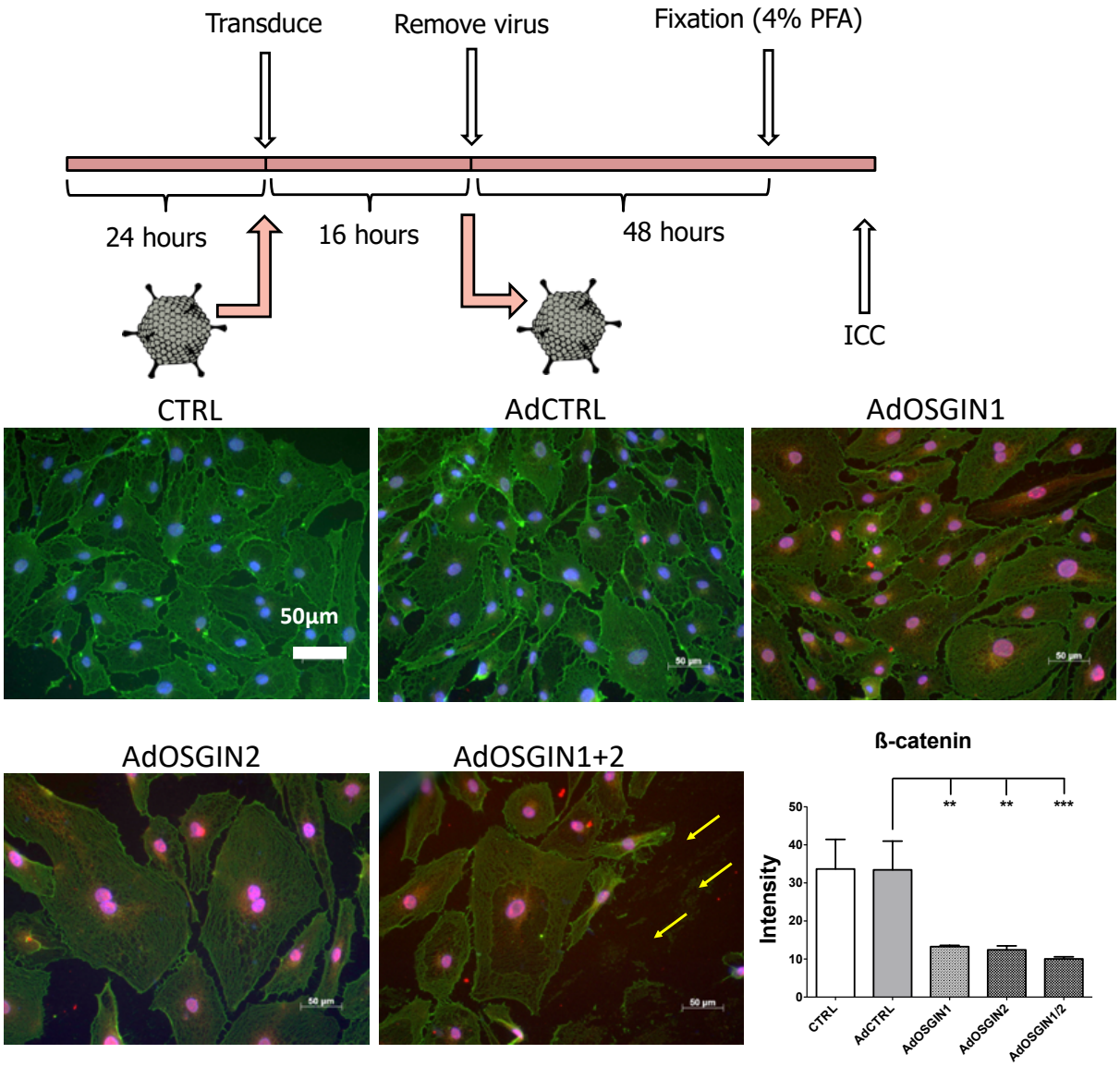

Figure 4.4). Immunofluorescence of β-catenin (Green), and OSGIN1 or 2 (Red) visualised by immunofluorescence microscopy. HCAECs grown on 0.1% gelatine coated chamber slide were transfected with adenovirus (OSGIN1, OSGIN2 and OSGIN1+2 overexpression) for 16 h at a total pfu of 400 per cell as described (Table 3.1). Images show that in the AdOSGIN2 and AdOSGIN1+2 conditions there is a loss of β-catenin staining intensity, both at the cell-cell junction and overall intensity compared to the ad AdCtrl and the non-transduced control. This analysis also highlights the changes in cell size induced by AdOSGIN2 and AdOSGIN1+2 transduction compared to AdCtrl and the control, as previously described (Figure 3.9-3.11). The yellow arrows show the loss of DAPI nuclear staining, suggesting the presence of a cell footprint caused by cell detachment. One-way Anova **p<0.01 and ***p<0.001 (n = 3).

Secondly, intercellular adhesion molecule VE-cadherin (Red) and tubulin (Green) were evaluated (Figure 4.5). VE-cadherin is a major endothelial adhesion molecule facilitating the formation of stable cell-cell junctions [442]. VE-cadherin expression and localisation to the intercellular boarders was reduced in AdOSGIN2 and AdOSGIN1+2 conditions, suggesting a weakening of cell-cell junctions. Tubulin, which is a major component of the

cytoskeleton, was almost absent in the conditions of AdOSGIN2 and AdOSGIN1+2. This analysis suggests that OSGIN1 and OSGIN2 not only have a detrimental effect on cell-cell contact and adhesion molecules, but also compromise cytoskeletal structure.

Finally, we analysed F-actin fibres and the integral focal adhesion protein vinculin. F-actin fibres are pivotal for cellular adhesion, mobility and cell contraction during cell division. We observed that AdOSGIN2 and combination of AdOSGIN1+2 reduced the intensity of F-actin staining, which might affect progression through the cell cycle. In the same way vinculin, a focal adhesion membrane-cytoskeletal protein associated with integrin adhesion molecules to the actin cytoskeleton, was also observed to be reduced in AdOSGIN2 and AdOSGIN1+2 conditions (Figure 4.5).

In addition, a frequent observation in all of these experiments, was detachment of ECs under static culture conditions. Evidence of large gaps in the cell culture, or evidence of remnants of cell 'footprints' were consistently observed in the OSGIN1+2 overexpression condition (marked by yellow arrows in Figures 4.5-4.6 and highlighted in Figure 4.7).

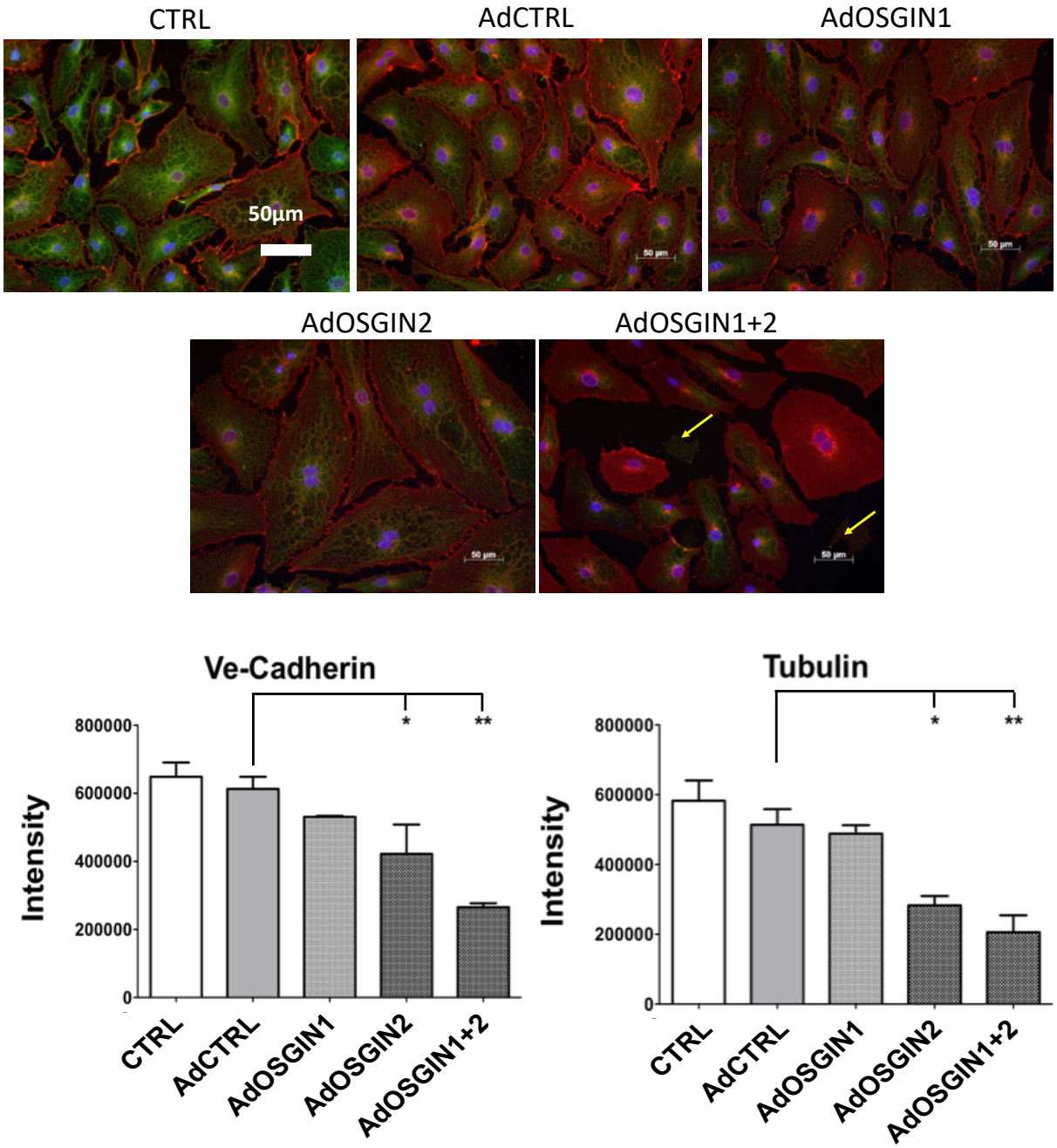

Figure 4.5). Immunofluorescence of Tubulin (Green) and VE-cadherin (Red), visualised by immunofluorescence microscopy HCAECs grown on 0.1% gelatine coated chamber slide were transfected with adenovirus (OSGIN1, OSGIN2 and OSGIN1+2 overexpression) for 16 h at a total pfu of 400 per cell as described (Table 3.1). Images show that in the OSGIN2 there is a loss of tubulin in 50% of the cells. OSGIN1+2 condition showed a loss of tubulin and VE-cadherin in 70% of the cells compared to the ad AdCtrl and the control. Furthermore, the yellow arrow shows the loss of DAPI nuclear staining, suggesting the presence of a cell footprint caused by cell detachment. One-way Anova *p<0.05 and **p<0.01 (n = 3).

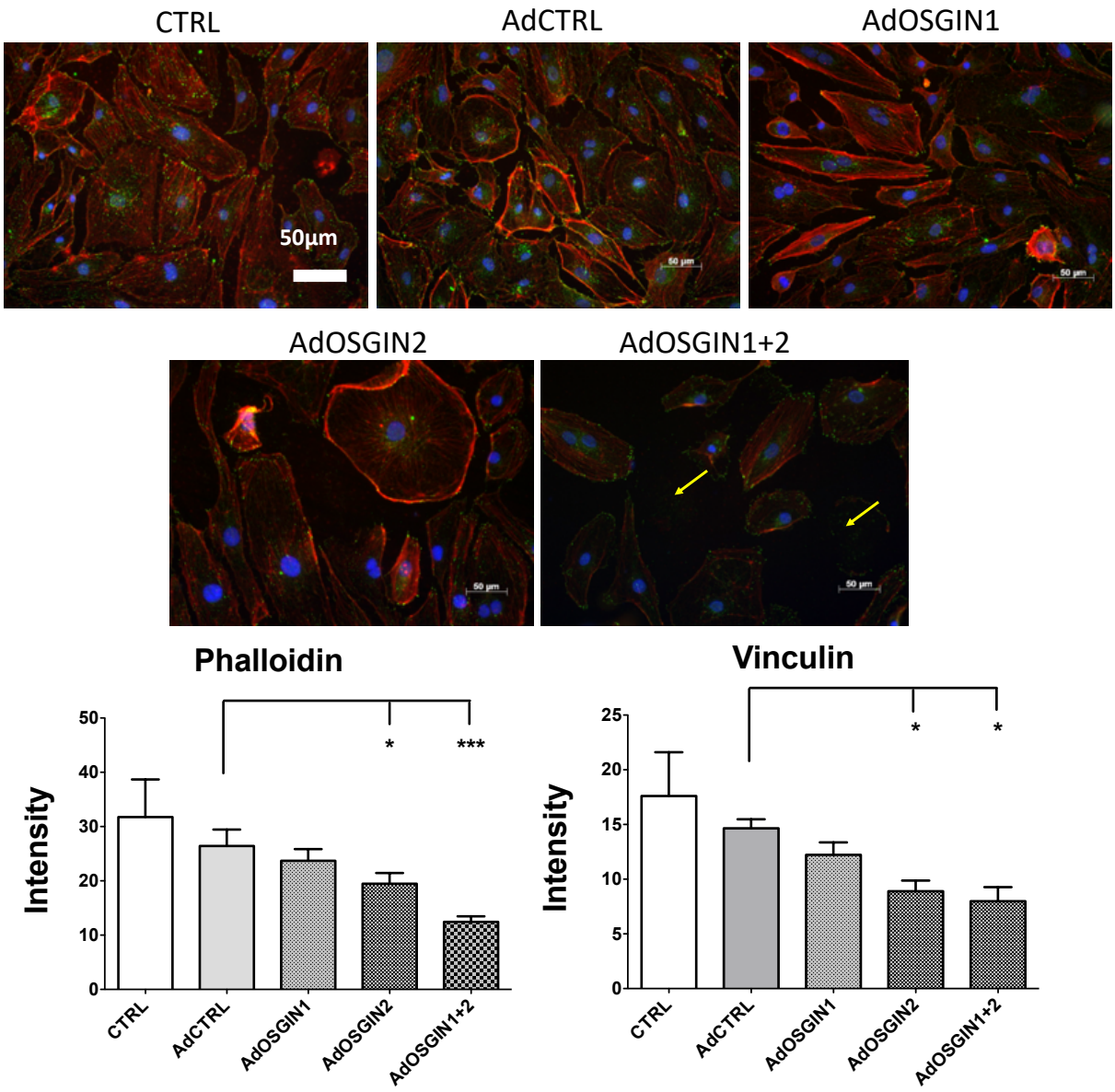

Figure 4.6). Immunofluorescence of vinculin (Green) and phalloidin (Red), visualised by immunofluorescence microscopy. HCAECs grown on 0.1% gelatine coated chamber slide were transfected with adenovirus (OSGIN1, OSGIN2 and OSGIN1+2 overexpression) for 16 h at a total pfu of 400 per cell as described (Table 3.1). Images show that in the AdOSGIN2 and AdOSGIN1+2 condition there is a loss of β-catenin compared to the ad AdCtrl and the control. Furthermore, the cell size changes for AdOSGIN2 and AdOSGIN1+2 compared to AdCtrl and the control. The yellow arrow shows the loss of DAPI nuclear staining, suggesting the presence of a cell footprint caused by cell detachment. Images show the loss of phalloidin in AdOSGIN1+2 transfected HCAECs. The yellow arrow shows the loss of DAPI nuclear staining, suggesting the presence of a cell footprint caused by cell detachment. One-way Anova *p<0.05 and ***p<0.001 (n = 3

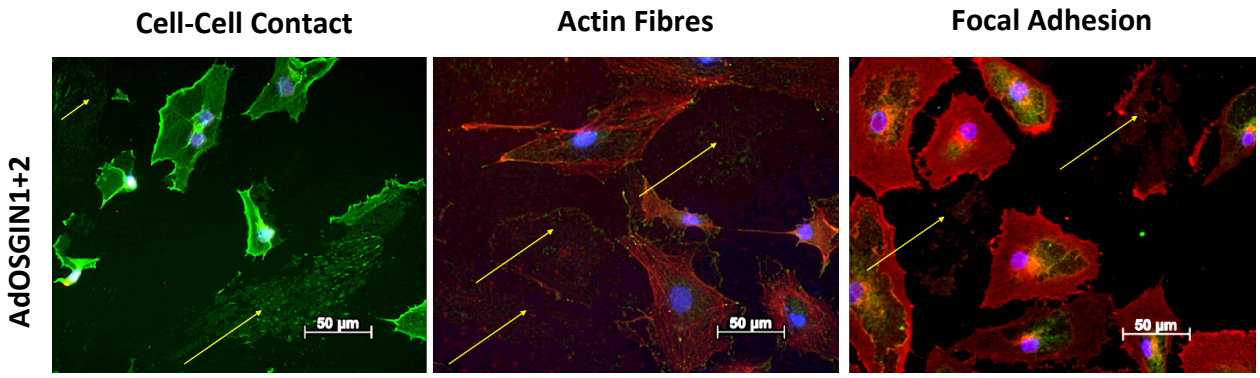

Figure 4.7). The above images are highlighting EC footprint in the condition of AdOSGIN1+2. Combined adenoviral overexpression of OSGIN1 and OSGIN2 promotes impairment of cell-cell contact (Left), loss in focal adhesion (centre) and disruption of cytoskeletal structure (Right). AdOSGIN1+2 HCAECs were showing detachment even in absence of shear stress, which suggest a weakening process on going in terms of cell adhesion.

4.7.2 RNAseq transcriptome analysis: uncovering the molecular mechanism of OSGIN1 and OSGIN2 and their combined effect on ECs

In order to better understand the consequence and molecular control of the effects of OSGIN1 and 2 overexpression, RNAseq transcriptome analysis was carried out using the genomics facility at the University of Manchester (Figure 4.8-4.9). Three independent batches of HCAECs were seeded in 6 well plates and transduced with AdCtrl, AdOSGIN1, AdOSGIN2, or AdOSGIN1+2 at a total of 400pfu/cell (as described Table 3.1). Subsequently, cells were lysed and total RNA purified using Norgen total RNA isolation Kit. 1µg of total RNA was used for RNAseq analysis. Following RNAseq, bioinformatic processing by D Ping Wang was performed to normalise the data between HCAEC batch to reduce the donor-specific effects and maximise the observation of treatment effect. RNAseq transcriptomics analysis (Figure 4.8) was performed on HCAECs transduced with adenoviral control, OSGIN1 adenovirus, OSGIN2 adenovirus and OSGIN1 and 2 (Figure 4.8-4.9). Following transcriptional analysis, 360 different genes were significantly changed over the 3 conditions, as shown in figure 4.10. Further analysis of the individual clusters was performed using Ingenuity, with the assistance of Dr Alexander Langford-Smith.

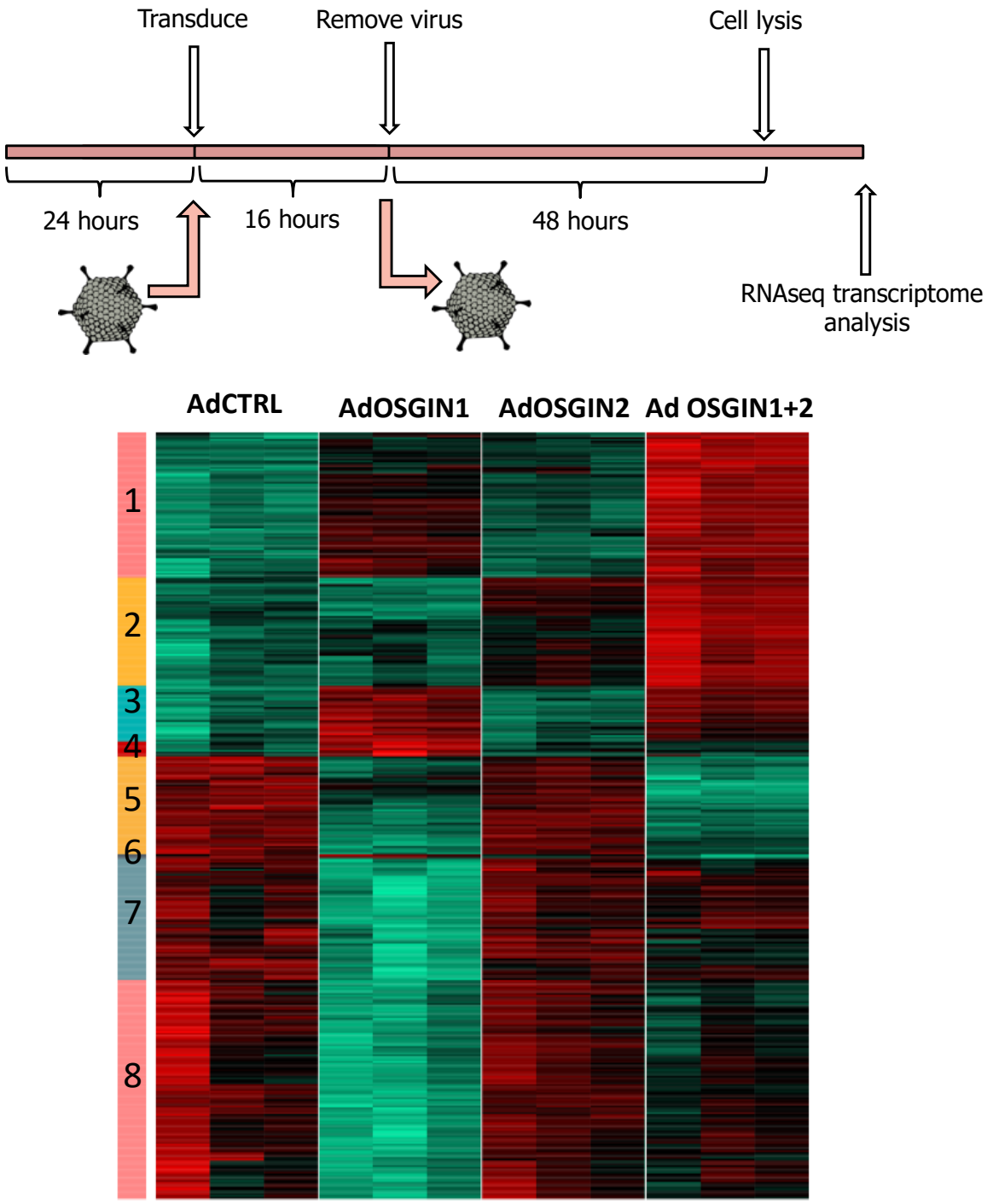

Figure 4.8). A) Schematic timeline for RNAseq transcriptome analysis. 1.7x 10^5 HCAECs were seeded and grown in a 6 well plate for 24 hrs. Transduction with adenoviral vector was carried out on the 2nd day (total pfu/cell of 400). 200 pfu/cell active vector (AdOSGIN1, AdOSGIN2) and 200pfu/cell of control virus were used for single gene transduction; for both OSGIN1 and 2 overexpression this consisted of 200pfu/cell of both vectors; AdCtrl (E1/E3 'empty' Ad vector), was used as the control (400pfu/cell). Virus was removed on the 3rd day. On the 4th day the media was removed, cells were washed with 1X PBS and lysed with 300µl of lysis buffer (with 1% β-mercaptoEtOH added).**B)** Heatmap of genes significantly changed between Adenoviral control and adenoviral overexpression of OSGIN1, OSGIN2 or OSGIN1+2, Green indicates down regulated genes, black no change and red up regulated genes. The cluster analysis was carried out on the DE genes identified with DESeq2 using a padj cut-off of 0.05, absolute log2 fold change cut-off of 0.5, and base Mean cut-off of 50. The Pearson distance was clustered with the hclust function and plotted with a R package of gplots. Clustering analysis reveals 8 clusters.

Gene Cluster

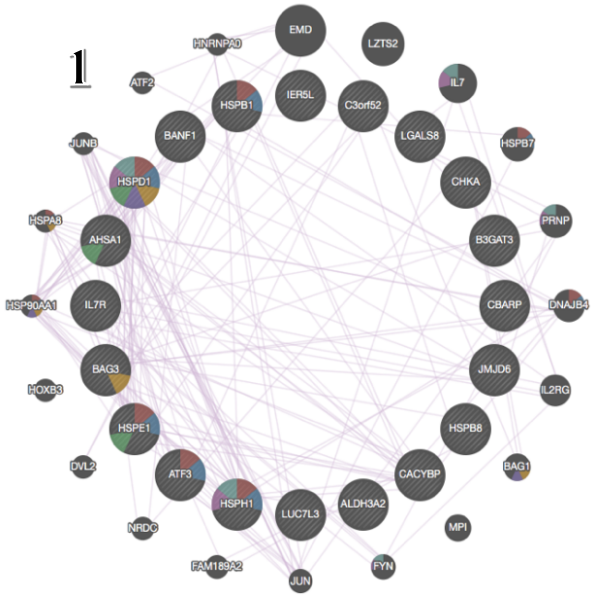

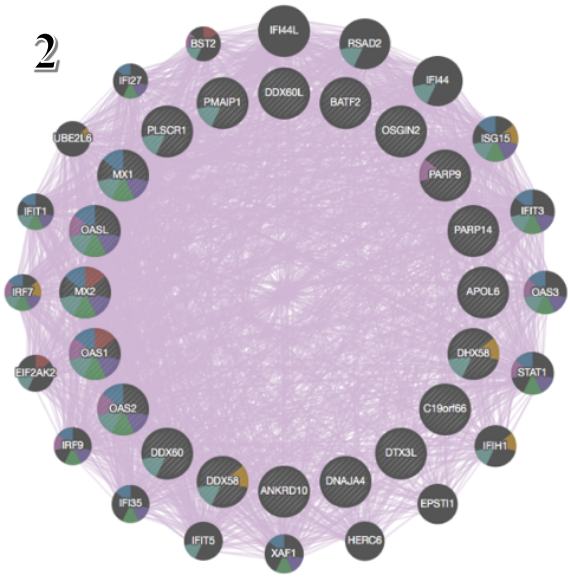

- response to topologically incorrect protein
- response to unfolded protein
- protein folding
- protein refolding
- chaperone binding
- regulation of lymphocyte activation
- regulation of leukocyte activation

- response to interferon-alpha
- regulation of type I interferon production
- response to type I interferon
- cellular response to type I interferon
- response to virus
- response to interferon-gamma
- type I interferon signaling pathway

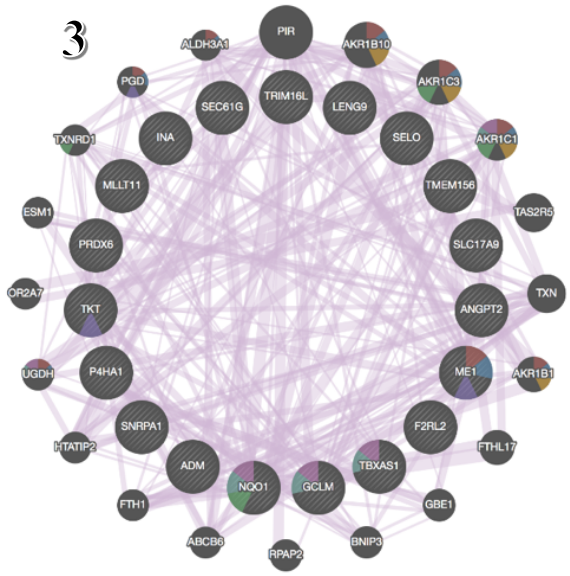

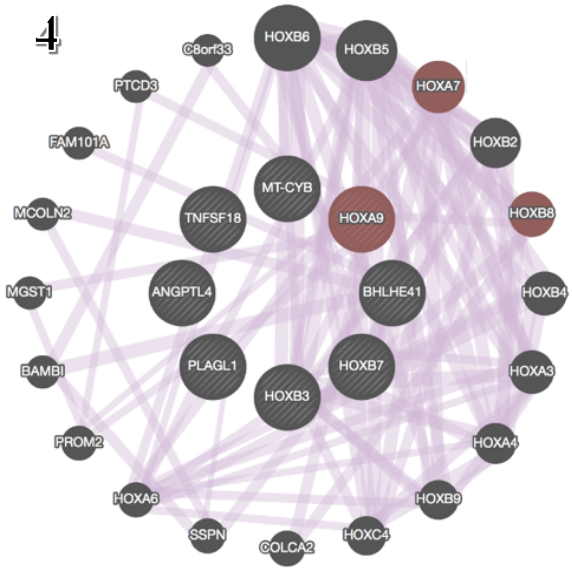

- oxidoreductase activity, acting on the CH-OH group of donors, NAD or NADP as acceptor
- oxidoreductase activity, acting on CH-OH group of donors
- quinone metabolic process
- oxidoreduction coenzyme metabolic process
- oxidoreductase activity, acting on NAD(P)H
- cellular response to xenobiotic stimulus
- xenobiotic metabolic process

- negative regulation of myeloid cell differentiation

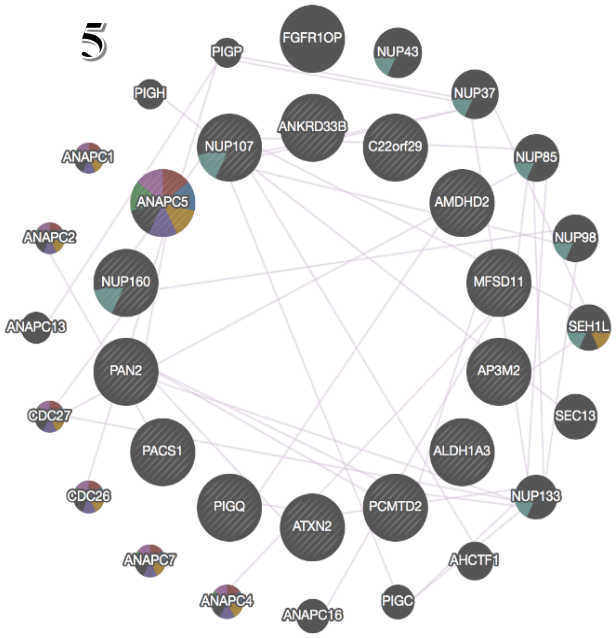

- mitotic spindle checkpoint
- metaphase/anaphase transition of cell cycle
- mitosis
- cell cycle checkpoint
- glucose transport
- negative regulation of cell cycle process
- negative regulation of cell cycle

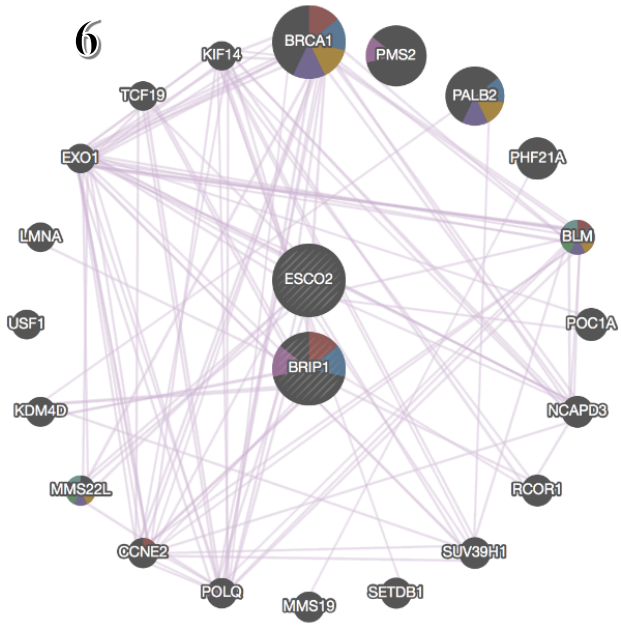

- cell cycle checkpoint
- double-strand break repair
- recombinational repair
- double-strand break repair via homologous recombination
- maintenance of fidelity involved in DNA-dependent DNA replication
- ATPase activity
- replication fork processing

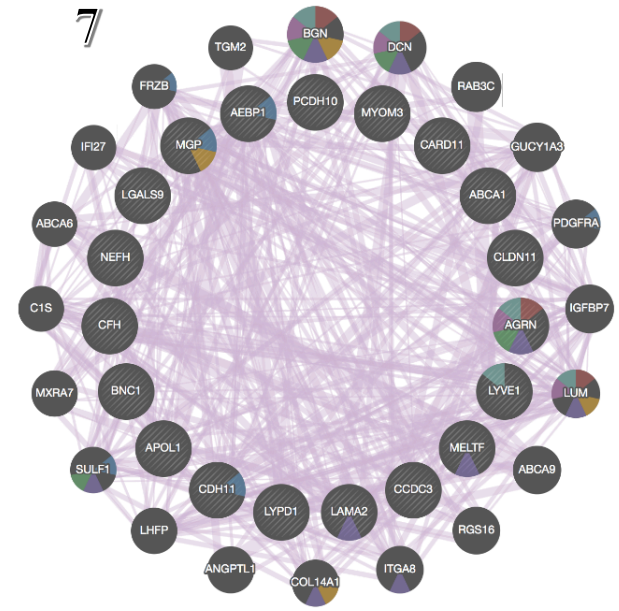

- lysosomal lumen
- skeletal system development
- extracellular matrix structural constituent
- extracellular matrix organization
- proteoglycan metabolic process
- vacuolar lumen
- aminoglycan metabolic process

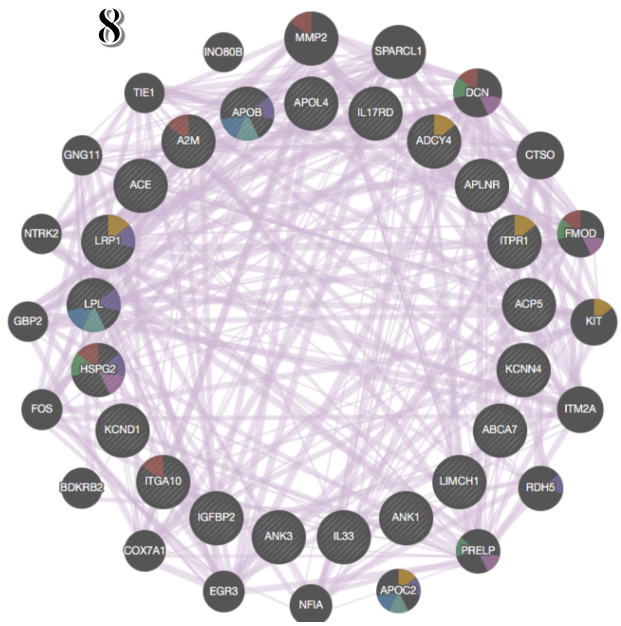

- regulation of lipase activity
- response to light stimulus
- vacuolar lumen
- protein-lipid complex remodeling
- macromolecular complex remodeling
- lysosomal lumen
- extracellular matrix organization

Upstream transcription factor

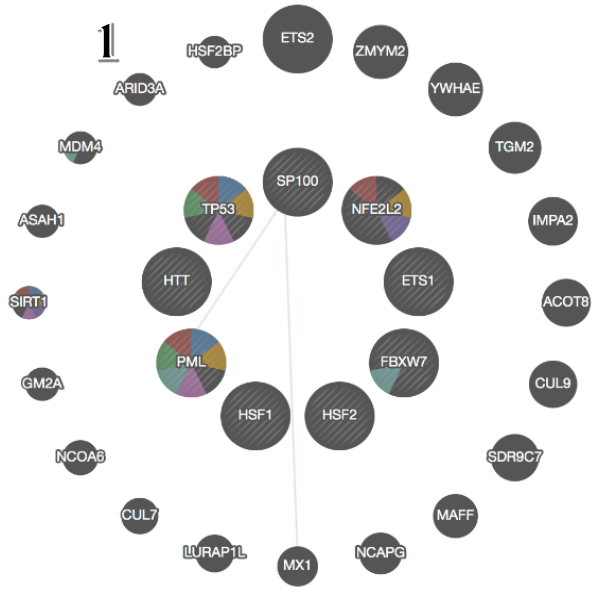

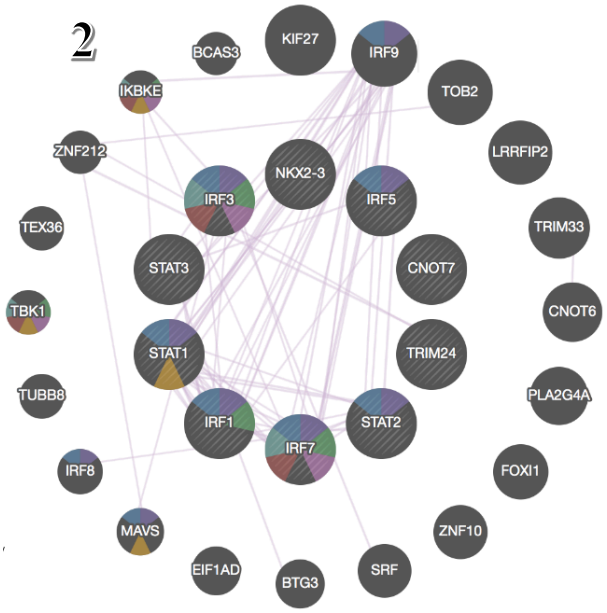

- cell aging
- response to oxidative stress
- negative regulation of cellular response to oxidative stress
- negative regulation of viral process
- aging
- cellular senescence
- regulation of protein stability

- type I interferon signaling pathway
- toll-like receptor signaling pathway
- TRIF-dependent toll-like receptor signaling pathway
- I-kappaB kinase/NF-kappaB signaling
- toll-like receptor 4 signaling pathway
- toll-like receptor 3 signaling pathway
- response to type I interferon

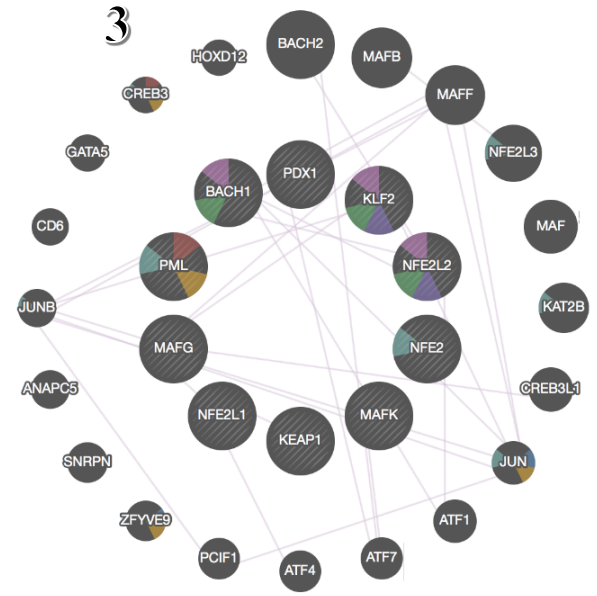

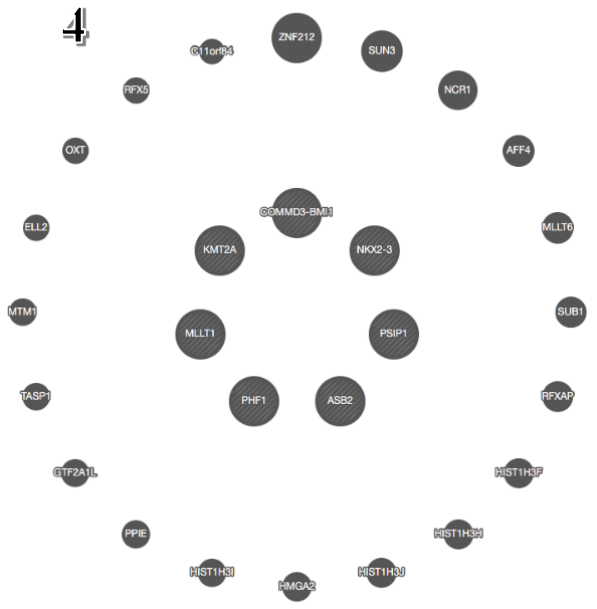

- positive regulation of defense response to virus by host
- SMAD protein import into nucleus
- protein localization to nucleus
- response to fluid shear stress
- regulation of DNA-templated transcription in response to stress
- transcription coactivator activity
- regulation of transcription from RNA polymerase II promoter in response to stress

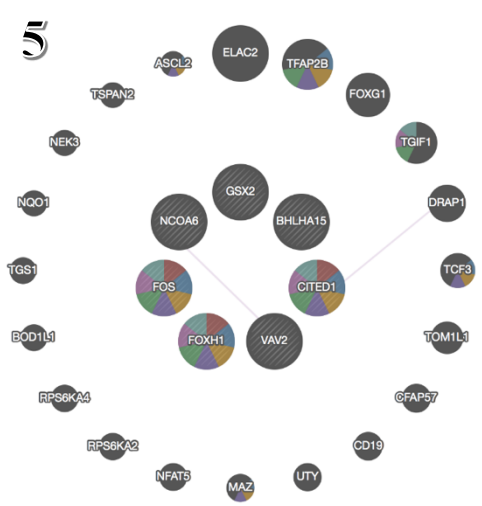

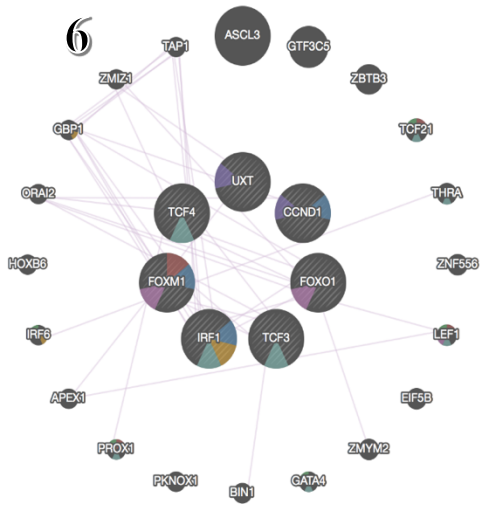

- SMAD binding
- regulatory region DNA binding
- transcription regulatory region DNA binding
- regulatory region nucleic acid binding
- transmembrane receptor protein serine/threonine kinase signaling pathway
- transforming growth factor beta receptor signaling pathway
- cellular response to transforming growth factor beta stimulus

- blood vessel morphogenesis
- cell cycle arrest
- interferon-gamma-mediated signaling pathway
- regulatory region nucleic acid binding
- DNA binding, bending
- transcription corepressor activity
- epithelial cell differentiation

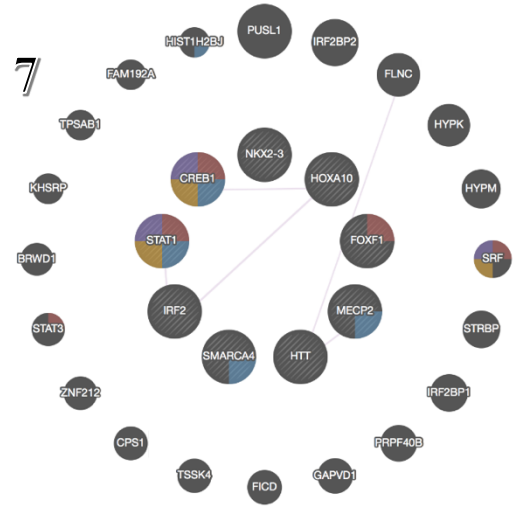

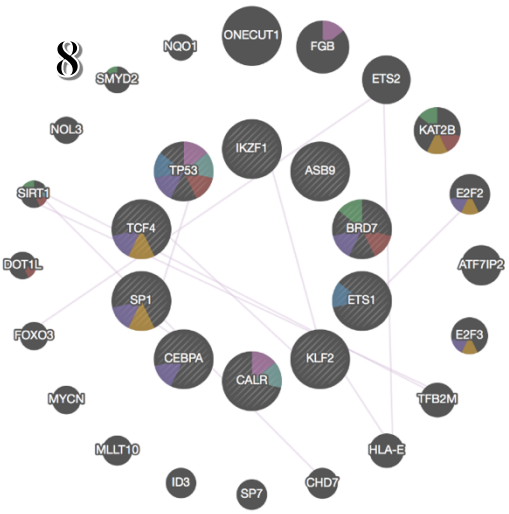

- sequence-specific DNA binding RNA polymerase II transcription factor activity
- chromatin
- RNA polymerase II regulatory region DNA binding
- RNA polymerase II regulatory region sequence-specific DNA binding

- chaperone binding
- cellular senescence
- histone modification
- transcription initiation from RNA polymerase II promoter
- transcription regulatory region DNA binding
- response to toxic substance
- peptidyl-lysine modification

Figure 4.9). Diagrams were generated by using GENEMANIA interconnection analysis. Each diagram represents a cluster and the respective upstream transcription factor regulation. Most of the clusters and the upstream regulator factor regulator pathways are associated with protein folding/refolding control, chaperone bindings, interferon signalling pathways activation, oxidoreductase activity, response to virus, xenobiotic stimulus and toxic substance, response to shear stress, DNA breaks, cell ageing, negative regulation of cell cycle process and arrest

A

OSGIN1 vs AdControl, significant: 285, fdr=0.05

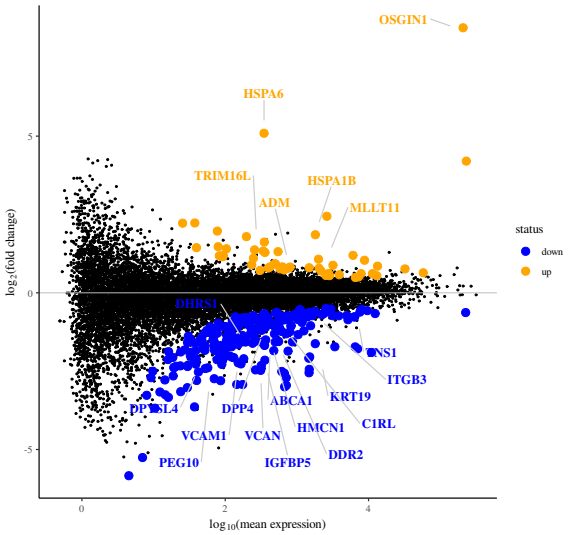

OSGIN2 vs AdControl, significant: 9, fdr=0.05

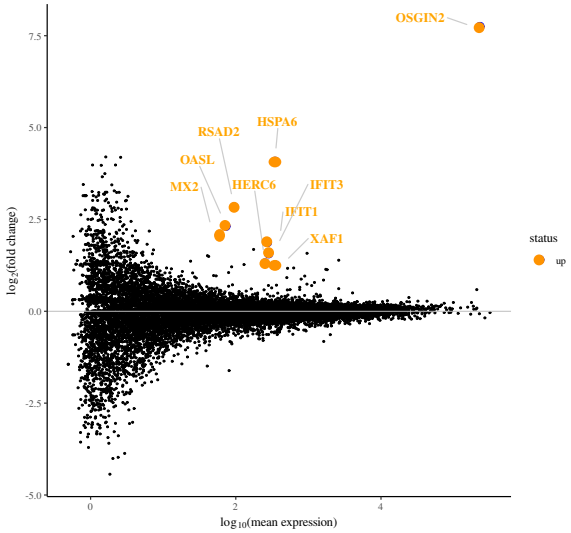

OSGIN1+2 vs AdControl, significant: 180, fdr=0.05

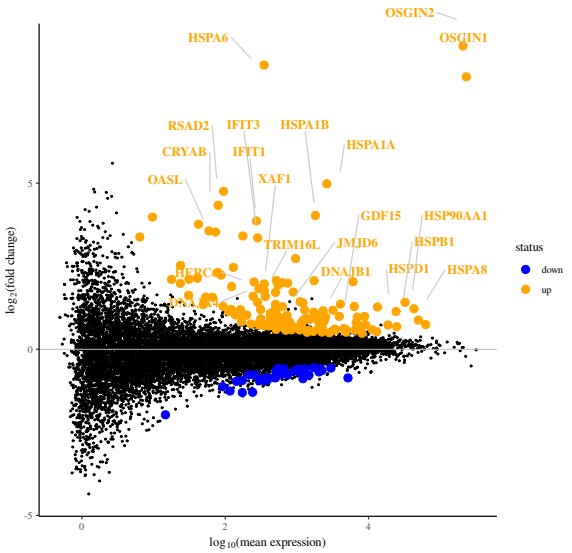

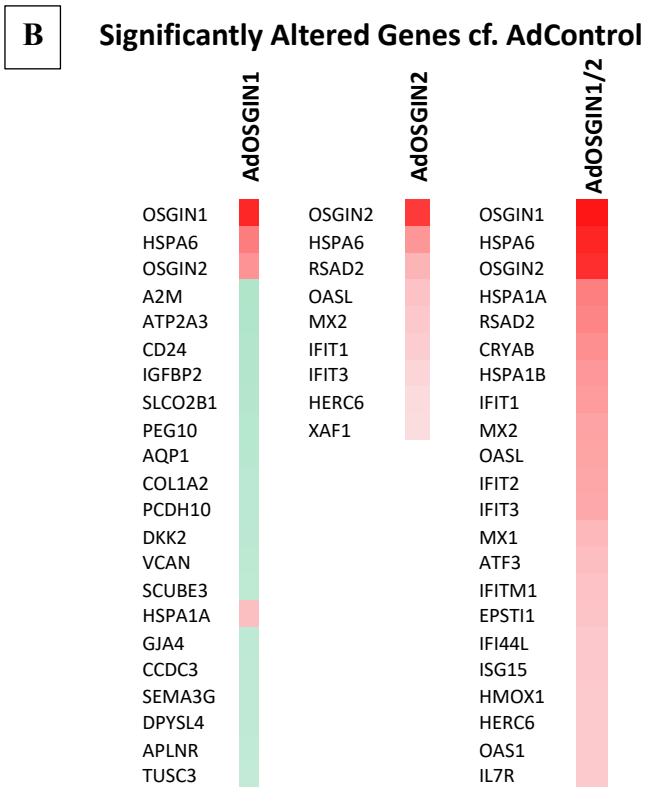

Figure 4.10). A) MA plots show the genes with the fold change by overexpression of OSGIN1, OSGIN2 or OSGIN1+2 compared to AdCtrl, yellow indicates upregulation and blue downregulation.
B) Summary of the MA plots. The genes with the most significantly/biggest fold change with an increase in expression are indicate in red an and green indicates a decrease. With AdOSGIN1, 235 genes changed significantly (p adjusted <0.05), 9 with AdOSGIN2 and 169 with AdOSGIN1+2 compared to AdCtrl.

Clustering analysis was carried out and eight clusters were identified and below summarised.

- Cluster 1: genes associated with the activation of the Ingenuity IPA canonical pathway NRF2-mediated Oxidative Stress Response, inhibition in eNOS Signalling and alteration in Protein Ubiquitination Pathway, Unfolded protein response (full list in Table 5 Appendix). These changes are predicted to be driven by the activation of Heat shock factor 1 (HSF1) and NRF2 (NFE2L2) (See Table 5 Appendix for all predicted regulators).
- Cluster 2 is associated with the activation of Interferon signalling which are driven by the activation of signal transducer and activator of transcription 1 (STAT1) and 2, Interferon regulatory factor 1 (IRF1), 3, 5, 7 and 9, and inhibition of tripartite motif-containing 24 (TRIM24) (Table 6 Appendix).
- Cluster 3 is related with NRF2-mediated Oxidative Stress Response pathway driven by NRF2 activation (Table 7 Appendix).

- Cluster 4 is related with negative regulation of cell differentiation (Table 8 Appendix).
- Cluster 5 and 6 are related with the activation of DNA double strand break repair, cell cycle check point, down regulation of cell cycle and cell cycle arrest confirming the results discussed in chapter 3 (Tables 9-10 Appendix).
- Cluster 7 and 8 are related with ECM reorganisation, proteoglycan metabolic process, cellular senescence and chaperone bindings which as mentioned in sections 4.2, 4.3 might be promote EC detachment (Tables 11-12 Appendix).
- Summary of the top 20 transcription factor regulators for AdOSGIN1, AdOSGIN2 and AdOSGIN1+2 is in figure 4.11. Here it was observed that AdOSGIN1s 20 transcription factor regulators are mainly associated with CMA and proteostasis pathways. AdOSGIN2s top 20 transcription factor regulators are mainly associated with signalling pathways, inhibition of NFKB and Trif-dependent Toll-like receptor pathway, and AdOSGIN1+2 top 20 transcription factor regulators are mainly involved with protein sumolation, response to TNFα and oxidative stress, interferon pathway activation and Toll-like receptor pathway.
- (Full detail of all clusters is in Tables 5 to 15 Appendix). 235 genes were significantly changed (p adjusted >0.05) with AdOSGIN1, 9 with AdOSGIN2 and 169 with AdOSGIN1 and 2 compared to AdCtrl (Figure 4.10).

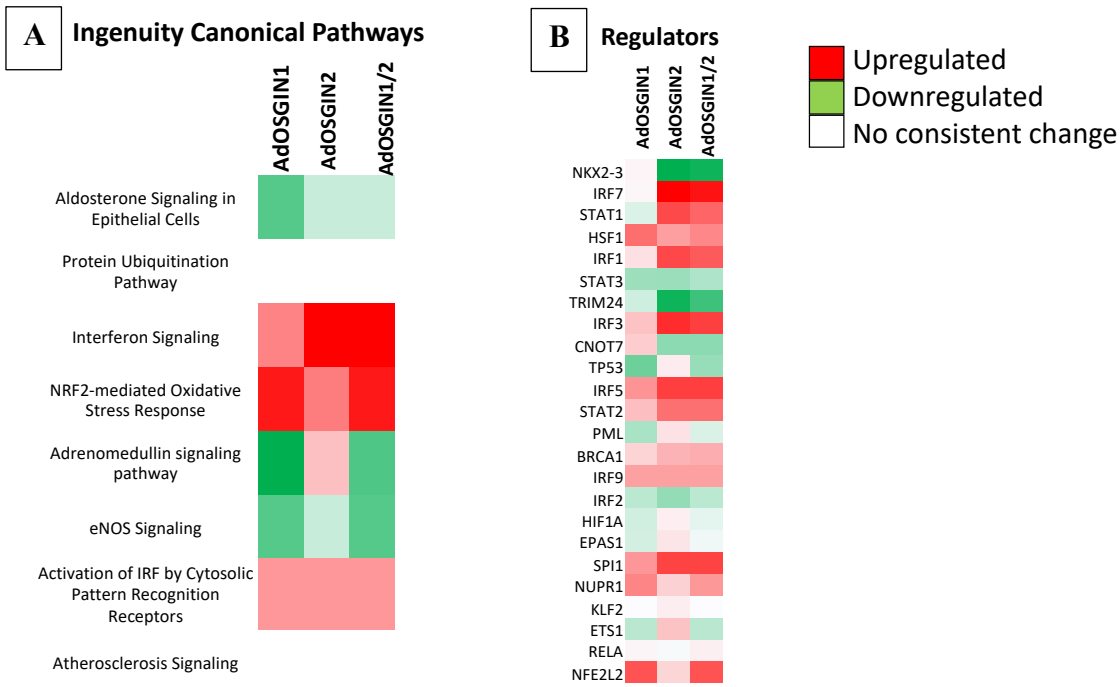

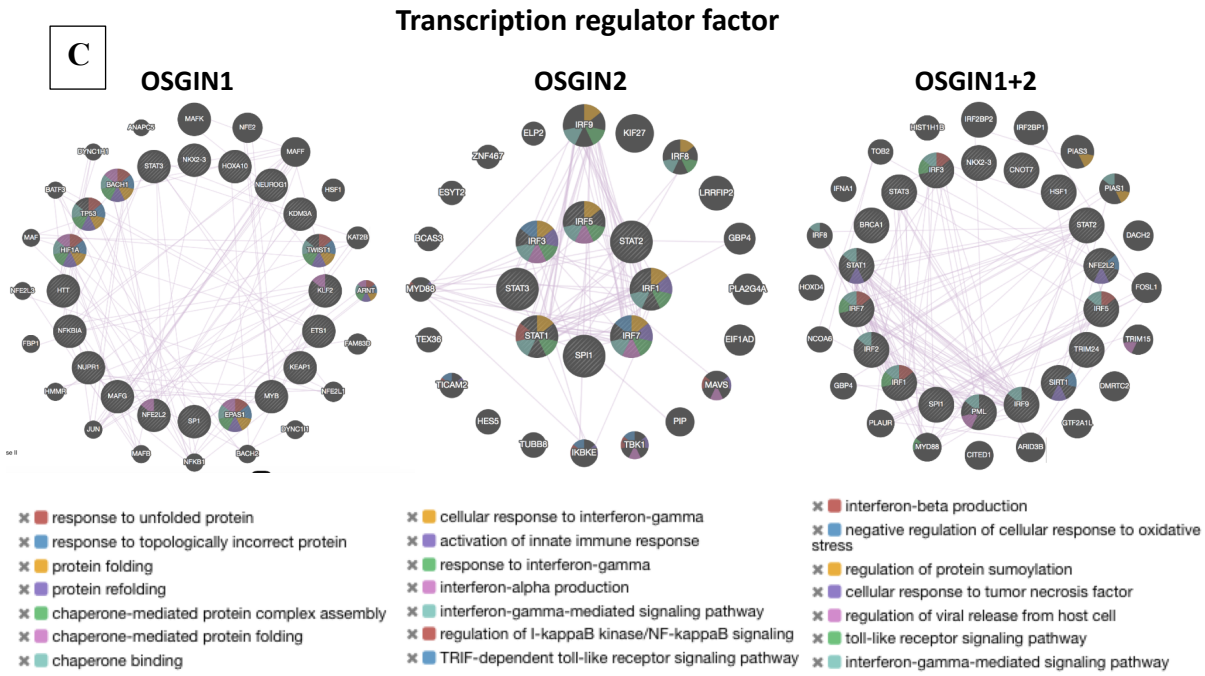

Figure 4.11). A) Ingenuity pathway analysis of the top predicted canonical pathways, red indicates a predicted activation and green a decrease. White indicates significant changes in genes in this pathway but do not consistently indicate an increase or decrease in the pathway, suggesting dysregulation. **B)** Ingenuity pathway analysis predicted upstream transcriptional regulators for genes changing within the heatmap, red indicates a predicted activation, white no change and green a decrease. **C)** The top 20 canonical regulators were analysed by GENEMANIA. Diagrams show co-expression of AdOSGIN1, AdOSGIN2 and combination of both transcription regulator factors. Analysis of AdOSGIN1 transcription regulator factors showed that are mainly associated with CMA and proteostasis pathways. AdOSGIN2s top 20 transcription regulator factors are associated with interferon signalling pathways, inhibition of NFKB and Trif-dependent Toll-like receptor pathway. AdOSGIN1+2 transcription regulator factors analysis are associated with protein sumolation, response to TNFα and oxidative stress, interferons pathway activation and Toll-like receptor pathway.

55% of the top 20 significant genes ranked by fold change were involved in interferon signalling or are downstream of interferon (IFIT1, MX2, OASL, IFIT2, IFIT3, MX1, IFITM1, EPSTI1, IFI44L, ISG15 and OAS1). The pivotal role of interferon is highlighted by the significant increase in genes involved with the interferon signalling ingenuity canonical pathway within all genes altered by OSGIN1, 2 or 1 and 2 (Figure 4.10A) and the predicted activation of upstream regulators IRF7, STAT1, IRF1, IRF3, IRF5, STAT2, BRACA1, IRF9 and SPI1, and inhibition of STAT3, TP53, IRF2 (Figure 4.11B).

30% of the top genes changed by AdOSGIN1 and 2 (HSPA6, HSPA1A, CRYAB, HSPA1B, ISG15 and HERC6) are associated with proteostasis and the genes in ingenuity canonical pathway Protein Ubiquitination Pathway are significantly altered.

25% of the top 20 have known to have interactions with the key proteostasis regulator BAG3 (HSPA6, HSPA1A, CRYAB, HSPA1B and ISG15 according to Inginuity IPA database) which is also upregulated (Figure 4.9). Furthermore, other interaction partners of BAG3:

STIP1, HSPB1, HSPB8, NQO1, HSP90AA1, HSP90AB1, DNAJB1, DNAJB6 HSPA4, P4HA2, SQSTM1/p62, HSPA8, TRIM69 are upregulated and CD40, DOCK8, CARMIL1, EVL, KRT19 and TFAP2A are downregulated (Table 13 Appendix) (Figure 4.11C).

Overall the transcriptomic analysis suggests the predominant pathways activated by OSGIN1+2 overexpression include regulation of NRF2- and interferon-controlled genes, and pronounced changes in genes involved in proteostasis, particularly those associated with BAG3-associated proteostasis.

4.7.3 OSGIN1 and OSGIN2 trigger CMA and impair physiological autophagic flux

To validate the results obtained from the RNAseq analysis and to further probe the genes involved in CMA, qPCR, western and ICC analysis of HCAECs transduced with AdOSGIN1 and AdOSGIN2 were performed. OSGIN1 and OSGIN2 significantly increased the mRNA level of classical autophagy and CMA genes. The autophagic mechanism is involved in both bulk degradation of primarily long-lived cytoplasmic proteins as well as in selective degradation of cytoplasmic organelles. The increased expression of multiple genes involved in the autophagic process might indicate the activation of a cellular response to increase autophagy to allow the cell to respond and adapt to perceived stress (Figure 4.12). Although macroautophagy and CMA represent separate entry points for proteostasis, they both result in the formation of the autophagolysosomal vesicles. There is no single marker of autophagy due to the complexity of this mechanism and its regulation, but SQSTM1/p62 binds directly LC3 [443] which results in specific degradation during autophagic process, and this makes SQSTM1/p62 a valuable marker to evaluate the autophagic flux [444]. Abnormal clearance of autophagic vesicles would result in an accumulation of punctate vesicular staining of SQSTM17p62 and lysosome-associated membrane glycoprotein 1 (LAMP1).

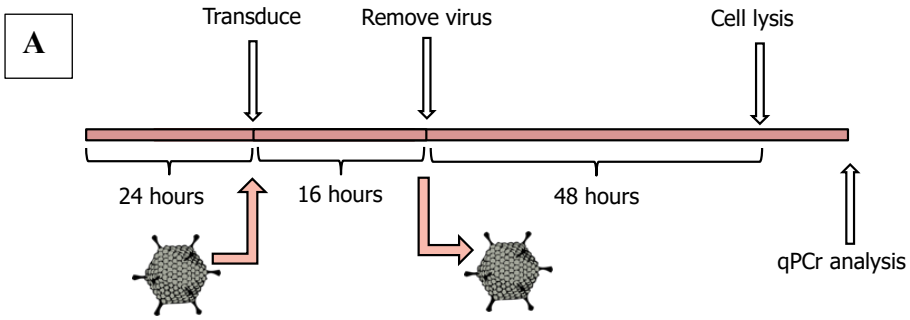

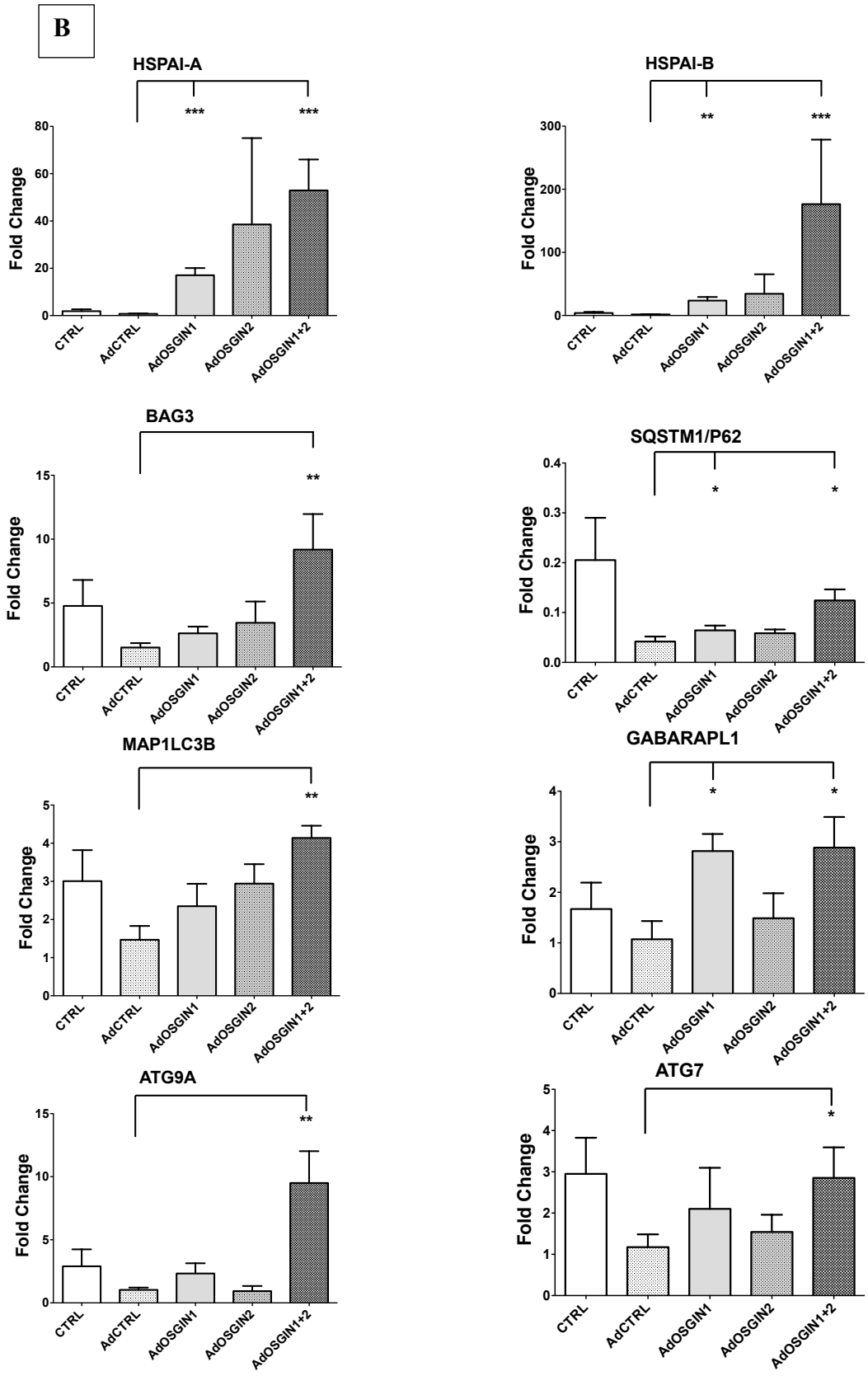

Figure 4.12). **A)** Timeline for mRNA analysis. 1.7x 10^5 HCAECs were seeded and grown in a 6 well plate for 24 hrs. Transduction with adenoviral vector was carried out the 2nd day (total pfu/cell of 400). 200 pfu/cell active vector (AdOSGIN1, AdOSGIN2) and 200pfu/cell of control virus were used for single gene transduction; for both OSGIN1 and 2 overexpression this consisted of 200pfu/cell of both vectors; AdCtrl (E1/E3 'empty' Ad vector), was used as the control (400pfu/cell). Virus was removed on 3rd day. On the 4th day the media

was removed, cells were washed with 1X PBS and lysate with 300µl of lysis buffer (3 µl of β-mercaptoEtOH was added). **B)** HCAECs were plated in 6 well plates and transduced with AdOSGIN1+2 at a pfu of 400 per cell as previously described (n=6 from different donors). RNA was purified using a Norgen Total RNA isolation kit and 250ng per condition used for reverse transcription. Changes in mRNA expression of key regulators of macroautophagy and chaperone-mediated autophagy pathway by OSGIN1+2 overexpression were assessed by qPCR, including F) HSPA1A; G) HSPA1B; H) BAG3; I) MAP1LC3B; J) SQSTM1/P62; K) ATG9A (**P<0.01 and ***P<0.001; n=6 One-way ANOVA) protein level quantification (Figure 4.14, 4.16). 1.7x 10^5 HCAECs were seeded and grown in a 6 well plate for 24 hrs. Transduction with adenoviral vector was carried out the 2nd day (total pfu/cell of 400). 200 pfu/cell active vector (AdOSGIN1, AdOSGIN2) and 200pfu/cell of control virus were used for single gene transduction; for both OSGIN1 and 2 overexpression this consisted of 200pfu/cell of both vectors; AdCtrl (E1/E3 'empty' Ad vector), was used as the control (400pfu/cell). Virus was removed on 3rd day. On the 4th day the media was removed, cells were washed with 1X PBS and lysate with 300µl of lysis buffer (3 µl of β-mercaptoEtOH was added).

Immunocytochemical staining for LAMP1 (Red) and SQSTM/p62 (Green) in HCAEC transduced with AdOSGIN1 and AdOSGIN2 (Figure 4.13) was performed.

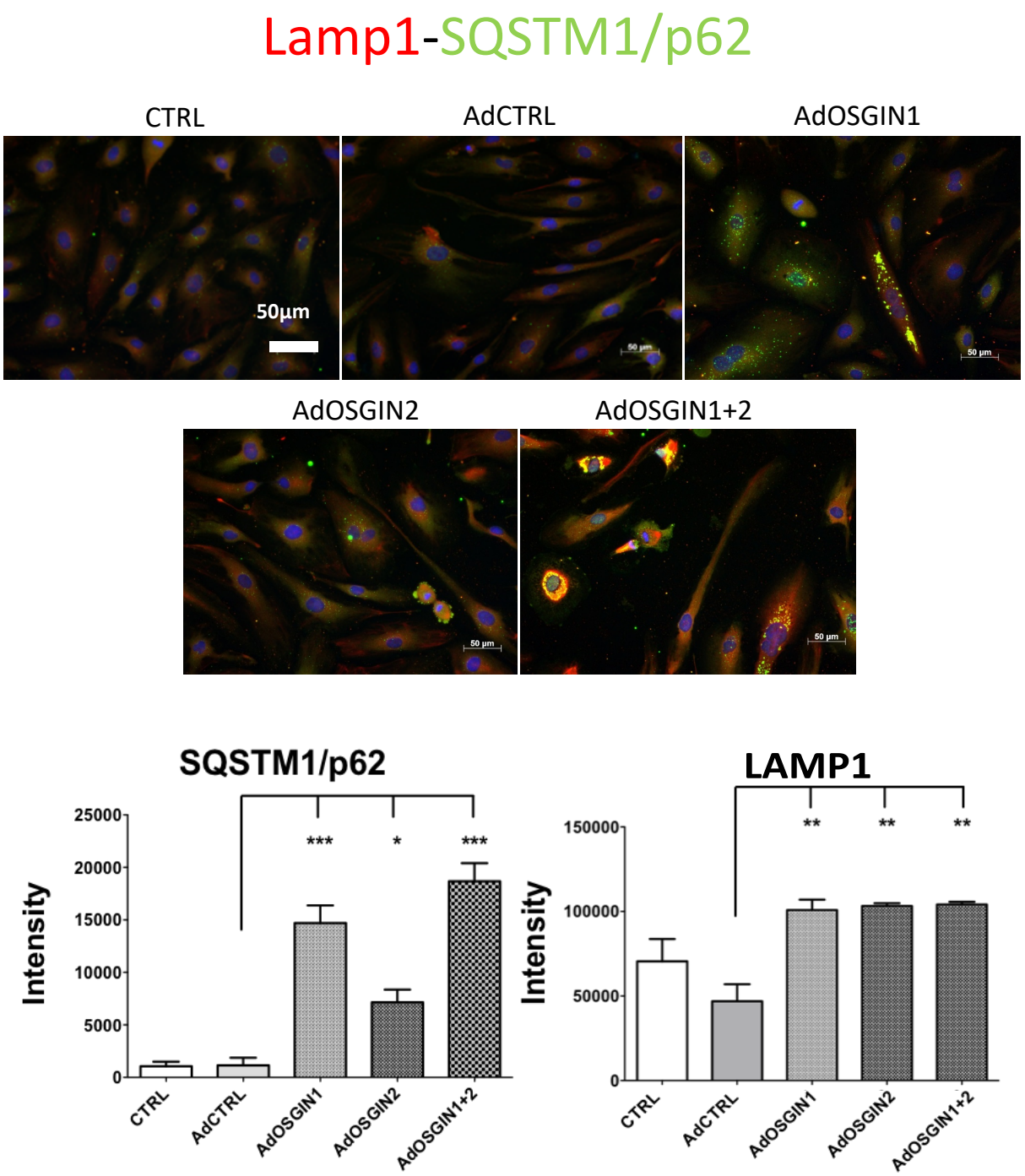

Figure 4.13). Immunofluorescence of SQSTM/p62 (Green) and LAMP1 (Red), demonstrate an accumulation of SQSTM/p62 and LAMP1 positive vesicles, indicative of a block in autophagic flux (*p<0.05, **p<0.01, ***p<0.001 n=3, one-way ANOVA). The experiment was carried out on a confluent layer of ECs in an 8 well chamber slide 0.1% gelatine coated. Transduction with adenoviral vector was carried out the 2nd day (total pfu/cell of 400). 200 pfu/cell active vector (AdOSGIN1, AdOSGIN2) and 200pfu/cell of control virus were used for single gene transduction; for both OSGIN1 and 2 overexpression this consisted of 200pfu/cell of both vectors; AdCtrl (E1/E3 'empty' Ad vector), was used as the control (400pfu/cell). Virus was removed on 3rd day. The 4th day the media was removed, cells were washed with 1X PBS and fixed in PFA 4% for 20'before immunostaining.

Immunocytochemical staining highlighted accumulation of LAMP1 and SQSTM/p62 positive vesicles which suggests a blockade of the autophagic flux. To confirm further, SQSTM/p62 accumulation was investigated using western blotting as shown in figure 4.14A-B.

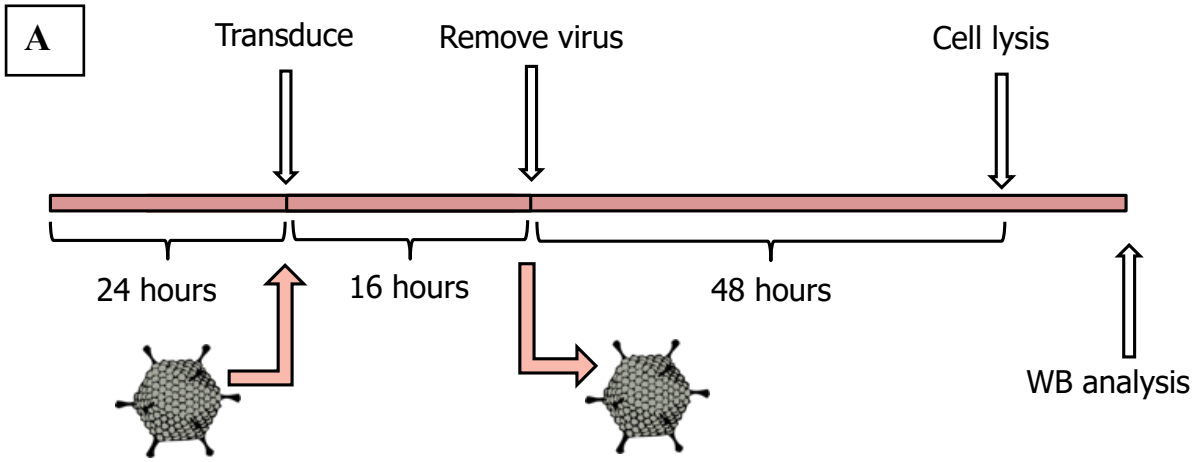

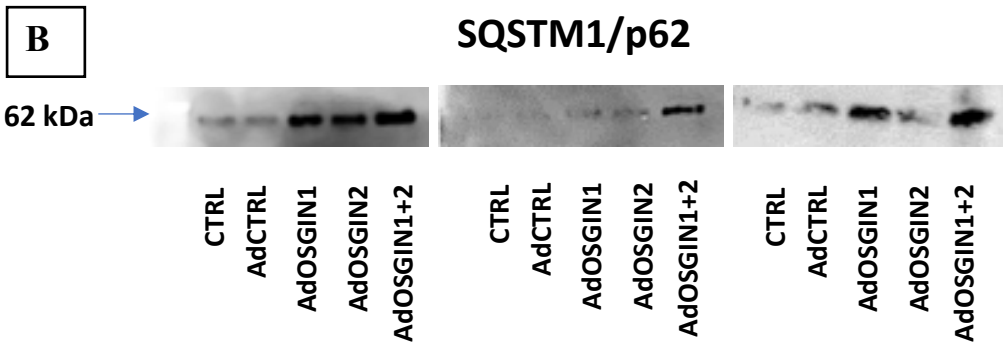

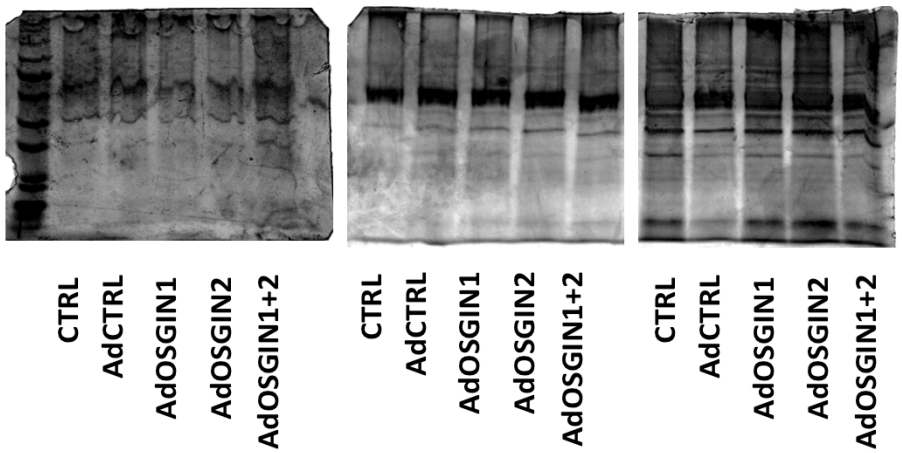

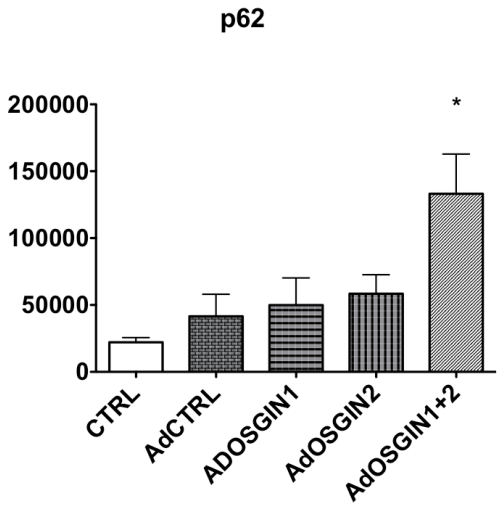

Figure 4.14). A) Timeline for the western blot experiment. B) SQSTM/p62 was evaluated through western blotting and its accumulation was reported in AdOSGIN1+2 condition (n=3). HCAECs were seeded in duplicate wells of a 24 well plate at $6x10^4$ cells per well. Transduction with adenoviral vector was carried out the 2nd day (total pfu/cell of 400). 200 pfu/cell active vector (AdOSGIN1, AdOSGIN2) and 200pfu/cell of control virus were used for single gene transduction; for both OSGIN1 and 2 overexpression this consisted of 200pfu/cell of both vectors; AdCtrl (E1/E3 'empty' Ad vector), was used as the control (400pfu/cell). Virus was removed on 3rd day. On the 4th day the media was removed, cells were washed with 1X PBS and lysate with cold RIPA buffer (1:1000 protease and phosphatase inhibitor was added). Total protein quantification was used to determine SQSTM/p62 accumulation (see Figure 4.14 for total protein). (n=3 independent experiments with HCAEC form different donors *$p<0.05$, one-way ANOVA).

This data suggests that OSGIN1 and OSGIN2 and in particular the combination of both genes, preclude the correct functionality of the autophagic mechanism, which promotes lysosomal accumulation and prevents normal degradation/recycling process of the cargo. In addition, HSP70 protein level was quantified by immunocytochemistry and also western blot analysis. As mentioned above CMA is responsible for the degradation of a subset of cytosolic proteins trough lysosomal degradation [269]. The KFERQ motif is recognized by a cytosolic chaperone HSP70, in complex with its cochaperones HSC70 [445], and differently from the canonical autophagy and microautophagy (see Introduction sections 1.91 and 1.95), once the CMA substrates are in the lysosomal lumen, they are rapidly degraded (5-10 min time) by lysosomal proteases. ICC staining and western blot analysis showed an increase in HSP70 protein levels, which matched the increase in HSP70 mRNA levels (Figure 4.15-4.16). Interestingly HSP70 is localised on the edge of the cells, which might affect adhesion molecules stability and consequently their degradation as they may interact with HSP70/BAG3 complex (Figure 4.15).

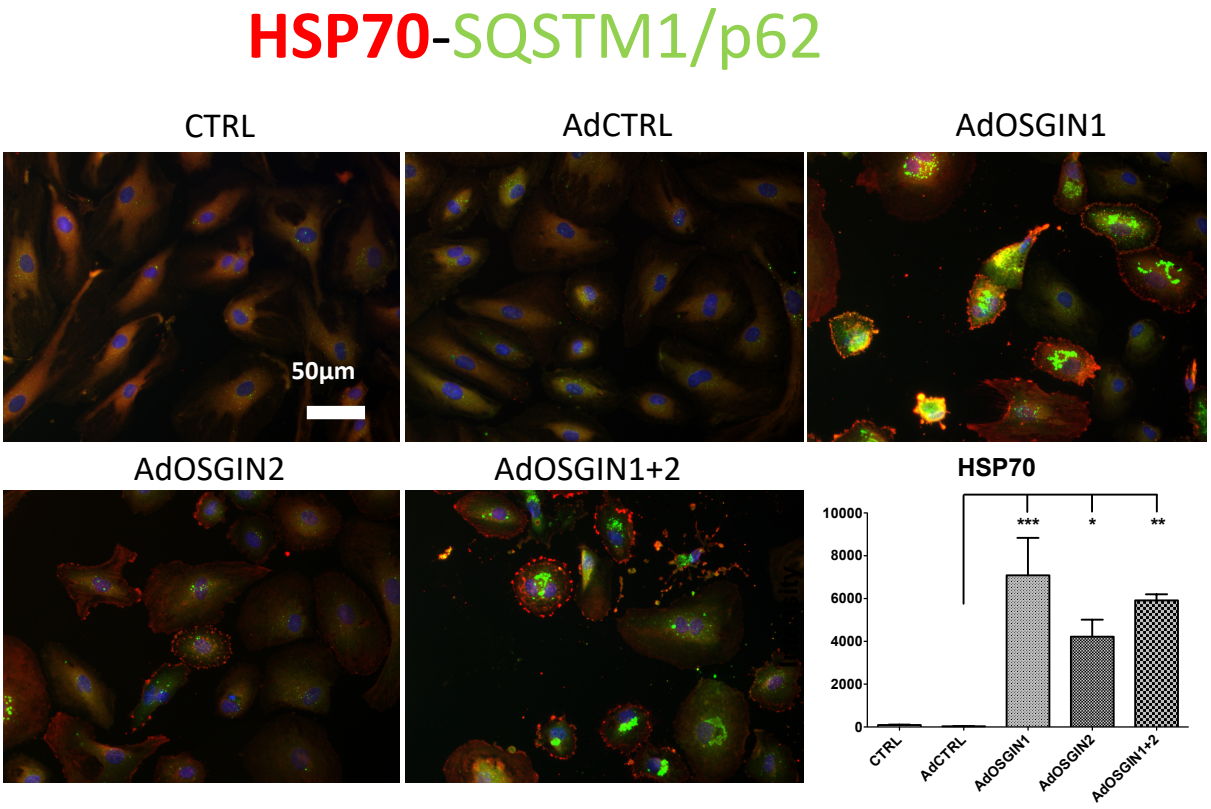

Figure 4.15). Immunofluorescence of SQSTM/p62 (in green) and HSP70 (in red) showed accumulation of both proteins (n=3). HCAECs were seeded in a 24 well plate in duplicate for 24 hrs. Transduction with adenoviral vector was carried out the 2nd day (total pfu/cell of 400). 200 pfu/cell active vector (AdOSGIN1, AdOSGIN2) and 200pfu/cell of control virus were used for single gene transduction; for both OSGIN1 and 2 overexpression this consisted of 200pfu/cell of both vectors; AdCtrl (E1/E3 'empty' Ad vector), was used as the control (400pfu/cell). Virus was removed on 3rd day. The 4th day the media was removed, cells were washed with 1X PBS and lysate with cold RIPA buffer (1:1000 protease and phosphatase inhibitor was added). Total protein quantification was used to determine SQSTM/p62 accumulation (Figure 4.14). Protein lysate was collected from 2 wells (in duplicate) of a 24 well plate. (*p<0.05, **p<0.01, ***p<0.001 one-way ANOVA).

Considering that CMA has been described as an emergency mechanism in case of canonical autophagy failure and that CMA substrates should be rapidly degraded, the presence of HSP70, concomitantly with p62, enhance the hypothesis of autophagic flux blockade.

HSP70 protein levels were further analysed and quantified by western blotting (Figure 4.16) and in all three conditions, AdOSGIN1, AdOSGIN2 and combination of both genes, HSP70 protein level was significantly higher, confirming ICC analysis.

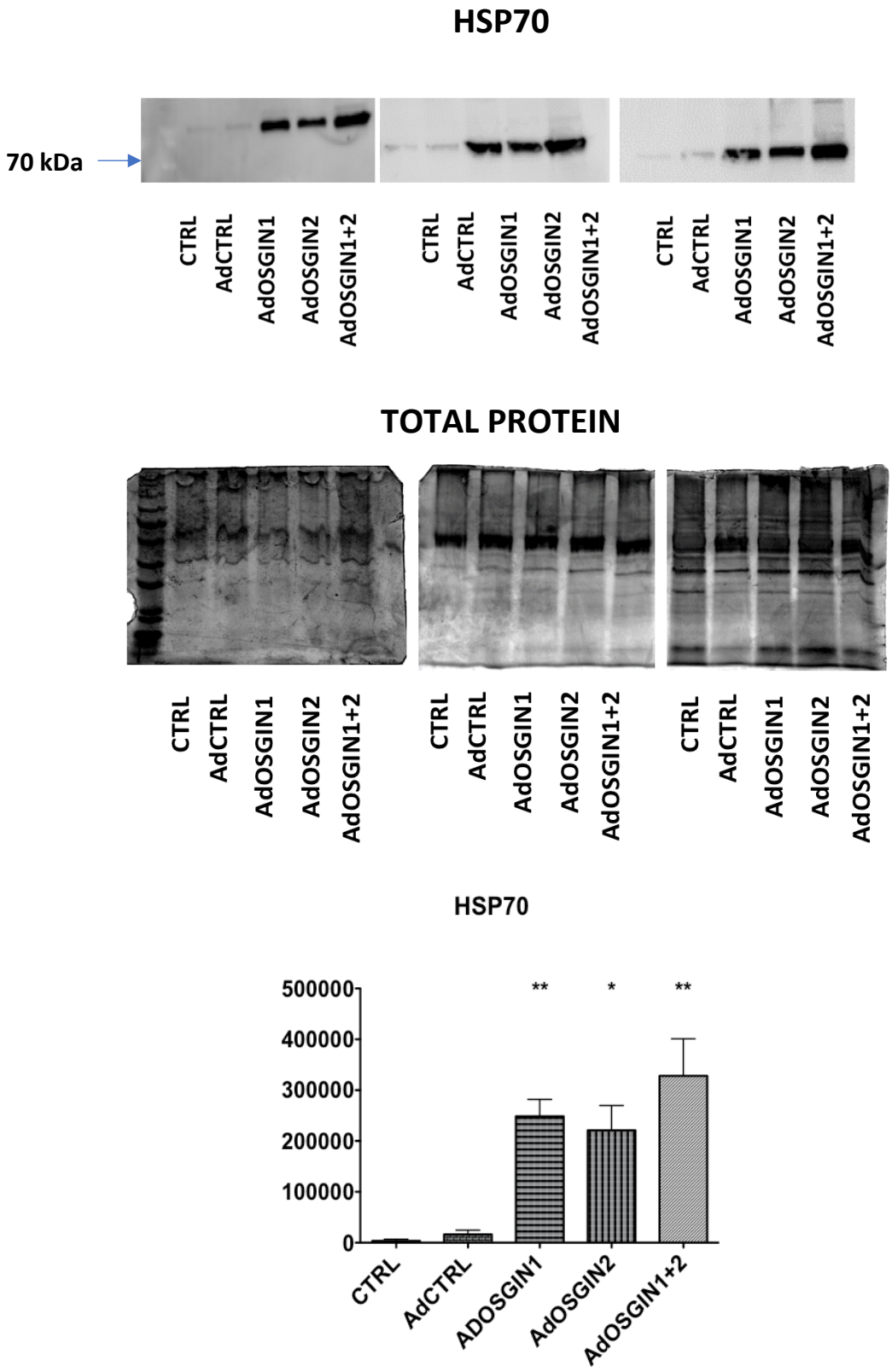

Figure 4.16). HSP70 was evaluated through western blotting and its accumulation was reported in AdOSGIN1+2 condition (n=3). Total protein quantification was used to determine SQSTM1/p62 and HSP70 level.

4.8 Discussion

In 2016 Belch *et al* [446] showed how the macroautophagy pathway is mediated by BAG3, HSP70 and SQSTM1/p62 targets aggregation-prone proteins through autophagy degradation. BAG3 therefore has been reported as an emergency system which switches from BAG1 during pathophysiological conditions [437] and how their levels are reciprocally regulated during ageing.

In 2009 Gamerdinger *et al* [447], using a well-known model of cell ageing developed by Nichols *et al* in 1977, showed that primary human cells which exhibit hallmarks of ageing, after a finite number of cell division become senescent with large morphology. Real time PCR showed a down regulation of BAG1 and 2 and up regulation of BAG3. These findings are in agreement with the data reported during this study suggesting that there is a tight link between cell morphology, cell ageing with following activation of senescence (described in Chapter 3) and autophagy pathways.

Here, the main genes involved in macroautophagy and CMA mechanisms were analysed by qPCr. It was observed that SQSTM1/p62, LC3B, Atg7, Atg8 (GABARAPL1) and atg9A were upregulated during the combined effect of AdOSGIN1 and 2 compared to AdCtrl. Furthermore, increased mRNA level of HSPA1A, HSPA1B (HSP70) and BAG3 was observed (Figure 4.8), suggesting a direct involvement of this mechanism during the process of plaque erosion.

The NRF2 antioxidant role regulates many genes in order to protect the cell against free radical and oxidative stress [122]. However, the data we provide here suggests that continually elevated NRF2 activation has an inhibitory effect of proteostasis, through the upregulation of OSGIN1 and OSGIN2. Previous work carried out in Dr White's laboratory showed that ESS in combination with TNFα and CSE, which contains high levels of reactive oxygen and free radicals [448], provokes NRF2 activation [116] and EC detachment [113]. Thus, environmental and haemodynamic stimuli synergise to further elevate NRF2 activation which potentially impairs adhesion of EC overlying stenotic plaques.

Results in Chapter 3 demonstrate that OSGIN1 and OSGIN2 are associated with cell cycle inhibition and increases in markers of senescence, which promotes changes in cell morphology and increases in cell size [449, 450]. The results in this chapter have showed that combined adenoviral overexpression of OSGIN1 and OSGIN2 is sufficient to trigger EC

detachment under static culture conditions. EC adhesion is modulated by three processes: interaction between ECM and focal adhesion, cell-cell contact, and intact cytoskeleton. Different markers for all processes were evaluated through ICC staining, which showed that OSGIN1 and 2 disrupt cytoskeletal structure in HCAECs with a heavy loss in tubulin and actin. It was also observed that they are responsible for reducing β catenin and VE-cadherin, weakening cell-cell contact and potentially augment EC permeability together with a decrease in the amount of focal adhesion. All three processes appear to be compromised with OSGIN1+2 overexpression, which severely impairs adhesome functionality. In addition, OSGIN1 and OSGIN2 overexpression affects cell height, this was observed to be up to 5-fold higher than the control and AdCtrl. This morphological change facilitates cell detachment when hit by ESS compared to a flat cell, in a scenario where cell structure and adhesion molecules are already compromised. Therefore, on a stenotic plaque, OSGIN1+2 upregulation would reduce the adhesive capacity of the cell, increment in EC height and together leading to erosion.

Data acquired from RNAseq transcriptome analysis, showed that after overexpression of OSGIN1 and 2, a third of the top gene changes are involved in the proteostasis mechanism, alongside an altered protein ubiquitination pathway. Interestingly, 11 of the top 20 genes significantly upregulated by OSGIN1, 2 or 1 and 2 show that their most relevant signalling and metabolic pathways, as well as the biological functions, are part of the interferon signalling pathway or downstream of interferon. Fascinatingly, OSGIN1+2 overexpression gives a signature for NRF2 regulated genes and interferon regulated genes. RNAseq transcriptome analysis suggests an alteration in the interferon signalling pathway, as well as strong changes in BAG3 and other genes responsible for the regulation of protein degradation, which as mentioned in the section 4.3 might lead to a loss in the adhesome functionality. OSGIN1 and 2 regulated genes might also be enhanced by interferon α signalling because of the presence of IRF3/7 binding sites in their promoter. Interestingly, downstream of NRF2, a high level of HSP70 was observed. HSP70 extracellular accumulation might have a protective effect in ECs [448], mediated through Trif-dependent TLR4 signalling [451], which activates IRF3/7, but for a better understanding of the impact of interferon α on endothelial erosion, further experiments and data from patients are necessary.

Sample analysis by qPCR also confirmed that OSGIN1 and OSGIN2 overexpression significantly enhanced expression HSPA1A and HSPA1B (HSP70) and BAG3 which supervises the correct protein folding in CMA. In addition, overexpression of BAG3 has been associated with loss in focal adhesion [435] which might explain EC detachment.

Next, OSGIN1 and OSGIN2 was also shown to promote significant increment in mRNA levels for the main genes involved in macroautophagy such as SQSTM1/p62, LC3B, GABARAPL1 (Atg8), atg7 and atg9A. Western blot analysis showed SQSTM1/p62 and HSP70 protein level accumulation, which suggests that there is a reduction in the autophagy flux.

Upregulation of the genes stated above suggests that damage in the cell activates the autophagy mechanism as a degradation pathway which is able to remove aggregates of toxic protein and non-functional organelles in order to prevent their detrimental effects. This supports the data that shows a block in the cell cycle in the attempt to repair the damage caused. However, an incomplete or inefficient process of clearance of cellular damage would explain the lack of cell recovery and its entrance in a cellular senescence state. Taking all this data together, a combination of OSGIN1 and 2 seems to promote EC detachment in an apoptosis independent manner. Combination of OSIGIN1 and 2 acts on EC adhesome by reducing its functionality, potentially by the overexpressing BAG3/p62 and BAG3/HSP70 complex which promotes focal adhesion weakening. Furthermore, OSGIN1 and 2 and constrains autophagic flux which it was observed to be crucial for strengthening the ECM/focal adhesion interaction in healthy cells. This would prevent ECs from re-establishing their interaction with the ECM facilitating cell detachment.

4.9 Key findings:

The key findings of the experiments described in this chapter are:

- EC functionality and intracellular junctions between ECs are pivotal for vascular integrity. Destabilization of endothelial junctions promote the disruption of the endothelial barrier which results in an increased EC permeability[452].Adenoviral overexpression of OSGIN2 and combination of OSGIN1 and OSGIN2 led to a loss of endothelial junction, impairing VE-cadherin and β-catenin. Furthermore, reduction of F-actin and tubulin was observed. Proatherogenic stimuli and oxidative stress promote endothelial microtubule functionality

damageand AdOSGIN2 and AdOSGIN1+2 might destabilize vascular integrity in a similar way, inducing EC permeability, and potentially increase cardiovascular risk.

- RNAseq transcriptome analysis showed that over the 3 conditions (AdOSGIN1, AdOSGIN2 and AdOSGIN1+2) vs AdCtrl, 360 genes were significantly regulated. Overall, the 8 clusters identified, showed their association with NRF2-mediated Oxidative Stress Response, inhibition in eNOS signalling and alteration in protein ubiquitination Pathway, unfolded protein response, which might be the link with CMA. These changes are driven by NRF2 and HSF1-regulated gene expression and pronounced changes in BAG3-regulated proteostasis.Furthermore, the activation of interferon signalling was observed, and interferon α signalling potentially enhanced the effect of OSGIN1 and OSGIN2 overexpression on their regulated gene. Among the genes involved in the CMA process during the correct folding protein control mechanism, HSPs (HSPA6, HSPA1A, HSPA1B) were confirmed by qPCr and western blot analysis. .
- Malfunction in the autophagy mechanism results in the accumulation of lysosomal vesicles.Autophagy has been described to have beneficial role in the clearance of misfolded or other harmful proteins. However, if this process is not rapid enough it results in the lysosomal vesicles being engulfed into the cytoplasm, which has a detrimental effect [211]. Constant activation of NRF2-regulated genes OSGIN1 and 2 lead to persistent activation of the autophagic process, which continuously overwhelms ECs with harmful proteins. SQSTM1/p62, usually rapidly removed during normal autophagy flux, was observed to be accumulated which clearly indicates a block in the natural autophagy progression, this potentially contributes to EC detachment.
- CMA autophagy regulates the selective degradation of cytosolic proteins in the cell. This mechanism has been shown to be reduced with age, which results in inefficient stress response and dysfunction. Similar behaviour has been reported with cellular senescence [453]. OSGIN1, OSGIN2 and a combination of both have shown to promote senescence in HCAECs and increase mRNA level of HSPA1A, HSPA1B (HSP70) and BAG3, which are the main players in CMA. Furthermore, accumulation of HSP70 has been observed by using both immunostaining and western blot analysis. This scenario suggests that CMA is impaired, and similarly to macroautophagy, results in a detrimental effect for the cell which alongside other data previously shown, facilitates EC detachment.

4.10 Summary:

This study is the first linking a non-canonical autophagy mechanism to plaque erosion, analysing the impact that NRF2 modulated genes, OSGIN1 and OSGIN2 have on EC molecules adhesion, cell-cell contact, morphology and cytoskeletal remodelling. Furthermore, CMA and autophagy mechanisms are inhibited (see chapter 5). Autophagy blockade is demonstrated by the accumulation of LAMP1, p62 and HSP70, which inhibits the autophagyc flux. These insults together exacerbate physiological cell functions and lead to endothelial detachment in the erosion of overlying stenotic plaque.

CHAPTER 5:
INVESTIGATING THE LINK BETWEEN NRF2, DYSFUNCTIONAL AUTOPHAGY AND ENDOTHELIAL ATTACHMENT

CHAPTER 5: INVESTIGATING THE LINK BETWEEN NRF2, DYSFUNCTIONAL AUTOPHAGY AND ENDOTHELIAL ATTACHMENT

5.1 Understanding the mechanism linking autophagy and atherosclerosis

As previously discussed in chapter 1, autophagy-mediated proteostasis plays an important homeostatic role in within the cell, in addition to its role in cellular adaptation. Consequently, it is involved in disease processes that promote atherosclerosis. The presence of increased vacuoles and inclusion bodies in the cytoplasm [293], inflammation (high TNFα level), ER stress, ox-LDL and ROS have all been identified or reported in atherosclerotic plaques. It is also noteworthy that these factors also promote the activation of autophagy highlighting the possibility that dysregulation of autophagy may play a part in atherosclerosis. Autophagy has a key role in protecting cells from ROS [22, 454], however over-activation of autophagy can reduce collagen synthesis and deposition [455] and induce cell death [456] that might promote plaque rupture and cardiovascular events [457]. In 2015 *Jiang et al.* [458] published an article "*p62 links autophagy and NRF2 signaling*" where it showed the mutual regulation of NRF2-inhibitor KEAP1 and SQSTM1/p62. This chapter investigates a role for autophagy in limiting endothelial adhesion, linking dysregulated proteostasis to the NRF2-regulated stress response.

A range of compounds to investigate these pathways, which are described below was used.

5.1.1 Bafilomycin A1

The vacuolar H+ ATPase commonly called V-ATPase is an electrogenic proton pump with the role of a pH lumen acidifier for intracellular and extracellular compartments. The first enzyme was discovered in yeast in 1981 by Oshumi and Anraku [459], where it was shown to be required for basic cellular physiology. V-ATPase was discovered in uni and multicellular organisms, including plants, showing its fundamental relevance for cellular survival. It has many roles and it has been found in different cellular locations, in particular in endomembrane organelles like endosomes and lysosomes, in the Golgi apparatus, endoplasmic reticulum and in coated vesicles. Acidic pH is necessary for the development of several processes such as endosomal ligand–receptor dissociation, hormone concentration, lysosomal degradation [460]. Autophagosome-lysosome membrane fusion and autolysosome acidification are the last steps in the process of autophagy (Figure 1.12).

Bafilomycin A1 (working concentration 30–100 nM) [461, 462] is a potent V-ATPase inhibitor, inhibiting acidification of lysosomes and preventing autophagosome-lysosome membrane fusion This is in contrast to NH4Cl or monensin, which do not promote vacuolization of lysosomes and therefore is commonly used to study the acidic compartments and the role of V-ATPase [463].

100nM bafilomycin A1 virtually inhibited endogenous protein degradation more efficiently than 10mM NH4Cl that neutralizes the acidity of the lysosomal compartment [464]. This shows the high efficiency of bafilomycin A1 against acidification of lysosomes and autolysosomes, in fact the autophagosomes that accumulated in the cytoplasm did not show any activity from the V-ATPase proton pump which blocked the fusion between autophagosomes and lysosomes with bafilomycin A1 [465].

5.1.2 Chloroquine (Chq)

Chq is a member of the quinonolone family and is a derivate of hydroxychloroquine and acts as a weak intercalating agent. It has been approved by the Food and Drug Administration (FDA) and it is mainly used against tumours through the inhibition of autophagy. Chq (10 to 300 μM) [466] acts as a lysosomotropic weak base and when it is in the monoprotonated form it engages with the lysosome becoming deprotonated and is sequestered inside the lysosome. During this process, chq is thought to alter the lysosomal pH inhibiting autophagic protein degradation [467]. In contrast to bafilomycin A1, Chq does not reduce LysoTracker puncta staining [468], instead promotes it indicating lysosomal enlargement. Even though extensive studies have not been carried out on the direct effect of Chq on mitochondria, it has been shown that in the case of cardiac pressure overload chq impairs mitochondrial functionality and quality [469]. It is well known that autophagy plays a major role in preserving mitochondria functionality through removing damaged mitochondria through mitophagy [470-472]. Failure to preserve appropriate mitochondria functionality leads to energy production impairment, increase in the production of ROS and therefore cytotoxicity, which has been extensively reported in both neurodegenerative and cardiovascular disease [473-475].

5.1.3 E64 – Cathepsins inhibitor

Cathepsins are a group of serine, cysteine and aspartyl proteases belonging to the papain family. Cathepsins play an important role in the degradation of lysosomal cargo and are

synthesized as an inactive precursor becoming a proteolytic active form during transport to the acidic environment of the endosomal/lysosomal compartment by autoprocessing or via the enzymatic activity of other cathepsins [476]. They are a major component of the lysosomal proteolytic capacity; however, they are also secreted from the cell and can play a role in degrading the extracellular matrix. For example, cathepsin L has potent elastase and collagenase activity and has been found to be highly expressed in the artery of apolipoprotein E-null mice [477-480].

E64 (working concentration 1-10μM) [481] is a potent selective inhibitor of cysteine proteases, binding its trans-epoxysuccinyl group with the thiol group of cathepsins B, H, and L to form a thioether linkage.

5.1.4 Pifithrin α

2-(2-Imino-4,5,6,7-tetrahydrobenzothiazol-3-yl)-1-p-tolylethanone-hydrobromide commonly known as pifithirin α (working concentration 5 20 μM)[482], has been used within the literature as an inhibitor of p53 mediated apoptosis and p53 dependent gene transcription. However, it has also been shown that pifithirin also reduces heat shock and glucocorticoid receptor (GR) signalling [483]. *Leu et al.* [484] demonstrated that pifithirin interacts with HSP70 and HSC70 [485] substrate binding domain (SBD) providing a mechanism that links all three pathways. HSP70 and HSC70 are highly homologous, but they do have some difference in terms of functionality which is related to the chaperone-based machinery pathway [486, 487].

Interestingly, it has been reported that administration of pifithirin promotes cell death without caspase activation [488] through dysfunctional autophagy. In fact, pifithirin treated cells showed a progressive accumulation of intracytoplasmic vacuoles, with SQSTM1/p62 accumulation (a marker of autophagy chapter 4 sections 4.2 and 4.5.2) and cathepsin activation (requires lysosomal acidification) in a dose dependent manner, suggesting inhibition of autophagy or defective autophagic/lysosomal degradation [489-493].

5.1.5 Ver155008 - HSP70 inhibitor

Ver155008 (Ver) (working concentration 15-30μM) [494] is a small molecule that interacts on the nucleotide binding domain in a half-open conformation, acting as a competitive ATP-inhibitor, preventing allosteric control between the substrate binding domain (SBD)

and the nucleotide binding domain [485, 495]). HSP70s interacts with its target protein via the C-terminal SBD through recognition Lys-Phe-Glu-Arg-Gln (KFERQ)-like motif [496]. This interaction is allosterically controlled by the N-terminal nucleotide binding domain which requires ATP hydrolysis. Crystal structure of HSP70 and HSC70 were crucial to elucidate their interaction with Ver155008 (Figure 5.1). The adenine of Ver inserts into the HSP70 adenine binding pocket between the amino acidic residues Arg-272 and 342 creating hydrogen bonds with the Oγ of the Ser-275 and N1 of the adenine ring. The O2 of Ver ribose side binds with Nζ through a hydrogen bond on the Lys-271. Another hydrogen bond is made by the O3 in the ribose group with a H_2O molecule on the residue Asp-234. Similar bonds to the Arg-272 and 342 are made by the dichlorobenzene and the 4-cyano-benzyloxymethyl [495].

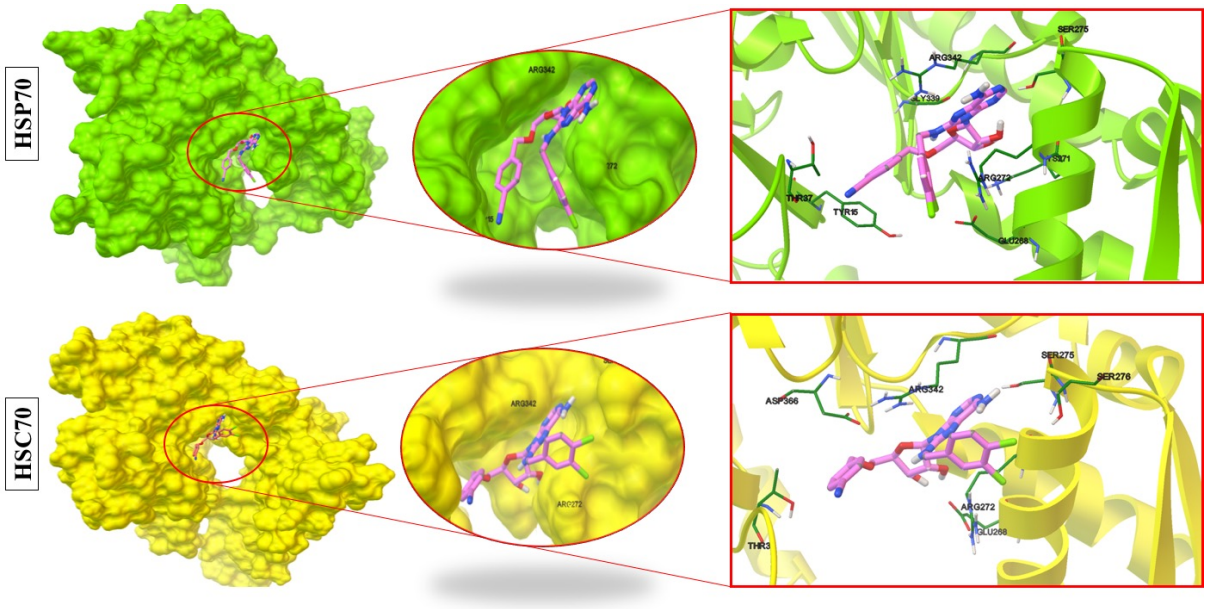

Figure 5.1). A) Ver155008 binds to the Nucleotide Binding Domain (NDB) of human HSP70. (A) Representative view of the NDB, and interaction of Ver155008 onto the NDB HSP70 protein binding site. **B)** Top-ranked docking pose of Ver155008 and its disposition within the NDB binding pocket of HSP70 protein. The protein is represented by molecular surfaces, and Ver155008 as coloured sticks. **C)** Ver155008 interacts with hydrogen bonds in HSP70 (Yellow) protein (Stick carbons are coloured in pink). The residues involved are Ser275 and Lys271, with binding energy score of -4.58Kcal/mol and predicted IC50 value of 439.5 micromolar. **D)** Ver155008 binds to the NBD of human HSC70. Representative view of Ver155008 onto the NBD HSC70 protein binding site. **E)** Top-ranked docking pose of VER-155008 and its disposition within the NBD binding pocket of HSC70 protein. The protein is represented by molecular surfaces, and Ver155008 as coloured sticks. **F)** Interaction between HSC70 (green) and Ver155008. Compound-HSC70 interaction involves hydrogen bonds. The residues implicated are Ser275 and Arg272, with binding energy score of -5.2Kcal/mol and predicted IC50 value of 154.87 micromolar.

Comparable behaviour has been shown for HSC70 with the only difference that on HSP70 it does not allow the complete closure of the central cleft of the Nucleotide Binding Domain (NBD) due to the absence of nucleotide exchange factor BAG1 which is known to cause a 14° outward rotation of NBD subdomain IIB [497] (Figure 5.1).

It was further reported that Ver inhibits HSP70's ATPase activity in a competitive manner and slows down nucleotide association, unlike pifithirin where, even at the high concentration, it doesn't affect the intrinsic ATP hydrolysis rate of the chaperone [484].

Finally, it has been demonstrated that Ver keeps the NBD in a conformation semi-opened between the closed nucleotide bound state, the opened conformation allows the interaction with nucleotide exchange factors of the BAG1 and HSP110 families. As a consequence of HSP70 inhibition, the functionality of ATPase activity of the SBD and the substrate release are reduced as well as its protein refolding capacity [498].

5.1.6 Metformin

Metformin (working concentration 100µM and 1mM) [499] is a FDA approved drug belonging to a class of drugs called biguanides, it is one of the most widely used drugs to treat type 2 diabetes [500] and malaria [501].

Metformin induces adenosine monophosphate-activated protein kinase (AMPK) activation. AMPK is a multi-subunit enzyme and it is the main regulator of lipid biosynthetic pathways due to the activation through phosphorylation and inactivation of key enzymes such as acetyl-CoA carboxylase (ACC) [502]. Furthermore, AMPK modulates metabolic regulation including fatty acid oxidation [503], muscle glucose uptake and gluconeogenesis [504]. Between 2010 and 2011, the role of AMPK was connected to autophagy [263, 505, 506], in particular AMPK is able to promote autophagy, activating directly autophagy-initiating kinase Ulk1 (homologue of yeast ATG1) through phosphorylation of Ser-317 and 777 in the condition of glucose starvation and repression of the mTOR complex-1 [507]. Autophagy induction through metformin administration was confirmed in 2016 by *Michiels et al.* [508] who showed a reduction in SQSTM1/p62 accumulation, suggesting an increase in autophagic flux. In mice and rats, metformin has been demonstrated to increase autophagic flux *in vivo*, in the brain [509, 510], kidney [511] and heart [512].

5.1.7 Rapamycin

Rapamycin (working concentration 20-100nM) [513, 514] is macrolide compound commonly used to coat coronary stents for its antiproliferative function. It also has an immunosuppressive function through inhibition of B and T lymphocyte activation through mTOR inhibition, impairing their sensitivity to interleukin-2 (IL-2) [515]. mTOR is a serine/threonine kinase and can form two different complexes mTORC1 and mTORC2 [516], depending on whether the complex includes the protein RAPTOR or RICTOR. These two complexes have different but complementary functions [517]. mTORC1 promotes cell proliferation as well as cell growth, it is involved in lipogenesis and protein synthesis through its targets S6 kinase 1 (S6K1), 4e-binding protein-1 (4eBP-1), hypoxia-inducible factor 1α (HIF1α) and CDKs [518]. Inhibition of mTORC1 leads to induction of autophagy, cellular growth and protein synthesis [519, 520].

Less is known about mTORC2, but it is involved in lipolysis, insulin sensitivity, cytoskeletal organization and it is responsible for the activation of the protein kinase B (AKT), serum/glucocorticoid-regulated kinase 1 (SGK1) as well as others. Inhibition of mTORC2 prevents cellular migration and cytoskeletal organization, it is the cause of insulin resistance and reduced life span of male mice [521]. mTORC1 and mTORC2 regulate each other's activity via a crosstalk mechanism [522, 523].

Rapamycin interacts with mTOR through the FKBP12/rapamycin-binding (FRB) domain, unlike other kinase inhibitors, which tend to target the catalytic ATP-binding site. The interaction between rapamycin and FRB is still unclear but it leads to specific inhibition of mTORC1. Rapamycin binding to FRB prevents mTOR autophosphorylation, the phosphorylation of 4EBP1 *in vitro,* [524]destabilising the mTOR-Raptor complex [525].

Although rapamycin can induce autophagy with the mechanism described above, it is also able to do so in a cyclical mTOR-independent pathway, which involves links between cAMP/Epac/PLC-ε/IP3 [526] and Ca^{2+}/calpain/Gsα signalling [527], most likely lowering the level of intracellular inositol 1,4,5-trisphosphate (IP3). Both these mechanisms of action have the potential, even with side effects, to induce the autophagic process [526].

5.2 Aim and objectives:

Aim: NRF2-regulate genes OSGIN1 and OSGIN2 appear to impair autophagic flow and increased HSP70/BAG3 complex in CMA. Establish whether the enhancement of autophagic flux is the key to restoring EC attachment.

This will be addressed in the following objectives:

- ESS in combination with CSE and TNFα promotes EC detachment. OSGIN1 and OSGIN2 mRNA levels were upregulated the most in ECs exposed to these conditions. Cell foot-prints were observed in static condition in the combination of AdOSGIN1+2. Next, ECs exposed to ESS with OSGIN1 and OSGIN2 overexpressed is going to be validated. Detached EC membrane integrity is going to be assessed.
- Deficit in autophagy pathway has been associated with cardiovascular pathologies. The combination of these two conditions has been linked, in particular, ageing and senescence of cells. AdOSGIN1 and 2 seem to promote EC detachment through inhibition of autophagy and impairment of autophagic flux. Chloroquine and Bafilomycin are drugs normally used in order decrease autophagy flux. Both compounds are going to be tested at low and moderate concentration. These conditions will be tested for EC detachment and compared with AdOSGIN1+2 combination condition.
- In physiologic conditions, cathepsin proteases are constrained into the lysosomes. Here, their role is to degrade unnecessary protein into amino acids and recycle them. One of the main cathepsins is cathepsin L [528]. OSGIN1 and OSGIN2 are responsible for lysosomal vesicles accumulation and therefore increment of cathepsins might be a direct consequence. Considering their nature, proteases cathepsins may potentially contribute to EC detachment. The presence of cathepsin L was therefore evaluated by immunocytochemical staining together with LAMP1.
- OSGIN1 and OSGIN2 in combination have shown to promote EC detachment, potentially inhibiting the autophagy mechanism and activating the HSP70/BAG3 complex in CMA. Bypass of a blockage of autophagy or HSP70 sequestration might be beneficial in order to re-establish the EC attachment. Several compounds (mentioned in sections 5.5.1-5.1.7) were tested in order to rescue ECs from detachment and concomitantly to dissect autophagy pathway.
- NRF2 is the main regulator in the antioxidant system. OSGIN1 and 2 triggered EC detachment potentially by dysfunctional autophagy or CMA signalling pathway. AdNRF2

overexpression on HCAECs exposed to ESS will be also evaluated in terms of EC detachment, autophagy/CMA mechanism and protein accumulation compared to AdOSGIN1 and 2.

5.3 Results

5.3.1 NRF2 participates in elevated flow endothelial cell detachment

This final results chapter aims to illustrate the contribution of NRF2 and OSGIN1+2 in the process of erosion of overlying stenotic plaques. Previous work by Dr Stephen White showed that under ESS, smoking-induces hyperactivation of NRF2 triggering EC detachment, which highlights a novel mechanism that contributes to endothelial erosion overlying stenotic plaques. NRF2 has been considered as protective in the presence of ROS, but chronic activation using CSE and TNFα on HCAECs did trigger EC detachment. Almost complete detachment was experienced when adding sulforaphane or isoliquiritigenin, which are pharmacological NRF2-activators. This indicates that NRF2 enhances cell loss rather than being protective. Similar to the results obtained for AdOSGIN1 and AdOSGIN2, adenoviral overexpression of NRF2 significantly inhibits cell proliferation (Figure 1.7C), implicating NRF2-dependent surveillance of ROS stress in regulating HCAEC replication, and therefore might be involved in the impairment of the endothelium to repair itself. In order to standardise the shearing force and to look at adhesion, experiments to assess the effects of NRF2 or OSGIN1+2 were carried out on 6-well plates located on the orbital shaker apparatus (section 2.7) [529, 530]. This also allowed the collection of HCAECs that have detached, which made it possible to examine their cell membrane integrity which would not have been possible because of the peristaltic pump contraction in the flow apparatus. Firstly, EC detachment between the flow apparatus in combination with ESS+CSE+TNFα versus orbital shaker with HCAECs transduced with AdNRF2 or AdOSGIN1+2 was compared. The two systems showed comparable results which confirmed the development of a simplified model without the need for ESS+CSE+TNFα (Figure 5.2).

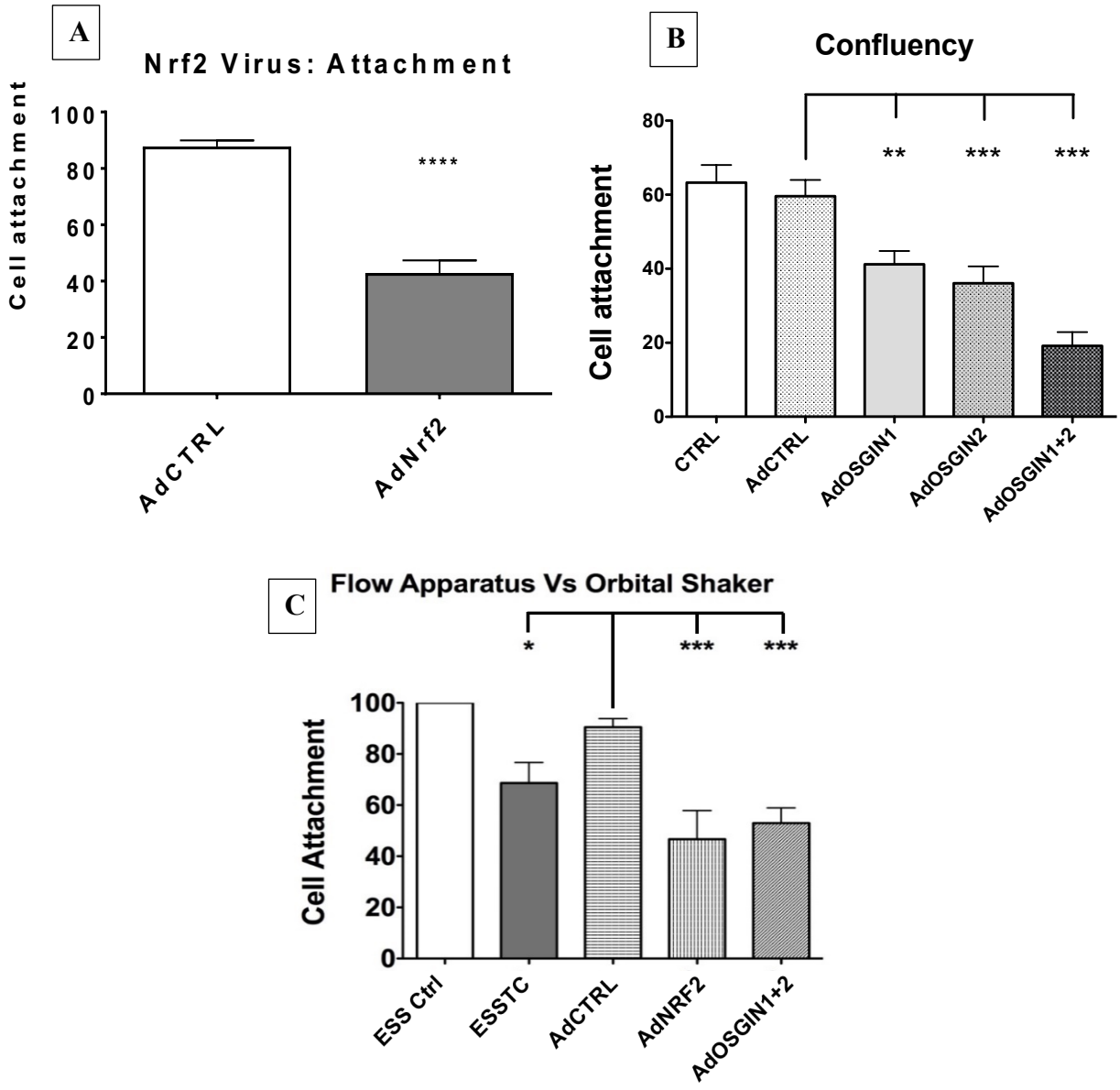

Figure 5.2). A-B) HCAECs were transfected with adenovirus (OSGIN1+2 and NRF2 overexpression) for 16 h at a total pfu of 400 per cell as described (Figure 4.1). The area of HCAECs exposed to flow for 72 hrs on orbital shaker model. Cell detachment was quantified by area on 5 random FoV images taken around the edge of the well, using FIJI Image J threshold function (*P<0.05, ***P<0.001 v ESS control; n=3 One-way ANOVA). **C)** EC detachment between flow apparatus and orbital shaker was quantified. In the flow apparatus HCAECs were exposed to ESS in combination with CSE+TNFα (ESSTC). ESS control from the flow apparatus didn't show any significant difference with AdCtrl in the orbital shaker model. ESSTC showed significant loss in EC attachment, however a non-significant difference was observed between ESSTC with AdNRF2 and AdOSGIN1+2.

5.3.2 OSGIN1 and OSGIN2, proteostasis and NRF2 regulate HCAEC adhesion

Adenoviral overexpression of OSGIN1 and 2 promoted EC detachment in both static (Chapter 4 Figures 4.4-4.7) and under shear stress (orbital shaker system experiment timeline figure 5.3A) conditions as shown in figure 5.3B. After 72 hrs exposure to shear stress, EC detachment was quantified. The orbital shaker system was chosen as a model to use because of the possibility of collecting detached cells and to analyse their membrane integrity using trypan blue exclusion as a measure of cell viability. The orbital shaker system made it possible to measure the area of detachment and to assess cell viability of the detached EC, supporting a non-apoptotic pathway of cell detachment as previously assessed in chapter 3 (Figure 5.3 C-D).

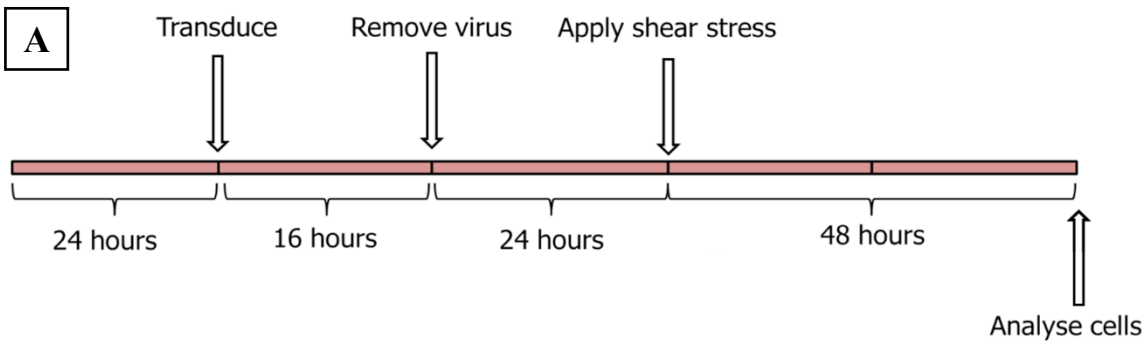

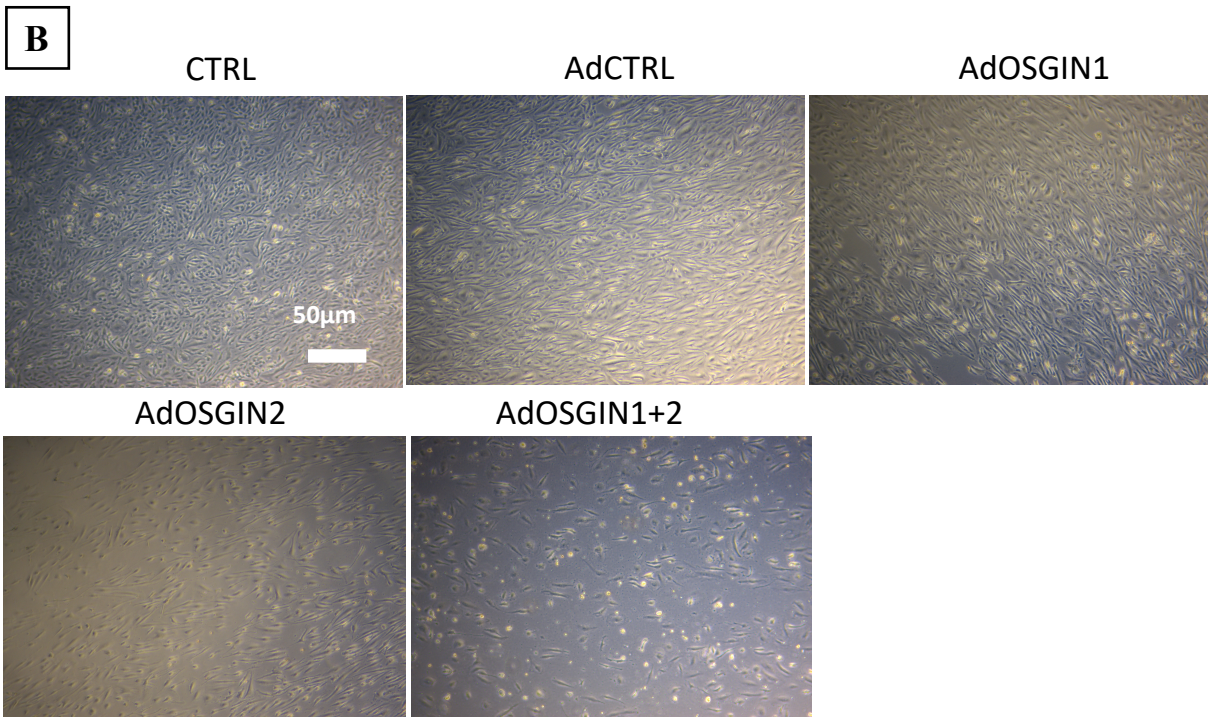

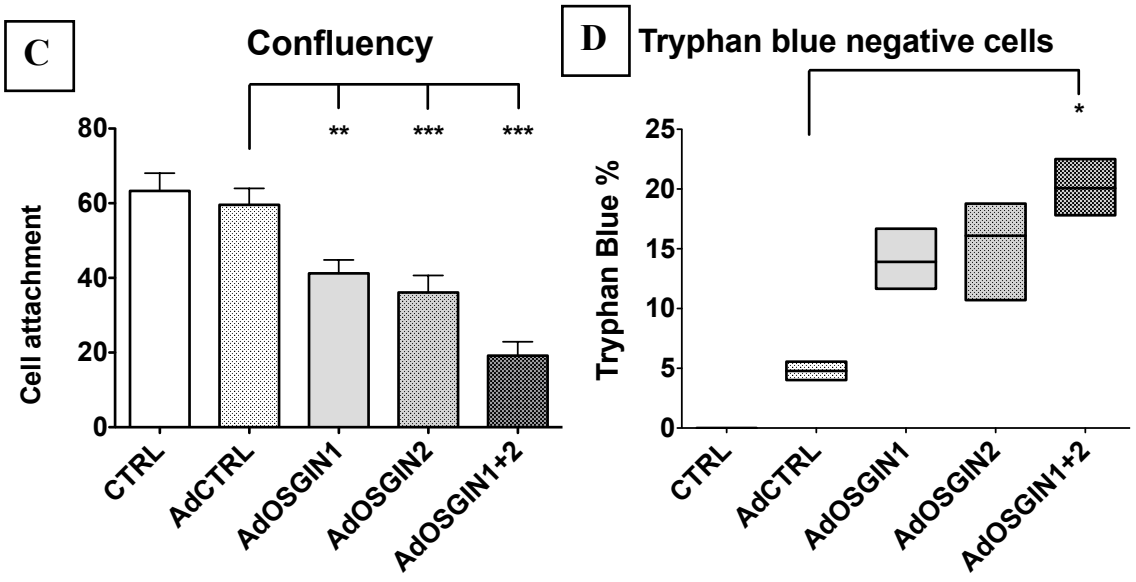

Figure 5.3). A) Timeline of adhesion experiments using the orbital shaker system as a model of shear stress. The experiment was carried out in a 6 well-plate, $2.5x10^5$ HCAECs per well were seeded in a 6 well plate on day 1. Transduction with adenoviral vector was carried out the 2nd day (total pfu/cell of 400). 200 pfu/cell active vector (AdOSGIN1, AdOSGIN2) and 200pfu/cell of control virus were used for single gene transduction, with 200pfu/cell of AdCtrl; for both OSGIN1 and 2 overexpression this consisted of 200pfu/cell of both vectors; AdCtrl (E1/E3 'empty' Ad vector), was used as the control (400pfu/cell). Virus was removed on day 3 and plates placed on the orbital shaker at 210RPM for 72 hrs before analysis. **B)** HCAECs were exposed to shear stress for 72 hrs using the orbital shaker system. At the end of 72 hrs the flow was stopped, and media was immediately collected. The wells were washed with cold PBS 1X and fixed with PFA 4%. Representative images of each condition are presented. **C)** Assessment of area of cell coverage**.** Quantification of endothelial cell detachment was measured by area on five random images on the edge of the well using ImageJ threshold function. Adenoviral overexpression of OSGIN1+2 triggers cell detachment (**P<0.01, ***P<0.001 v AdCtrl; n=3, One-way ANOVA). **D)** Media was collected, and detached cells displayed a significant maintenance of cell membrane integrity (*P<0.05 v AdCtrl; n=3 One-way ANOVA).

5.3.3 Inhibition of autophagy leads to EC detachment

Following our observation that genes involved in chaperone mediated autophagy were upregulated by OSGIN1+2 overexpression (array data and figures 4.9-4.13), we investigated the effects of reducing autophagic flux on HCAEC adhesion, by exposing HCAECs to two inhibitors of autophagy. Cells were incubated with two different doses: low doses of chq (150μM) or bafilomycin A1 (50nM) (Figure 5.4 A-B), or moderate doses (300μM, 100nM Figure 5.4), in order to pharmacologically reduce autophagic flux. In both circumstances cell detachment was observed with similar maintenance of membrane integrity (Figure 5.4D-F).

Interestingly, co-treatment of OSGIN1+2 overexpression with both chq or bafilomycin did not enhance cell detachment or alter cell integrity, suggesting that a reduction in autophagic flux by either chq or bafilomycin, or OSGIN1+2 overexpression may follow a similar pathway in regulating cell adhesion (Figure 5.4C-E).

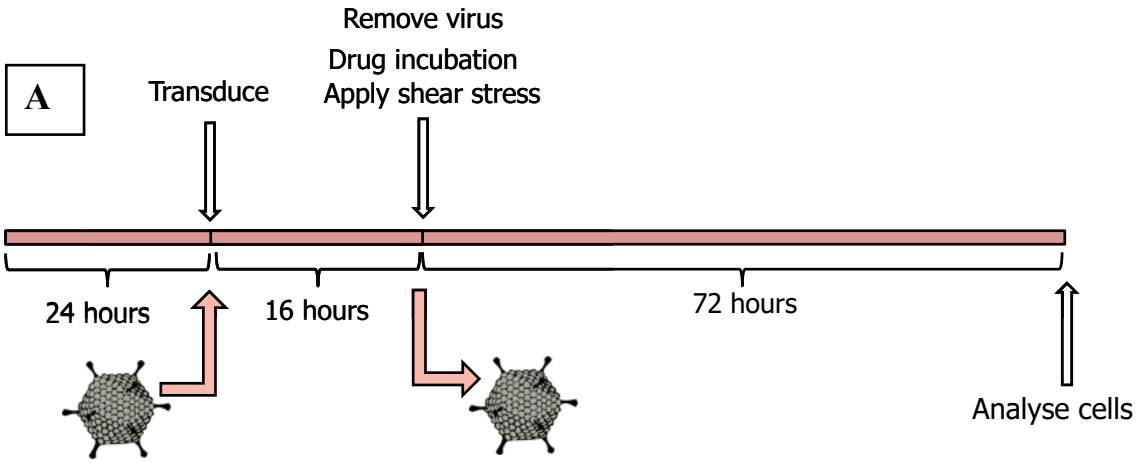
A
Transduce
Remove virus
Drug incubation
Apply shear stress
24 hours
16 hours
72 hours
Analyse cells

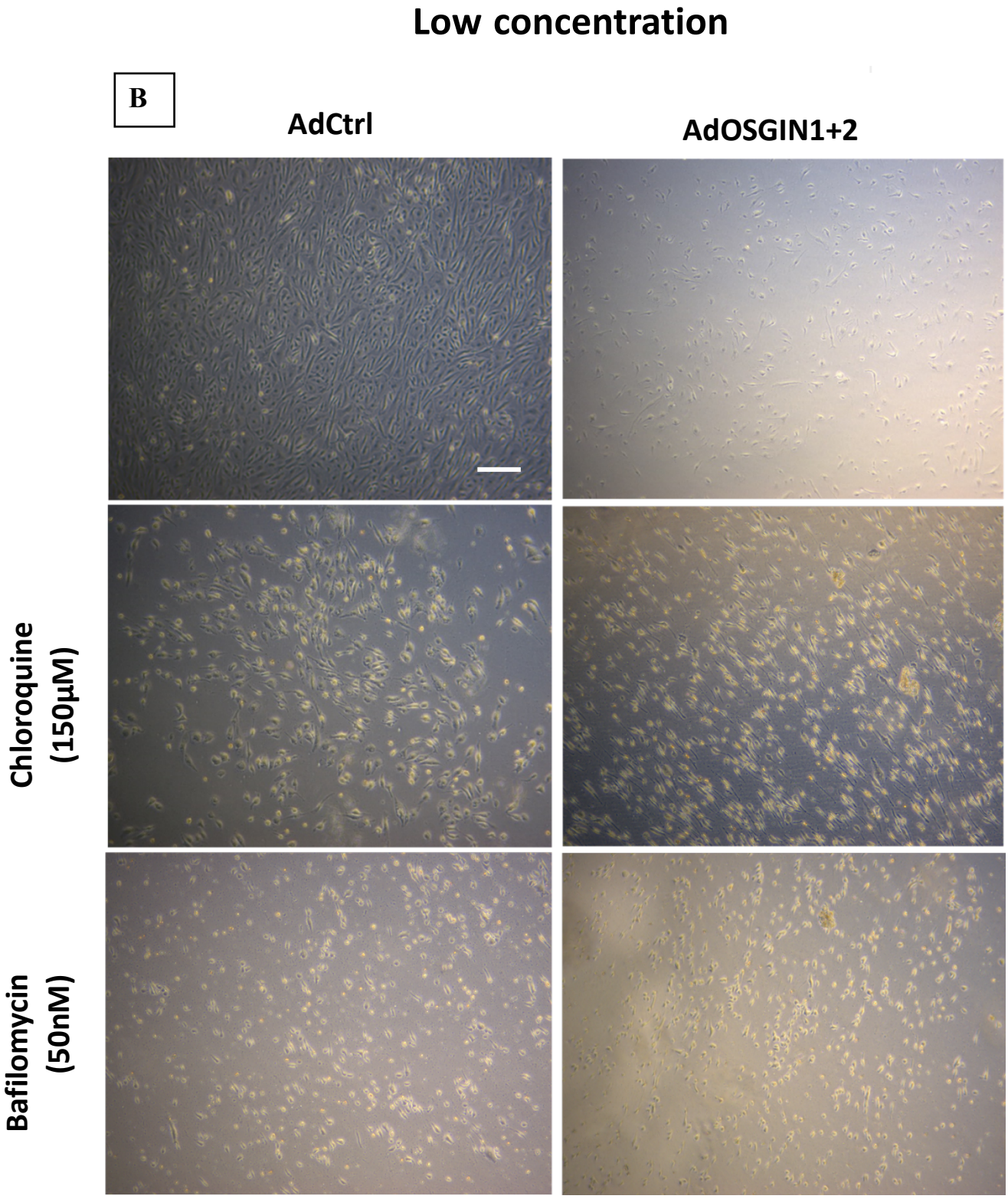
Low concentration
B
AdCtrl
AdOSGIN1+2
Chloroquine (150µM)
Bafilomycin (50nM)

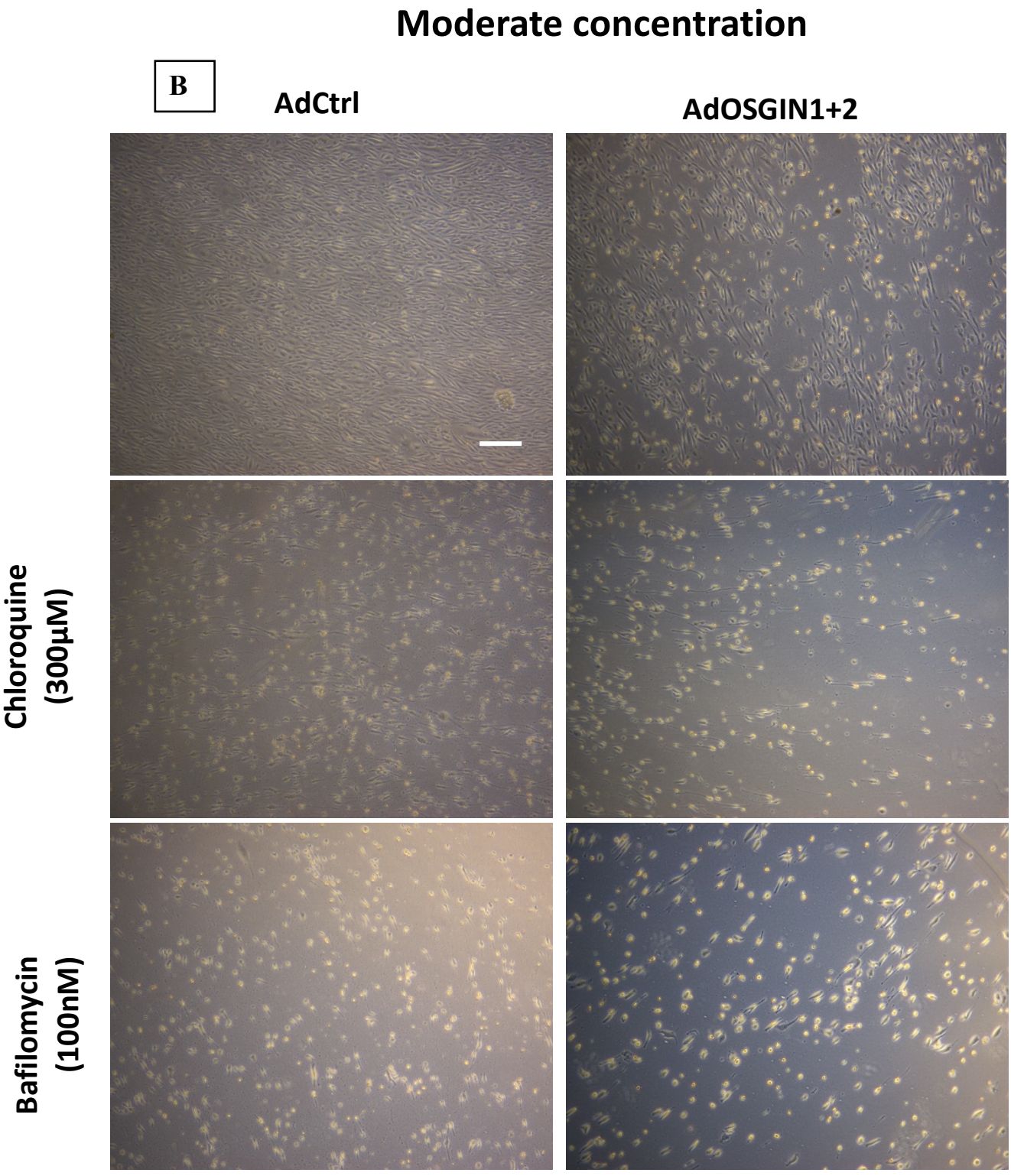
Moderate concentration
B
AdCtrl
AdOSGIN1+2
Chloroquine (300µM)
Bafilomycin (100nM)

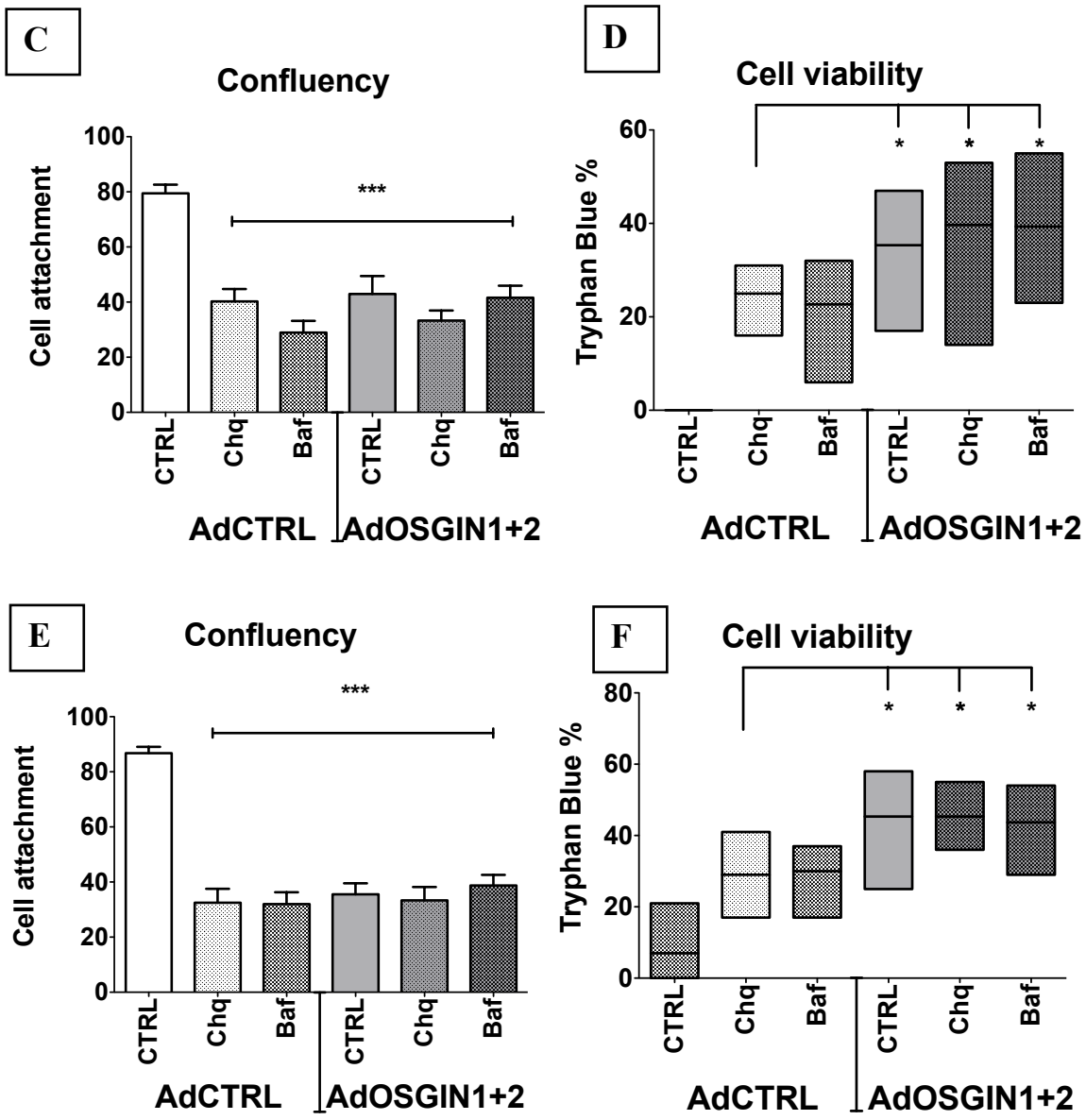

Figure 5.4). A) Timeline of adhesion experiments with inhibitors of autophagy. The experimental design was the same for the previous experiment, except that Chq or Baf were added at the commencement of shear stress using the orbital shaker **B)** Following exposure to shear stress for 72hrs, media was immediately collected for analysis of detached cells. The wells were washed with cold PBS 1X and fixed with PFA 4%. Representative images are presented for both doses of Chq or Baf. HCAECs + Chq (150-300µM), Bafilomycin (50-100nM), or OSGIN1+2 overexpression showed induced comparable, non-synergistic detachment. **C-E)** Quantification of EC detachment was quantified by area of cell coverage on 5 FoV taken around the edge of the well, using ImageJ threshold function. (**P<0.01 and ***P<0.001 v AdCtrl, n=4, Two-way ANOVA). **D-F)** a similar maintenance of membrane integrity was observed between Chq, Baf and OSGIN1+2 treatment (*P<0.05 v AdCtrl, n=4, Two-way ANOVA).

5.3.4 Potential role of cathepsins in OSGIN1+2 mediated detachment

Reduction in autophagic flux would result in the accumulation of lysosomes within the cell, with the potential for accumulation of proteases that could affect cell adhesion if released

from the cell. We observed an accumulation of lysosomes with OSGIN1+2 overexpression (see Figure 4.13 Chapter 4). Cathepsin L is essential for the correct degradation of lysosomal cargo, and during a blockage of autophagic process, it can accumulate inside lysosomes, where it will become activated under low pH conditions. To assess this possibility, ICC staining was carried out in order to quantify cathepsin L and determine its co-location with lysosomes (Figure 5.5).

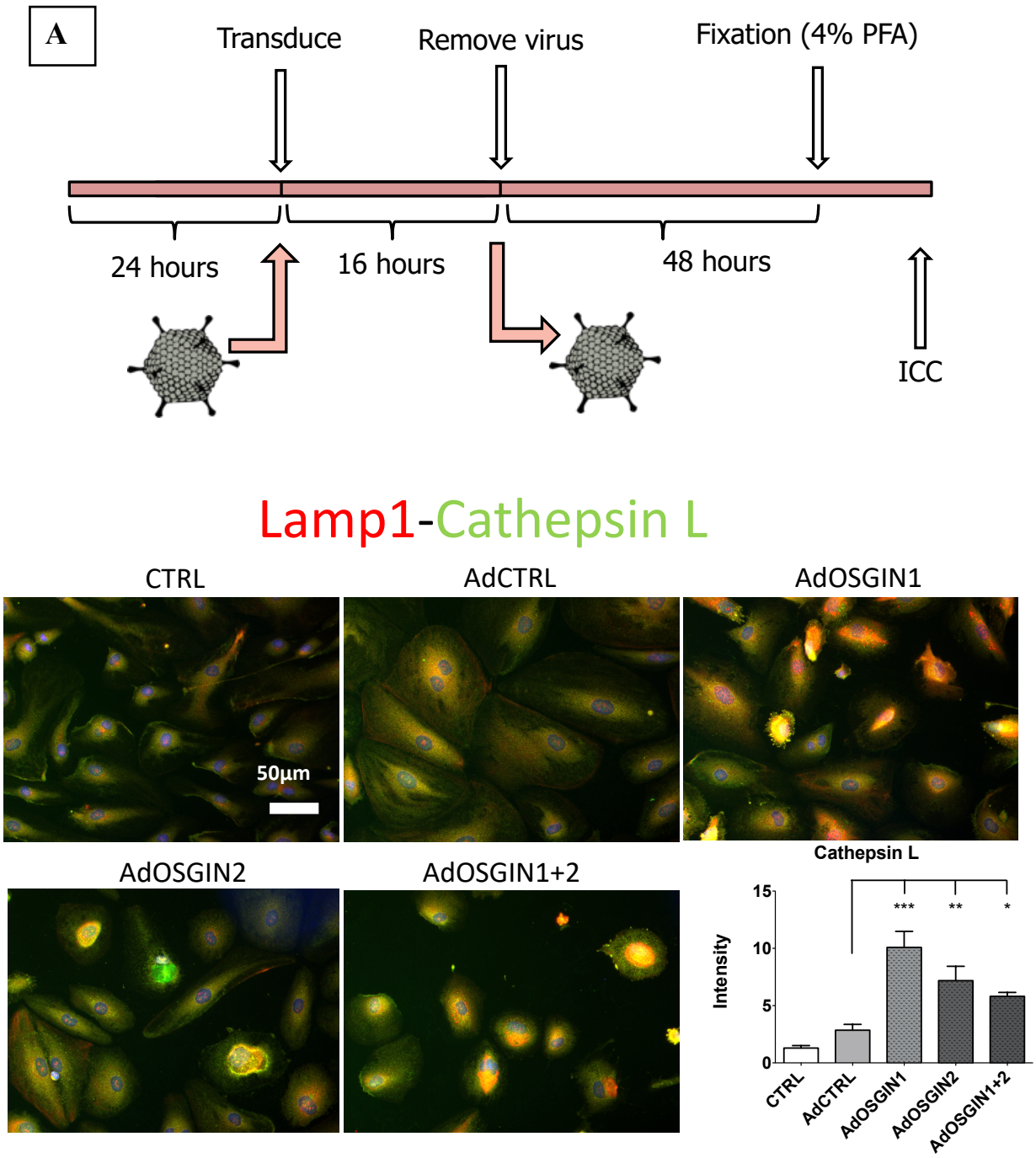

Figure 5.5). Immunofluorescence of cathepsin L (Green) and LAMP1 (Red) demonstrate an accumulation of cathepsin L in LAMP1 positive vesicles, indicative of their intracellular accumulation. **A)** Timeline for examination of Cathepsin L with OSGIN1+2 overexpression. HCAECs grown on 0.1% gelatine coated chamber slide were transfected with adenovirus (OSGIN1, OSGIN2 and OSGIN1+2 overexpression) for 16 h. Transduction with adenoviral vector was carried out the 2nd day (total pfu/cell of 400). 200 pfu/cell active vector (AdOSGIN1, AdOSGIN2) and 200pfu/cell of control virus were used for single gene transduction; for both OSGIN1 and 2 overexpression this consisted of 200pfu/cell of both vectors; AdCtrl (E1/E3 'empty' Ad vector), was used as the control (400pfu/cell). Virus was removed on 3rd day. The 4th day the media was removed, cells were washed with 1X PBS and fixed in PFA 4% for 20' before immunostaining. **B)** representative images of HCAEC transduced with OSGIN1+2 (n=3).

ICC staining of cathepsin L and LAMP1 showed a co-localisation and accumulation of the two proteins. It suggests the autophagic flux is reduced, in accordance with the previous data shown in chapter 4 about SQSTM1/p62. However, this experiment does not show whether cathepsin L is acting outside the lysosome and contributing to HCAEC detachment. This was investigated in the experiments below using a cathepsin B, H and L inhibitor E64 (see Figures 5.6A-B).

5.3.5 Investigating the potential mechanism of OSGIN1+2-mediated HCAEC detachment

Taking all these data together, cell detachment might result from either the block of autophagic flux affecting the function of the cytoskeleton or adhesome or the release of activated proteases from the lysosome, exemplified by cathepsin L. In order to have a better understanding, ECs were incubated with different compounds with the purpose to dissect autophagy or cathepsin activity. A pilot study was carried out in order to evaluate dose and toxicity. Three technical replicates were used per condition. Under LSS on the orbital shaker system ECs (AdCtrl and AdOSGIN1+2 overexpressed) were treated with low dose and moderate dose of pifithirin (10-20μM), Ver155008 (15-30μM), metformin (100μM and 1mM) and rapamycin (20-100nM). Regarding the inhibition of cathepsin L activity, as mentioned above, E64 was used at 1μM and 10μM, keeping in mind that pifithirin also impairs the activation of cathepsin L (Figure 5.6 A-C).

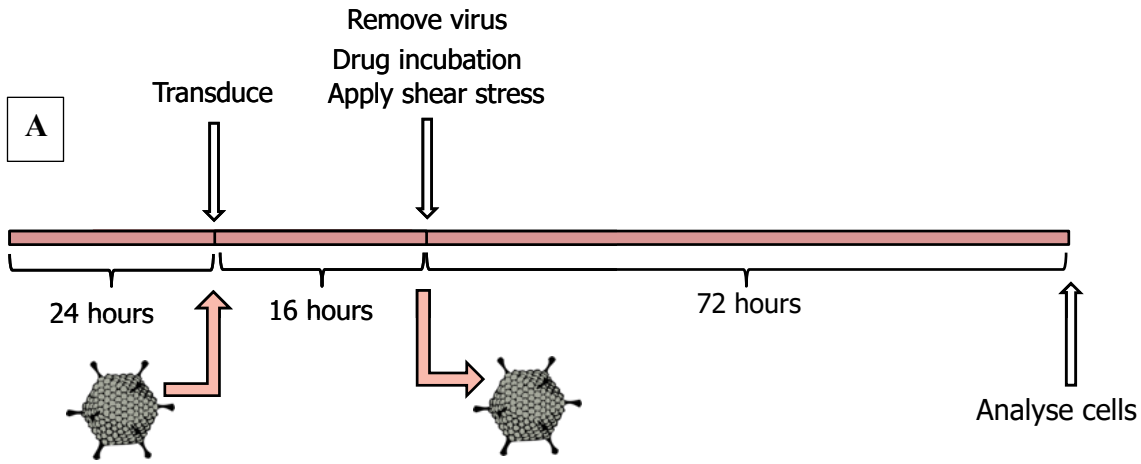

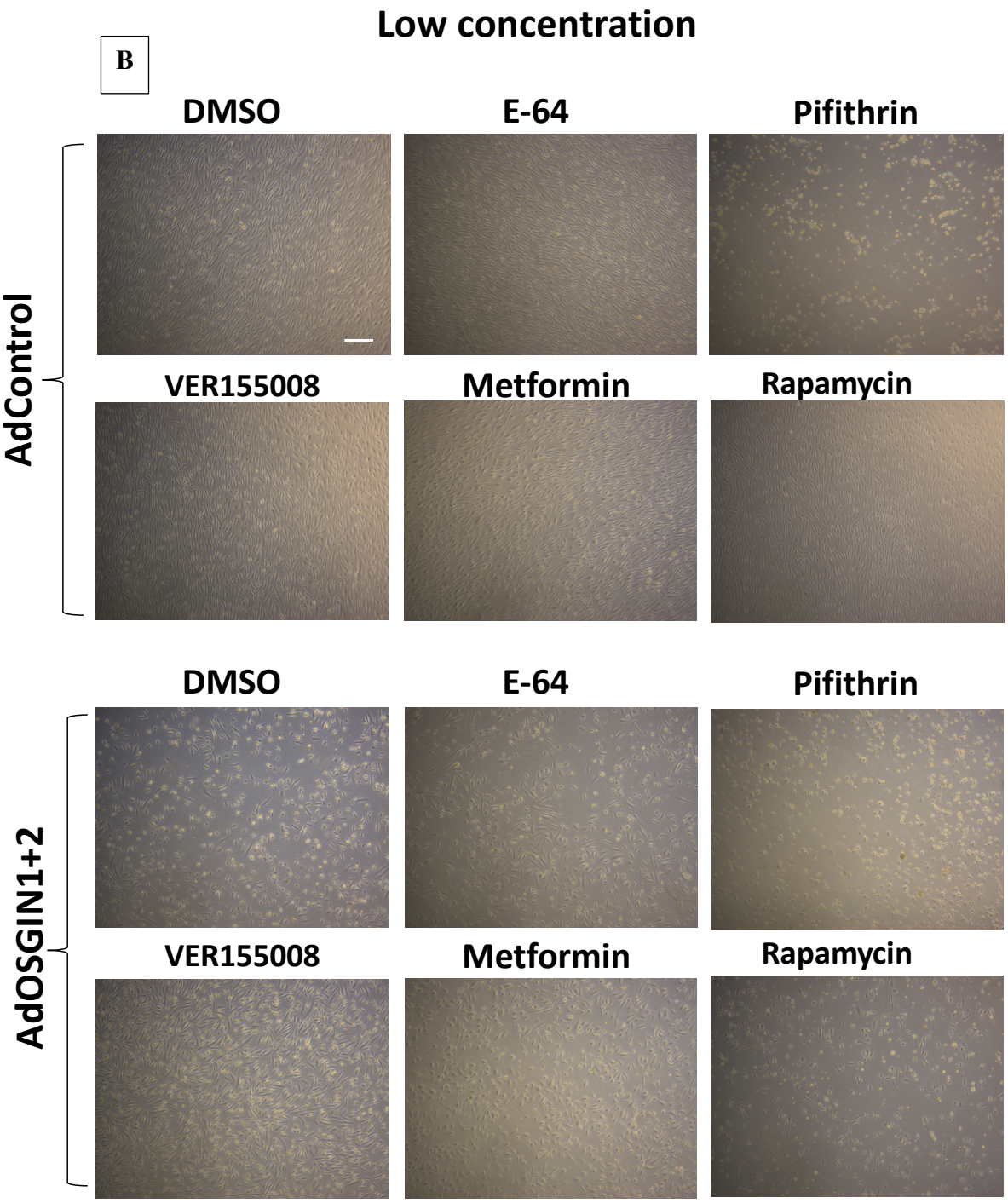
Low concentration
B
DMSO
E-64
Pifithrin
AdControl
VER155008
Metformin
Rapamycin
DMSO
E-64
Pifithrin
AdOSGIN1+2
VER155008
Metformin
Rapamycin

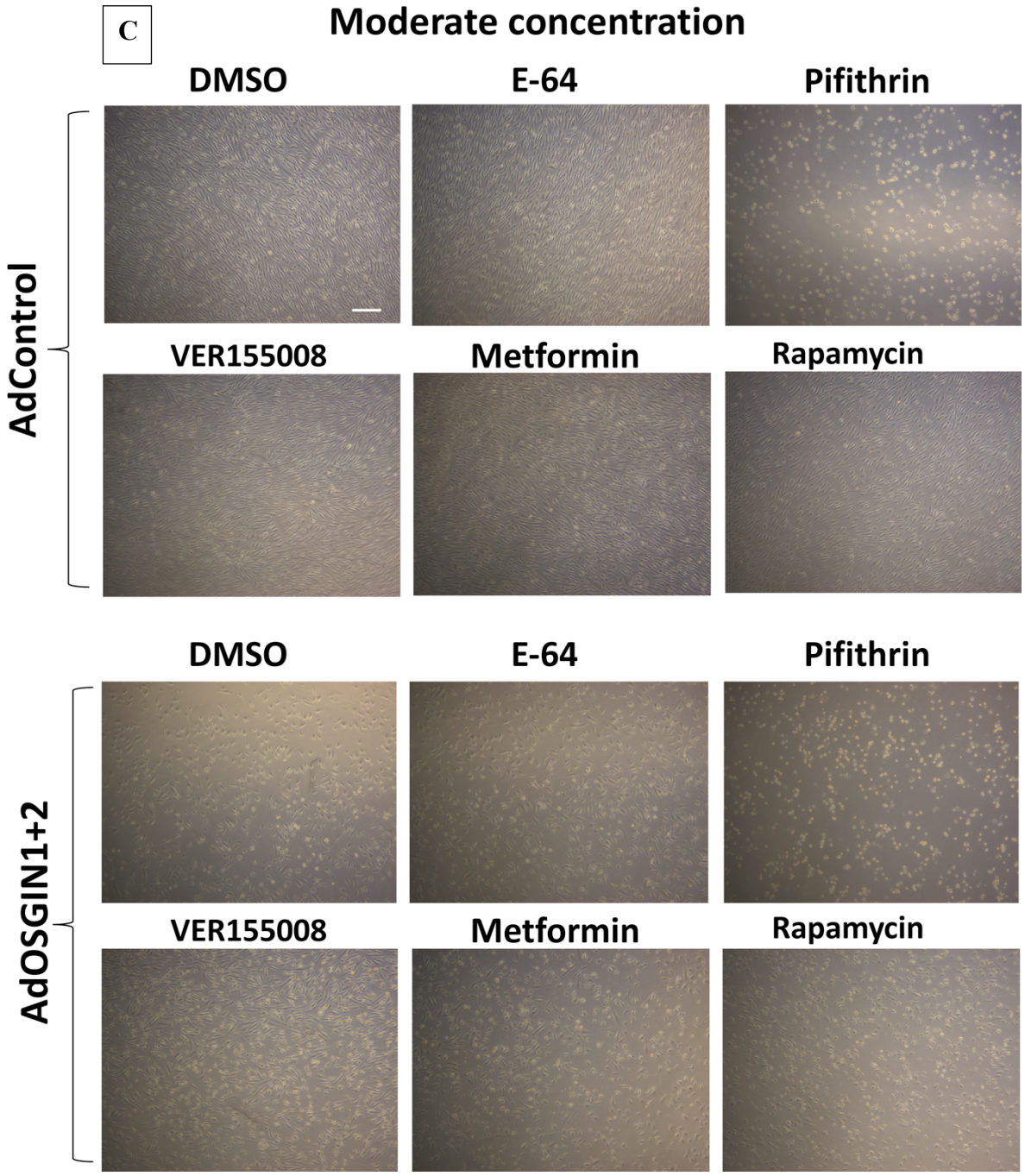
C
Moderate concentration
DMSO
E-64
Pifithrin
AdControl
VER155008
Metformin
Rapamycin
DMSO
E-64
Pifithrin
AdOSGIN1+2
VER155008
Metformin
Rapamycin

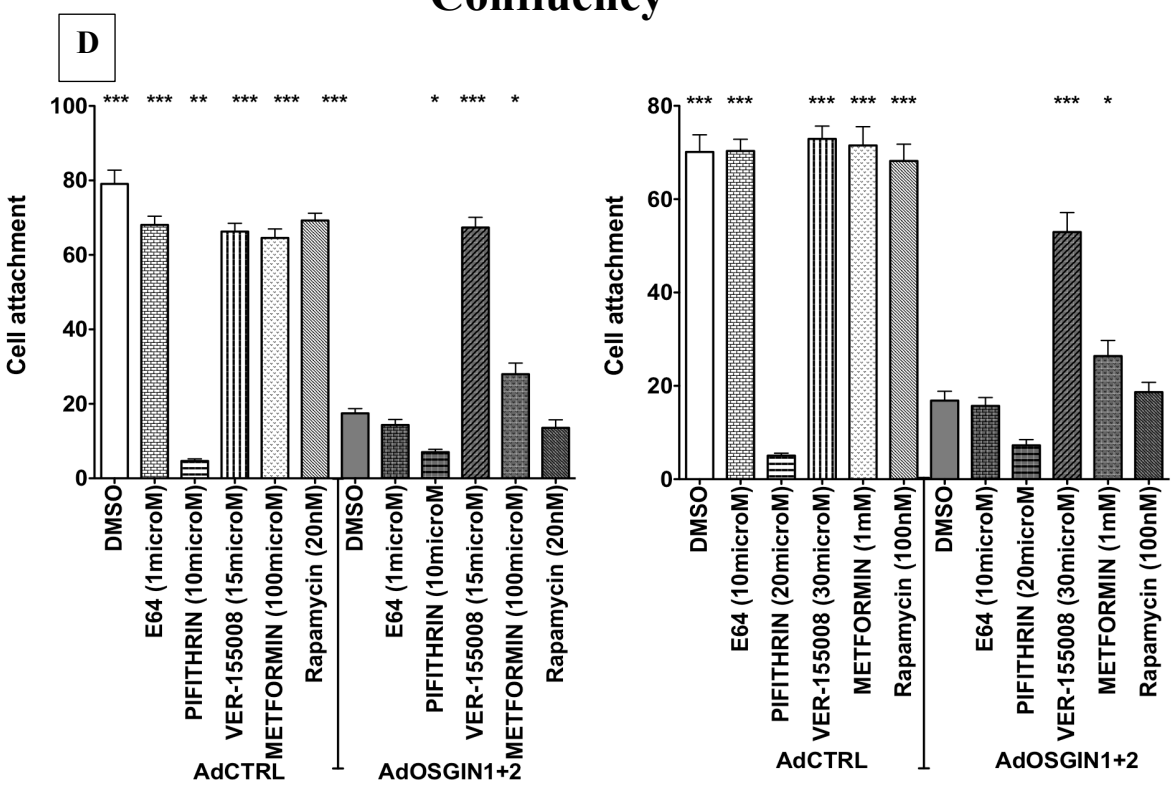

Figure 5.6). A) Timeline of HCAEC adhesion experiment. **B)** The experiment was carried out in a 6 well plate on day 1. Transduction with adenoviral vector was carried out on the 2nd day (total pfu/cell of 400). 200 pfu/cell active vector (AdOSGIN1, AdOSGIN2) and 200pfu/cell of control virus was used for a single gene transduction; for both OSGIN1 and 2 overexpression this consisted of 200pfu/cell of both vectors; AdCtrl (E1/E3 'empty' Ad vector) was used as the control (400pfu/cell). Virus was removed on the 3rd day and HCAECs were exposed to ESS ± compounds for 72 hrs using the orbital shaker system. AdCtrl and AdOSGIN1+2 ECs were treated with a low dose of E64 (1μM), pifithirin (10μM), Ver155008 (15μM), metformin (100μM) and rapamycin (20nM). The wells were washed with cold PBS 1X and fixed with PFA 4%. Eight random FoV were taken around the edge of the well and quantified with FIJI image J software. Representative images are provided (n=1, 3 technical replicates). **C)** AdCtrl and AdOSGIN1+2 ECs were treated with low dose of E64 (10μM), pifithirin (20μM), Ver155008 (30μM), metformin (1mM) and rapamycin (100nM) as described above. The wells were washed with cold PBS 1X and fixed with PFA 4%. Eight random FoV were taken around the edge of the well and quantified with FIJI image J software. Representative images are presented (n=1, 3 technical replicates). **D)** Quantification of cell adhesion was quantified by percentage of area of cell attached on 5 random FoV taken around the edge of the well, using FIJI Image J threshold function. (*P<0.05, **P<0.01 and ***P<0.001 v AdCtrl, n=1, 3 technical replicates, Two-way ANOVA).

The mechanism that leads to OSGIN1+2 mediated endothelial detachment is complex and during the pilot study several drugs were tested with the purpose to evaluate the correct doses to use, assess cytotoxicity and ameliorate EC response to ESS concomitantly with autophagy inhibition. Interesting results were observed during the experiment described above. The use of E64 cathepsin inhibitor didn't compromise the state of ECs in the control condition but in AdOSGIN1+2 it also did not improve EC attachment. This outcome suggests that even if cathepsins may affect ECs, their activity is not fundamental in the process of plaque erosion. Noteworthy pifithirin, which is supposed to impair the process

of enzyme maturation, further confirms that cathepsin function is not a priority for ECs. Interestingly, pifithirin promoted EC detachment in both AdCtrl and AdOSGIN1+2. As mentioned above (section 5.1.4) pifithirin α promotes cell death in the case of no caspase activation [488] which is in accordance with data obtained (chapter 3, section 3.4.7), and leads to dysfunctional autophagy, exacerbating EC detachment. Considering that AdOSGIN1+2 acts as an autophagy inhibitor promoting erosion, it is possible that pifithirin provokes a similar outcome. Rapamycin instead did not reduce EC attachment on the AdCtrl but on the other end it didn't improve the AdOSGIN1+2 condition, which suggests a mTOR-independent mechanism as a regulator in the process of erosion of plaques. The two last compounds tested, Ver155008 and Metformin, instead showed promising results. Ver155008 was the best option against AdOSGIN1+2 and it seems to work by sequestering HSP70 and partially inhibiting it and its complex(es), reducing the functionality of ATPase activity of the SBD and slowing down the protein refolding process. Metformin acts through AMPK activation, which is a mTOR-independent mechanism. This result would explain why rapamycin, which is an mTOR inhibitor, did not improve EC erosion. Metformin treatment has been proven to ameliorate the risk of cardiovascular insults in 30% of cases [531], which is interesting considering that by coincidence the rate of myocardial infarction (MI) due to erosion of overlying stenotic plaques is about the same percentage. Furthermore, it seems that the blockage of autophagy gets bypassed by the use of metformin (data showed below section 5.3.6) which clears SQSTM1/p62and accumulation.

5.3.6 HSP70 inhibition or activation of AMPK with metformin limits detachment

Based on the initial observations from the pilot experiment above, metformin and Ver155008 were added to ECs under ESS on the orbital shaker in order to replicate previous results. AdNRF2 overexpression was also included in this analysis. After 72hrs of shear stress AdCtrl, AdOSGIN1+2 and AdNRF2 $\pm$ metformin or Ver155008 were assessed (Figure 5.7).

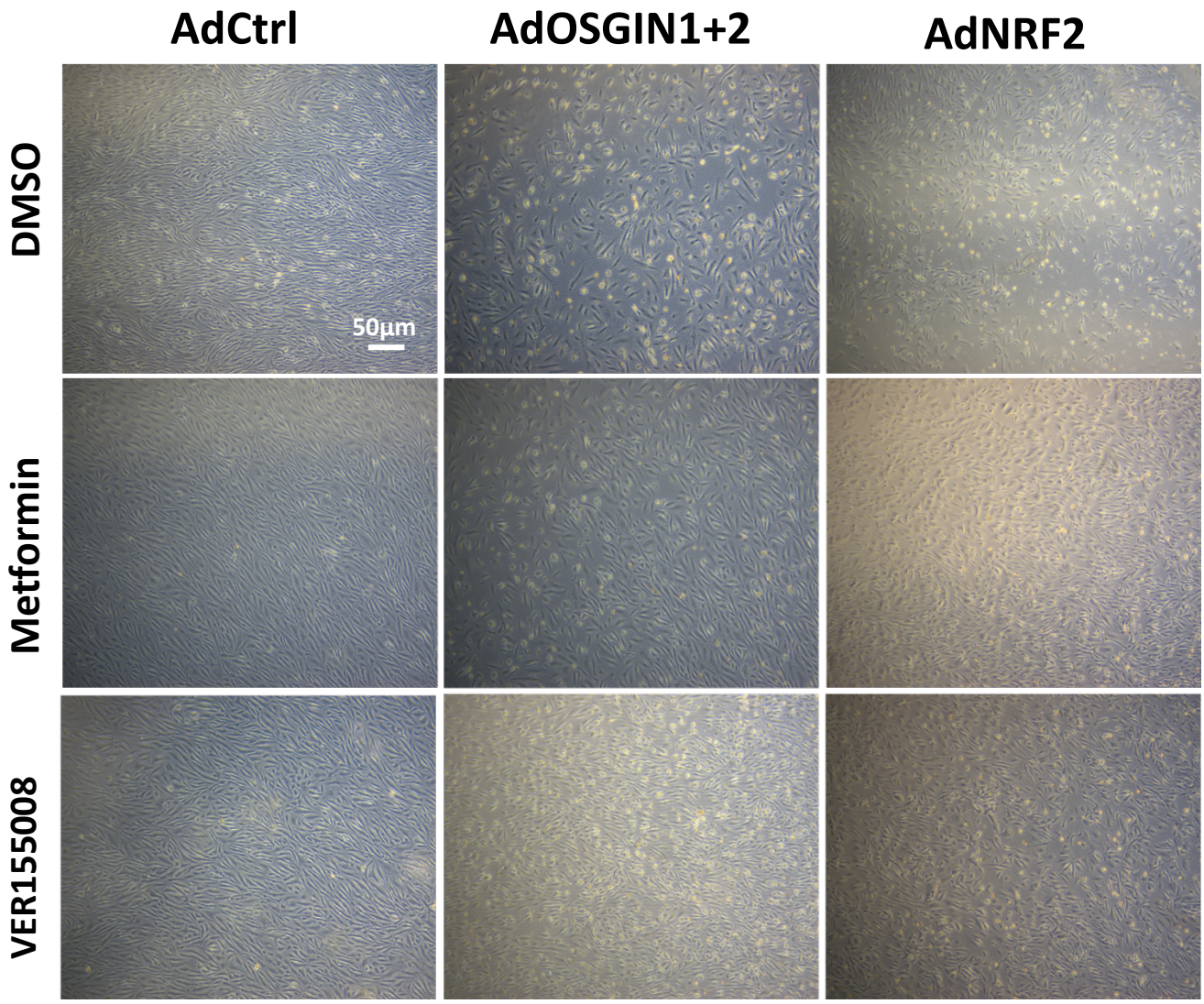

Figure 5.7). The experiment was carried out as described in figure 5.6A. A confluent layer of ECs were seeded on a 6 well plate. Transduction with adenoviral vector was carried out after 24 hrs (total pfu/cell of 400). 200 pfu/cell active vector (AdOSGIN1, AdOSGIN2) and 200pfu/cell of control virus were used for single gene transduction; for both OSGIN1 and 2 overexpression this consisted of 200pfu/cell of both vectors; AdCtrl (E1/E3 'empty' Ad vector) was used as the control (400pfu/cell). Media was replaced and HCAECs were incubated ± compounds and exposed to flow for 72hrs using the orbital shaker. EC detachment was quantified by the area of cells attached on 6 random FoV taken around the edge of the well using FIJI Image J threshold function.

Because of the change in cell size, depth (and therefore assumed volume) and an increase in number of nuclei per cell (chapter 3 section 3.4.4), calculation of cell detachment is potentially confounded as fewer cells may occupy greater relative area, normalisation by protein content is compromised by an increase in cell volume and quantification by DNA by the increase in multinucleated cells. To ensure any bias in these assessments did not affect the result, all three methods were used to assess cell detachment (Percentage area

coverage Figure 5.8A). BCA total protein quantification of cell lysate Figure 5.8B, and total DNA content of cell lysate Figure 5.8C. All three methods of assessment gave equivalent results, with enhanced adhesion in the presence of Ver155008 and Metformin for both OSGIN1+2 and NRF2-mediated cell detachment.

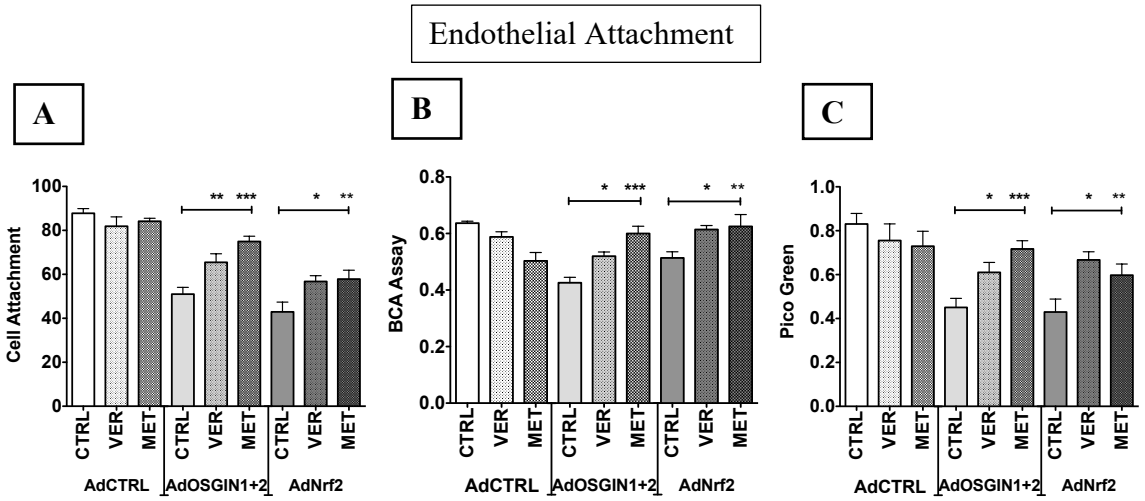

Figure 5.8). Quantification of experiment described in figure 5.7. HCAECs exposed to flow for 72 hrs in the orbital shaker were lysate for protein and DNA quantification. Comparison of different normalisation techniques. **A)** cell detachment as percentage coverage. **B**) cell detachment calculated by DNA content of cell lysate **C**) cell detachment by protein concentration of cell lysate. All three different quantifications showed equivalent results as presented in the first graph on the left. OSGIN1+2 and NRF2-mediated cell detachment was reduced by co-treatment with Ver155008 (15μM), or Metformin (100μM); (*P<0.05, **P<0.01, ***P<0.001, n=3 Two-way ANOVA).

Components of the HSP70/BAG3 proteostasis pathway were highly upregulated by OSGIN1+2 overexpression, indicating a potential role of dysregulated chaperone-mediated autophagy in cell detachment. Inhibition of the HSP70 nucleotide binding site activity using Ver15008 was able to reduce both OSGIN1+2 and NRF2-mediated cell detachment. In addition, HSP70 expression was potentially inhibited [102] and metformin promoted canonical macro-autophagy by activation of AMPK, potentially bypassing a block in chaperone-mediated autophagy. Accumulation of proteins involved in autophagy were assessed by western blot analysis to investigate the mode of action of Ver15008 and Metformin (Figure 5.9).

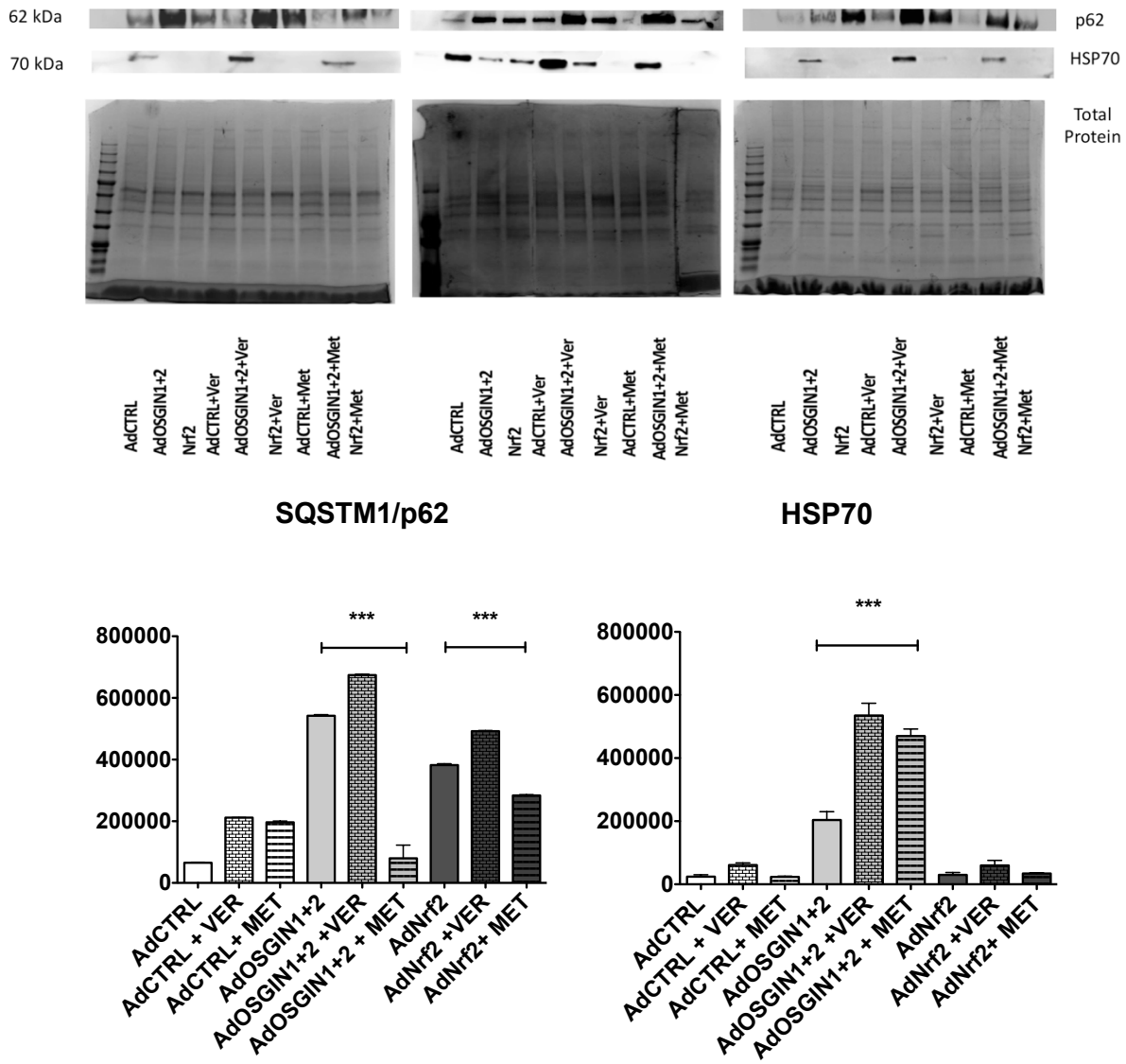

Figure 5.9). A) Adenoviral overexpression was carried out in HCAECs in order to overexpress AdOSGIN1+2 and AdNRF2. HCAECs exposed to flow and incubated with Metformin and Ver155008 (see timeline Figure 5.7) were washed with 1X PBS and lysate with cold RIPA buffer (1:1000 protease and phosphatase inhibitor were added). Western blot analysis was carried on the samples shown in 5.7. 15µg of protein, quantified by BCA assay (Thermo fisher) were loaded per lane. 10% polyacrylamide gel was used. Proteins were loaded and run at 90V in the stacking gel in order for them to align and at 150 V in the running gel. Protein higher than 90 kDa were transferred by using wet transfer (Thermo Fisher) for 1 hr at 35 V, while proteins lower than 90kDa were transfer by using semidry transfer method (BioRad) for 1 hr 30' at 18V. Proteins were transferred onto a nitrocellulose or PVDF membrane, blocked with BSA or milk in TBST for 1 hr according to the datasheet. Antibody (ab) concentration was optimised (See Table 1 Appendix for full detail) and the membrane and primary ab were incubated for 16 hrs. The membrane was washed three times with TBST and incubated with the secondary ab. Immobilon ECL solution was used to develop the membrane and ChemiDoc™ Touch Gel Imaging System for image acquisition. Total protein quantification was used to determine SQSTM1/p62, and HSP70 protein levels. 10% polyacrylamide gel was stained by using Coomassie brilliant blue and band densities were quantified after the gel was de-stained. **B)** Rescue experiments were carried out on orbital shaker using Metformin and Ver155008. Following orbital shaker experiments, ECs were lysate and total protein quantification was used to determine (a)SQSTM1/p62 and (b)HSP70 (western blotting analysis). OSGIN1+2 and NRF2-mediated cell detachment was reduced by co-treatment with Ver155008 (15µM), or Metformin (100µM); (*P<0.05, **P<0.01, ***P<0.001, n=3 Two-way ANOVA).

Metformin, but not VER-155008 treatment reversed SQSTM1/p62 protein accumulation following AdOSGIN1+2 and AdNRF2 overexpression (***P<0.001, n=3, Two-Way ANOVA).

Consistent with the increase in mRNA and proteins as assessed by qPCR, western blot and ICC (Figures 4.13-4.15) OSGIN1+2 increased the accumulation of p62, which was also seen for AdNRF2 treatment. Ver155008 increased the accumulation of p62 (seen in the AdCtrl, AdOSGIN1+2 and AdNRF2). Metformin reduced the accumulation of p62 with both AdOSGIN1+2 and AdNRF2 treatment, consistent with a potential increase in macroautophagy clearing p62 accumulation.

Similarly, OSGIN1+2 overexpression increased the accumulation of HSP70, confirming the results seen in figure 4.15. Neither Ver155008, or Metformin affected this accumulation, highlighting that the beneficial effects of Ver155008 are not mediated through regulating HSP70 expression or clearance from the cell. Interestingly, NRF2 did not increase the accumulation of HSP70, suggesting any effect on chaperone mediated autophagy by NRF2, does not require HSP70 overexpression and that basal levels of HSP70 are sufficient to mediate a deleterious effect on cell adhesion, which could be prevented by treatment with Ver155008.

5.4 Discussion

The NRF2 antioxidant system is generally well known as an athero-protective mechanism that protects the cell against ROS [532]. Laminar shear stress stimulates NRF2 activity in ECs through the upregulation of KLF2 [152]. Upregulation of NRF2-regulated genes was also observed in response to ESS, combined with CSE and TNFα [150]. This haemodynamic environment is permissive for triggering EC detachment which was recapitulated by adenoviral overexpression of NRF2 (Figure 5.8A). Similarly, detachment of HCAECs could be induced by overexpression of two NRF2-regulated genes, OSGIN1 and OSGIN2 (Figure 5.8B). Therefore, HCAEC detachment could be triggered by the combination of ESS+TNFα+CSE, NRF2 overexpression or OSGIN1+2 overexpression. This detachment was independent of a signature of apoptosis (Figure 3.16) with detached cells maintaining a significant degree of membrane integrity (Figure 5.4D).

Beyond the observations on HCAEC detachment, my work starts to dissect the mechanism by which the hyperactivation of the NRF2 system mediates cell detachment. Drawing on the wider literature, I present a proposed mechanism of action for NRF2 and OSGIN1+2 (Figure 5.10) where AdNRF2 and AdOSGIN2 act as autophagy inhibitors. Inhibition of the natural autophagy process results in the impairment of the autophagic flux, which in turn triggers CMA.

CMA degrades dangerous or aberrant proteins by both ubiquitin-proteasome machinery or by using the autophagic-lysosomal system through HSP70/BAG3 complex (Figure 1.12). Both mRNAs of BAG3, HSP70 and SQSTM1/p62 and protein levels of HSP70 and SQSTM1/p62 accumulated with AdOSGIN1+2 transduction in both static conditions (Figure 4.12, 4.15-4.16, 5.9B) and on exposure to flow using the orbital shaker system. The HSP70/BAG3 complex in concert with SQSTM1/p62 selectively targets aggregation-prone proteins and leads to autophagic degradation and therefore might target EC adhesome, impairing cell-cell contact and focal adhesion.

HSP70 has a pivotal role in CMA, and in physiological conditions HSP70 forms a complex with BAG1 and leads to protein degradation by the ubiquitin-proteasome system, but in pathophysiological conditions the HSP70/BAG1 complex switches to HSP70/BAG3 where degradation of protein occurs by sequestration and final lysosomal degradation. Importantly, it has been shown that HSP70/BAG3 function affects cell adhesome,

degrading focal adhesion in many types of cells, such as epithelial, SMC and even cancer cells [425, 533-535]. Clearly, if this process is triggered by OSGIN1+2 overexpression, it would promote EC detachment, especially if this occurs on a stenotic plaque where the ECs are exposed to ESS. Furthermore, impairment of the natural autophagy flux leads to SQSTM1/p62 accumulation, which has dramatic consequences for the cell. SQSTM1/p62 has been shown to bind KEAP1, which normally inhibits NRF2, sequestering KEAP1 for degradation and therefore amplifying a loop that further enhances NRF2 activity [458] and further increasing the inhibition of autophagic flux. Inhibition of autophagy by low or moderate doses of Bafilomycin or Chloroquine, also triggered cell detachment, adding weight to this theory. Interestingly, the combination of the two autophagy inhibitors with OSGIN1+2 overexpression did not increase cell detachment or effect cell membrane integrity suggesting they operate via the same mechanism. AdOSGIN1+2 increased SQSTM1/p62 and HSP70 accumulation (Figure 5.9B), and SQSTM1/p62 accumulation was corrected by metformin treatment. This data, alongside the set of experiments carried out in chapter 4, proposes a novel mechanism for NRF2/OSGIN1+2-mediated HCAEC detachment via the inhibition of the autophagy pathway that may have great insight for endothelial erosion overlying stenotic plaques.

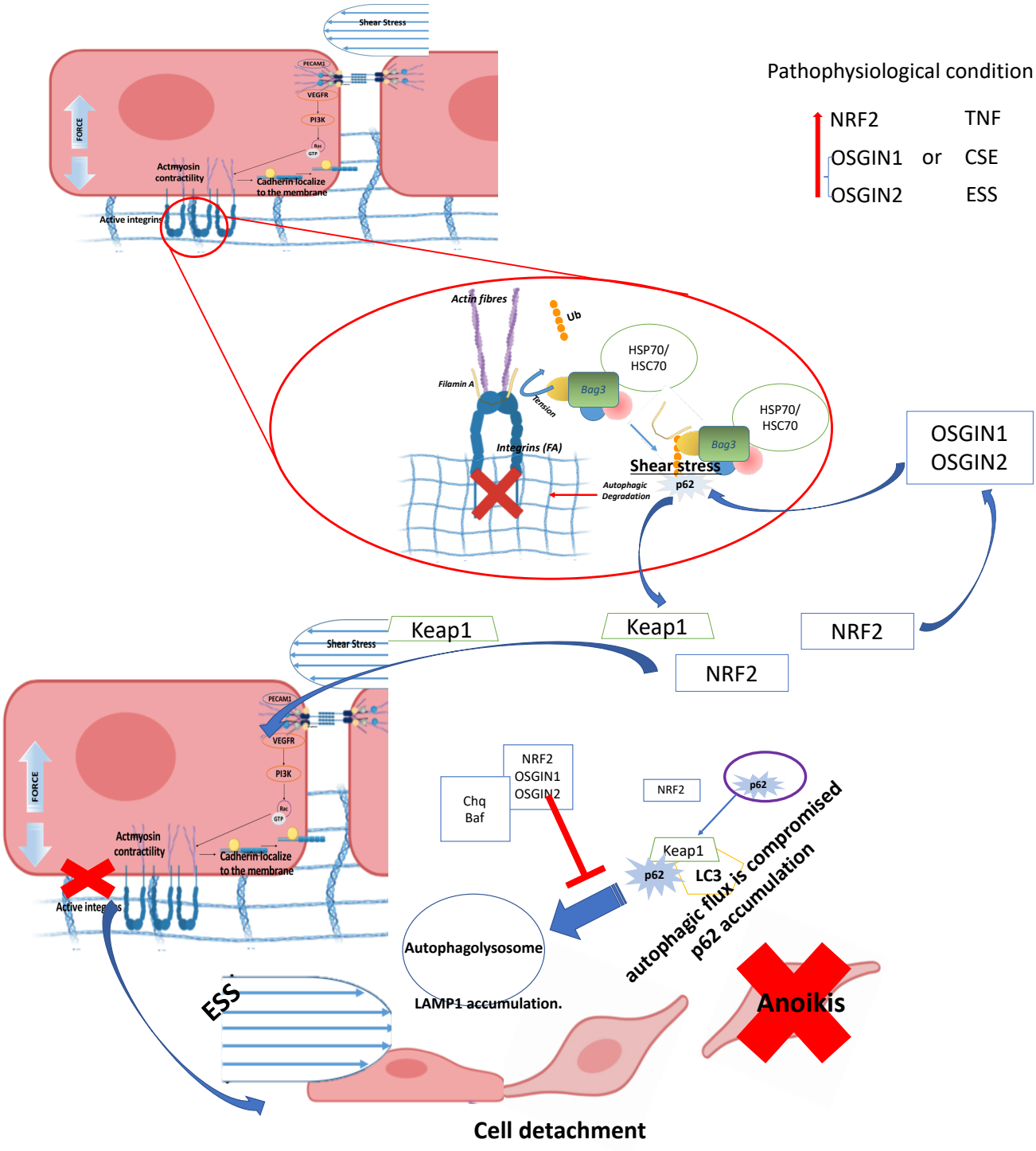

Figure 5.10). Schematic representation of NRF2-OSGIN1+2 mechanism of action. NRF2 constant activation either by Adenoviral overexpression or by the combination of ESS+TNFα and CSE triggers OSGIN1 and OSGIN2. OSGIN1 and 2 promote accumulation of SQSTM1/p62 which interacts with NRF2-inhibitor KEAP1, leading to a constant activation and nuclear translocation of NRF2. This process activates a NRF2/p62 overexpression loop which leads to SQSTM1/p2 accumulation and finally dysfunctional autophagy, impairing autophagic flux (comparable to autophagy inhibition mediated by Baf and Chq). Here, an emergency autophagy mechanism (CMA) is triggered by the substitution of the complex HSP70/BAG1 with HSP70/BAG3. Chronic activation of HSP70/BAG3 targets EC adhesome, which promotes focal adhesion degradation and facilitates EC detachment. ECs detached in an apoptotic-independent mechanism due to adhesome proteins weakening and ESS force which will lead to anoikis.

Several compounds were tested during a pilot study in order to dissect the autophagy mechanism, and cathepsin protease inhibitors were also incubated with HCAECs exposed to flow after adenoviral overexpression of OSGIN1+2. Cathepsin L, which has been observed to be located in lysosomal vesicles, did not lead to any improvement in EC attachment after incubation with E64, which suggests that even if there is an accumulation of cathepsins, they do not play a major role in our model of HCAEC detachment.

In order to bypass the blockage of autophagy, four compounds were incubated with HCAECs and exposed to flow after adenoviral overexpression of NRF2 and OSGIN1+2. Pifithirin was the only compound which showed a detrimental effect on HCAECs in both AdCtrl, AdOSGIN1+2 conditions. Its mechanism of action is not completely clear, but it seems to have a inhibitory effect on heat shock and GR signalling and leads to cell death in a caspase independent manner [488]. Rapamycin destabilised the complex mTOR-Raptor [525] but did not have any significant effect on cell attachment. Rapamycin inefficacy suggests that EC detachment occurs through an mTOR independent mechanism.

The two compounds metformin and ver155008 demonstrated an ability to improve EC attachment. Metformin was reported to enhance autophagy in the brain [509, 510] and heart [512]. Metformin triggers AMP kinase, activating directly autophagy-initiating kinase Ulk1. It was also shown to reduce SQSTM1/p62 accumulation in AdOSGIN1+2 and AdNRF2 HCAECs exposed to flow (Figure 5.9B) supporting the notion that it increased macro-autophagic flux. A proposed mechanism of action is shown in figure 5.11. It has been observed that an acute autophagic response would promote a cell survival mechanism that represses anoikis which would allow the cell to reattach. In contrast, prolonged ECM detachment followed by an impaired durable autophagy response from the cell would result in increased motility [413], promoting EC detachment in the erosion of overlying stenotic plaques and eventually anoikis. Metformin bypasses the inhibition of autophagy by NRF2 or OSGIN1+2 through activation of ULK1, leading to a clearance of SQSTM1/p62 accumulation in both conditions. Clearance of SQSTM1/p62 re-equilibrates the interaction between KEAP1-NRF2, which would prevent the amplification loop between NRF2 and SQSTM1/p62. Further to CMA, even really low levels of the HSP70/BAG3 complex is sufficient to promote adhesome disruption by efficiently locking target proteins [425, 536]. This is possible by the association of HSP70/BAG3 complex with short hydrophobic peptide

segments in the target proteins. HSP70 binding and release cycle is driven by a switch between low affinity to high affinity ADP bound state [496]. However, after incubation with metformin, NRF2 is sequestered by its inhibitor KEAP1, and HSP70/BAG3 complex might be dissociated in favour of HSP70/BAG1, resulting in a more physiological condition [437]. Metformin would potentially rescue ECs due to the autophagy response normalisation which results in an improvement of EC attachment [413].

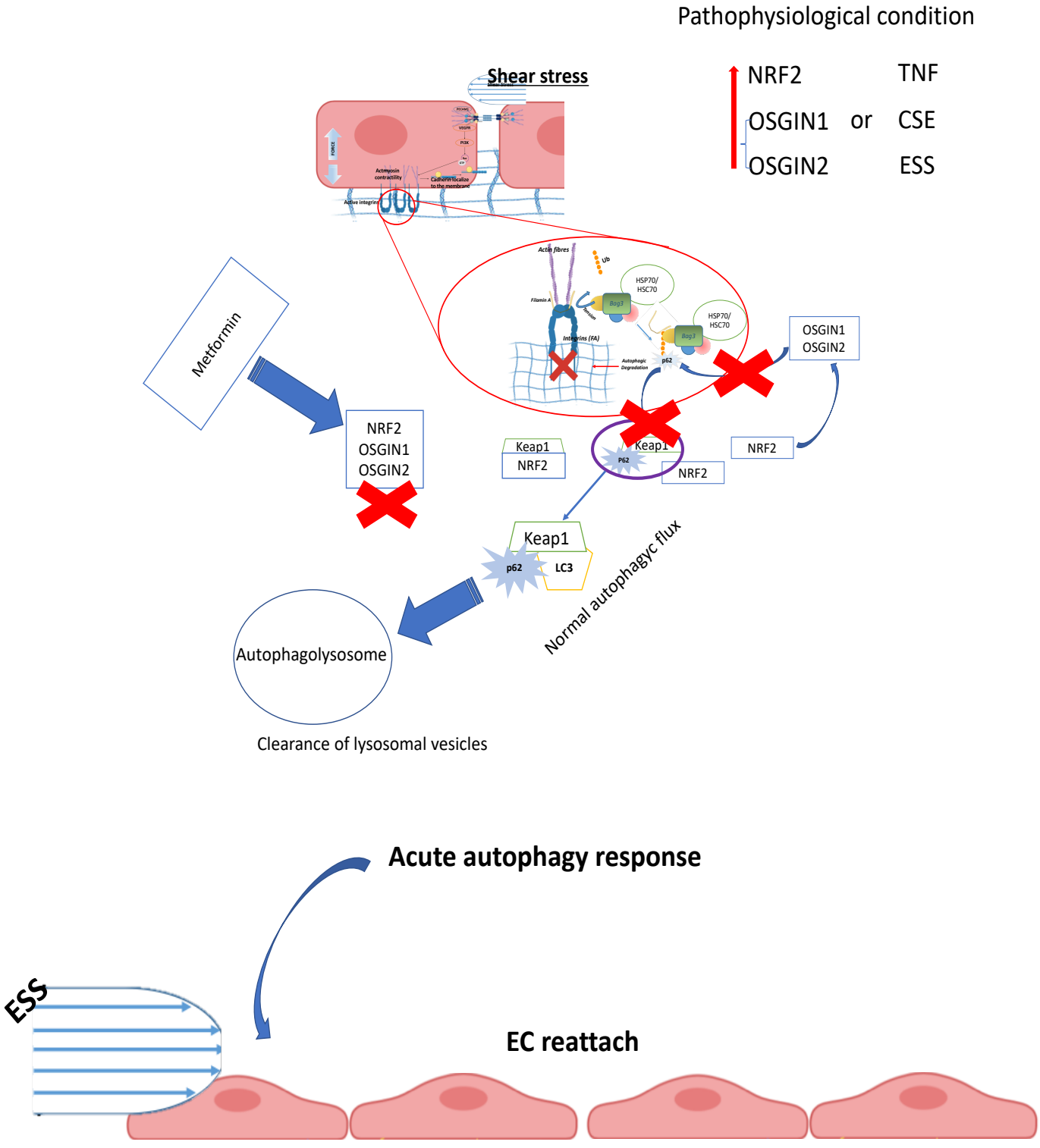

Figure 5.11). Schematic representation of metformin mechanism of action. Impairment of autophagy flux is removed by metformin. Rebalance of the normal autophagy flux promotes clearance of SQSTM1/p62 accumulation. Reduction in SQSTM1/p62 protein release iNRF2, KEAP1, which interacts with NRF2 blocking its nuclear localisation. Furthermore, acute autophagy response mediated by metformin promotes cell attachment.

Differently from metformin, Ver15008 selectively sequesters and inhibits HSP70's ATPase activity in a competitive manner. Ver155008 was shown to improve EC attachment in both AdOSGIN1+2 and AdNRF2 conditions, without reducing the accumulation of SQSTM1/p62 and HSP70 proteins. Additional experiments to determine if Ver155008 promotes HSP70/BAG1 association or prevents the pathophysiological HSP70/BAG3 complex are required to illuminate the mechanism; however, it would appear that it prevents the HSP70/BAG3 complex from degrading focal adhesions [437]. Therefore, Ver155008 treatment would not regenerate autophagic flux, impaired by NRF2 or OSGIN1+2 but it would selectively inhibit the function of HSP70 and its complex allowing the cells maintain more stable adhesome complexes and more robust focal adhesions (Figure 5.12).

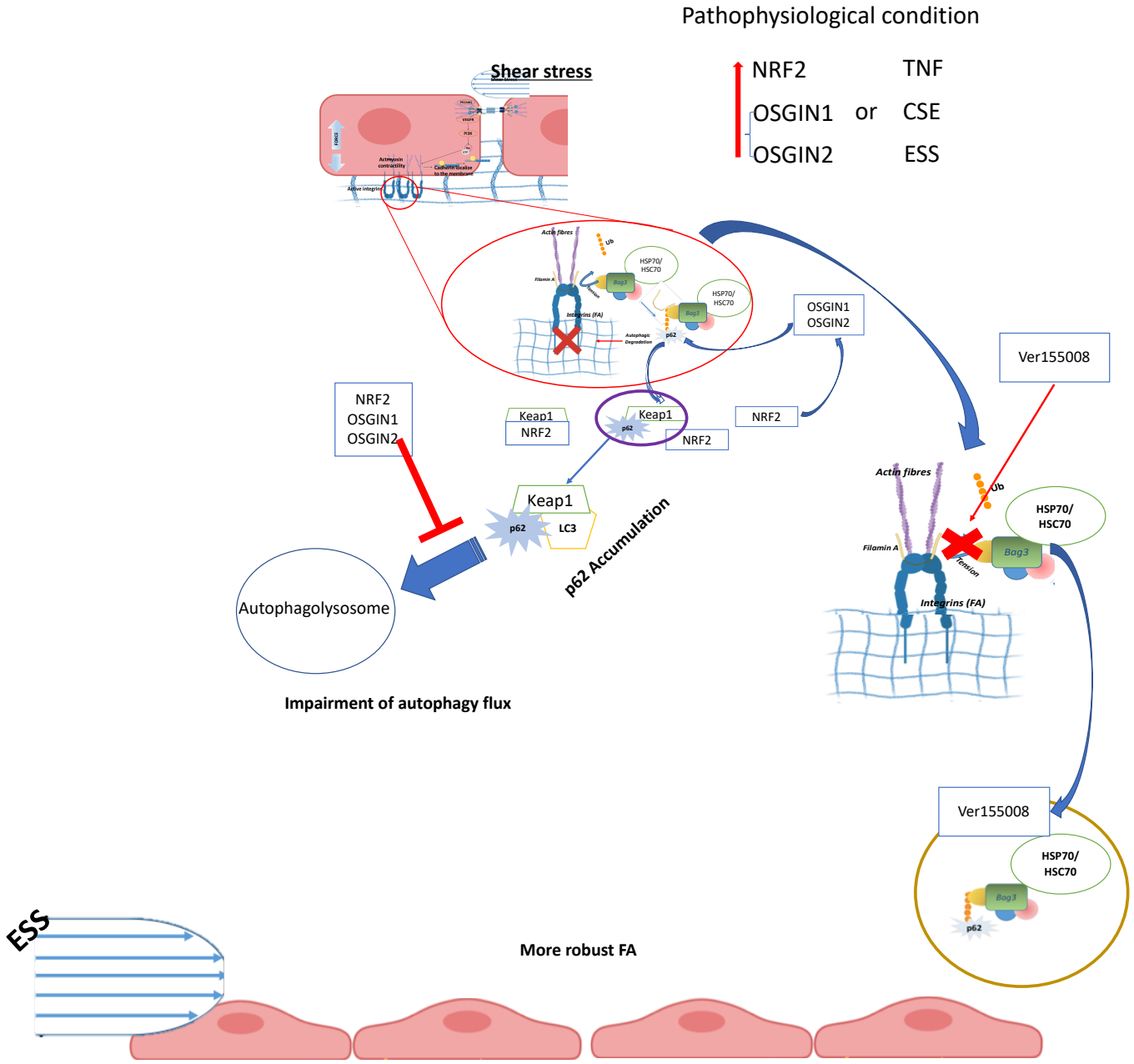

Figure 5.12). Schematic representation of Ver155008 mechanism of action. Although the impairment of autophagic flux promoted by NRF2 or OSGIN1+2, ver155008 sequesters HSP70/BAG3 complex inhibiting its action against the EC adhesome. HSP70/BAG3 complex, which is triggered during pathophysiological conditions, is therefore incapable to degrade focal adhesion. In this scenario, ver155008 improves EC attachment by protecting EC/ECM interaction which results in more robust focal adhesion.

Although these data are promising in terms a novel therapeutic treatment against NRF2/OSGIN1+2-mediated cell detachment, this work has been carried out only on HCAECs and it should be noted that unexpected cell type-dependent effects may occur. Further studies are therefore necessary to fully elucidate the mechanism and cellular

diversity of plaque erosion in order to challenge the application of autophagy-stimulating therapies (See Table 4 Appendix for compounds details).

5.5 Key findings:

- AdOSGIN1, AdOSGIN2 and in particular a combination of both promotes significant EC detachment under flow. The AdOSGIN1+2 condition showed a significant number of detached ECs alive, further supporting the theory of an apoptosis-independent mechanism promoting cell detachment.
- The two autophagy inhibitors were added into the media after adenoviral overexpression and cells were exposed to flow. EC detachment was observed in AdOSGIN1+2 with either chloroquine or bafilomycin. Furthermore, detachment was not enhanced, and cell integrity was not altered which suggests that impairment of autophagic flux by AdOSGIN1+2, chloroquine or bafilomycin regulates cell adhesion.
- AdOSGIN1+2 are responsible for reducing autophagic flux which led to lysosomal vesicles accumulation. Immunocytochemical staining co-localised LAMP1 and cathepsin L. AdOSGIN1+2 showed an increment of LAMP1 and cathepsin L protein, however AdOSGIN1+2 HCAECs exposed to flow incubated with cathepsin inhibitor did not improve EC attachment. This suggests that the presence of cathepsin proteases is not sufficient to promote EC detachment and their inhibition is not beneficial.
- Considering that the combined effect of AdOSGIN1+2 leads to a blockage of the natural autophagy process, various compounds described in sections 5.1.1 - 5.1.7 were used in order to enhance the autophagic mechanism. The two compounds, metformin and ver155008, were both able to improve cell attachment respectively by activating AMP-kinase pathways and by sequestering HSP70. Both AdOSGIN1+2 and AdNRF2 HAECs exposed to flow plus the compounds showed a significant improvement in cell attachment, which suggests that inhibition of HSP70 or activation of AMP-kinase reverses cell detachment driven by either OSGIN1 and OSGIN2 or NRF2 overexpression.
- Here, HSP70 and SQSTM1/p62 accumulation was assessed in HCAECs exposed to flow in AdNRF2 and AdOSGIN1+2. Metformin showed a significant decrease in the level of SQSTM1/p62 accumulation in both AdNRF2 and AdOSGIN1+2. Ver155008 improved cell attachment by sequestering HSP70 which, in pathophysiological conditions in CMA, links with BAG3 and potentially SQSTM1/p62 [437]. This study is the first to show that the use of ver155008 and metformin in a model of erosion respectively modified and reduced SQSTM1/p62 accumulation. This is a pioneering study proposing the use of ver155008 and metformin as a therapy against erosion of overlying stenotic plaques.

5.6 Summary

Overexpression of OSGIN1 and OSGIN2 in HCAECs triggered cell detachment, equivalent to NRF2 overexpression which was quantified by exposure to shear stress using the orbital shaker model. Detached cells were analysed for membrane integrity using trypan blue exclusion, which demonstrated that a significant proportion of detached cells remained integral, supporting a non-apoptotic mechanism. Incubation with low doses of chloroquine (150μM) or bafilomycin (50nM) or moderate doses (300μM, 100nM) to inhibit autophagy also triggered cell detachment with similar maintenance of membrane integrity. Co-treatment of OSGIN1+2 overexpression with either chloroquine or bafilomycin did not enhance cell detachment or alter cell integrity, suggesting a reduction in autophagic flux by either chloroquine or bafilomycin, or OSGIN1+2 overexpression which is capable of regulating cell adhesion. Inhibition of cathepsins activity using E64 (1μM and 10μM) did not reduce or enhance EC detachment, suggesting that it is not a primary mechanism involved in endothelial erosion. On the contrary, the use of Pifithirin α (10μM and 20μM) exacerbates EC detachment in both control and OSGIN1+2 conditions, this is likely to be due to its non-specific activity or because it promotes cell death in the case of no caspase activation (Chapter 4), leading to dysfunctional autophagy. Rapamycin did not display any significant improvement in cell attachment which indicates an mTOR-independent mechanism. Finally, this study demonstrates that inhibition of HSPA1A/HSPA1B nucleotide binding site with ver155008 reduced cell detachment, suggesting a role of chaperone-mediated autophagy in regulating cell adhesion. This supports the observation that AMP kinase activation by metformin, which promotes macroautophagy, potentially bypasses the blockade in chaperone-mediated autophagy and normalises p62 protein levels, also suggesting a clearance of autophagic vesicles and improvement of autophagic flux which stabilizes the attachment to a substrate of HCAEC overexpressing either NRF2 or OSGIN1+2.

CHAPTER 6: GENERAL DISCUSSION, CLOSING REMARKS, FUTURE WORK AND LIMITATIONS

CHAPTER 6: GENERAL DISCUSSION

The research carried out during this PhD has focused on understanding the molecular mechanism that might contribute towards endothelial erosion of stenotic atherosclerotic plaques. I investigated the impact that biomechanically-amplified NRF2-regulated genes affected endothelial adhesion. During this project combined activation of multiple pathways such as autophagy and senescence, triggered by adenoviral overexpression of NRF2, OSGIN1 and 2 led to endothelial detachment in our *in vitro* model. The data discussed here advances understanding of the ECs molecular mechanism activated in response to ROS, pathways that might contribute in the pathophysiology of plaque erosion, and a potential therapy against endothelial dysfunction-induced desquamation.

6.1 Investigation into the biological process of eroded plaque exposed to ESS: responsible genes

The vascular endothelium is a key player in the maintenance of vascular tone and the prevention of atherosclerosis. Endothelial dysfunction is induced by multiple factors including disturbed flow, inflammatory mediators and oxidants derived from cigarette smoke. It is known to promote coronary atherosclerosis and increase the likelihood of myocardial infarctions (MI) and strokes [537]. Conversely, laminar flow protects against endothelial dysfunction, at least in the initial phases of atherogenesis. Endothelial erosion of plaques is the underlying mechanism that causes about 30% of heart attacks [16]. Prior to the completion of this PhD, the molecular mechanism behind erosion of underlying stenotic plaques exposed to ESS had not been studied. It was known that mechanosensitive ECs, are regulated by flow, however plaque erosion was suggested to be due to enhanced rates of apoptosis in the distal region of atherosclerotic plaques exposed to OSS [9]. To investigate potential mechanisms, we identified that OCT-defined plaque erosions occur most frequently on stenotic plaques where the endothelium is exposed to elevated flow. This would argue against an apoptotic mechanism for plaque erosion as this flow environment protects from, rather than promotes apoptosis [59]. Using an *in vitro* model that exposed HCAEC to the elevated flow and smoking-induced dysfunction, endothelial detachment was observed. The combined effects of CSE and TNFα on HCAECs promoted 30% of detachment and increased the level of several genes, among which NRF2, which is the principal gene controlling the antioxidant system [113].

Analysis of ECs under these criteria identified two novel flow and smoking responsive genes, OSGIN1 and OSGIN2 which are highly upregulated in the HCAECs exposed to ESS in combination with CSE and TNFα. Not much was known about these genes, especially related with CVD, but they appear to be most strongly upregulated under conditions that promoted endothelial detachment, suggesting they may be involved in this process.

6.2 NRF2 enhance EC detachment under ESS: tackling the dogma of NRF2 protective effect

NRF2 it is commonly considered as "the Master Regulator of Anti-Oxidative Responses". Although in the context of atherosclerosis, there is no doubt about the protective role of NRF2 against ROS [538], its beneficial effects lay on a very precarious balance. NRF2 dysregulation or uncontrolled activation, which can be chronic in heavy smokers, provokes a detrimental effect which exacerbates a microenvironment already affected by noxious stimulai. In support of this theory, global deletion of NRF2 (NRF2-/-) in hypercholesterolemic mice has been shown to decrease atherosclerosis, even though there is a reduction in antioxidant defense [182, 539] and inflammation [540]. Previous work showed that HCAECs exposed to ESS in combination with CSE and TNFα have increased levels of NRF2-responsive genes [116], and concomitantly decreased EC proliferation rates and cell detachment [113] (Figure 1.7).

Attempts to dissect the mechanism using an apoptosis inhibitor (Z-VAD-FMK), a pan matrix metalloproteinase inhibitor (GM6001), rosuvastatin, or necrostatin-1 failed to prevent cell detachment [113]. Treatment with activators of Nrf2 exacerbated, rather than prevented cell loss, eluding to a role in mediating cell detachment. Therefore, in order to further investigate the function of NRF2, NRF2 was overexpressed by using adenoviral vector in HCAECs and subsequently exposed to shear stress using an orbital shaker system [529, 530] (Figure 5.2). AdNRF2 was shown to significantly increase EC detachment (Figure 5.8), supporting the implication of NRF2-regulated gene expression in endothelial detachment. These observations raise a cautionary note on modulation of NRF2 as an adjunctive therapy to prolong lifespan [541, 542]. The multiple levels of control that exist to regulate NRF2 activity strengthen this concern [122] by indicating the necessity for tight regulation of the NRF2-dependent transcriptional program. Further experiments on HCAECs exposed to ESS and incubated with CSE and TNFα showed the highest levels of two NRF2-regulated

genes OSGIN1 and OSGIN2 coincided with detachment (Figure 3.1). This scenario highlights the importance of ESS in triggering a complex shear-dependent pattern of regulation of OSGIN1+2 and that the ESS-induced changes in EC phenotype might promote plaque erosion, in addition to any mechanical contribution to detachment caused by the increase in shear stress.

Furthermore, significantly higher OSGIN1 and OSGIN2 protein levels were observed in the aortas of mice exposed to tobacco smoke for 3 months compared to the control mice (Figure 3.2) supporting the relevance of our *in vitro* findings.

6.3 NRF2 executioners: OSGIN1 and OSGIN2

Not much is known about OSGIN1 and even less about his poorly characterised homolog OSGIN2, especially in the context of vascular biology. It is known that both have similar molecular weights of around 60 kDa, they have a similar predicted structure with 50% amino acid sequence identity (Figure 1.11) and they are well conserved among species. Their conservation suggests an essential role within the cell. To dissect the role of OSGIN1 and OSGIN2 adenoviral viral overexpression was performed in HCAECs. Combined overexpression of both genes in HCAECs in static culture triggered cell detachment, highlighted by the presence of cell-prints visible during immunocytochemical analysis. In order to evaluate whether apoptosis is the mechanism responsible, multiple caspase assays and western blot analysis of PARP, which is considered the main target for caspase 3, were performed. Interestingly, none of the experiments indicated an increased caspase activity or PARP cleavage supporting the hypothesis that this represents a novel apoptosis-independent and mechanism triggering EC desquamation. This observation is in concordance with the inclusion of a caspase inhibitor having no effect on cell detachment in the ESS+CSE+TNFα *in vitro* model and a recent paper published by Brennan *et al.* [197]. Transcriptomic analysis was performed on HCAECs transduced with AdCtrl, AdOSGIN1, AdOSGIN2, or AdOSGIN1+2, 360 genes which had significant changes in their expression over the three conditions were observed (Figure 4.9). Eight clusters were identified, among which cluster one has been significantly enriched in genes associated with the activation of the Ingenuity IPA canonical pathway NRF2-mediated Oxidative Stress Response, eNOS signalling inhibition. Interestingly, there was also an alteration in the protein ubiquitination pathway and unfolded protein response driven by the activation of the transcription factor

genes HSF1 and Nrf2 (See Table 15 Appendix). Furthermore, RNAseq suggests an involvement of interferon α signalling (Cluster 2) which might enhance the gene expression pattern promoted by AdOSGIN1+2 because of the numerous regulated genes with IRF3/7 binding sites in their promoters. For interferon α signalling, out of the 20 genes, five (CRYAB, HSPA1A, HSPA1B and ISG15) have greater changes in expression and all five were found to be related with proteostasis or proteostasis regulator BAG3. Other BAG3 regulators among which HSP90AA1, HSP90AB1, SQSTM1/p62 and HSPA8 were also involved.

This data suggests that alterations in NRF2-mediated Oxidative Stress Response and unfolded protein quality control pathways might be the missing link in oxidative stress response pathway with CMA.

6.4 Function of OSGIN1 and OSGIN2 in HCAECs

Considering the lack of information for NRF2 regulated genes OSGIN1 and OSGIN2, adenoviral overexpression was carried out in order to evaluate their role in HCAECs. First, identifying whether OSGIN1 and/or OSGIN2 were able to translocate from the nuclei to the mitochondria, as suggested by Brennan et al in astrocytes [197] which might help identify their mode of action. In opposition to Brennan, AdOSGIN1 and 2 in HCAECs are localised exclusively in the nucleus, despite the lack of an obvious nuclear localisation sequence using cNLS Mapper[543], or SeqNLS [544]. In order to evaluate whether OSGIN1 and 2 affects cellular proliferation comparable with the data previously obtained with AdNRF2[113], BrdU incorporation assays (Figure 3.7) and propidium iodide FACS analysis demonstrated that OSGIN1+2 overexpression inhibited cell proliferation, inducing cell cycle arrest in S-phase (Figure 3.12). AdOSGIN1 and 2 gave rise to a multitude of multinucleated cells (Figure 3.8), demonstrating that OSGIN2 overexpression allowed nuclear division but prevented the final cytokinesis event, blocking G2-M progression (Figure 3.12). Further investigation of this peculiarity revealed that inhibition of proliferation is associated with the induction of senescence. HCAECs were positive for senescence-associated β-galactosidase (Figure 3.15), which is a commonly accepted marker of high lysosomal activity. Additionally, an increased expression of the marker of senescence was assessed, in particular, p16 and p21 (Figure 3.13 - 3.14), and which were shown to inhibit cyclins cdk4 and cdk6 which are expressed during the cell cycle between

S-phase and G2-M [302]. Furthermore, overexpression of both genes OSGIN1+2 dramatically affected cell morphology, increasing cell size and depth indicative of a hypertrophic cell morphology in accordance with a senescent phenotype [303].

6.5 Upregulation of OSGIN1 And OSGIN2 dramatically modify cell size, disrupt cell structure and focal adhesions

A hypertrophic cell morphology is reported to be peculiar in senescence phenotypes undergoing structural and functional changes that strongly compromise every aspect of cell physiology. Nonetheless the impact of senescence on cytoskeletal reorganization is poorly understood [545]. Integrity of the cytoskeleton and focal adhesion is required for stable cell adhesion and in ECs, in order to avoid detachment caused by elevated shear stress. Overexpression of OSGIN1 and OSGIN2 triggered profound alterations in cell structure. Enlarged HCAEC size and dysmorphic nuclei were observed respectively (Figures 3.8 and 3.10), furthermore a collapse of the actin fibres and tubulin networks with an overall reduction in staining for actin, tubulin and vinculin were observed (Figure 4.4 – 4.7). Interestingly, confocal Z-stack analysis (Figure 3.11) shows a 5-fold increase in cell height compared to the control which, in a scenario were the cytoskeletal reorganisation function and cell adhesion stability is impaired, might be a further reason to promote EC desquamation, providing a larger protrusion into the lumen and amplifying their exposure to ESS. The cause might be the concomitant accumulation of autophagic vesicles within HCAECs and the expression of the genes involved in HSP70/BAG3-controlled CMA pathway. Both BAG3 and HSP70 (Figure 4.12) showed higher levels of expression following adenoviral overexpression of OSGIN1 and OSGIN2. It is possible that the complex HSP70/BAG3 promotes degradation of dysfunctional or misfolded focal adhesion and cytoskeletal structure proteins during proteostasis control.

It was observed that in eroded plaques the sub-endothelial matrix is high in versican and hyaluronan [42]. Recently it was shown that high levels of the enzyme hyaluronidase 2 (HYAL2) degrades high-molecular-weight hyaluronan to its proinflammatory 20-kDa isoform [112], therefore hyaluronan and versican may regulate vascular inflammation in atherosclerosis [546, 547] and regulate processes that modulate endothelial erosion. Hyaluronan (and biglycan) can bind to and activate TLR2 and TLR4 [63, 548] and TLR2 engagement has been suggested as the mechanism that promotes endothelial detachment

on the distal area of eroded plaques exposed to OSS. In the same way, TLR4 activation, which is normally activated by bacterial endotoxin, a pathogen-associated molecular pattern (PAMP), may also be activated by damage-associated molecular pattern (DAMP) proteins such as HSP70 [549], promoting EC desquamation through increased Trif-dependent activation of IRF3 signalling. Further studies are necessary in order to investigate TLR4-dependent amplification of detachment.

6.6 NRF2, OSGIN1 and OSGIN2 promote detachment though dysfunctional autophagy: mechanism and potential therapy

Overexpression of OSGIN1 and OSGIN2 in HCAECs exposed to shear stress on the orbital shaker model promoted detachment comparable to AdNRF2 (Figure 5.2). Analysis by trypan blue exclusion showed that many of the detached cells retained their membrane integrity, supporting the theory of a non-apoptotic mechanism of detachment. Based on the observation that OSGIN1+2 overexpression markedly enhanced the HSP70/BAG3 proteostasis pathway and the anti-apoptotic mechanism, autophagy was the logical path to follow.

HCAECs incubated with autophagy inhibitors using two different concentrations, low doses of chloroquine (150μM) or bafilomycin (50nM) to inhibit autophagy (Figure 5.4A), or moderate doses (300μM, 100nM Figure 5.4B) also triggered cell detachment with similar maintenance of membrane integrity (Figure 5.4 C, D, E and F). Interestingly, co-treatment of ECs with OSGIN1+2 overexpression with either chloroquine or bafilomycin did not enhance cell detachment or alter cell integrity, suggesting a reduction in autophagic flux by either chloroquine or bafilomycin, or by OSGIN1+2 overexpression may be responsible for detachment (Figure 5.4 C, D, E and F).

Impairment of autophagic flux is an important characteristic of oxidative stress-induced senescence [301], where, although autophagic gene expression and structures increase, the accumulation of SQSTM1/p62 indicates an impaired autophagic flux with lysosomal dysfunction [550]. SQSTM1/p62 accumulation is considered the main marker of dysfunctional autophagy [444], it was observed in both static (Figure 4.13 and 4.14) and under flow conditions (Figure 5.9 in HCAECs transduced with OSGIN1+2 and NRF2 adenoviral vectors, with increased accumulation of lysosomal vesicles (Figure 4.13) and

autophagy-related gene expression levels (Figure 4.12). The putative mechanism of action leading to EC detachment is summarized in figure 6.1.

In response to detachment, healthy cells can trigger an acute increase autophagic flux, promoting cell survival by repressing apoptosis and affording some time for the cell to rebuild its connection with ECM (Discussed in chapter 4). Sustained overexpression of NRF2 or OSGIN1 and OSGIN2 inhibits autophagic flux (Figure 5.10), which may be promoted by further activation of NRF2 and SQSTM1/p62 [413], providing an amplification of detrimental signalling within the cell. Here, SQSTM1/p62 binds KEAP1, promoting NRF2 nuclear translocation and NRF2-regulated gene expression. Failure in the macroautophagy mechanism triggers the activation of selective autophagy or CMA, where cells respond to inhibition of macroautophagy by constitutively activating CMA [551, 552]. Activation of CMA has also been observed in the case of inhibition of the proteasome [553, 554], and represents a switch from physiological to pathological conditions. We observed a large increase in the expression level of HSP701A, HSP701B and BAG3 suggesting an increase in CMA, and activation of this stress-activated proteostatic pathway [267]. Furthermore, BAG3 expression is normally low in physiological conditions and BAG1 is the predominant protein that binds HSP70, forming the HSP70/BAG1 complex. However, in pathological conditions this balance switches towards BAG3 and replaces BAG1 in the HSP70/BAG1 complex. HSP70/BAG3 is therefore activated and is accompanied by CMA activation [437]. HSP70/BAG3 complex has been observed to degrade filamin A, which is an essential linking protein that bridges the actin cytoskeleton and focal adhesion complexes and therefore may limit EC/ECM interaction and promote detachment. Failing to maintain this interaction leads to EC detachment and which may be followed by anoikis [555].

HCAECs exposed to shear stress were treated with several compounds in order to reduce EC detachment. Particular attention was given to dissecting a potential role of dysregulated chaperone-mediated autophagy in cell detachment by inhibiting HSP70 nucleotide binding site using Ver155008 or bypassing the autophagy inhibition by activating AMP kinase with metformin. Both Ver155008 and metformin reduced cell detachment, this was induced by either OSGIN1+2 or NRF2 overexpression which modified the accumulation of autophagic vesicle markers SQSTM1/p62 (Figure 5.8, 5.9). This

supports the hypothesis that OSGIN1+2 dysregulation of chaperone-mediated autophagy mediates NRF2-mediated cell detachment.

6.7 Closing remarks

NRF2 signalling involves a large network of interacting members, with multiple levels of complexity. From the variety of NRF2 regulated gene activation, two in particular, OSGIN1 and OSGIN2 can reproduce the effects seen by NRF2 overexpression and are therefore likely to be responsible for NRF2-triggered EC detachment. It is possible that high levels of the combination of OSGIN1 and 2 combine to promote HCAECs detachment. OSGIN1 and OSGIN2 channelled their effect into two main branches of signalling: CMA and senescence. CMA proteostasis controlled by the HSP70/BAG3 complex and arrest of cell cycle by senescence activation pathways leads to disruption of cytoskeletal structure and impairment of focal adhesion molecules crucial for EC adhesion [556, 557]. The ability of metformin and Ver155008 to partially rescue the deficit in adhesion represents a novel axis for therapeutic intervention and may become a potential therapy in ACS patients.

6.8 Future works

These findings demonstrate that under elevated flow, smoking-induced hyperactivation of NRF2 and NRF2-regulated genes OSGIN1 and 2 can trigger endothelial cell detachment, highlighting a novel mechanism that could contribute to ACS involving endothelial erosion overlying stenotic plaques. However, advances in our understanding of the mechanism of erosion of plaques have been made during this study, some interesting questions have arisen during this PhD and will form the basis of future hypothesis-driven investigations to shed light on the intricate mechanism of endothelial dysfunction in erosion overlying stenotic plaques.

6.8.1 How does NR3F2 trigger SQSTM1/p62 accumulation, leading to reduce autophagic flux?

Results suggested that ECs transduced by NRF2 adenoviral vectors inhibit autophagic flux, with an observed accumulation of SQSTM1/p62 protein and lysosomal activity. Several independent groups [558-560] identified the direct interaction between SQSTM1/p62 and KEAP1, which appears to inhibit the ability of KEAP1 to promote NRF2 degradation, followed by NRF2 nuclear translocation and associated gene expression. Both during this PhD and previous work it was observed that increased oxidative stress leads to impaired

autophagy. Furthermore, it was observed that the overexpression of the downstream NRF2-regulated genes OSGIN1 and 2, either alone or in combination, have the potential to drive SQSTM1/p62 gene transcription and protein accumulation. This interesting result shifts the axis from a one-way pathway SQSTM1/p62→NRF2 activation to a two-way pathway of mutual stimulation SQSTM1/p62 ↔ NRF2, which can act in an amplification loop and promote the chronic triggering of NRF2 activation and blockage of autophagic flux through SQSTM1/p62 accumulation.

6.8.2 Regulation of OSGIN1 and 2 can improve endothelial dysfunction by preventing autophagy blockage and senescence?

During this study it was observed that the role of OSGIN1 and 2 in promoting cell senescence by the increased expression of p16 and p21, which inhibits cdk4/6 and leads to a mitotic senescence transition. Stress response can trigger multiple effector mechanisms whose combination determines the phenotypic quality. A subset of autophagy-related genes have been reported to be upregulated during senescence [316]. Overexpression of OSGIN1 and 2 have been shown to be responsible for multiple genes commonly known to be involved in autophagy, but at the protein level they decrease autophagic flux, displaying accumulation of SQSTM1/p62. How OSGIN1 and OSGIN2 promotes a blockage in autophagy is still not known. To answer this question, further dissection of the mechanism of action of OSGIN1 and 2 is necessary. KO or TET-system on/off viral vector of OSGIN1 and 2 might be give better idea on their molecular mechanism.

6.8.3 Is the HSP70/BAG3 complex responsible for EC detachment?

This study demonstrated that overexpression of OSGIN1 and 2 promotes high transcription level of HSPA1A/HSPA1B or HSP70. Concomitantly BAG3 expression was also increased. BAG3 overexpression has been shown to result in a decrease in migration and adhesion to matrix [435], the decrease was reversed by deletion of the BAG3 proline-rich (PXXP) domain, indicating that an interaction of BAG3 with a SH3 domain-containing protein was crucial [533]. Other separate studies have proved the active interaction between HSP70 and BAG3 in the formation of the HSP70/BAG3 complex [434, 561]. Of particular interest Hutt et al observed that silencing HSP70-specific nucleotide exchange factor BAG3 improved cell stability, restoration of cell-surface function, protein trafficking, and

autophagic flux [562]. Still very little is known about the HSP70/BAG3 complex, but it participates in a range of disease states [437] which highlights the necessity to dissect further the role of dysregulated autophagy in the modulation of endothelial adhesion.

6.8.4 How does the activity of TLR2 and TLR4 in erosion of overlying stenotic plaque exposed to ESS affects endothelial adhesion molecules?

Eroded plaque sub-endothelial matrix composition is abundant in versican, glycosaminoglycan and hyaluronan [42]. Degradation of hyaluronan in its proinflammatory 20-kDa isoform might lead to inflammation in atherosclerosis by the modulation of TLR2 and 4 [63, 548, 563]. In the area exposed to OSS, TLR2 signalling may predispose ECs to endothelial desquamation, apoptosis and NET formation [9, 71, 564]. However, exposure to laminar shear inhibits apoptosis in endothelial cells overlying atherosclerotic plaques [59]. Furthermore, the experiments proposed in this study define a mechanism of endothelial detachment which is apoptosis independent. Further studies should address the differential effects on cell death pathways of hyaluronan and HSP70 signalling through TLR2 and TLR4 under various flow conditions. In addition, the relative adhesive quality of a sub-endothelial matrix containing a higher proportion of hyaluronan and versican and possible contributions of extracellular matrix-degrading hydrolases requires elucidation, especially under elevated flow conditions [107, 565]. These observations put a spotlight on the role of TLR2 and TLR4 and their ligands hyaluronan and HSP70, in modulating endothelial erosion in both hemodynamic environments.

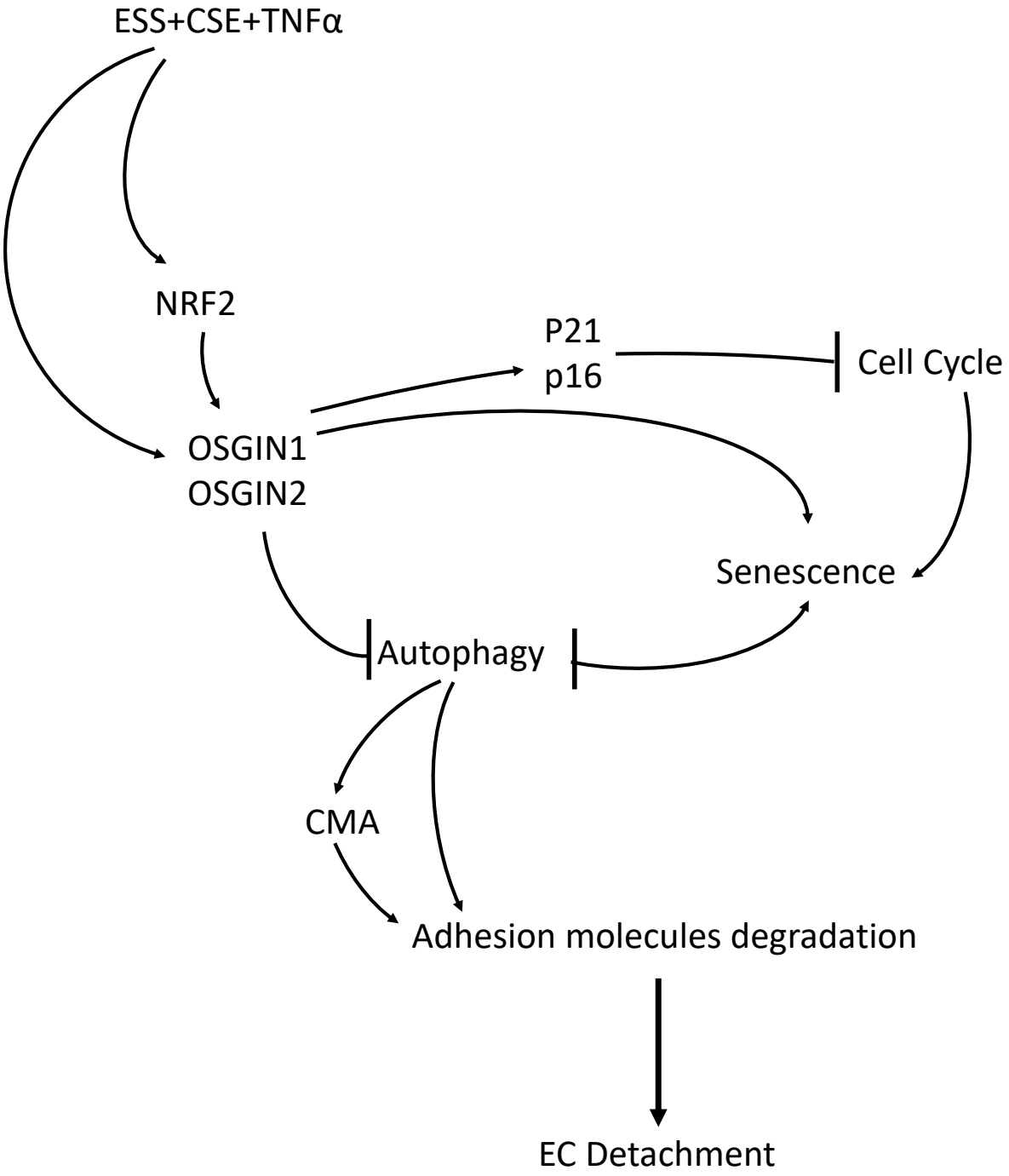

Figure 6.1). Putative mechanism of action leading to detachment. ESS+CSE+TNFα leads to NRF2-signalling pathway activation and the overexpression of two NRF2-regulated genes OSGIN1 and OSGIN2. OSGIN1 and OSGIN2 inhibit autophagy and blockage of cell cycle, promoting cellular senescence. Furthermore, inhibition of autophagy activates the emergency CMA mechanism, which might be responsible for adhesion molecule degradation and consequently EC detachment.

6.9 Study limitations

- Although HCAECs are the more appropriate type of cells for carrying out a study on endothelial detachment on plaque erosion, during this PhD the cross-talk between HCAECs and other type of cells (such as SMC and leukocytes) in the artery was not evaluated. This PhD focused on creating a simple model of erosion and further improvement, such as co-culture of HCAECs and other arterial representative cells would give a wider understanding about the effect of detachment.

- An *in vitro* model of erosion was used in order to evaluate what is occurring in HCACEs exposed to ESS in smokers. This model only shows what is occurring in particular circumstances and only focused on the last stage of plaque erosion at the moment of endothelial detachment. Creating an *in vivo* model of plaque erosion would give a better understanding about this pathology.

- Plaque erosion of an atherosclerotic plaque is a complicated pathology which involves a combined effect of several hits. During this PhD only two genes were evaluated. Their contribution on endothelial detachment have been studied, but many others might take part in this scenario. Further analysis of other genes, with particular attention on those involved in the molecular pathways described during this PhD will improve our knowledge on endothelial erosion of atherosclerotic plaques.

- Although an improvement of endothelial attachment was shown when HCAECs were treated with Metformin and Ver155008 *in vitro*, it is difficult to assess the real potential of these two compounds without the possibility to test them *in vivo*. Furthermore, the combination of both compounds might enhance their effect, giving a better outcome in terms of improving endothelial attachment, but this was not investigated during this PhD.

APPENDIX

Table 1. Primary Antibodies, dilutions and methodology used in Western Blotting

	Primary ab	**Blocking Solution**	**Secondary ab**
OSGIN1 (Biorbyt orb100666)	Rabbit-antiOSGIN1 (1:1000) O/N 4°C	1% BSA	Monoclonal Secondary HRP anti rabbit (1:1000-1 hr) in TBSTween
OSGIN2 (Biorbyt orb185683)	Rabbit-antiOSGIN2 (1:500) O/N 4°C	1% BSA	Monoclonal Secondary HRP-anti rabbit (1:1000-1 hr) in TBSTween
PARP cleavage (Cell Signaling D64E10)	Rabbit anti-PARP (1:1000) O/N 4°C	0,5% BSA	Monoclonal Secondary HRP-anti rabbit (1:2000-1 hr) in TBSTween
SQSTM1/p62 (Abcam ab56416)	Mouse anti-p62 (1:1000) O/N 4°C	3% Milk	Monoclonal Secondary HRP-anti mouse (1:5000-1 hr) in TBSTween
HSP70 (Abcam ab45133)	Rabbit anti-HSP70 (1:1000) O/N 4°C	5% Milk	Monoclonal Secondary HRP-anti rabbit (1:5000-1 hr) in TBSTween

Table 2. Antibodies used in Immunocytochemical analysis

Antibody	**Type**	**Dilution**	**Company**
OSGIN1	Rabbit	1:100	(Biorbyt orb100666)
OSGIN2	Rabbit	1:75	(Biorbyt orb185683)
VE-Cadherin	Rabbit	1:400	(Cell Signalling D87F2)
β-Catenin	Mouse	1:100	(BD Transduction Laboratories 610153)
Vinculin	Mouse	1:400	(Sigma V4505)
Mab113	Mouse	1:100	(Abcam ab92824)
Tubulin	Already conjugated (Green)	1:1000	(Abcam ab64503)
Phalloidin	Already conjugated (Red)	1:250	(Sigma P1951)
HSP70	Rabbit	1:400	(Abcam ab45133)
LAMP1	Rabbit	1:100	(Abcam ab24170)

SQSTM1/p62	mouse	1:200	(Abcam ab56416)

Secondary Antibody description

Alexa fluor488	Anti-mouse or rabbit	1:200	Invitrogen
Alexa fluor647	Anti-mouse or rabbit	1:200	Invitrogen

Table 3. Primer sequences used for real-time PCR

p21 (SW878F/879R)	F CTCAGGGTCGAAAACGGCGG R GTGGGCGGATTAGGGCTTCCT
p16 (SW926F/927R)	F CGAGCTCGGCCCTGGAG R TCGGGCGCTGCCCATCAT
HSPA1A (SW355F/356R)	F TGAGGAGCTGCTGCGACAGT R GGCTGGAAACGGAACACTGG
HSPA1B (SW357F/358R)	F TGTTGAGTTTCCGGCGTTCC R AACACCCCCACGCAGGAGTA
BAG3 (SW966F/967R)	F GCGGGGCATGCCAGAAACCA R CTGGCCGGGTAACGTTCTGCT
ATG7 (SW894F/895R)	F GGACTGGCCGTGATTGCAGGA R ATCCGATCGTCACTGCTGCTGG
ATG9A (SW938F/939R)	F AGAGGCGCTACGGTGGCATC R GCCTTGATGCCGACTGCCCA
MAP1LC3B (SW934F/935R)	F CGCCCAGATCCCTGCACCAT R AGCATTGAGCTGTAAGCGCCTTCT
SQSTM1/p62 (SW936F/937R)	F GGACGGGGACTTGGTTGCCTT R CGGGTTCCTACCACAGGCCC
GABARAPL1/ATG8 (SW940F/941R)	F CGGACAGGGTCCCCGTGATTG R AGCACTGGTGGGAGGGATGGT
GAPDH (SW180F/181R)	F CGGATTTGGTCGTATTGGGCG R GCCTTCTCCATGGTGGTGAAGAC

Table 4. Chemical compounds added during orbital shaker experiment

Compounds	Work concentration	Brand	Dissolved in
Chloroquine	100 or 300μM	Sigma	MV2 media
Bafilomycin	50nM or 100nM	Sigma	DMSO
Metformin	100μM-1mM	Sigma	MV2 media
VER-155008	15-30μM	Sigma	DMSO
E64	1-10μM	Sigma	MV2 media
Pifithrin α	10-20μM	Sigma	DMSO
Rapamycin	20-100nM	Sigma	DMSO

Table 5. Cluster 1, Genes and top 10 canonical pathways and regulators.

Genes		Ingenuity Canonical Pathways	Upstream Transcriptional Regulator
AHSA1	HSPB1	Aldosterone Signaling in Epithelial Cells	HSF1
ALDH3A2	HSPB8	Protein Ubiquitination Pathway	FBXW7
ATF3	HSPD1	NRF2-mediated Oxidative Stress Response	PML
B3GAT3	HSPE1	Unfolded protein response	SP100
BAG3	HSPH1	Glucocorticoid Receptor Signaling	NFE2L2
BANF1	IER5L	eNOS Signaling	TP53
C3orf52	IL7R	Aryl Hydrocarbon Receptor Signaling	ETS1
CACYBP	JMJD6	Huntington's Disease Signaling	HSF2
CBARP	LGALS8	Xenobiotic Metabolism Signaling	HTT
CHKA	LUC7L3	Ingenuity Canonical Pathways	NUPR1
CHORDC1	MICB		
CPNE8	MLKL		

CRYAB	MRPL18
CRYZ	MSX1
DEDD2	NAPG
DNAJA1	NDRG1
DNAJB1	OSGIN1
DNAJB6	P4HA2
EVI2B	PATL1
FKBP4	PAXBP1
FTL	PLAUR
GDF15	PLEKHB2
HIF3A	PRPF38B
HIST2H2BE	PTGES3
HMOX1	RNF19B
HSP90AA1	RSRP1
HSP90AB1	SNX3
HSPA1A	SPATS2L
HSPA1B	SQSTM1
HSPA4	STIP1
HSPA6	TRIM16
HSPA8	TSPYL2

Table 6. Cluster 2, Genes and top 10 canonical pathways and regulators.

Genes	
ANKRD10	MX1
APOL6	MX2
BATF2	OAS1
C19orf66	OAS2
DDX58	OASL
DDX60	OSGIN2
DDX60L	PARP14
DHX58	PARP9
DNAJA4	PLSCR1
DTX3L	PMAIP1
EIF2AK2	PPP1R18
EPSTI1	RSAD2
GBP1	SAMD9
GCH1	SAMD9L
HERC6	SERPINH1
IFI35	SLC15A3
IFI44L	SLC37A1
IFIH1	SP110
IFIT1	TAP1
IFIT2	TRIM21
IFIT3	TRIM26
IFIT5	TRIM69
IFITM1	UBC
IRF7	UBE2L6
ISG15	XAF1
LY6E	

Ingenuity Canonical Pathways
Interferon Signaling
Activation of IRF by Cytosolic Pattern Recognition Receptors
Role of Pattern Recognition Receptors in Recognition of Bacteria and Viruses
Role of RIG1-like Receptors in Antiviral Innate Immunity
Tetrahydrobiopterin Biosynthesis I
Tetrahydrobiopterin Biosynthesis II
Retinoic acid Mediated Apoptosis Signaling
Toll-like Receptor Signaling
Death Receptor Signaling
Protein Ubiquitination Pathway

Upstream Transcriptional Regulator
IRF7
STAT1
IRF1
NKX2-3
IRF3
IRF5
TRIM24
CNOT7
STAT3
STAT2

Table 7. Cluster 3, Genes and top 10 canonical pathways and regulators.

Genes		Ingenuity Canonical Pathways	Upstream Transcriptional Regulator
ADM	PRDX6	NRF2-mediated Oxidative Stress Response	MAFG
ANGPT2	SBDSP1	Glutathione Biosynthesis	BACH1
F2RL2	SEC61G	Pentose Phosphate Pathway (Non-oxidative Branch)	NFE2L2
GCLM	SELO	Superoxide Radicals Degradation	KEAP1
INA	SLC17A9	Prostanoid Biosynthesis	MAFK
LENG9	SNRPA1	Phagosome Maturation	NFE2
ME1	TBXAS1	Pentose Phosphate Pathway	PML
MLLT11	TKT	γ-glutamyl Cycle	KLF2
NQO1	TMEM156	Glutathione Redox Reactions I	NFE2L1
P4HA1	TRIM16L	Gluconeogenesis I	PDX1
PDE4B	UPP1		
PLPP2	XPOT		
PRDX1	ZDHHC6		

Table 8. Cluster 4, Genes and top 10 canonical pathways and regulators.

Genes	Ingenuity Canonical Pathways	Upstream Transcriptional Regulator
ANGPTL4	Oxidative Phosphorylation	PHF1
CTD-2015G9.2	Mitochondrial Dysfunction	COMMD3-BMI1
HOXA9	Sirtuin Signaling Pathway	KMT2A
HOXB7		MLLT1
MT-CYB		ASB2
RPSAP58		NKX2-3
TNFSF18		PSIP1
		HOXB3
		BHLHE41
		PLAGL1

Table 9. Cluster 5, Genes and top 10 canonical pathways and regulators.

Genes	
ALDH1A3	MFSD11
AMDHD2	NUP107
ANAPC5	NUP160
ANKRD33B	PACS1
AP3M2	PAN2
ATXN2	PCMTD2
C22orf29	PIGQ
CAPN11	PLA2G4C
CHD1L	PLD1
CLIP4	PPCS
CPNE5	RCBTB1
DFNA5	RFC3
DHRS1	RNF123
DHRS11	SESTD1
EEF2K	SLC35E2B
EVL	SMARCC2
HAS3	STK38L
HERC2	SYNE2
ITPR3	TGFA
KRIT1	UQCRC2
LETMD1	VPS13C
LRRC16A	WDR59
MED12	ZC3H7A

Ingenuity Canonical Pathways
Coenzyme A Biosynthesis
N-acetylglucosamine Degradation I
Phospholipases
Endothelin-1 Signaling
N-acetylglucosamine Degradation II
Role of BRCA1 in DNA Damage Response
Non-Small Cell Lung Cancer Signaling
Phospholipase C Signaling
Antioxidant Action of Vitamin C
Pancreatic Adenocarcinoma Signaling

Upstream Transcriptional Regulator
FOXH1
CITED1
Ncoa6
GSX2
BHLHA15
FOS
VAV2

Table 10. Cluster 6, Genes and top 10 canonical pathways and regulators.

Genes	
BRIP1	
ESCO2	

Ingenuity Canonical Pathways
Role of BRCA1 in DNA Damage Response

Upstream Transcriptional Regulator
CCND1
UXT
FOXM1
IRF1
TCF4
TCF3
FOXO1

Table 11. Cluster 7, Genes and top 10 canonical pathways and regulators.

Genes	
ABCA1	LAMA2
AEBP1	LGALS9
AGRN	LYPD1
APOL1	LYVE1
BNC1	MELTF
CARD11	MGP
CCDC3	MYOM3
CDH11	NEAT1
CFH	NEFH
CLDN11	PCDH10
CSF2RB	PCDH17
CTHRC1	PLCB2
CX3CL1	PLCD1
DDR2	PLCL1
DGKA	POSTN

Ingenuity Canonical Pathways
Adrenomedullin signaling pathway
Role of Macrophages, Fibroblasts and Endothelial Cells in Rheumatoid Arthritis
Antioxidant Action of Vitamin C
P2Y Purigenic Receptor Signaling Pathway
Phospholipases
Wnt/Ca+ pathway
Melatonin Signaling
GPCR-Mediated Integration of Enteroendocrine Signaling Exemplified by an L Cell
Aldosterone Signaling in Epithelial Cells
Agrin Interactions at Neuromuscular Junction

Upstream Transcriptional Regulator
HTT
NKX2-3
HOXA10
CREB1
SMARCA4
MECP2
STAT1
FOXF1
IRF2
ATF4

DKK2	PSMB9
DOCK5	PTPRU
DOCK8	SAT1
DPP4	SELENBP1
ERAP1	SEMA7A
FAM129A	SLITRK4
FRAS1	ST6GALNAC1
GATSL3	STXBP2
HSPA12B	TACSTD2
IGFBP5	TFAP2A
IL18R1	TRPV2
ITGB3	TUSC3
KLF4	VCAM1
KRT19	

Table 12. Cluster 8, Genes and top 10 canonical pathways and regulators.

Genes	HSPG2
A2M	IGFBP2
ABCA7	IL17RD
ACE	IL33
ACP5	ITGA10
ADCY4	ITPR1
ANK1	KCND1
ANK3	KCNN4
APLNR	LIMCH1
APOB	LPL
APOL4	LRP1
AQP1	MAMDC2
AQP3	MAN1C1

Ingenuity Canonical Pathways
Atherosclerosis Signaling
Inhibition of Matrix Metalloproteases
Adrenomedullin Signaling pathway
Gap Junction Signaling
GP6 Signaling Pathway
eNOS Signaling
Hepatic Fibrosis / Hepatic Stellate Cell Activation
Renin-Angiotensin Signaling
Breast Cancer Regulation by Stathmin1
Dopamine-DARPP32 Feedback in cAMP Signaling

Upstream Transcriptional Regulator
KLF2
TP53
SP1
TCF4
CALR
CEBPA
BRD7
ETS1
IKZF1
ASB9

ARHGEF9	MAN2B2
ATHL1	MFAP2
ATP2A3	MMP17
B3GNT9	MYO18A
BTN3A3	NPR1
C10orf10	PBX1
C10orf128	PCMTD1
C10orf54	PEG10
C14orf132	PIDD1
C1RL	PIK3R3
CALCOCO1	PLPP3
CCND2	PPARGC1B
CD24	PPP1R14A
CD40	PTGIS
CECR1	RAPGEF5
CFI	RP1-152L7.5
CKB	RRAGB
CMKLR1	SCUBE3
COL17A1	SEMA3G
COL1A2	SGCE
COL4A5	SIAE
COLEC12	SIDT2
DPYSL4	SLC16A14
DYSF	SLC46A3
EDA2R	SLCO2A1
ENTPD1	SLCO2B1
EPS8L2	SNED1
ERV3-1	SORT1
FBLN2	STAB1
FBN1	SULF1
FKBP9	TMOD1
GAA	TNFRSF14
GAL3ST4	TNS1
GJA4	TPCN1
GJA5	TRIM66
GPR146	USHBP1
HEG1	VASH1
HHAT	VCAN
HMCN1	ZNF366

Table 13. AdOSGIN1 vs AdCtrl, Genes and top 20 canonical pathways and regulators.

Genes					Ingenuity Canonical Pathways	Upstream Transcriptional Regulator
A2M	CMKLR1	HSPA1B	OSGIN2	SLITRK4	Aldosterone Signaling in Epithelial Cells	TP53
ABCA1	COL17A1	HSPA4	P4HA1	SNED1	Adrenomedullin signaling pathway	EPAS1
ABCA7	COL1A2	HSPA6	PACS1	SNRPA1	Atherosclerosis Signaling	HIF1A
ACE	COL4A5	HSPB8	PAN2	SORT1	eNOS Signaling	KLF2
ACP5	COLEC12	HSPD1	PBX1	ST6GALNAC1	Hepatic Fibrosis / Hepatic Stellate Cell Activation	NKX2-3
ADCY4	CPNE5	HSPG2	PCDH10	STAB1	Sperm Motility	NEUROG1
ADM	CRYAB	IGFBP2	PCDH17	STK38L	Cellular Effects of Sildenafil (Viagra)	SP1
AEBP1	CSF2RB	IGFBP5	PCMTD1	STXBP2	Dopamine-DARPP32 Feedback in cAMP Signaling	NFKBIA
AGRN	CTD-2015G9.2	IL17RD	PCMTD2	SULF1	Gap Junction Signaling	ETS1
ALDH1A3	CTHRC1	IL18R1	PDE4B	SYNE2	Prostanoid Biosynthesis	HTT
AMDHD2	CX3CL1	IL33	PEG10	TACSTD2	Endothelin-1 Signaling	STAT3
ANGPT2	DDR2	INA	PIDD1	TBXAS1	GP6 Signaling Pathway	NUPR1
ANGPTL4	DGKA	ITGA10	PIK3R3	TFAP2A	GPCR-Mediated Integration of Enteroendocrine Signaling Exemplified by an L Cell	TWIST1
ANK1	DHRS1	ITGB3	PLA2G4C	TGFA	Synaptic Long-Term Depression	MAFG
ANK3	DKK2	ITPR1	PLCB2	TKT	Neuropathic Pain Signaling in Dorsal Horn Neurons	MYB

ANKRD33B	DOCK5	ITPR3	PLCD1	TMEM156
AP3M2	DOCK8	JMJD6	PLCL1	TMOD1
APLNR	DPP4	KCND1	PLPP2	TNFRSF14
APOB	DPYSL4	KCNN4	PLPP3	TNFSF18
APOL1	DYSF	KLF4	POSTN	TNS1
APOL4	EDA2R	KRT19	PPARGC1B	TPCN1
AQP1	ENTPD1	LAMA2	PPP1R14A	TRIM16
AQP3	EPS8L2	LENG9	PRDX1	TRIM16L
ARHGEF9	ERAP1	LETMD1	PRDX6	TRIM66
ATHL1	ERV3-1	LGALS9	PSMB9	TRPV2
ATP2A3	EVL	LIMCH1	PTGES3	TUSC3
B3GNT9	F2RL2	LPL	PTGIS	UPP1
BNC1	FAM129A	LRP1	PTPRU	UQCRC2
BTN3A3	FBLN2	LRRC16A	RAPGEF5	USHBP1
C10orf10	FBN1	LYPD1	RCBTB1	VASH1
C10orf128	FKBP4	LYVE1	RNF123	VCAM1
C10orf54	FKBP9	MAMDC2	RP1-152L7.5	VCAN
C14orf132	FRAS1	MAN1C1	RPSAP58	VPS13C
C1RL	GAA	MAN2B2	RRAGB	XPOT
CACYBP	GAL3ST4	ME1	SAT1	ZNF366
CALCOCO1	GATSL3	MELTF	SCUBE3	
CAPN11	GCLM	MFAP2	SEC61G	
CARD11	GDF15	MFSD11	SELENBP1	
CCDC3	GJA4	MGP	SELO	
CCND2	GJA5	MLLT11	SEMA3G	

Dendritic Cell Maturation
Phospholipases
Inhibition of Matrix Metalloproteases
Thrombin Signaling
Protein Ubiquitination Pathway

KEAP1
KDM3A
BACH1
NFE2L2
HOXA10

CD24	GPR146	MMP17	SEMA7A	
CD40	HEG1	MT-CYB	SGCE	
CDH11	HHAT	MYO18A	SIAE	
CECR1	HMCN1	MYOM3	SIDT2	
CFH	HMOX1	NEAT1	SLC16A14	
CFI	HOXA9	NEFH	SLC17A9	
CHORDC1	HOXB7	NPR1	SLC35E2B	
CKB	HSP90AA1	NQO1	SLC46A3	
CLDN11	HSPA12B	NUP160	SLCO2A1	
CLIP4	HSPA1A	OSGIN1	SLCO2B1	

Table 14. AdOSGIN2 vs AdCtrl, Genes and top 20 canonical pathways and regulators.

Genes	Ingenuity Canonical Pathways	Upstream Transcriptional Regulator
HERC6	Interferon Signaling	IRF7
HSPA6	Role of Lipids/Lipid Rafts in the Pathogenesis of Influenza	STAT3
IFIT1	Unfolded protein response	STAT1
IFIT3	Aldosterone Signaling in Epithelial Cells	IRF1
MX2	eNOS Signaling	IRF5
OASL	Huntington's Disease Signaling	IRF3
OSGIN2	Protein Ubiquitination Pathway	STAT2
RSAD2	Glucocorticoid Receptor Signaling	SPI1
XAF1		TRIM24
		NFATC2
		IRF9
		MSC
		BRCA1
		SP100
		IKZF3
		SIRT1
		CNOT7
		SQSTM1
		POU2AF1
		HOXD10

Tables 15. AdOSGIN1&2 vs AdCtrl, Genes and top 20 canonical pathways and regulators.

Genes				Ingenuity Canonical Pathways	Upstream Transcriptional Regulator
AHSA1	GCLM	NUP107	TRIM16	Aldosterone Signaling in Epithelial Cells	IRF7
ALDH3A2	GDF15	OAS1	TRIM16L	Protein Ubiquitination Pathway	HSF1
AMDHD2	HAS3	OAS2	TRIM21	Interferon Signaling	NKX2-3
ANAPC5	HERC2	OASL	TRIM26	NRF2-mediated Oxidative Stress Response	STAT1
ANGPT2	HERC6	OSGIN1	TRIM69	Activation of IRF by Cytosolic Pattern Recognition Receptors	IRF5
ANKRD10	HIF3A	OSGIN2	TSPYL2	Unfolded protein response	IRF1
AP3M2	HIST2H2BE	P4HA1	UBC	Role of Pattern Recognition Receptors in Recognition of Bacteria and Viruses	CNOT7
APOL6	HMOX1	P4HA2	UBE2L6	Role of RIG1-like Receptors in Antiviral Innate Immunity	TRIM24
ATF3	HSP90AA1	PACS1	UQCRC2	eNOS Signaling	IRF3
ATXN2	HSP90AB1	PARP14	UTP3	Glucocorticoid Receptor Signaling	STAT2
B3GAT3	HSPA1A	PARP9	VPS13C	Aryl Hydrocarbon Receptor Signaling	STAT3
BAG3	HSPA1B	PATL1	WDR59	Pathogenesis of Multiple Sclerosis	IRF9
BANF1	HSPA4	PAXBP1	XAF1	Hypoxia Signaling in the	SPI1

BATF2	HSPA6	PIGQ	ZC3H7A
BRIP1	HSPA8	PLAUR	ZDHHC6
C19orf66	HSPB1	PLD1	ZFAND2A
C22orf29	HSPB8	PLEKHB2	ZNF207
C3orf52	HSPD1	PLSCR1	ZNF622
CACYBP	HSPE1	PMAIP1	
CBARP	HSPH1	PPCS	
CHD1L	IER5L	PPP1R18	
CHKA	IFI35	PRDX1	
CHORDC1	IFI44L	PRPF38B	
CLIP4	IFIH1	PTGES3	
CPNE8	IFIT1	RCBTB1	
CRYAB	IFIT2	RFC3	
CRYZ	IFIT3	RNF123	
DDX58	IFIT5	RNF19B	
DDX60	IFITM1	RSAD2	
DDX60L	IL7R	RSRP1	
DEDD2	IRF7	SAMD9	
DFNA5	ISG15	SAMD9L	
DHRS1	ITPR3	SBDSP1	
DHRS11	JMJD6	SEC61G	

Cardiovascular System
Huntington's Disease Signaling
Choline Biosynthesis III
Primary Immunodeficiency Signaling
Xenobiotic Metabolism Signaling
Mitotic Roles of Polo-Like Kinase
IL-17A Signaling in Gastric Cells
Coenzyme A Biosynthesis

PML
BRCA1
SIRT1
IRF2
NFE2L2
FBXW7
TP53

DHX58	KRIT1	SELO	
DNAJA1	LGALS8	SERPINH1	
DNAJA4	LUC7L3	SESTD1	
DNAJB1	LY6E	SLC15A3	
DNAJB6	MED12	SLC35E2B	
DTX3L	MFSD11	SLC37A1	
EEF2K	MICB	SMARCC2	
EIF2AK2	MLKL	SNX3	
EPSTI1	MLLT11	SP110	
ESCO2	MRPL18	SPATS2L	
EVI2B	MSX1	SQSTM1	
EVL	MX1	STIP1	
FKBP4	MX2	SYNE2	
FTL	NAPG	TAP1	
GBP1	NDRG1	TGFA	
GCH1	NQO1	TKT	

References

1. Johnson, G., *1. On certain points in the Anatomy and Pathology of Bright's Disease of the Kidney. 2. On the Influence of the Minute Blood-vessels upon the Circulation.* Med Chir Trans, 1868. **51**: p. 57-78 3.
2. Konstantinov, I.E., N. Mejevoi, and N.M. Anichkov, *Nikolai N. Anichkov and his theory of atherosclerosis.* Tex Heart Inst J, 2006. **33**(4): p. 417-23.
3. Lobstein, J.F., *Traité d'anatomie pathologique. Vol. 2.* . 1833.
4. Mönckenberg, *Über die reine Mediaverkalkung der Extremitätenarterien und ihr Verhalten zur Arteriosklerose.* 1903.
5. Thompson, R.C., et al., *Atherosclerosis across 4000 years of human history: the Horus study of four ancient populations.* Lancet, 2013. **381**(9873): p. 1211-22.
6. Strong, J.P. and G.H. Mc, Jr., *The natural history of coronary atherosclerosis.* Am J Pathol, 1962. **40**: p. 37-49.
7. Barquera, S., et al., *Global Overview of the Epidemiology of Atherosclerotic Cardiovascular Disease.* Arch Med Res, 2015. **46**(5): p. 328-38.
8. Lozano, R., et al., *Global and regional mortality from 235 causes of death for 20 age groups in 1990 and 2010: a systematic analysis for the Global Burden of Disease Study 2010.* Lancet, 2012. **380**(9859): p. 2095-128.
9. Libby, P., et al., *Reassessing the Mechanisms of Acute Coronary Syndromes.* Circ Res, 2019. **124**(1): p. 150-160.
10. Farb, A., et al., *Coronary plaque erosion without rupture into a lipid core. A frequent cause of coronary thrombosis in sudden coronary death.* Circulation, 1996. **93**(7): p. 1354-63.
11. Jia, H., et al., *In vivo diagnosis of plaque erosion and calcified nodule in patients with acute coronary syndrome by intravascular optical coherence tomography.* J Am Coll Cardiol, 2013. **62**(19): p. 1748-58.
12. Niccoli, G., et al., *Plaque rupture and intact fibrous cap assessed by optical coherence tomography portend different outcomes in patients with acute coronary syndrome.* Eur Heart J, 2015. **36**(22): p. 1377-84.
13. Higuma, T., et al., *A Combined Optical Coherence Tomography and Intravascular Ultrasound Study on Plaque Rupture, Plaque Erosion, and Calcified Nodule in Patients With ST-Segment Elevation Myocardial Infarction: Incidence, Morphologic Characteristics, and Outcomes After Percutaneous Coronary Intervention.* JACC Cardiovasc Interv, 2015. **8**(9): p. 1166-1176.
14. Schwartz, R.S., et al., *Microemboli and microvascular obstruction in acute coronary thrombosis and sudden coronary death: relation to epicardial plaque histopathology.* J Am Coll Cardiol, 2009. **54**(23): p. 2167-73.
15. White, S.J., A.C. Newby, and T.W. Johnson, *Endothelial erosion of plaques as a substrate for coronary thrombosis.* Thromb Haemost, 2016. **115**(3): p. 509-19.
16. Dai, J., et al., *In vivo predictors of plaque erosion in patients with ST-segment elevation myocardial infarction: a clinical, angiographical, and intravascular optical coherence tomography study.* Eur Heart J, 2018. **39**(22): p. 2077-2085.
17. Tavora, F., et al., *Sudden coronary death caused by pathologic intimal thickening without atheromatous plaque formation.* Cardiovasc Pathol, 2011. **20**(1): p. 51-7.
18. Virmani, R., et al., *Lessons from sudden coronary death: a comprehensive morphological classification scheme for atherosclerotic lesions.* Arterioscler Thromb Vasc Biol, 2000. **20**(5): p. 1262-75.
19. Kolodgie, F.D., et al., *Pathology of atherosclerosis and stenting.* Neuroimaging Clin N Am, 2007. **17**(3): p. 285-301, vii.
20. Roth, G.A., et al., *Global and regional patterns in cardiovascular mortality from 1990 to 2013.* Circulation, 2015. **132**(17): p. 1667-78.

21. Berk, B.C., et al., *Atheroprotective Mechanisms Activated by Fluid Shear Stress in Endothelial Cells.* Drug News Perspect, 2002. **15**(3): p. 133-139.
22. Li, X., et al., *Shear stress in atherosclerotic plaque determination.* DNA Cell Biol, 2014. **33**(12): p. 830-8.
23. Chatzizisis, Y.S., et al., *Role of endothelial shear stress in the natural history of coronary atherosclerosis and vascular remodeling: molecular, cellular, and vascular behavior.* J Am Coll Cardiol, 2007. **49**(25): p. 2379-93.
24. Feldman, C.L., et al., *Determination of in vivo velocity and endothelial shear stress patterns with phasic flow in human coronary arteries: a methodology to predict progression of coronary atherosclerosis.* Am Heart J, 2002. **143**(6): p. 931-9.
25. MacIsaac, A.I., J.D. Thomas, and E.J. Topol, *Toward the quiescent coronary plaque.* J Am Coll Cardiol, 1993. **22**(4): p. 1228-41.
26. Malek, A.M., S.L. Alper, and S. Izumo, *Hemodynamic shear stress and its role in atherosclerosis.* JAMA, 1999. **282**(21): p. 2035-42.
27. Gimbrone, M.A., Jr., et al., *Endothelial dysfunction, hemodynamic forces, and atherogenesis.* Ann N Y Acad Sci, 2000. **902**: p. 230-9; discussion 239-40.
28. Heo, K.S., K. Fujiwara, and J. Abe, *Shear stress and atherosclerosis.* Mol Cells, 2014. **37**(6): p. 435-40.
29. Reinhart-King, C.A., K. Fujiwara, and B.C. Berk, *Physiologic stress-mediated signaling in the endothelium.* Methods Enzymol, 2008. **443**: p. 25-44.
30. Traub, O. and B.C. Berk, *Laminar shear stress: mechanisms by which endothelial cells transduce an atheroprotective force.* Arterioscler Thromb Vasc Biol, 1998. **18**(5): p. 677-85.
31. Koskinas, K.C., et al., *Role of endothelial shear stress in stent restenosis and thrombosis: pathophysiologic mechanisms and implications for clinical translation.* J Am Coll Cardiol, 2012. **59**(15): p. 1337-49.
32. Heo, K.S., et al., *PKCzeta mediates disturbed flow-induced endothelial apoptosis via p53 SUMOylation.* J Cell Biol, 2011. **193**(5): p. 867-84.
33. Cunningham KS1, G.A., *The role of shear stress in the pathogenesis of atherosclerosis.* 2005.
34. Chiu, J.J. and S. Chien, *Effects of disturbed flow on vascular endothelium: pathophysiological basis and clinical perspectives.* Physiol Rev, 2011. **91**(1): p. 327-87.
35. Chen, J., et al., *alphavbeta3 Integrins Mediate Flow-Induced NF-kappaB Activation, Proinflammatory Gene Expression, and Early Atherogenic Inflammation.* Am J Pathol, 2015. **185**(9): p. 2575-89.
36. Dimmeler, S., et al., *Shear stress inhibits apoptosis of human endothelial cells.* FEBS Lett, 1996. **399**(1-2): p. 71-4.
37. Hermann, C., A.M. Zeiher, and S. Dimmeler, *Shear stress inhibits H2O2-induced apoptosis of human endothelial cells by modulation of the glutathione redox cycle and nitric oxide synthase.* Arterioscler Thromb Vasc Biol, 1997. **17**(12): p. 3588-92.
38. Guagliumi, G., et al., *Mechanisms of atherothrombosis and vascular response to primary percutaneous coronary intervention in women versus men with acute myocardial infarction: results of the OCTAVIA study.* JACC Cardiovasc Interv, 2014. **7**(9): p. 958-68.
39. Sun, Z., *Atherosclerosis and atheroma plaque rupture: normal anatomy of vasa vasorum and their role associated with atherosclerosis.* ScientificWorldJournal, 2014. **2014**: p. 285058.
40. Virmani, R., et al., *Vulnerable plaque: the pathology of unstable coronary lesions.* J Interv Cardiol, 2002. **15**(6): p. 439-46.
41. Manduteanu, I. and M. Simionescu, *Inflammation in atherosclerosis: a cause or a result of vascular disorders?* J Cell Mol Med, 2012. **16**(9): p. 1978-90.

42. Kolodgie, F.D., et al., *Differential accumulation of proteoglycans and hyaluronan in culprit lesions: insights into plaque erosion.* Arterioscler Thromb Vasc Biol, 2002. **22**(10): p. 1642-8.
43. Sato, Y., et al., *Proportion of fibrin and platelets differs in thrombi on ruptured and eroded coronary atherosclerotic plaques in humans.* Heart, 2005. **91**(4): p. 526-530.
44. Burke, A.P., et al., *34th Bethesda Conference: Task force #2--What is the pathologic basis for new atherosclerosis imaging techniques?* J Am Coll Cardiol, 2003. **41**(11): p. 1874-86.
45. Nilsson, J., *Atherosclerotic plaque vulnerability in the statin era.* Eur Heart J, 2017. **38**(21): p. 1638-1644.
46. Lee, S.E., et al., *Effects of Statins on Coronary Atherosclerotic Plaques: The PARADIGM Study.* JACC Cardiovasc Imaging, 2018. **11**(10): p. 1475-1484.
47. Bohula, E.A., et al., *Inflammatory and Cholesterol Risk in the FOURIER Trial.* Circulation, 2018. **138**(2): p. 131-140.
48. Pradhan, A.D., et al., *Residual Inflammatory Risk on Treatment With PCSK9 Inhibition and Statin Therapy.* Circulation, 2018. **138**(2): p. 141-149.
49. Libby, P. and G. Pasterkamp, *Requiem for the 'vulnerable plaque'.* Eur Heart J, 2015. **36**(43): p. 2984-7.
50. Pasterkamp, G., H.M. den Ruijter, and P. Libby, *Temporal shifts in clinical presentation and underlying mechanisms of atherosclerotic disease.* Nat Rev Cardiol, 2017. **14**(1): p. 21-29.
51. Kramer, M.C., et al., *Relationship of thrombus healing to underlying plaque morphology in sudden coronary death.* J Am Coll Cardiol, 2010. **55**(2): p. 122-32.
52. Virmani, R., et al., *Pathology of the vulnerable plaque.* J Am Coll Cardiol, 2006. **47**(8 Suppl): p. C13-8.
53. Burke, A.P., et al., *Effect of risk factors on the mechanism of acute thrombosis and sudden coronary death in women.* Circulation, 1998. **97**(21): p. 2110-6.
54. Rittersma, S.Z., et al., *Plaque instability frequently occurs days or weeks before occlusive coronary thrombosis: a pathological thrombectomy study in primary percutaneous coronary intervention.* Circulation, 2005. **111**(9): p. 1160-5.
55. Mangold, A., et al., *Coronary neutrophil extracellular trap burden and deoxyribonuclease activity in ST-elevation acute coronary syndrome are predictors of ST-segment resolution and infarct size.* Circ Res, 2015. **116**(7): p. 1182-92.
56. Libby P, G.P., Schoen FJ, Lee RT. , *The vascular biology of the acute coronary syndromes. In: Topol EJ, ed. Acute Coronary Syndromes. .* 2000.
57. Liu, P., M. Sun, and S. Sader, *Matrix metalloproteinases in cardiovascular disease.* Can J Cardiol, 2006. **22 Suppl B**: p. 25B-30B.
58. van der Wal, A.C., et al., *Site of intimal rupture or erosion of thrombosed coronary atherosclerotic plaques is characterized by an inflammatory process irrespective of the dominant plaque morphology.* Circulation, 1994. **89**(1): p. 36-44.
59. Tricot, O., et al., *Relation between endothelial cell apoptosis and blood flow direction in human atherosclerotic plaques.* Circulation, 2000. **101**(21): p. 2450-2453.
60. Mullick, A.E., P.S. Tobias, and L.K. Curtiss, *Modulation of atherosclerosis in mice by Toll-like receptor 2.* J Clin Invest, 2005. **115**(11): p. 3149-56.
61. Mullick, A.E., P.S. Tobias, and L.K. Curtiss, *Toll-like receptors and atherosclerosis: key contributors in disease and health?* Immunol Res, 2006. **34**(3): p. 193-209.
62. Quillard, T., et al., *Mechanisms of erosion of atherosclerotic plaques.* Curr Opin Lipidol, 2017. **28**(5): p. 434-441.
63. Erridge, C., *Endogenous ligands of TLR2 and TLR4: agonists or assistants?* J Leukoc Biol, 2010. **87**(6): p. 989-99.
64. Kaplan, M.J. and M. Radic, *Neutrophil extracellular traps: double-edged swords of innate immunity.* J Immunol, 2012. **189**(6): p. 2689-95.

65. Yipp, B.G., et al., *Infection-induced NETosis is a dynamic process involving neutrophil multitasking in vivo.* Nat Med, 2012. **18**(9): p. 1386-93.
66. Quillard, T., et al., *TLR2 and neutrophils potentiate endothelial stress, apoptosis and detachment: implications for superficial erosion.* Eur Heart J, 2015. **36**(22): p. 1394-404.
67. Chow, A.K., J. Cena, and R. Schulz, *Acute actions and novel targets of matrix metalloproteinases in the heart and vasculature.* Br J Pharmacol, 2007. **152**(2): p. 189-205.
68. Birge, R.B. and D.S. Ucker, *Innate apoptotic immunity: the calming touch of death.* Cell Death Differ, 2008. **15**(7): p. 1096-102.
69. Mullick, A.E., et al., *Increased endothelial expression of Toll-like receptor 2 at sites of disturbed blood flow exacerbates early atherogenic events.* J Exp Med, 2008. **205**(2): p. 373-83.
70. Dunzendorfer, S., H.K. Lee, and P.S. Tobias, *Flow-dependent regulation of endothelial Toll-like receptor 2 expression through inhibition of SP1 activity.* Circ Res, 2004. **95**(7): p. 684-91.
71. Franck, G., et al., *Flow Perturbation Mediates Neutrophil Recruitment and Potentiates Endothelial Injury via TLR2 in Mice: Implications for Superficial Erosion.* Circ Res, 2017. **121**(1): p. 31-42.
72. Bentzon, J.F. and E. Falk, *Plaque Erosion: New Insights From the Road Less Travelled.* Circ Res, 2017. **121**(1): p. 8-10.
73. Ferrante, G., et al., *High levels of systemic myeloperoxidase are associated with coronary plaque erosion in patients with acute coronary syndromes: a clinicopathological study.* Circulation, 2010. **122**(24): p. 2505-13.
74. Heiss, E.H., et al., *Active NF-E2-related factor (Nrf2) contributes to keep endothelial NO synthase (eNOS) in the coupled state: role of reactive oxygen species (ROS), eNOS, and heme oxygenase (HO-1) levels.* J Biol Chem, 2009. **284**(46): p. 31579-86.
75. Kolodgie, F.D., et al., *The accumulation of specific types of proteoglycans in eroded plaques: a role in coronary thrombosis in the absence of rupture.* Curr Opin Lipidol, 2004. **15**(5): p. 575-82.
76. Taylor, K.R., et al., *Hyaluronan fragments stimulate endothelial recognition of injury through TLR4.* J Biol Chem, 2004. **279**(17): p. 17079-84.
77. Scheibner, K.A., et al., *Hyaluronan fragments act as an endogenous danger signal by engaging TLR2.* J Immunol, 2006. **177**(2): p. 1272-81.
78. Wright, H.L., et al., *Neutrophil function in inflammation and inflammatory diseases.* Rheumatology (Oxford), 2010. **49**(9): p. 1618-31.
79. Bertheloot, D. and E. Latz, *HMGB1, IL-1alpha, IL-33 and S100 proteins: dual-function alarmins.* Cell Mol Immunol, 2017. **14**(1): p. 43-64.
80. Laman, J.D., et al., *Significance of peptidoglycan, a proinflammatory bacterial antigen in atherosclerotic arteries and its association with vulnerable plaques.* Am J Cardiol, 2002. **90**(2): p. 119-23.
81. Nijhuis, M.M., et al., *Peptidoglycan increases firm adhesion of monocytes under flow conditions and primes monocyte chemotaxis.* J Vasc Res, 2007. **44**(3): p. 214-22.
82. Delgado-Rizo, V., et al., *Neutrophil Extracellular Traps and Its Implications in Inflammation: An Overview.* Front Immunol, 2017. **8**: p. 81.
83. Yipp, B.G. and P. Kubes, *NETosis: how vital is it?* Blood, 2013. **122**(16): p. 2784-94.
84. Doring, Y., O. Soehnlein, and C. Weber, *Neutrophil Extracellular Traps in Atherosclerosis and Atherothrombosis.* Circ Res, 2017. **120**(4): p. 736-743.
85. de Buhr, N. and M. von Kockritz-Blickwede, *How Neutrophil Extracellular Traps Become Visible.* J Immunol Res, 2016. **2016**: p. 4604713.
86. Zhao, W., D.K. Fogg, and M.J. Kaplan, *A novel image-based quantitative method for the characterization of NETosis.* J Immunol Methods, 2015. **423**: p. 104-10.

87. Pilsczek, F.H., et al., *A novel mechanism of rapid nuclear neutrophil extracellular trap formation in response to Staphylococcus aureus.* J Immunol, 2010. **185**(12): p. 7413-25.
88. Wong, K.W. and W.R. Jacobs, Jr., *Mycobacterium tuberculosis exploits human interferon gamma to stimulate macrophage extracellular trap formation and necrosis.* J Infect Dis, 2013. **208**(1): p. 109-19.
89. Wang, Y., et al., *Differential microbicidal effects of human histone proteins H2A and H2B on Leishmania promastigotes and amastigotes.* Infect Immun, 2011. **79**(3): p. 1124-33.
90. Lewis, H.D., et al., *Inhibition of PAD4 activity is sufficient to disrupt mouse and human NET formation.* Nat Chem Biol, 2015. **11**(3): p. 189-91.
91. Li, P., et al., *PAD4 is essential for antibacterial innate immunity mediated by neutrophil extracellular traps.* J Exp Med, 2010. **207**(9): p. 1853-62.
92. Neeli, I., S.N. Khan, and M. Radic, *Histone deimination as a response to inflammatory stimuli in neutrophils.* J Immunol, 2008. **180**(3): p. 1895-902.
93. Brinkmann, V. and A. Zychlinsky, *Beneficial suicide: why neutrophils die to make NETs.* Nat Rev Microbiol, 2007. **5**(8): p. 577-82.
94. Xu, J., et al., *Extracellular histones are major mediators of death in sepsis.* Nat Med, 2009. **15**(11): p. 1318-21.
95. Hansson, G.K. and A. Hermansson, *The immune system in atherosclerosis.* Nat Immunol, 2011. **12**(3): p. 204-12.
96. Yamamoto, E., et al., *Endothelial Shear Stress and Plaque Erosion: A Computational Fluid Dynamics and Optical Coherence Tomography Study.* JACC Cardiovasc Imaging, 2019. **12**(2): p. 374-375.
97. Gould, K.L., K. Lipscomb, and G.W. Hamilton, *Physiologic basis for assessing critical coronary stenosis. Instantaneous flow response and regional distribution during coronary hyperemia as measures of coronary flow reserve.* Am J Cardiol, 1974. **33**(1): p. 87-94.
98. Duerrschmidt, N., et al., *NO-mediated regulation of NAD(P)H oxidase by laminar shear stress in human endothelial cells.* J Physiol, 2006. **576**(Pt 2): p. 557-67.
99. Dekker, R.J., et al., *Prolonged fluid shear stress induces a distinct set of endothelial cell genes, most specifically lung Kruppel-like factor (KLF2).* Blood, 2002. **100**(5): p. 1689-1698.
100. Villarreal, G., Jr., et al., *Defining the regulation of KLF4 expression and its downstream transcriptional targets in vascular endothelial cells.* Biochem Biophys Res Commun, 2010. **391**(1): p. 984-9.
101. Dai, G., et al., *Biomechanical forces in atherosclerosis-resistant vascular regions regulate endothelial redox balance via phosphoinositol 3-kinase/Akt-dependent activation of Nrf2.* Circ Res, 2007. **101**(7): p. 723-33.
102. White, S.J., et al., *Characterization of the differential response of endothelial cells exposed to normal and elevated laminar shear stress.* J Cell Physiol, 2011. **226**(11): p. 2841-8.
103. Warboys, C.M., et al., *The role of blood flow in determining the sites of atherosclerotic plaques.* F1000 Med Rep, 2011. **3**: p. 5.
104. Hahn, C. and M.A. Schwartz, *Mechanotransduction in vascular physiology and atherogenesis.* Nat Rev Mol Cell Biol, 2009. **10**(1): p. 53-62.
105. Dai, G., et al., *Distinct endothelial phenotypes evoked by arterial waveforms derived from atherosclerosis-susceptible and -resistant regions of human vasculature.* Proc Natl Acad Sci U S A, 2004. **101**(41): p. 14871-6.
106. Stone, P.H., et al., *Prediction of progression of coronary artery disease and clinical outcomes using vascular profiling of endothelial shear stress and arterial plaque characteristics: the PREDICTION Study.* Circulation, 2012. **126**(2): p. 172-81.

107. Hazell, G.G., et al., *PI16 is a shear stress and inflammation-regulated inhibitor of MMP2.* Sci Rep, 2016. **6**: p. 39553.
108. Stone, P.H., et al., *Effect of endothelial shear stress on the progression of coronary artery disease, vascular remodeling, and in-stent restenosis in humans: in vivo 6-month follow-up study.* Circulation, 2003. **108**(4): p. 438-44.
109. Gijsen, F.J., et al., *Strain distribution over plaques in human coronary arteries relates to shear stress.* Am J Physiol Heart Circ Physiol, 2008. **295**(4): p. H1608-14.
110. Torii, R., et al., *Stress phase angle depicts differences in coronary artery hemodynamics due to changes in flow and geometry after percutaneous coronary intervention.* Am J Physiol Heart Circ Physiol, 2009. **296**(3): p. H765-76.
111. Virmani, R., et al., *Atherosclerotic plaque progression and vulnerability to rupture: angiogenesis as a source of intraplaque hemorrhage.* Arterioscler Thromb Vasc Biol, 2005. **25**(10): p. 2054-61.
112. Pedicino, D., et al., *Alterations of Hyaluronan Metabolism in Acute Coronary Syndrome: Implications for Plaque Erosion.* J Am Coll Cardiol, 2018. **72**(13): p. 1490-1503.
113. Satta, S., *A pivotal role for Nrf2 in endothelial detachment– implications for endothelial erosion of stenotic plaques*

. 2019.
114. Teasdale, J.E., et al., *Cigarette smoke extract profoundly suppresses TNFα-mediated proinflammatory gene expression through upregulation of ATF3 in human coronary artery endothelial cells.* Scientific Reports, 2017. **7**: p. 39945.
115. Kim, K.H., et al., *Expression of stress-response ATF3 is mediated by Nrf2 in astrocytes.* Nucleic Acids Res, 2010. **38**(1): p. 48-59.
116. Teasdale, J.E., et al., *Cigarette smoke extract profoundly suppresses TNFalpha-mediated proinflammatory gene expression through upregulation of ATF3 in human coronary artery endothelial cells.* Sci Rep, 2017. **7**: p. 39945.
117. Birben, E., et al., *Oxidative stress and antioxidant defense.* World Allergy Organ J, 2012. **5**(1): p. 9-19.
118. Moi, P., et al., *Isolation of NF-E2-related factor 2 (Nrf2), a NF-E2-like basic leucine zipper transcriptional activator that binds to the tandem NF-E2/AP1 repeat of the beta-globin locus control region.* Proc Natl Acad Sci U S A, 1994. **91**(21): p. 9926-30.
119. Zhang, M., et al., *Emerging roles of Nrf2 and phase II antioxidant enzymes in neuroprotection.* Prog Neurobiol, 2013. **100**: p. 30-47.
120. Nguyen, T., P. Nioi, and C.B. Pickett, *The Nrf2-antioxidant response element signaling pathway and its activation by oxidative stress.* J Biol Chem, 2009. **284**(20): p. 13291-5.
121. Forman, H.J., K.J. Davies, and F. Ursini, *How do nutritional antioxidants really work: nucleophilic tone and para-hormesis versus free radical scavenging in vivo.* Free Radic Biol Med, 2014. **66**: p. 24-35.
122. Satta, S., et al., *The Role of Nrf2 in Cardiovascular Function and Disease.* Oxid Med Cell Longev, 2017. **2017**: p. 9237263.
123. Itoh, K., et al., *An Nrf2/small Maf heterodimer mediates the induction of phase II detoxifying enzyme genes through antioxidant response elements.* Biochem Biophys Res Commun, 1997. **236**(2): p. 313-22.
124. Tong, K.I., et al., *Keap1 recruits Neh2 through binding to ETGE and DLG motifs: characterization of the two-site molecular recognition model.* Mol Cell Biol, 2006. **26**(8): p. 2887-900.
125. Nioi, P., et al., *The carboxy-terminal Neh3 domain of Nrf2 is required for transcriptional activation.* Mol Cell Biol, 2005. **25**(24): p. 10895-906.

126. Katoh, Y., et al., *Two domains of Nrf2 cooperatively bind CBP, a CREB binding protein, and synergistically activate transcription.* Genes Cells, 2001. **6**(10): p. 857-68.
127. Sun, Z., Y.E. Chin, and D.D. Zhang, *Acetylation of Nrf2 by p300/CBP augments promoter-specific DNA binding of Nrf2 during the antioxidant response.* Mol Cell Biol, 2009. **29**(10): p. 2658-72.
128. Li, W., S.W. Yu, and A.N. Kong, *Nrf2 possesses a redox-sensitive nuclear exporting signal in the Neh5 transactivation domain.* J Biol Chem, 2006. **281**(37): p. 27251-63.
129. Rada, P., et al., *SCF/{beta}-TrCP promotes glycogen synthase kinase 3-dependent degradation of the Nrf2 transcription factor in a Keap1-independent manner.* Mol Cell Biol, 2011. **31**(6): p. 1121-33.
130. Wang, H., et al., *RXRalpha inhibits the NRF2-ARE signaling pathway through a direct interaction with the Neh7 domain of NRF2.* Cancer Res, 2013. **73**(10): p. 3097-108.
131. Zipper, L.M. and R.T. Mulcahy, *The Keap1 BTB/POZ dimerization function is required to sequester Nrf2 in cytoplasm.* J Biol Chem, 2002. **277**(39): p. 36544-52.
132. Canning, P., F.J. Sorrell, and A.N. Bullock, *Structural basis of Keap1 interactions with Nrf2.* Free Radic Biol Med, 2015. **88**(Pt B): p. 101-107.
133. Yamamoto, T., et al., *Physiological significance of reactive cysteine residues of Keap1 in determining Nrf2 activity.* Mol Cell Biol, 2008. **28**(8): p. 2758-70.
134. Itoh, K., J. Mimura, and M. Yamamoto, *Discovery of the negative regulator of Nrf2, Keap1: a historical overview.* Antioxid Redox Signal, 2010. **13**(11): p. 1665-78.
135. Itoh, K., et al., *Keap1 represses nuclear activation of antioxidant responsive elements by Nrf2 through binding to the amino-terminal Neh2 domain.* Genes Dev, 1999. **13**(1): p. 76-86.
136. Wakabayashi, N., et al., *Protection against electrophile and oxidant stress by induction of the phase 2 response: fate of cysteines of the Keap1 sensor modified by inducers.* Proc Natl Acad Sci U S A, 2004. **101**(7): p. 2040-5.
137. Dinkova-Kostova, A.T., et al., *Direct evidence that sulfhydryl groups of Keap1 are the sensors regulating induction of phase 2 enzymes that protect against carcinogens and oxidants.* Proc Natl Acad Sci U S A, 2002. **99**(18): p. 11908-13.
138. Blank, V., *Small Maf proteins in mammalian gene control: mere dimerization partners or dynamic transcriptional regulators?* J Mol Biol, 2008. **376**(4): p. 913-25.
139. Wasserman, W.W. and W.E. Fahl, *Functional antioxidant responsive elements.* Proc Natl Acad Sci U S A, 1997. **94**(10): p. 5361-6.
140. Camp, N.D., et al., *Wilms tumor gene on X chromosome (WTX) inhibits degradation of NRF2 protein through competitive binding to KEAP1 protein.* J Biol Chem, 2012. **287**(9): p. 6539-50.
141. Chen, W., et al., *Direct interaction between Nrf2 and p21(Cip1/WAF1) upregulates the Nrf2-mediated antioxidant response.* Mol Cell, 2009. **34**(6): p. 663-73.
142. Hast, B.E., et al., *Proteomic analysis of ubiquitin ligase KEAP1 reveals associated proteins that inhibit NRF2 ubiquitination.* Cancer Res, 2013. **73**(7): p. 2199-210.
143. Kumar, V., et al., *Novel chalcone derivatives as potent Nrf2 activators in mice and human lung epithelial cells.* J Med Chem, 2011. **54**(12): p. 4147-59.
144. Bryan, H.K., et al., *The Nrf2 cell defence pathway: Keap1-dependent and -independent mechanisms of regulation.* Biochem Pharmacol, 2013. **85**(6): p. 705-17.
145. Cuendet, M., et al., *Quinone reductase induction as a biomarker for cancer chemoprevention.* J Nat Prod, 2006. **69**(3): p. 460-3.
146. McMahon, M., et al., *Keap1-dependent proteasomal degradation of transcription factor Nrf2 contributes to the negative regulation of antioxidant response element-driven gene expression.* J Biol Chem, 2003. **278**(24): p. 21592-600.

147. Jyrkkanen, H.K., et al., *Nrf2 regulates antioxidant gene expression evoked by oxidized phospholipids in endothelial cells and murine arteries in vivo.* Circ Res, 2008. **103**(1): p. e1-9.
148. McMahon, M., et al., *Keap1 perceives stress via three sensors for the endogenous signaling molecules nitric oxide, zinc, and alkenals.* Proc Natl Acad Sci U S A, 2010. **107**(44): p. 18838-43.
149. Rangasamy, T., et al., *Genetic ablation of Nrf2 enhances susceptibility to cigarette smoke-induced emphysema in mice.* J Clin Invest, 2004. **114**(9): p. 1248-59.
150. Teasdale, J.E., et al., *Cigarette smoke but not electronic cigarette aerosol activates a stress response in human coronary artery endothelial cells in culture.* Drug Alcohol Depend, 2016. **163**: p. 256-60.
151. Rushworth, S.A., S. Shah, and D.J. MacEwan, *TNF mediates the sustained activation of Nrf2 in human monocytes.* J Immunol, 2011. **187**(2): p. 702-7.
152. Fledderus, J.O., et al., *KLF2 primes the antioxidant transcription factor Nrf2 for activation in endothelial cells.* Arterioscler Thromb Vasc Biol, 2008. **28**(7): p. 1339-46.
153. Hosoya, T., et al., *Differential responses of the Nrf2-Keap1 system to laminar and oscillatory shear stresses in endothelial cells.* J Biol Chem, 2005. **280**(29): p. 27244-50.
154. Warabi, E., et al., *Shear stress stabilizes NF-E2-related factor 2 and induces antioxidant genes in endothelial cells: role of reactive oxygen/nitrogen species.* Free Radic Biol Med, 2007. **42**(2): p. 260-9.
155. Chen, X.L., et al., *Laminar flow induction of antioxidant response element-mediated genes in endothelial cells. A novel anti-inflammatory mechanism.* J Biol Chem, 2003. **278**(2): p. 703-11.
156. Keum, Y.S., et al., *Mechanism of action of sulforaphane: inhibition of p38 mitogen-activated protein kinase isoforms contributing to the induction of antioxidant response element-mediated heme oxygenase-1 in human hepatoma HepG2 cells.* Cancer Res, 2006. **66**(17): p. 8804-13.
157. Lee, D.S., et al., *The cytoprotective effect of sulfuretin against tert-butyl hydroperoxide-induced hepatotoxicity through Nrf2/ARE and JNK/ERK MAPK-mediated heme oxygenase-1 expression.* Int J Mol Sci, 2014. **15**(5): p. 8863-77.
158. Park, S.H., et al., *Tumor necrosis factor induces GSK3 kinase-mediated cross-tolerance to endotoxin in macrophages.* Nat Immunol, 2011. **12**(7): p. 607-15.
159. Lee, J. and M.S. Kim, *The role of GSK3 in glucose homeostasis and the development of insulin resistance.* Diabetes Res Clin Pract, 2007. **77 Suppl 1**: p. S49-57.
160. Rushworth, S.A., et al., *The high Nrf2 expression in human acute myeloid leukemia is driven by NF-kappaB and underlies its chemo-resistance.* Blood, 2012. **120**(26): p. 5188-98.
161. Kim, S.W., et al., *Up-down regulation of HO-1 and iNOS gene expressions by ethyl pyruvate via recruiting p300 to Nrf2 and depriving It from p65.* Free Radic Biol Med, 2013. **65**: p. 468-476.
162. Soares, M.P., et al., *Heme oxygenase-1 modulates the expression of adhesion molecules associated with endothelial cell activation.* J Immunol, 2004. **172**(6): p. 3553-63.
163. Olson, C.M., et al., *p38 mitogen-activated protein kinase controls NF-kappaB transcriptional activation and tumor necrosis factor alpha production through RelA phosphorylation mediated by mitogen- and stress-activated protein kinase 1 in response to Borrelia burgdorferi antigens.* Infect Immun, 2007. **75**(1): p. 270-7.
164. Mitra, A., et al., *Cardioprotective role of P38 MAPK during myocardial infarction via parallel activation of alpha-crystallin B and Nrf2.* J Cell Physiol, 2014. **229**(9): p. 1272-82.

165. Kobayashi, A., et al., *Oxidative stress sensor Keap1 functions as an adaptor for Cul3-based E3 ligase to regulate proteasomal degradation of Nrf2.* Mol Cell Biol, 2004. **24**(16): p. 7130-9.
166. Karapetian, R.N., et al., *Nuclear oncoprotein prothymosin alpha is a partner of Keap1: implications for expression of oxidative stress-protecting genes.* Mol Cell Biol, 2005. **25**(3): p. 1089-99.
167. Igarashi, K., et al., *Multivalent DNA binding complex generated by small Maf and Bach1 as a possible biochemical basis for beta-globin locus control region complex.* J Biol Chem, 1998. **273**(19): p. 11783-90.
168. Hoshino, H., et al., *Oxidative stress abolishes leptomycin B-sensitive nuclear export of transcription repressor Bach2 that counteracts activation of Maf recognition element.* J Biol Chem, 2000. **275**(20): p. 15370-6.
169. Dhakshinamoorthy, S., et al., *Bach1 competes with Nrf2 leading to negative regulation of the antioxidant response element (ARE)-mediated NAD(P)H:quinone oxidoreductase 1 gene expression and induction in response to antioxidants.* J Biol Chem, 2005. **280**(17): p. 16891-900.
170. Suzuki, H., et al., *Cadmium induces nuclear export of Bach1, a transcriptional repressor of heme oxygenase-1 gene.* J Biol Chem, 2003. **278**(49): p. 49246-53.
171. Huang, H.C., T. Nguyen, and C.B. Pickett, *Phosphorylation of Nrf2 at Ser-40 by protein kinase C regulates antioxidant response element-mediated transcription.* J Biol Chem, 2002. **277**(45): p. 42769-74.
172. Chen, J.S., et al., *Nrf-2 mediated heme oxygenase-1 expression, an antioxidant-independent mechanism, contributes to anti-atherogenesis and vascular protective effects of Ginkgo biloba extract.* Atherosclerosis, 2011. **214**(2): p. 301-9.
173. Chen, L.H., et al., *Expression, purification, and in vitro refolding of a humanized single-chain Fv antibody against human CTLA4 (CD152).* Protein Expr Purif, 2006. **46**(2): p. 495-502.
174. Yang, H.L., et al., *Anti-angiogenic properties of coenzyme Q0 through downregulation of MMP-9/NF-kappaB and upregulation of HO-1 signaling in TNF-alpha-activated human endothelial cells.* Biochem Pharmacol, 2015. **98**(1): p. 144-56.
175. Cheng, X., R.C. Siow, and G.E. Mann, *Impaired redox signaling and antioxidant gene expression in endothelial cells in diabetes: a role for mitochondria and the nuclear factor-E2-related factor 2-Kelch-like ECH-associated protein 1 defense pathway.* Antioxid Redox Signal, 2011. **14**(3): p. 469-87.
176. Mahmoud, A.M., et al., *A novel role for small molecule glycomimetics in the protection against lipid-induced endothelial dysfunction: Involvement of Akt/eNOS and Nrf2/ARE signaling.* Biochim Biophys Acta Gen Subj, 2017. **1861**(1 Pt A): p. 3311-3322.
177. Lo, S.C. and M. Hannink, *PGAM5 tethers a ternary complex containing Keap1 and Nrf2 to mitochondria.* Exp Cell Res, 2008. **314**(8): p. 1789-803.
178. Song, J., et al., *Glutathione protects brain endothelial cells from hydrogen peroxide-induced oxidative stress by increasing nrf2 expression.* Exp Neurobiol, 2014. **23**(1): p. 93-103.
179. Chen, B., et al., *The role of Nrf2 in oxidative stress-induced endothelial injuries.* J Endocrinol, 2015. **225**(3): p. R83-99.
180. Lee, O.H., et al., *An auto-regulatory loop between stress sensors INrf2 and Nrf2 controls their cellular abundance.* J Biol Chem, 2007. **282**(50): p. 36412-20.
181. Wakabayashi, N., et al., *Keap1-null mutation leads to postnatal lethality due to constitutive Nrf2 activation.* Nat Genet, 2003. **35**(3): p. 238-45.
182. Barajas, B., et al., *NF-E2-related factor 2 promotes atherosclerosis by effects on plasma lipoproteins and cholesterol transport that overshadow antioxidant protection.* Arterioscler Thromb Vasc Biol, 2011. **31**(1): p. 58-66.

183. Zgheib, E., et al., *Investigation of Nrf2, AhR and ATF4 Activation in Toxicogenomic Databases.* Front Genet, 2018. **9**: p. 429.
184. Huynh, H., et al., *Cloning and Characterization of a Novel Pregnancy-Induced Growth Inhibitor in Mammary Gland.* Endocrinology, 2001. **142**(8): p. 3607-3615.
185. Wang, T., et al., *Bone marrow stromal cell-derived growth inhibitor inhibits growth and migration of breast cancer cells via induction of cell cycle arrest and apoptosis.* J Biol Chem, 2005. **280**(6): p. 4374-82.
186. Ong, C.K., et al., *The role of 5' untranslated region in translational suppression of OKL38 mRNA in hepatocellular carcinoma.* Oncogene, 2007. **26**(8): p. 1155-65.
187. Ong, C.K., et al., *Genomic structure of human OKL38 gene and its differential expression in kidney carcinogenesis.* J Biol Chem, 2004. **279**(1): p. 743-54.
188. J Hu, Y.W., *OSGIN1 (oxidative stress induced growth inhibitor 1).* Atlas Genet Cytogenet Oncol Haematol. 2015;19(2):117-120., 2014.
189. Marchler-Bauer, A., et al., *CDD: conserved domains and protein three-dimensional structure.* Nucleic Acids Res, 2013. **41**(Database issue): p. D348-52.
190. Rundlof, A.K., et al., *Quantification of alternative mRNA species and identification of thioredoxin reductase 1 isoforms in human tumor cells.* Differentiation, 2007. **75**(2): p. 123-32.
191. Osburn, W.O., et al., *Increased colonic inflammatory injury and formation of aberrant crypt foci in Nrf2-deficient mice upon dextran sulfate treatment.* Int J Cancer, 2007. **121**(9): p. 1883-91.
192. Osborne, S.A. and K.F. Tonissen, *Genomic organisation and alternative splicing of mouse and human thioredoxin reductase 1 genes.* BMC Genomics, 2001. **2**: p. 10.
193. Yao, H., et al., *Histone Arg modifications and p53 regulate the expression of OKL38, a mediator of apoptosis.* J Biol Chem, 2008. **283**(29): p. 20060-8.
194. Li, R., et al., *OKL38 is an oxidative stress response gene stimulated by oxidized phospholipids.* J Lipid Res, 2007. **48**(3): p. 709-15.
195. Yan, X., et al., *Fatty acid epoxyisoprostane E2 stimulates an oxidative stress response in endothelial cells.* Biochem Biophys Res Commun, 2014. **444**(1): p. 69-74.
196. Hu, J., et al., *Interaction of OKL38 and p53 in regulating mitochondrial structure and function.* PLoS One, 2012. **7**(8): p. e43362.
197. Brennan, M.S., et al., *The NRF2 transcriptional target, OSGIN1, contributes to monomethyl fumarate-mediated cytoprotection in human astrocytes.* Sci Rep, 2017. **7**: p. 42054.
198. Treumer, F., et al., *Dimethylfumarate is a potent inducer of apoptosis in human T cells.* J Invest Dermatol, 2003. **121**(6): p. 1383-8.
199. Wang, G., et al., *Role of OSGIN1 in mediating smoking-induced autophagy in the human airway epithelium.* Autophagy, 2017. **13**(7): p. 1205-1220.
200. Fujii, S., et al., *Insufficient autophagy promotes bronchial epithelial cell senescence in chronic obstructive pulmonary disease.* Oncoimmunology, 2012. **1**(5): p. 630-641.
201. Hwang, J.W., et al., *Cigarette smoke-induced autophagy is regulated by SIRT1-PARP-1-dependent mechanism: implication in pathogenesis of COPD.* Arch Biochem Biophys, 2010. **500**(2): p. 203-9.
202. Kim, H.P., et al., *Autophagic proteins regulate cigarette smoke-induced apoptosis: protective role of heme oxygenase-1.* Autophagy, 2008. **4**(7): p. 887-95.
203. Takasaka, N., et al., *Autophagy induction by SIRT6 through attenuation of insulin-like growth factor signaling is involved in the regulation of human bronchial epithelial cell senescence.* J Immunol, 2014. **192**(3): p. 958-68.
204. Ito, S., et al., *PARK2-mediated mitophagy is involved in regulation of HBEC senescence in COPD pathogenesis.* Autophagy, 2015. **11**(3): p. 547-59.
205. Isomura, M., et al., *Sequence analysis of a total of three megabases of DNA in two regions of chromosome 8p.* DNA Res, 1999. **6**(6): p. 387-400.

206. Deter, R.L. and C. De Duve, *Influence of glucagon, an inducer of cellular autophagy, on some physical properties of rat liver lysosomes.* J Cell Biol, 1967. **33**(2): p. 437-49.
207. Nakatogawa, H., et al., *Dynamics and diversity in autophagy mechanisms: lessons from yeast.* Nat Rev Mol Cell Biol, 2009. **10**(7): p. 458-67.
208. Levine, B. and G. Kroemer, *Autophagy in the pathogenesis of disease.* Cell, 2008. **132**(1): p. 27-42.
209. Xie, Z. and D.J. Klionsky, *Autophagosome formation: core machinery and adaptations.* Nat Cell Biol, 2007. **9**(10): p. 1102-9.
210. Klionsky, D.J., *Autophagy: from phenomenology to molecular understanding in less than a decade.* Nat Rev Mol Cell Biol, 2007. **8**(11): p. 931-7.
211. Mizushima, N., *Autophagy: process and function.* Genes Dev, 2007. **21**(22): p. 2861-73.
212. Liu, Y., et al., *Autosis is a Na+,K+-ATPase-regulated form of cell death triggered by autophagy-inducing peptides, starvation, and hypoxia-ischemia.* Proc Natl Acad Sci U S A, 2013. **110**(51): p. 20364-71.
213. Munoz-Pinedo, C. and S.J. Martin, *Autosis: a new addition to the cell death Tower of Babel.* Cell Death Dis, 2014. **5**: p. e1319.
214. Levine, B. and D.J. Klionsky, *Development by self-digestion: molecular mechanisms and biological functions of autophagy.* Dev Cell, 2004. **6**(4): p. 463-77.
215. Klionsky, D.J., et al., *A comprehensive glossary of autophagy-related molecules and processes (2nd edition).* Autophagy, 2011. **7**(11): p. 1273-94.
216. Yorimitsu, T. and D.J. Klionsky, *Autophagy: molecular machinery for self-eating.* Cell Death Differ, 2005. **12 Suppl 2**: p. 1542-52.
217. Chen, Y. and D.J. Klionsky, *The regulation of autophagy - unanswered questions.* J Cell Sci, 2011. **124**(Pt 2): p. 161-70.
218. Itakura, E. and N. Mizushima, *Characterization of autophagosome formation site by a hierarchical analysis of mammalian Atg proteins.* Autophagy, 2010. **6**(6): p. 764-76.
219. Hayashi-Nishino, M., et al., *A subdomain of the endoplasmic reticulum forms a cradle for autophagosome formation.* Nat Cell Biol, 2009. **11**(12): p. 1433-7.
220. Yla-Anttila, P., et al., *3D tomography reveals connections between the phagophore and endoplasmic reticulum.* Autophagy, 2009. **5**(8): p. 1180-5.
221. He, C. and D.J. Klionsky, *Regulation mechanisms and signaling pathways of autophagy.* Annu Rev Genet, 2009. **43**: p. 67-93.
222. Takahashi, Y., et al., *Bif-1 regulates Atg9 trafficking by mediating the fission of Golgi membranes during autophagy.* Autophagy, 2011. **7**(1): p. 61-73.
223. Ravikumar, B., et al., *Plasma membrane contributes to the formation of pre-autophagosomal structures.* Nat Cell Biol, 2010. **12**(8): p. 747-57.
224. Ravikumar, B., K. Moreau, and D.C. Rubinsztein, *Plasma membrane helps autophagosomes grow.* Autophagy, 2010. **6**(8): p. 1184-6.
225. Hailey, D.W., et al., *Mitochondria supply membranes for autophagosome biogenesis during starvation.* Cell, 2010. **141**(4): p. 656-67.
226. Mijaljica, D., M. Prescott, and R.J. Devenish, *The intriguing life of autophagosomes.* Int J Mol Sci, 2012. **13**(3): p. 3618-35.
227. Yang, Z. and D.J. Klionsky, *An overview of the molecular mechanism of autophagy.* Curr Top Microbiol Immunol, 2009. **335**: p. 1-32.
228. Hara, T., et al., *FIP200, a ULK-interacting protein, is required for autophagosome formation in mammalian cells.* J Cell Biol, 2008. **181**(3): p. 497-510.
229. Ganley, I.G., et al., *ULK1.ATG13.FIP200 complex mediates mTOR signaling and is essential for autophagy.* J Biol Chem, 2009. **284**(18): p. 12297-305.
230. Hosokawa, N., et al., *Nutrient-dependent mTORC1 association with the ULK1-Atg13-FIP200 complex required for autophagy.* Mol Biol Cell, 2009. **20**(7): p. 1981-91.

231. Jung, C.H., et al., *ULK-Atg13-FIP200 complexes mediate mTOR signaling to the autophagy machinery.* Mol Biol Cell, 2009. **20**(7): p. 1992-2003.
232. Itoh, T., et al., *Golgi-resident small GTPase Rab33B interacts with Atg16L and modulates autophagosome formation.* Mol Biol Cell, 2008. **19**(7): p. 2916-25.
233. Takahashi, Y., C.L. Meyerkord, and H.G. Wang, *Bif-1/endophilin B1: a candidate for crescent driving force in autophagy.* Cell Death Differ, 2009. **16**(7): p. 947-55.
234. Fimia, G.M., et al., *Ambra1 regulates autophagy and development of the nervous system.* Nature, 2007. **447**(7148): p. 1121-5.
235. Mizushima, N., et al., *Mouse Apg16L, a novel WD-repeat protein, targets to the autophagic isolation membrane with the Apg12-Apg5 conjugate.* J Cell Sci, 2003. **116**(Pt 9): p. 1679-88.
236. Ohsumi, Y., *Molecular dissection of autophagy: two ubiquitin-like systems.* Nat Rev Mol Cell Biol, 2001. **2**(3): p. 211-6.
237. Weidberg, H., E. Shvets, and Z. Elazar, *Biogenesis and cargo selectivity of autophagosomes.* Annu Rev Biochem, 2011. **80**: p. 125-56.
238. Mizushima, N., et al., *Dissection of autophagosome formation using Apg5-deficient mouse embryonic stem cells.* J Cell Biol, 2001. **152**(4): p. 657-68.
239. Lee, I.H. and T. Finkel, *Regulation of autophagy by the p300 acetyltransferase.* J Biol Chem, 2009. **284**(10): p. 6322-8.
240. Ichimura, Y., et al., *A ubiquitin-like system mediates protein lipidation.* Nature, 2000. **408**(6811): p. 488-92.
241. Hanada, T., et al., *The Atg12-Atg5 conjugate has a novel E3-like activity for protein lipidation in autophagy.* J Biol Chem, 2007. **282**(52): p. 37298-302.
242. Fujita, N., et al., *The Atg16L complex specifies the site of LC3 lipidation for membrane biogenesis in autophagy.* Mol Biol Cell, 2008. **19**(5): p. 2092-100.
243. Nair, U., et al., *A role for Atg8-PE deconjugation in autophagosome biogenesis.* Autophagy, 2012. **8**(5): p. 780-93.
244. Geng, J. and D.J. Klionsky, *The Atg8 and Atg12 ubiquitin-like conjugation systems in macroautophagy. 'Protein modifications: beyond the usual suspects' review series.* EMBO Rep, 2008. **9**(9): p. 859-64.
245. Satyavarapu, E.M., et al., *Autophagy-independent induction of LC3B through oxidative stress reveals its non-canonical role in anoikis of ovarian cancer cells.* Cell Death Dis, 2018. **9**(10): p. 934.
246. Kabeya, Y., et al., *LC3, a mammalian homologue of yeast Apg8p, is localized in autophagosome membranes after processing.* EMBO J, 2000. **19**(21): p. 5720-8.
247. Xie, Z., U. Nair, and D.J. Klionsky, *Atg8 controls phagophore expansion during autophagosome formation.* Mol Biol Cell, 2008. **19**(8): p. 3290-8.
248. Stephan, J.S., et al., *The Tor and cAMP-dependent protein kinase signaling pathways coordinately control autophagy in Saccharomyces cerevisiae.* Autophagy, 2010. **6**(2): p. 294-5.
249. Budovskaya, Y.V., et al., *The Ras/cAMP-dependent protein kinase signaling pathway regulates an early step of the autophagy process in Saccharomyces cerevisiae.* J Biol Chem, 2004. **279**(20): p. 20663-71.
250. Cherra, S.J., 3rd, et al., *Regulation of the autophagy protein LC3 by phosphorylation.* J Cell Biol, 2010. **190**(4): p. 533-9.
251. Blancquaert, S., et al., *cAMP-dependent activation of mammalian target of rapamycin (mTOR) in thyroid cells. Implication in mitogenesis and activation of CDK4.* Mol Endocrinol, 2010. **24**(7): p. 1453-68.
252. Mavrakis, M., et al., *Depletion of type IA regulatory subunit (RIalpha) of protein kinase A (PKA) in mammalian cells and tissues activates mTOR and causes autophagic deficiency.* Hum Mol Genet, 2006. **15**(19): p. 2962-71.

253. Alers, S., et al., *Role of AMPK-mTOR-Ulk1/2 in the regulation of autophagy: cross talk, shortcuts, and feedbacks.* Mol Cell Biol, 2012. **32**(1): p. 2-11.
254. Meley, D., et al., *AMP-activated protein kinase and the regulation of autophagic proteolysis.* J Biol Chem, 2006. **281**(46): p. 34870-9.
255. Hardie, D.G., *AMP-activated/SNF1 protein kinases: conserved guardians of cellular energy.* Nat Rev Mol Cell Biol, 2007. **8**(10): p. 774-85.
256. Inoki, K., T. Zhu, and K.L. Guan, *TSC2 mediates cellular energy response to control cell growth and survival.* Cell, 2003. **115**(5): p. 577-90.
257. Yang, Z. and D.J. Klionsky, *Mammalian autophagy: core molecular machinery and signaling regulation.* Curr Opin Cell Biol, 2010. **22**(2): p. 124-31.
258. Gwinn, D.M., et al., *AMPK phosphorylation of raptor mediates a metabolic checkpoint.* Mol Cell, 2008. **30**(2): p. 214-26.
259. Gorlach, A., et al., *Calcium and ROS: A mutual interplay.* Redox Biol, 2015. **6**: p. 260-271.
260. Egan, D.F., et al., *Phosphorylation of ULK1 (hATG1) by AMP-activated protein kinase connects energy sensing to mitophagy.* Science, 2011. **331**(6016): p. 456-61.
261. Hoyer-Hansen, M., et al., *Control of macroautophagy by calcium, calmodulin-dependent kinase kinase-beta, and Bcl-2.* Mol Cell, 2007. **25**(2): p. 193-205.
262. Kim, J., et al., *AMPK and mTOR regulate autophagy through direct phosphorylation of Ulk1.* Nat Cell Biol, 2011. **13**(2): p. 132-41.
263. Lee, J.W., et al., *The association of AMPK with ULK1 regulates autophagy.* PLoS One, 2010. **5**(11): p. e15394.
264. Shang, L., et al., *Nutrient starvation elicits an acute autophagic response mediated by Ulk1 dephosphorylation and its subsequent dissociation from AMPK.* Proc Natl Acad Sci U S A, 2011. **108**(12): p. 4788-93.
265. Ding, W.X., et al., *Differential effects of endoplasmic reticulum stress-induced autophagy on cell survival.* J Biol Chem, 2007. **282**(7): p. 4702-10.
266. Chiang, H.L. and J.F. Dice, *Peptide sequences that target proteins for enhanced degradation during serum withdrawal.* J Biol Chem, 1988. **263**(14): p. 6797-805.
267. Arias, E. and A.M. Cuervo, *Chaperone-mediated autophagy in protein quality control.* Curr Opin Cell Biol, 2011. **23**(2): p. 184-9.
268. Pereira, L., J.P. Girardi, and M. Bakovic, *Forms, crosstalks, and the role of phospholipid biosynthesis in autophagy.* Int J Cell Biol, 2012. **2012**: p. 931956.
269. Dice, J.F., *Peptide sequences that target cytosolic proteins for lysosomal proteolysis.* Trends Biochem Sci, 1990. **15**(8): p. 305-9.
270. Bandyopadhyay, U., et al., *Identification of regulators of chaperone-mediated autophagy.* Mol Cell, 2010. **39**(4): p. 535-47.
271. Napolitano, G., et al., *Impairment of chaperone-mediated autophagy leads to selective lysosomal degradation defects in the lysosomal storage disease cystinosis.* EMBO Mol Med, 2015. **7**(2): p. 158-74.
272. Cuervo, A.M. and J.F. Dice, *A receptor for the selective uptake and degradation of proteins by lysosomes.* Science, 1996. **273**(5274): p. 501-3.
273. Bandyopadhyay, U., et al., *The chaperone-mediated autophagy receptor organizes in dynamic protein complexes at the lysosomal membrane.* Mol Cell Biol, 2008. **28**(18): p. 5747-63.
274. Kiffin, R., et al., *Activation of chaperone-mediated autophagy during oxidative stress.* Mol Biol Cell, 2004. **15**(11): p. 4829-40.
275. Cuervo, A.M., et al., *Direct lysosomal uptake of alpha 2-microglobulin contributes to chemically induced nephropathy.* Kidney Int, 1999. **55**(2): p. 529-45.
276. Cuervo, A.M., et al., *Activation of a selective pathway of lysosomal proteolysis in rat liver by prolonged starvation.* Am J Physiol, 1995. **269**(5 Pt 1): p. C1200-8.

277. Kirkin, V., et al., *NBR1 cooperates with p62 in selective autophagy of ubiquitinated targets.* Autophagy, 2009. **5**(5): p. 732-3.
278. Kirkin, V., et al., *A role for ubiquitin in selective autophagy.* Mol Cell, 2009. **34**(3): p. 259-69.
279. Lamark, T., et al., *NBR1 and p62 as cargo receptors for selective autophagy of ubiquitinated targets.* Cell Cycle, 2009. **8**(13): p. 1986-90.
280. De Duve, C. and R. Wattiaux, *Functions of lysosomes.* Annu Rev Physiol, 1966. **28**: p. 435-92.
281. Li, W.W., J. Li, and J.K. Bao, *Microautophagy: lesser-known self-eating.* Cell Mol Life Sci, 2012. **69**(7): p. 1125-36.
282. Kunz, J.B., H. Schwarz, and A. Mayer, *Determination of four sequential stages during microautophagy in vitro.* J Biol Chem, 2004. **279**(11): p. 9987-96.
283. Uttenweiler, A., H. Schwarz, and A. Mayer, *Microautophagic vacuole invagination requires calmodulin in a Ca2+-independent function.* J Biol Chem, 2005. **280**(39): p. 33289-97.
284. Muller, O., et al., *Autophagic tubes: vacuolar invaginations involved in lateral membrane sorting and inverse vesicle budding.* J Cell Biol, 2000. **151**(3): p. 519-28.
285. Doelling, J.H., et al., *The APG8/12-activating enzyme APG7 is required for proper nutrient recycling and senescence in Arabidopsis thaliana.* J Biol Chem, 2002. **277**(36): p. 33105-14.
286. Sou, Y.S., et al., *The Atg8 conjugation system is indispensable for proper development of autophagic isolation membranes in mice.* Mol Biol Cell, 2008. **19**(11): p. 4762-75.
287. Sattler, T. and A. Mayer, *Cell-free reconstitution of microautophagic vacuole invagination and vesicle formation.* J Cell Biol, 2000. **151**(3): p. 529-38.
288. Uttenweiler, A. and A. Mayer, *Microautophagy in the yeast Saccharomyces cerevisiae.* Methods Mol Biol, 2008. **445**: p. 245-59.
289. Yang, Z. and D.J. Klionsky, *Permeases recycle amino acids resulting from autophagy.* Autophagy, 2007. **3**(2): p. 149-50.
290. Mijaljica, D., M. Prescott, and R.J. Devenish, *Microautophagy in mammalian cells: revisiting a 40-year-old conundrum.* Autophagy, 2011. **7**(7): p. 673-82.
291. Parzych, K.R. and D.J. Klionsky, *An overview of autophagy: morphology, mechanism, and regulation.* Antioxid Redox Signal, 2014. **20**(3): p. 460-73.
292. Sun, Y., *Autophagy: A new target for the treatment of atherosclerosis*. 2018.
293. Perrotta, I., *The use of electron microscopy for the detection of autophagy in human atherosclerosis.* Micron, 2013. **50**: p. 7-13.
294. Ouimet, M., *Autophagy in obesity and atherosclerosis: Interrelationships between cholesterol homeostasis, lipoprotein metabolism and autophagy in macrophages and other systems.* Biochim Biophys Acta, 2013. **1831**(6): p. 1124-33.
295. Margariti, A., et al., *XBP1 mRNA splicing triggers an autophagic response in endothelial cells through BECLIN-1 transcriptional activation.* J Biol Chem, 2013. **288**(2): p. 859-72.
296. Muller, C., et al., *Oxidized LDLs trigger endoplasmic reticulum stress and autophagy: prevention by HDLs.* Autophagy, 2011. **7**(5): p. 541-3.
297. Monastyrska, I., et al., *Multiple roles of the cytoskeleton in autophagy.* Biol Rev Camb Philos Soc, 2009. **84**(3): p. 431-48.
298. Liu, Y. and B. Levine, *Autosis and autophagic cell death: the dark side of autophagy.* Cell Death Differ, 2015. **22**(3): p. 367-76.
299. Li, R., et al., *Disturbed Flow Induces Autophagy, but Impairs Autophagic Flux to Perturb Mitochondrial Homeostasis.* Antioxid Redox Signal, 2015. **23**(15): p. 1207-19.

300. Han, X., et al., *AMPK activation protects cells from oxidative stress-induced senescence via autophagic flux restoration and intracellular NAD(+) elevation.* Aging Cell, 2016. **15**(3): p. 416-27.
301. Tai, H., et al., *Autophagy impairment with lysosomal and mitochondrial dysfunction is an important characteristic of oxidative stress-induced senescence.* Autophagy, 2017. **13**(1): p. 99-113.
302. Wyllie, F.S., et al., *S phase cell-cycle arrest following DNA damage is independent of the p53/p21(WAF1) signalling pathway.* Oncogene, 1996. **12**(5): p. 1077-82.
303. Capparelli, C., et al., *CDK inhibitors (p16/p19/p21) induce senescence and autophagy in cancer-associated fibroblasts, "fueling" tumor growth via paracrine interactions, without an increase in neo-angiogenesis.* Cell Cycle, 2012. **11**(19): p. 3599-610.
304. Nam, H.Y., et al., *Prolonged autophagy by MTOR inhibitor leads radioresistant cancer cells into senescence.* Autophagy, 2013. **9**(10): p. 1631-2.
305. Kwon, Y., et al., *Autophagy Is Pro-Senescence When Seen in Close-Up, but Anti-Senescence in Long-Shot.* Mol Cells, 2017. **40**(9): p. 607-612.
306. Pyo, J.O., et al., *Overexpression of Atg5 in mice activates autophagy and extends lifespan.* Nat Commun, 2013. **4**: p. 2300.
307. Lakatta, E.G. and D. Levy, *Arterial and cardiac aging: major shareholders in cardiovascular disease enterprises: Part I: aging arteries: a "set up" for vascular disease.* Circulation, 2003. **107**(1): p. 139-46.
308. Nussenzweig, S.C., S. Verma, and T. Finkel, *The role of autophagy in vascular biology.* Circ Res, 2015. **116**(3): p. 480-8.
309. North, B.J. and D.A. Sinclair, *The intersection between aging and cardiovascular disease.* Circ Res, 2012. **110**(8): p. 1097-108.
310. Mei, Y., et al., *Autophagy and oxidative stress in cardiovascular diseases.* Biochim Biophys Acta, 2015. **1852**(2): p. 243-51.
311. LaRocca, T.J., et al., *Translational evidence that impaired autophagy contributes to arterial ageing.* J Physiol, 2012. **590**(14): p. 3305-16.
312. LaRocca, T.J., et al., *Mitochondrial quality control and age-associated arterial stiffening.* Exp Gerontol, 2014. **58**: p. 78-82.
313. LaRocca, T.J., et al., *The autophagy enhancer spermidine reverses arterial aging.* Mech Ageing Dev, 2013. **134**(7-8): p. 314-20.
314. Blagosklonny, M.V., *Cell cycle arrest is not senescence.* Aging (Albany NY), 2011. **3**(2): p. 94-101.
315. Chandler, H. and G. Peters, *Stressing the cell cycle in senescence and aging.* Curr Opin Cell Biol, 2013. **25**(6): p. 765-71.
316. Young, A.R., et al., *Autophagy mediates the mitotic senescence transition.* Genes Dev, 2009. **23**(7): p. 798-803.
317. Cho, S. and E.S. Hwang, *Status of mTOR activity may phenotypically differentiate senescence and quiescence.* Mol Cells, 2012. **33**(6): p. 597-604.
318. Jeyapalan, J.C. and J.M. Sedivy, *Cellular senescence and organismal aging.* Mech Ageing Dev, 2008. **129**(7-8): p. 467-74.
319. Leontieva, O.V., et al., *Elimination of proliferating cells unmasks the shift from senescence to quiescence caused by rapamycin.* PLoS One, 2011. **6**(10): p. e26126.
320. Blagosklonny, M.V., *Hypoxia, MTOR and autophagy: converging on senescence or quiescence.* Autophagy, 2013. **9**(2): p. 260-2.
321. Yu, Q., et al., *DNA-damage-induced type I interferon promotes senescence and inhibits stem cell function.* Cell Rep, 2015. **11**(5): p. 785-797.
322. Kim, K.S., et al., *Interferon-gamma induces cellular senescence through p53-dependent DNA damage signaling in human endothelial cells.* Mech Ageing Dev, 2009. **130**(3): p. 179-88.

323. Duan, X., et al., *Differential roles for the interferon-inducible IFI16 and AIM2 innate immune sensors for cytosolic DNA in cellular senescence of human fibroblasts.* Mol Cancer Res, 2011. **9**(5): p. 589-602.
324. Almontashiri, N.A., et al., *Interferon-gamma activates expression of p15 and p16 regardless of 9p21.3 coronary artery disease risk genotype.* J Am Coll Cardiol, 2013. **61**(2): p. 143-7.
325. Warboys, C.M., et al., *Disturbed flow promotes endothelial senescence via a p53-dependent pathway.* Arterioscler Thromb Vasc Biol, 2014. **34**(5): p. 985-95.
326. S, A., *FastQC A Quality Control tool for High Throughput Sequence Data.* 2018.
327. R:CoreTeam, *R: A language and environment for statistical computing. R Foundation for Statistical Computing.* 2014.
328. [Warnes GR, B.B., Bonebakker L, Gentleman R, Huber W, Liaw A, Lumley T, Maechler M, Magnusson A, Moeller S, Schwartz M and Venables B., *gplots: Various R Programming Tools for Plotting Data. .* 2016.
329. Grant, R.A., et al., *The effects of smoking on whisker movements: A quantitative measure of exploratory behaviour in rodents.* Behav Processes, 2016. **128**: p. 17-23.
330. A. T. A. Boraei, P.K.S., M. Sechi, S. Satta, *Discovery of novel functionalized 1,2,4-triazoles as PARP-1 inhibitors in breast cancer: design, synthesis and antitumor activity evaluation.* European Journal of Medicinal Chemistry 2019.
331. Sechi, M., et al., *Design and synthesis of novel dihydroxyindole-2-carboxylic acids as HIV-1 integrase inhibitors.* Antivir Chem Chemother, 2004. **15**(2): p. 67-81.
332. Burke, A.P., et al., *Coronary risk factors and plaque morphology in men with coronary disease who died suddenly.* N Engl J Med, 1997. **336**(18): p. 1276-82.
333. Messner, B. and D. Bernhard, *Smoking and cardiovascular disease: mechanisms of endothelial dysfunction and early atherogenesis.* Arterioscler Thromb Vasc Biol, 2014. **34**(3): p. 509-15.
334. Malumbres, M. and M. Barbacid, *Cell cycle, CDKs and cancer: a changing paradigm.* Nat Rev Cancer, 2009. **9**(3): p. 153-66.
335. Pavlides, S.C., et al., *TGF-beta activates APC through Cdh1 binding for Cks1 and Skp2 proteasomal destruction stabilizing p27kip1 for normal endometrial growth.* Cell Cycle, 2016. **15**(7): p. 931-47.
336. Lee, E.W., et al., *Differential regulation of p53 and p21 by MKRN1 E3 ligase controls cell cycle arrest and apoptosis.* EMBO J, 2009. **28**(14): p. 2100-13.
337. Yagi, A., et al., *GADD34 induces p53 phosphorylation and p21/WAF1 transcription.* J Cell Biochem, 2003. **90**(6): p. 1242-9.
338. Xu, H., et al., *Dux4 induces cell cycle arrest at G1 phase through upregulation of p21 expression.* Biochem Biophys Res Commun, 2014. **446**(1): p. 235-40.
339. Choi, W.I., et al., *Role of promyelocytic leukemia zinc finger (PLZF) in cell proliferation and cyclin-dependent kinase inhibitor 1A (p21WAF/CDKN1A) gene repression.* J Biol Chem, 2014. **289**(27): p. 18625-40.
340. Hydbring, P., M. Malumbres, and P. Sicinski, *Non-canonical functions of cell cycle cyclins and cyclin-dependent kinases.* Nat Rev Mol Cell Biol, 2016. **17**(5): p. 280-92.
341. Abbas, T. and A. Dutta, *p21 in cancer: intricate networks and multiple activities.* Nat Rev Cancer, 2009. **9**(6): p. 400-14.
342. Meikrantz, W. and R. Schlegel, *Apoptosis and the cell cycle.* J Cell Biochem, 1995. **58**(2): p. 160-74.
343. Browne, S.J., et al., *The adenomatous polyposis coli protein and retinoblastoma protein are cleaved early in apoptosis and are potential substrates for caspases.* Cell Death Differ, 1998. **5**(3): p. 206-13.
344. Ovadya, Y. and V. Krizhanovsky, *Strategies targeting cellular senescence.* J Clin Invest, 2018. **128**(4): p. 1247-1254.

345. Campisi, J., *The biology of replicative senescence.* Eur J Cancer, 1997. **33**(5): p. 703-9.
346. Childs, B.G., et al., *Senescence and apoptosis: dueling or complementary cell fates?* EMBO Rep, 2014. **15**(11): p. 1139-53.
347. Seluanov, A., et al., *Change of the death pathway in senescent human fibroblasts in response to DNA damage is caused by an inability to stabilize p53.* Mol Cell Biol, 2001. **21**(5): p. 1552-64.
348. Bernard, D., et al., *The c-Rel transcription factor can both induce and inhibit apoptosis in the same cells via the upregulation of MnSOD.* Oncogene, 2002. **21**(28): p. 4392-402.
349. Wang, E., *Senescent human fibroblasts resist programmed cell death, and failure to suppress bcl2 is involved.* Cancer Res, 1995. **55**(11): p. 2284-92.
350. Ressler, S., et al., *p16INK4A is a robust in vivo biomarker of cellular aging in human skin.* Aging Cell, 2006. **5**(5): p. 379-89.
351. Jeyapalan, J.C., et al., *Accumulation of senescent cells in mitotic tissue of aging primates.* Mech Ageing Dev, 2007. **128**(1): p. 36-44.
352. Shay, J.W. and I.B. Roninson, *Hallmarks of senescence in carcinogenesis and cancer therapy.* Oncogene, 2004. **23**(16): p. 2919-33.
353. Demaria, M., et al., *Cellular Senescence Promotes Adverse Effects of Chemotherapy and Cancer Relapse.* Cancer Discov, 2017. **7**(2): p. 165-176.
354. Schosserer, M., J. Grillari, and M. Breitenbach, *The Dual Role of Cellular Senescence in Developing Tumors and Their Response to Cancer Therapy.* Front Oncol, 2017. **7**: p. 278.
355. Di Micco, R., et al., *Oncogene-induced senescence is a DNA damage response triggered by DNA hyper-replication.* Nature, 2006. **444**(7119): p. 638-42.
356. Mallette, F.A., M.F. Gaumont-Leclerc, and G. Ferbeyre, *The DNA damage signaling pathway is a critical mediator of oncogene-induced senescence.* Genes Dev, 2007. **21**(1): p. 43-8.
357. Childs, B.G., H. Li, and J.M. van Deursen, *Senescent cells: a therapeutic target for cardiovascular disease.* J Clin Invest, 2018. **128**(4): p. 1217-1228.
358. Velichko, A.K., et al., *Mechanism of heat stress-induced cellular senescence elucidates the exclusive vulnerability of early S-phase cells to mild genotoxic stress.* Nucleic Acids Res, 2015. **43**(13): p. 6309-20.
359. Sun, P., et al., *PRAK is essential for ras-induced senescence and tumor suppression.* Cell, 2007. **128**(2): p. 295-308.
360. Alcorta, D.A., et al., *Involvement of the cyclin-dependent kinase inhibitor p16 (INK4a) in replicative senescence of normal human fibroblasts.* Proc Natl Acad Sci U S A, 1996. **93**(24): p. 13742-7.
361. Zhao, H. and Z. Darzynkiewicz, *Biomarkers of cell senescence assessed by imaging cytometry.* Methods Mol Biol, 2013. **965**: p. 83-92.
362. Kuilman, T., et al., *The essence of senescence.* Genes Dev, 2010. **24**(22): p. 2463-79.
363. Blasco, M.A., et al., *Telomere shortening and tumor formation by mouse cells lacking telomerase RNA.* Cell, 1997. **91**(1): p. 25-34.
364. Artandi, S.E., et al., *Telomere dysfunction promotes non-reciprocal translocations and epithelial cancers in mice.* Nature, 2000. **406**(6796): p. 641-5.
365. Toettcher, J.E., et al., *Distinct mechanisms act in concert to mediate cell cycle arrest.* Proc Natl Acad Sci U S A, 2009. **106**(3): p. 785-90.
366. Toledo, L.I., et al., *ATR prohibits replication catastrophe by preventing global exhaustion of RPA.* Cell, 2013. **155**(5): p. 1088-103.
367. Dimri, G.P., et al., *A biomarker that identifies senescent human cells in culture and in aging skin in vivo.* Proc Natl Acad Sci U S A, 1995. **92**(20): p. 9363-7.

368. Childs, B.G., et al., *Senescent intimal foam cells are deleterious at all stages of atherosclerosis.* Science, 2016. **354**(6311): p. 472-477.
369. Bennett, M.R. and M.C. Clarke, *Killing the old: cell senescence in atherosclerosis.* Nat Rev Cardiol, 2017. **14**(3): p. 132.
370. Kurz, D.J., et al., *Senescence-associated (beta)-galactosidase reflects an increase in lysosomal mass during replicative ageing of human endothelial cells.* J Cell Sci, 2000. **113 (Pt 20)**: p. 3613-22.
371. Elmore, S., *Apoptosis: a review of programmed cell death.* Toxicol Pathol, 2007. **35**(4): p. 495-516.
372. Rock, K.L. and H. Kono, *The inflammatory response to cell death.* Annu Rev Pathol, 2008. **3**: p. 99-126.
373. Stone, P.H., et al., *Role of Low Endothelial Shear Stress and Plaque Characteristics in the Prediction of Nonculprit Major Adverse Cardiac Events: The PROSPECT Study.* JACC Cardiovasc Imaging, 2018. **11**(3): p. 462-471.
374. Chatzizisis, Y.S., et al., *Prediction of the localization of high-risk coronary atherosclerotic plaques on the basis of low endothelial shear stress: an intravascular ultrasound and histopathology natural history study.* Circulation, 2008. **117**(8): p. 993-1002.
375. Antoniadis, A.P. and P.H. Stone, *Evolving understanding of the heterogeneous natural history of individual coronary artery plaques and the role of local endothelial shear stress.* Curr Opin Cardiol, 2017. **32**(6): p. 748-754.
376. Zakkar, M., et al., *Increased endothelial mitogen-activated protein kinase phosphatase-1 expression suppresses proinflammatory activation at sites that are resistant to atherosclerosis.* Circ Res, 2008. **103**(7): p. 726-32.
377. Durand, E., et al., *In vivo induction of endothelial apoptosis leads to vessel thrombosis and endothelial denudation: a clue to the understanding of the mechanisms of thrombotic plaque erosion.* Circulation, 2004. **109**(21): p. 2503-6.
378. Giannopoulos, A.A., et al., *Erosion of Thin-Cap Fibroatheroma in an Area of Low Endothelial Shear Stress: Anatomy and Local Hemodynamic Environment Dictate Outcomes.* JACC Cardiovasc Interv, 2016. **9**(8): p. e77-e78.
379. Vergallo, R., et al., *Coronary plaque erosion developing in an area of high endothelial shear stress: insights from serial optical coherence tomography imaging.* Coron Artery Dis, 2019. **30**(1): p. 74-75.
380. Rajendran, P., et al., *The vascular endothelium and human diseases.* Int J Biol Sci, 2013. **9**(10): p. 1057-69.
381. Mundi, S., et al., *Endothelial permeability, LDL deposition, and cardiovascular risk factors-a review.* Cardiovasc Res, 2018. **114**(1): p. 35-52.
382. Ballermann, B.J., et al., *Shear stress and the endothelium.* Kidney Int Suppl, 1998. **67**: p. S100-8.
383. Chen, C.S., J. Tan, and J. Tien, *Mechanotransduction at cell-matrix and cell-cell contacts.* Annu Rev Biomed Eng, 2004. **6**: p. 275-302.
384. Favero, G., et al., *Endothelium and its alterations in cardiovascular diseases: life style intervention.* Biomed Res Int, 2014. **2014**: p. 801896.
385. Reitsma, S., et al., *The endothelial glycocalyx: composition, functions, and visualization.* Pflugers Arch, 2007. **454**(3): p. 345-59.
386. Hisamatsu, T., et al., *Smoking, Smoking Cessation, and Measures of Subclinical Atherosclerosis in Multiple Vascular Beds in Japanese Men.* J Am Heart Assoc, 2016. **5**(9).
387. Krupski, W.C., *The peripheral vascular consequences of smoking.* Ann Vasc Surg, 1991. **5**(3): p. 291-304.
388. Barbieri, S.S. and B.B. Weksler, *Tobacco smoke cooperates with interleukin-1beta to alter beta-catenin trafficking in vascular endothelium resulting in increased*

permeability and induction of cyclooxygenase-2 expression in vitro and in vivo. FASEB J, 2007. **21**(8): p. 1831-43.
389. Jaimes, E.A., et al., *Stable compounds of cigarette smoke induce endothelial superoxide anion production via NADPH oxidase activation.* Arterioscler Thromb Vasc Biol, 2004. **24**(6): p. 1031-6.
390. Barbieri, S.S., et al., *Suppressing PTEN activity by tobacco smoke plus interleukin-1beta modulates dissociation of VE-cadherin/beta-catenin complexes in endothelium.* Arterioscler Thromb Vasc Biol, 2008. **28**(4): p. 732-8.
391. Bernhard, D., et al., *Cigarette smoke metal-catalyzed protein oxidation leads to vascular endothelial cell contraction by depolymerization of microtubules.* FASEB J, 2005. **19**(9): p. 1096-107.
392. Auernheimer, V., et al., *Vinculin phosphorylation at residues Y100 and Y1065 is required for cellular force transmission.* J Cell Sci, 2015. **128**(18): p. 3435-43.
393. Bays, J.L., et al., *Vinculin phosphorylation differentially regulates mechanotransduction at cell-cell and cell-matrix adhesions.* J Cell Biol, 2014. **205**(2): p. 251-63.
394. Mui, K.L., C.S. Chen, and R.K. Assoian, *The mechanical regulation of integrin-cadherin crosstalk organizes cells, signaling and forces.* J Cell Sci, 2016. **129**(6): p. 1093-100.
395. Nagafuchi, A. and M. Takeichi, *Transmembrane control of cadherin-mediated cell adhesion: a 94 kDa protein functionally associated with a specific region of the cytoplasmic domain of E-cadherin.* Cell Regul, 1989. **1**(1): p. 37-44.
396. Buckley, C.D., et al., *Cell adhesion. The minimal cadherin-catenin complex binds to actin filaments under force.* Science, 2014. **346**(6209): p. 1254211.
397. Gates, J. and M. Peifer, *Can 1000 reviews be wrong? Actin, alpha-Catenin, and adherens junctions.* Cell, 2005. **123**(5): p. 769-72.
398. Tabas, I., K.J. Williams, and J. Boren, *Subendothelial lipoprotein retention as the initiating process in atherosclerosis: update and therapeutic implications.* Circulation, 2007. **116**(16): p. 1832-44.
399. Libby, P., et al., *Inflammation in atherosclerosis: from pathophysiology to practice.* J Am Coll Cardiol, 2009. **54**(23): p. 2129-38.
400. Giampietro, C., *VE-cadherin complex plasticity: EPS8 and YAP play relay at adherens junctions.* Tissue Barriers, 2016. **4**(4): p. e1232024.
401. Dejana, E., et al., *Organization and signaling of endothelial cell-to-cell junctions in various regions of the blood and lymphatic vascular trees.* Cell Tissue Res, 2009. **335**(1): p. 17-25.
402. Dejana, E. and D. Vestweber, *The role of VE-cadherin in vascular morphogenesis and permeability control.* Prog Mol Biol Transl Sci, 2013. **116**: p. 119-44.
403. Weiss, E.E., et al., *Vinculin is part of the cadherin-catenin junctional complex: complex formation between alpha-catenin and vinculin.* J Cell Biol, 1998. **141**(3): p. 755-64.
404. Knudsen, K.A., et al., *Interaction of alpha-actinin with the cadherin/catenin cell-cell adhesion complex via alpha-catenin.* J Cell Biol, 1995. **130**(1): p. 67-77.
405. Furukawa, K.T., et al., *The Epithelial Circumferential Actin Belt Regulates YAP/TAZ through Nucleocytoplasmic Shuttling of Merlin.* Cell Rep, 2017. **20**(6): p. 1435-1447.
406. Chervin-Petinot, A., et al., *Epithelial protein lost in neoplasm (EPLIN) interacts with alpha-catenin and actin filaments in endothelial cells and stabilizes vascular capillary network in vitro.* J Biol Chem, 2012. **287**(10): p. 7556-72.
407. Huveneers, S., et al., *Vinculin associates with endothelial VE-cadherin junctions to control force-dependent remodeling.* J Cell Biol, 2012. **196**(5): p. 641-52.

408. Komarova, Y.A., et al., *VE-cadherin signaling induces EB3 phosphorylation to suppress microtubule growth and assemble adherens junctions.* Mol Cell, 2012. **48**(6): p. 914-25.
409. Frisch, S.M. and H. Francis, *Disruption of epithelial cell-matrix interactions induces apoptosis.* J Cell Biol, 1994. **124**(4): p. 619-26.
410. Frisch, S.M. and E. Ruoslahti, *Integrins and anoikis.* Curr Opin Cell Biol, 1997. **9**(5): p. 701-6.
411. vom Dahl, S., et al., *Involvement of integrins in osmosensing and signaling toward autophagic proteolysis in rat liver.* J Biol Chem, 2003. **278**(29): p. 27088-95.
412. Schliess, F., et al., *Involvement of integrins and Src in insulin signaling toward autophagic proteolysis in rat liver.* J Biol Chem, 2004. **279**(20): p. 21294-301.
413. Vlahakis, A. and J. Debnath, *The Interconnections between Autophagy and Integrin-Mediated Cell Adhesion.* J Mol Biol, 2017. **429**(4): p. 515-530.
414. Tuloup-Minguez, V., et al., *Autophagy modulates cell migration and beta1 integrin membrane recycling.* Cell Cycle, 2013. **12**(20): p. 3317-28.
415. Kenific, C.M., et al., *NBR1 enables autophagy-dependent focal adhesion turnover.* J Cell Biol, 2016. **212**(5): p. 577-90.
416. Sharifi, M.N., et al., *Autophagy Promotes Focal Adhesion Disassembly and Cell Motility of Metastatic Tumor Cells through the Direct Interaction of Paxillin with LC3.* Cell Rep, 2016. **15**(8): p. 1660-72.
417. Fung, C., et al., *Induction of autophagy during extracellular matrix detachment promotes cell survival.* Mol Biol Cell, 2008. **19**(3): p. 797-806.
418. Chen, N. and J. Debnath, *IkappaB kinase complex (IKK) triggers detachment-induced autophagy in mammary epithelial cells independently of the PI3K-AKT-MTORC1 pathway.* Autophagy, 2013. **9**(8): p. 1214-27.
419. Miranti, C.K. and J.S. Brugge, *Sensing the environment: a historical perspective on integrin signal transduction.* Nat Cell Biol, 2002. **4**(4): p. E83-90.
420. Kenific, C.M., T. Wittmann, and J. Debnath, *Autophagy in adhesion and migration.* J Cell Sci, 2016. **129**(20): p. 3685-3693.
421. Nobes, C.D. and A. Hall, *Rho GTPases control polarity, protrusion, and adhesion during cell movement.* J Cell Biol, 1999. **144**(6): p. 1235-44.
422. Belaid, A., et al., *Autophagy plays a critical role in the degradation of active RHOA, the control of cell cytokinesis, and genomic stability.* Cancer Res, 2013. **73**(14): p. 4311-22.
423. Ma, Z., et al., *p66Shc mediates anoikis through RhoA.* J Cell Biol, 2007. **179**(1): p. 23-31.
424. Razinia, Z., et al., *Filamins in mechanosensing and signaling.* Annu Rev Biophys, 2012. **41**: p. 227-46.
425. Ulbricht, A., et al., *Cellular mechanotransduction relies on tension-induced and chaperone-assisted autophagy.* Curr Biol, 2013. **23**(5): p. 430-5.
426. Kaushik, S. and A.M. Cuervo, *Chaperone-mediated autophagy: a unique way to enter the lysosome world.* Trends Cell Biol, 2012. **22**(8): p. 407-17.
427. Choi, A.M., S.W. Ryter, and B. Levine, *Autophagy in human health and disease.* N Engl J Med, 2013. **368**(19): p. 1845-6.
428. Klionsky, D.J., *Autophagy revisited: a conversation with Christian de Duve.* Autophagy, 2008. **4**(6): p. 740-3.
429. McHugh, D. and J. Gil, *Senescence and aging: Causes, consequences, and therapeutic avenues.* J Cell Biol, 2018. **217**(1): p. 65-77.
430. Hohfeld, J., Y. Minami, and F.U. Hartl, *Hip, a novel cochaperone involved in the eukaryotic Hsc70/Hsp40 reaction cycle.* Cell, 1995. **83**(4): p. 589-98.

431. Beere, H.M., et al., *Heat-shock protein 70 inhibits apoptosis by preventing recruitment of procaspase-9 to the Apaf-1 apoptosome.* Nat Cell Biol, 2000. **2**(8): p. 469-75.
432. Lee, J.S., J.J. Lee, and J.S. Seo, *HSP70 deficiency results in activation of c-Jun N-terminal Kinase, extracellular signal-regulated kinase, and caspase-3 in hyperosmolarity-induced apoptosis.* J Biol Chem, 2005. **280**(8): p. 6634-41.
433. Guerriero, L., et al., *The anti-apoptotic BAG3 protein is involved in BRAF inhibitor resistance in melanoma cells.* Oncotarget, 2017. **8**(46): p. 80393-80404.
434. Meriin, A.B., et al., *Hsp70-Bag3 complex is a hub for proteotoxicity-induced signaling that controls protein aggregation.* Proc Natl Acad Sci U S A, 2018. **115**(30): p. E7043-E7052.
435. Rosati, A., et al., *BAG3: a multifaceted protein that regulates major cell pathways.* Cell Death Dis, 2011. **2**: p. e141.
436. Das, C.K., et al., *BAG3 Overexpression and Cytoprotective Autophagy Mediate Apoptosis Resistance in Chemoresistant Breast Cancer Cells.* Neoplasia, 2018. **20**(3): p. 263-279.
437. Sturner, E. and C. Behl, *The Role of the Multifunctional BAG3 Protein in Cellular Protein Quality Control and in Disease.* Front Mol Neurosci, 2017. **10**: p. 177.
438. Caron, J.M., *Alteration of microtubule physiology in hepatocytes by insulin.* J Cell Physiol, 1989. **138**(3): p. 603-10.
439. Adiguzel, E., et al., *Collagens in the progression and complications of atherosclerosis.* Vasc Med, 2009. **14**(1): p. 73-89.
440. Rodriguez, I. and M. Gonzalez, *Physiological mechanisms of vascular response induced by shear stress and effect of exercise in systemic and placental circulation.* Front Pharmacol, 2014. **5**: p. 209.
441. Vion, A.C., et al., *Autophagy is required for endothelial cell alignment and atheroprotection under physiological blood flow.* Proc Natl Acad Sci U S A, 2017. **114**(41): p. E8675-E8684.
442. Vestweber, D., *VE-cadherin: the major endothelial adhesion molecule controlling cellular junctions and blood vessel formation.* Arterioscler Thromb Vasc Biol, 2008. **28**(2): p. 223-32.
443. Klionsky, D.J., et al., *Guidelines for the use and interpretation of assays for monitoring autophagy in higher eukaryotes.* Autophagy, 2008. **4**(2): p. 151-75.
444. Bjorkoy, G., et al., *Monitoring autophagic degradation of p62/SQSTM1.* Methods Enzymol, 2009. **452**: p. 181-97.
445. Chiang, H.L., et al., *A role for a 70-kilodalton heat shock protein in lysosomal degradation of intracellular proteins.* Science, 1989. **246**(4928): p. 382-5.
446. Behl, C., *Breaking BAG: The Co-Chaperone BAG3 in Health and Disease.* Trends Pharmacol Sci, 2016. **37**(8): p. 672-688.
447. Gamerdinger, M., et al., *Protein quality control during aging involves recruitment of the macroautophagy pathway by BAG3.* EMBO J, 2009. **28**(7): p. 889-901.
448. Valavanidis, A., T. Vlachogianni, and K. Fiotakis, *Tobacco smoke: involvement of reactive oxygen species and stable free radicals in mechanisms of oxidative damage, carcinogenesis and synergistic effects with other respirable particles.* Int J Environ Res Public Health, 2009. **6**(2): p. 445-62.
449. Llanos, S., et al., *Lysosomal trapping of palbociclib and its functional implications.* Oncogene, 2019. **38**(20): p. 3886-3902.
450. Huang, T. and J.A. Rivera-Perez, *Senescence-associated beta-galactosidase activity marks the visceral endoderm of mouse embryos but is not indicative of senescence.* Genesis, 2014. **52**(4): p. 300-8.
451. Zhang, Y., et al., *A protective Hsp70-TLR4 pathway in lethal oxidant lung injury.* J Immunol, 2013. **191**(3): p. 1393-403.

452. Chistiakov, D.A., A.N. Orekhov, and Y.V. Bobryshev, *Endothelial Barrier and Its Abnormalities in Cardiovascular Disease.* Front Physiol, 2015. **6**: p. 365.
453. Moreno-Blas, D., E. Gorostieta-Salas, and S. Castro-Obregon, *Connecting chaperone-mediated autophagy dysfunction to cellular senescence.* Ageing Res Rev, 2018. **41**: p. 34-41.
454. Guo, F.X., et al., *Shear Stress in Autophagy and Its Possible Mechanisms in the Process of Atherosclerosis.* DNA Cell Biol, 2017. **36**(5): p. 335-346.
455. Kawano, S., et al., *Autophagy promotes degradation of internalized collagen and regulates distribution of focal adhesions to suppress cell adhesion.* Biol Open, 2017. **6**(11): p. 1644-1653.
456. Martinet, W. and G.R. De Meyer, *Autophagy in atherosclerosis: a cell survival and death phenomenon with therapeutic potential.* Circ Res, 2009. **104**(3): p. 304-17.
457. De Meyer, G.R. and W. Martinet, *Autophagy in the cardiovascular system.* Biochim Biophys Acta, 2009. **1793**(9): p. 1485-95.
458. Jiang, T., et al., *p62 links autophagy and Nrf2 signaling.* Free Radic Biol Med, 2015. **88**(Pt B): p. 199-204.
459. Ohsumi, Y. and Y. Anraku, *Active transport of basic amino acids driven by a proton motive force in vacuolar membrane vesicles of Saccharomyces cerevisiae.* J Biol Chem, 1981. **256**(5): p. 2079-82.
460. Forgac, M., *Vacuolar ATPases: rotary proton pumps in physiology and pathophysiology.* Nat Rev Mol Cell Biol, 2007. **8**(11): p. 917-29.
461. Redmann, M., et al., *Inhibition of autophagy with bafilomycin and chloroquine decreases mitochondrial quality and bioenergetic function in primary neurons.* Redox Biol, 2017. **11**: p. 73-81.
462. Klionsky, D.J., et al., *Does bafilomycin A1 block the fusion of autophagosomes with lysosomes?* Autophagy, 2008. **4**(7): p. 849-50.
463. Tougard, C., et al., *Effect of monensin on secretory pathway in GH3 prolactin cells. A cytochemical study.* J Histochem Cytochem, 1983. **31**(6): p. 745-54.
464. Jacquin, E., et al., *Pharmacological modulators of autophagy activate a parallel noncanonical pathway driving unconventional LC3 lipidation.* Autophagy, 2017. **13**(5): p. 854-867.
465. Mauvezin, C. and T.P. Neufeld, *Bafilomycin A1 disrupts autophagic flux by inhibiting both V-ATPase-dependent acidification and Ca-P60A/SERCA-dependent autophagosome-lysosome fusion.* Autophagy, 2015. **11**(8): p. 1437-8.
466. Saito, Y., et al., *Transient acceleration of autophagic degradation by pharmacological Nrf2 activation is important for retinal pigment epithelium cell survival.* Redox Biol, 2018. **19**: p. 354-363.
467. Bowman, E.J., A. Siebers, and K. Altendorf, *Bafilomycins: a class of inhibitors of membrane ATPases from microorganisms, animal cells, and plant cells.* Proc Natl Acad Sci U S A, 1988. **85**(21): p. 7972-6.
468. Mauthe, M., et al., *Chloroquine inhibits autophagic flux by decreasing autophagosome-lysosome fusion.* Autophagy, 2018. **14**(8): p. 1435-1455.
469. Chaanine, A.H., et al., *High-dose chloroquine is metabolically cardiotoxic by inducing lysosomes and mitochondria dysfunction in a rat model of pressure overload hypertrophy.* Physiol Rep, 2015. **3**(7).
470. Zhang, J., *Autophagy and Mitophagy in Cellular Damage Control.* Redox Biol, 2013. **1**(1): p. 19-23.
471. Johri, A. and M.F. Beal, *Mitochondrial dysfunction in neurodegenerative diseases.* J Pharmacol Exp Ther, 2012. **342**(3): p. 619-30.
472. Mitchell, T., et al., *Convergent mechanisms for dysregulation of mitochondrial quality control in metabolic disease: implications for mitochondrial therapeutics.* Biochem Soc Trans, 2013. **41**(1): p. 127-33.

473. Dodson, M., V. Darley-Usmar, and J. Zhang, *Cellular metabolic and autophagic pathways: traffic control by redox signaling.* Free Radic Biol Med, 2013. **63**: p. 207-21.
474. Redmann, M., et al., *Mitophagy mechanisms and role in human diseases.* Int J Biochem Cell Biol, 2014. **53**: p. 127-33.
475. Hill, B.G., et al., *Integration of cellular bioenergetics with mitochondrial quality control and autophagy.* Biol Chem, 2012. **393**(12): p. 1485-1512.
476. Collette, J., et al., *Biosynthesis and alternate targeting of the lysosomal cysteine protease cathepsin L.* Int Rev Cytol, 2004. **241**: p. 1-51.
477. Jormsjo, S., et al., *Differential expression of cysteine and aspartic proteases during progression of atherosclerosis in apolipoprotein E-deficient mice.* Am J Pathol, 2002. **161**(3): p. 939-45.
478. Tan, G.J., et al., *Cathepsins mediate tumor metastasis.* World J Biol Chem, 2013. **4**(4): p. 91-101.
479. Joyce, J.A. and D. Hanahan, *Multiple roles for cysteine cathepsins in cancer.* Cell Cycle, 2004. **3**(12): p. 1516-619.
480. Gocheva, V. and J.A. Joyce, *Cysteine cathepsins and the cutting edge of cancer invasion.* Cell Cycle, 2007. **6**(1): p. 60-4.
481. Wilder, C.L., et al., *Differential cathepsin responses to inhibitor-induced feedback: E-64 and cystatin C elevate active cathepsin S and suppress active cathepsin L in breast cancer cells.* Int J Biochem Cell Biol, 2016. **79**: p. 199-208.
482. McKeon, A.M., et al., *Novel Improved Synthesis of HSP70 Inhibitor, Pifithrin-mu. In Vitro Synergy Quantification of Pifithrin-mu Combined with Pt Drugs in Prostate and Colorectal Cancer Cells.* Molecules, 2016. **21**(7).
483. Murphy, P.J., et al., *Pifithrin-alpha inhibits p53 signaling after interaction of the tumor suppressor protein with hsp90 and its nuclear translocation.* J Biol Chem, 2004. **279**(29): p. 30195-201.
484. Leu, J.I., et al., *A small molecule inhibitor of inducible heat shock protein 70.* Mol Cell, 2009. **36**(1): p. 15-27.
485. Leu, J.I., et al., *HSP70 inhibition by the small-molecule 2-phenylethynesulfonamide impairs protein clearance pathways in tumor cells.* Mol Cancer Res, 2011. **9**(7): p. 936-47.
486. Tutar, Y., Y. Song, and D.C. Masison, *Primate chaperones Hsc70 (constitutive) and Hsp70 (induced) differ functionally in supporting growth and prion propagation in Saccharomyces cerevisiae.* Genetics, 2006. **172**(2): p. 851-61.
487. Rohde, M., et al., *Members of the heat-shock protein 70 family promote cancer cell growth by distinct mechanisms.* Genes Dev, 2005. **19**(5): p. 570-82.
488. Leu, J.I. and D.L. George, *Hepatic IGFBP1 is a prosurvival factor that binds to BAK, protects the liver from apoptosis, and antagonizes the proapoptotic actions of p53 at mitochondria.* Genes Dev, 2007. **21**(23): p. 3095-109.
489. Bjorkoy, G., et al., *p62/SQSTM1 forms protein aggregates degraded by autophagy and has a protective effect on huntingtin-induced cell death.* J Cell Biol, 2005. **171**(4): p. 603-14.
490. Komatsu, M., et al., *Homeostatic levels of p62 control cytoplasmic inclusion body formation in autophagy-deficient mice.* Cell, 2007. **131**(6): p. 1149-63.
491. Pankiv, S., et al., *p62/SQSTM1 binds directly to Atg8/LC3 to facilitate degradation of ubiquitinated protein aggregates by autophagy.* J Biol Chem, 2007. **282**(33): p. 24131-45.
492. Ichimura, Y., et al., *Structural basis for sorting mechanism of p62 in selective autophagy.* J Biol Chem, 2008. **283**(33): p. 22847-57.
493. Shvets, E., E. Fass, and Z. Elazar, *Utilizing flow cytometry to monitor autophagy in living mammalian cells.* Autophagy, 2008. **4**(5): p. 621-8.

494. Chatterjee, M., et al., *The PI3K/Akt signaling pathway regulates the expression of Hsp70, which critically contributes to Hsp90-chaperone function and tumor cell survival in multiple myeloma.* Haematologica, 2013. **98**(7): p. 1132-41.
495. Schlecht, R., et al., *Functional analysis of Hsp70 inhibitors.* PLoS One, 2013. **8**(11): p. e78443.
496. Mayer, M.P. and B. Bukau, *Hsp70 chaperones: cellular functions and molecular mechanism.* Cell Mol Life Sci, 2005. **62**(6): p. 670-84.
497. Sondermann, H., et al., *Structure of a Bag/Hsc70 complex: convergent functional evolution of Hsp70 nucleotide exchange factors.* Science, 2001. **291**(5508): p. 1553-7.
498. Sharma, D. and D.C. Masison, *Hsp70 structure, function, regulation and influence on yeast prions.* Protein Pept Lett, 2009. **16**(6): p. 571-81.
499. Wang, G.Y., et al., *Autophagy was involved in the protective effect of metformin on hyperglycemia-induced cardiomyocyte apoptosis and Connexin43 downregulation in H9c2 cells.* Int J Med Sci, 2017. **14**(7): p. 698-704.
500. Stumvoll, M., et al., *Metabolic effects of metformin in non-insulin-dependent diabetes mellitus.* N Engl J Med, 1995. **333**(9): p. 550-4.
501. Kalra, S., et al., *Malaria and diabetes.* J Pak Med Assoc, 2017. **67**(5): p. 810-813.
502. Hardie, D.G. and D. Carling, *The AMP-activated protein kinase--fuel gauge of the mammalian cell?* Eur J Biochem, 1997. **246**(2): p. 259-73.
503. Winder, W.W. and D.G. Hardie, *AMP-activated protein kinase, a metabolic master switch: possible roles in type 2 diabetes.* Am J Physiol, 1999. **277**(1): p. E1-10.
504. Lochhead, P.A., et al., *5-aminoimidazole-4-carboxamide riboside mimics the effects of insulin on the expression of the 2 key gluconeogenic genes PEPCK and glucose-6-phosphatase.* Diabetes, 2000. **49**(6): p. 896-903.
505. Hardie, D.G., *AMPK and autophagy get connected.* EMBO J, 2011. **30**(4): p. 634-5.
506. Zhao, M. and D.J. Klionsky, *AMPK-dependent phosphorylation of ULK1 induces autophagy.* Cell Metab, 2011. **13**(2): p. 119-20.
507. Shigemitsu, K., et al., *Regulation of translational effectors by amino acid and mammalian target of rapamycin signaling pathways. Possible involvement of autophagy in cultured hepatoma cells.* J Biol Chem, 1999. **274**(2): p. 1058-65.
508. CF, M., *Metformin Attenuates Expression of Endothelial Cell Adhesion Molecules and Formation of Atherosclerotic Plaques via Autophagy Induction.* . SciMed Central 2016.
509. Son, S.M., et al., *Metformin Facilitates Amyloid-beta Generation by beta- and gamma-Secretases via Autophagy Activation.* J Alzheimers Dis, 2016. **51**(4): p. 1197-208.
510. Jiang, T., et al., *Acute metformin preconditioning confers neuroprotection against focal cerebral ischaemia by pre-activation of AMPK-dependent autophagy.* Br J Pharmacol, 2014. **171**(13): p. 3146-57.
511. Li, J., et al., *Metformin Protects Against Cisplatin-Induced Tubular Cell Apoptosis and Acute Kidney Injury via AMPKalpha-regulated Autophagy Induction.* Sci Rep, 2016. **6**: p. 23975.
512. Xie, Z., et al., *Improvement of cardiac functions by chronic metformin treatment is associated with enhanced cardiac autophagy in diabetic OVE26 mice.* Diabetes, 2011. **60**(6): p. 1770-8.
513. Kapuy, O., P.K. Vinod, and G. Banhegyi, *mTOR inhibition increases cell viability via autophagy induction during endoplasmic reticulum stress - An experimental and modeling study.* FEBS Open Bio, 2014. **4**: p. 704-13.
514. Foster, D.A. and A. Toschi, *Targeting mTOR with rapamycin: one dose does not fit all.* Cell Cycle, 2009. **8**(7): p. 1026-9.
515. Mukherjee, S. and U. Mukherjee, *A comprehensive review of immunosuppression used for liver transplantation.* J Transplant, 2009. **2009**: p. 701464.

516. Santulli, G. and H. Totary-Jain, *Tailoring mTOR-based therapy: molecular evidence and clinical challenges.* Pharmacogenomics, 2013. **14**(12): p. 1517-26.
517. Huang, J. and B.D. Manning, *A complex interplay between Akt, TSC2 and the two mTOR complexes.* Biochem Soc Trans, 2009. **37**(Pt 1): p. 217-22.
518. Morita, M., et al., *mTORC1 controls mitochondrial activity and biogenesis through 4E-BP-dependent translational regulation.* Cell Metab, 2013. **18**(5): p. 698-711.
519. Dowling, R.J., et al., *Dissecting the role of mTOR: lessons from mTOR inhibitors.* Biochim Biophys Acta, 2010. **1804**(3): p. 433-9.
520. Martinet, W., H. De Loof, and G.R. De Meyer, *mTOR inhibition: a promising strategy for stabilization of atherosclerotic plaques.* Atherosclerosis, 2014. **233**(2): p. 601-7.
521. Lamming, D.W., *mTORC2 takes the longevity stAGE.* Oncotarget, 2014. **5**(17): p. 7214-5.
522. Julien, L.A., et al., *mTORC1-activated S6K1 phosphorylates Rictor on threonine 1135 and regulates mTORC2 signaling.* Mol Cell Biol, 2010. **30**(4): p. 908-21.
523. Urbanska, M., et al., *Mammalian target of rapamycin complex 1 (mTORC1) and 2 (mTORC2) control the dendritic arbor morphology of hippocampal neurons.* J Biol Chem, 2012. **287**(36): p. 30240-56.
524. Jacinto, E., et al., *Mammalian TOR complex 2 controls the actin cytoskeleton and is rapamycin insensitive.* Nat Cell Biol, 2004. **6**(11): p. 1122-8.
525. Kim, D.H., et al., *mTOR interacts with raptor to form a nutrient-sensitive complex that signals to the cell growth machinery.* Cell, 2002. **110**(2): p. 163-75.
526. Sarkar, S., et al., *Lithium induces autophagy by inhibiting inositol monophosphatase.* J Cell Biol, 2005. **170**(7): p. 1101-11.
527. Williams, A., et al., *Novel targets for Huntington's disease in an mTOR-independent autophagy pathway.* Nat Chem Biol, 2008. **4**(5): p. 295-305.
528. Gu, W.W., et al., *Autophagy and cathepsin L are involved in the antinociceptive effect of DMBC in a mouse acetic acid-writhing model.* Acta Pharmacol Sin, 2013. **34**(8): p. 1007-12.
529. Warboys, C.M., et al., *Acute and chronic exposure to shear stress have opposite effects on endothelial permeability to macromolecules.* Am J Physiol Heart Circ Physiol, 2010. **298**(6): p. H1850-6.
530. Potter, C.M., et al., *Role of shear stress in endothelial cell morphology and expression of cyclooxygenase isoforms.* Arterioscler Thromb Vasc Biol, 2011. **31**(2): p. 384-91.
531. Hippisley-Cox, J. and C. Coupland, *Diabetes treatments and risk of heart failure, cardiovascular disease, and all cause mortality: cohort study in primary care.* BMJ, 2016. **354**: p. i3477.
532. Chen, X.L., et al., *Activation of Nrf2/ARE pathway protects endothelial cells from oxidant injury and inhibits inflammatory gene expression.* Am J Physiol Heart Circ Physiol, 2006. **290**(5): p. H1862-70.
533. Kassis, J.N., et al., *CAIR-1/BAG-3 modulates cell adhesion and migration by downregulating activity of focal adhesion proteins.* Exp Cell Res, 2006. **312**(15): p. 2962-71.
534. Carrizzo, A., et al., *The prosurvival protein BAG3: a new participant in vascular homeostasis.* Cell Death Dis, 2016. **7**(10): p. e2431.
535. Radons, J., *The human HSP70 family of chaperones: where do we stand?* Cell Stress Chaperones, 2016. **21**(3): p. 379-404.
536. Fernandez-Fernandez, M.R. and J.M. Valpuesta, *Hsp70 chaperone: a master player in protein homeostasis.* F1000Res, 2018. **7**.
537. Friedman, G.D., L.G. Dales, and H.K. Ury, *Mortality in middle-aged smokers and nonsmokers.* N Engl J Med, 1979. **300**(5): p. 213-7.

538. Vomund, S., et al., *Nrf2, the Master Regulator of Anti-Oxidative Responses.* Int J Mol Sci, 2017. **18**(12).
539. Sussan, T.E., et al., *Disruption of Nrf2, a key inducer of antioxidant defenses, attenuates ApoE-mediated atherosclerosis in mice.* PLoS One, 2008. **3**(11): p. e3791.
540. Zakkar, M., et al., *Activation of Nrf2 in endothelial cells protects arteries from exhibiting a proinflammatory state.* Arterioscler Thromb Vasc Biol, 2009. **29**(11): p. 1851-7.
541. Lewis, K.N., et al., *Regulation of Nrf2 signaling and longevity in naturally long-lived rodents.* Proc Natl Acad Sci U S A, 2015. **112**(12): p. 3722-7.
542. Bruns, D.R., et al., *Nrf2 Signaling and the Slowed Aging Phenotype: Evidence from Long-Lived Models.* Oxid Med Cell Longev, 2015. **2015**: p. 732596.
543. Kosugi, S., et al., *Systematic identification of cell cycle-dependent yeast nucleocytoplasmic shuttling proteins by prediction of composite motifs.* Proc Natl Acad Sci U S A, 2009. **106**(25): p. 10171-6.
544. Lin, J.R. and J. Hu, *SeqNLS: nuclear localization signal prediction based on frequent pattern mining and linear motif scoring.* PLoS One, 2013. **8**(10): p. e76864.
545. Moujaber, O., et al., *Cellular senescence is associated with reorganization of the microtubule cytoskeleton.* Cell Mol Life Sci, 2019. **76**(6): p. 1169-1183.
546. Wight, T.N., *A role for proteoglycans in vascular disease.* Matrix Biol, 2018. **71-72**: p. 396-420.
547. Fischer, J.W., *Role of hyaluronan in atherosclerosis: Current knowledge and open questions.* Matrix Biol, 2019. **78-79**: p. 324-336.
548. Schaefer, L., et al., *The matrix component biglycan is proinflammatory and signals through Toll-like receptors 4 and 2 in macrophages.* J Clin Invest, 2005. **115**(8): p. 2223-33.
549. Luong, M., et al., *Stimulation of TLR4 by recombinant HSP70 requires structural integrity of the HSP70 protein itself.* J Inflamm (Lond), 2012. **9**: p. 11.
550. Sarkar, C., et al., *Impaired autophagy flux is associated with neuronal cell death after traumatic brain injury.* Autophagy, 2014. **10**(12): p. 2208-22.
551. Rodriguez-Muela, N., et al., *Balance between autophagic pathways preserves retinal homeostasis.* Aging Cell, 2013. **12**(3): p. 478-88.
552. Kaushik, S., et al., *Constitutive activation of chaperone-mediated autophagy in cells with impaired macroautophagy.* Mol Biol Cell, 2008. **19**(5): p. 2179-92.
553. Koga, H., et al., *A photoconvertible fluorescent reporter to track chaperone-mediated autophagy.* Nat Commun, 2011. **2**: p. 386.
554. Chava, S., et al., *Chaperone-mediated autophagy compensates for impaired macroautophagy in the cirrhotic liver to promote hepatocellular carcinoma.* Oncotarget, 2017. **8**(25): p. 40019-40036.
555. Bonnans, C., J. Chou, and Z. Werb, *Remodelling the extracellular matrix in development and disease.* Nat Rev Mol Cell Biol, 2014. **15**(12): p. 786-801.
556. Kathage, B., et al., *The cochaperone BAG3 coordinates protein synthesis and autophagy under mechanical strain through spatial regulation of mTORC1.* Biochim Biophys Acta Mol Cell Res, 2017. **1864**(1): p. 62-75.
557. Iwasaki, M., et al., *BAG3 regulates motility and adhesion of epithelial cancer cells.* Cancer Res, 2007. **67**(21): p. 10252-9.
558. Komatsu, M., et al., *The selective autophagy substrate p62 activates the stress responsive transcription factor Nrf2 through inactivation of Keap1.* Nat Cell Biol, 2010. **12**(3): p. 213-23.
559. Lau, A., et al., *A noncanonical mechanism of Nrf2 activation by autophagy deficiency: direct interaction between Keap1 and p62.* Mol Cell Biol, 2010. **30**(13): p. 3275-85.

560. Fan, W., et al., *Keap1 facilitates p62-mediated ubiquitin aggregate clearance via autophagy.* Autophagy, 2010. **6**(5): p. 614-21.
561. Li, X., et al., *Validation of the Hsp70-Bag3 protein-protein interaction as a potential therapeutic target in cancer.* Mol Cancer Ther, 2015. **14**(3): p. 642-8.
562. Hutt, D.M., et al., *Silencing of the Hsp70-specific nucleotide-exchange factor BAG3 corrects the F508del-CFTR variant by restoring autophagy.* J Biol Chem, 2018. **293**(35): p. 13682-13695.
563. Campo, G.M., et al., *Hyaluronan differently modulates TLR-4 and the inflammatory response in mouse chondrocytes.* Biofactors, 2012. **38**(1): p. 69-76.
564. Franck, G., et al., *Roles of PAD4 and NETosis in Experimental Atherosclerosis and Arterial Injury: Implications for Superficial Erosion.* Circ Res, 2018. **123**(1): p. 33-42.
565. Mayranpaa, M.I., et al., *Desquamation of human coronary artery endothelium by human mast cell proteases: implications for plaque erosion.* Coron Artery Dis, 2006. **17**(7): p. 611-21.